Elliptically Polarizing Undulators for the ARPES beamline at the Solaris Light Source

Erik Wallén*

December 20, 2011.

*Email: erik.wallen@maxlab.lu.se, Telephone +46 46 222 33 56, Address: E. Wallén, MAX-lab, Box 118, SE-22100 Lund, Sweden

Contents

1 Introduction and summary

This report contains the magnetic models, the expected heat loads, the expected synchrotron radiation properties, and the expected tune shifts at different modes of operation for 3 different elliptically polarizing undulators which might be possible to use for the ARPES beamline at the 1.5 GeV Solaris Lights source [1]. The magnetic modeling has been carried out with the software package Radia [2].

1.1 Beam parameters of the 1.5 GeV Solaris storage ring

The parameters of the stored electron beam in the middle of the straight sections the 1.5 GeV Solaris storage ring are given below in Table 1 [3] and the parameters in Table 1 have been used for the brilliance and angular spectral flux calculations in this report.

Table 1: Beam parameters in the middle of the straight sections of the Solaris 1.5 GeV Ring [3]

Beam Energy	1.5	GeV
Beam Current	300	mA
Energy Spread (rms)	0.0010	
Horizontal Beta Function	5.672	m
Horizontal Emittance	5.985	nmrad
Vertical Beta Function	2.837	m
Vertical Emittance	59.85	pmrad
σ_h rms horizontal beam size	184.2	μm
$\sigma_{h'}$ rms horizontal beam divergence	32.48	μrad
σ_v rms vertical beam size	13.03	μm
$\sigma_{v'}$ rms vertical beam divergence	4.593	μrad

1.2 Summary of the model calculations

The 3 different modeled elliptically polarizing undulators have the period lengths 96, 90, and 72 mm and they are called epu96, epu90, and epu72. The lengths, magnetic gaps and period lengths are given in Table 2. The total length is approximately 2.6 m and the magnetic gap is 13 mm for all three undulators. The magnetic peak field and effective field and the K_x-value are given in Table 3. The emitted synchrotron radiation power and on-axis power density are given in Table 4. The vertical and horizontal tune shifts are given in Table 5.

Each elliptically polarizing undulator has been modeled in four different modes, called XXPlan, XXHeli, XXIncl, XXVert, where XX stands for the name of the undulator. XXPlan stands for planar mode giving horizontal polarization of the emitted synchrotron radiation. XXHeli stands for helical mode giving circular polarization of the emitted synchrotron radiation. XXIncl stands for inclined mode giving a 45 degree tilt in polarization plane of the emitted synchrotron radiation. XXVert stands for vertical mode giving vertical polarization of the emitted synchrotron radiation.

All the 3 elliptically polarizing undulators will give rise to strong dynamical multipoles when they are operating in other modes than the planar mode. The tune shifts at different modes will probably have to be compensated for by using current strips along the vacuum chamber [4]. The current strips will require at least 1.4 mm of vertical aperture. The vacuum chamber should hence not be thicker than approximately 11 mm at the straight sections.

Table 2: The length, minimum magnetic gap and period lengths for the modeled elliptically polarizing undulators.

Name	Length [mm]	Gap [mm]	Period Length [mm]
epu96	2515.99	13	96
epu90	2539.68	13	90
epu72	2610.74	13	72

Table 3: The maximum magnetic peak field and effective field and the K_x-value of the modeled elliptically polarizing undulators.

Name	Peak Field [T]	effective Field [T]	effective K_x-value
epu96	1.244	1.295	11.6115
epu90	1.235	1.279	10.7513
epu72	1.168	1.194	8.02941

Table 4: The maximum emitted SR power and on-axis power density of the modeled elliptically polarizing undulators.

Name	SR Power [kW]	On-axis power density [kW/mrad^2]
epu96	1.80196	0.532925
epu90	1.77425	0.568397
epu72	1.58953	0.687494

Table 5: The vertical and horizontal tune shifts of the modeled elliptically polarizing undulators when they are operating in the planar mode.

Name	Vertical Tune Shift	Horizontal Tune Shift
epu96	2.06482×10^{-2}	1.06846×10^{-2}
epu90	1.95636×10^{-2}	9.42675×10^{-3}
epu72	1.62824×10^{-2}	5.95767×10^{-3}

2 The elliptically polarizing undulator epu96

2.1 Modes of operation in the elliptically polarizing undulator epu96

Horizontal polarisation of the emitted synchrotron radiation from the epu96 (Period=96 mm, Gap=13mm) is found in the planar mode when there is no movement of the sub-girders.

Circular polarisation is found in the elliptical mode of operation for a symmetric sub-grider movement of 26.4797 mm. Figure 1 shows the vertical and horizontal magnetic field for the epu96 when operating in the helical mode.

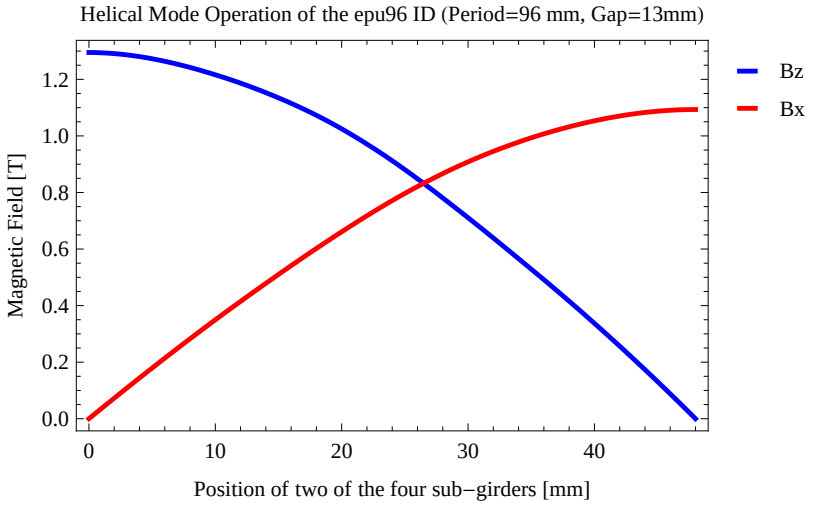

[hb]

Figure 1: Vertical and horizontal magnetic field for the the epu96 when operating in the helical mode for different positions for two of the four sub-girders

45 degree polarisation is found in the inclined mode of operation for an assymetric sub-grider movement of 25.2657 mm. Figure 2 shows the vertical and horizontal magnetic field for the epu96 when operating in the inclined mode.

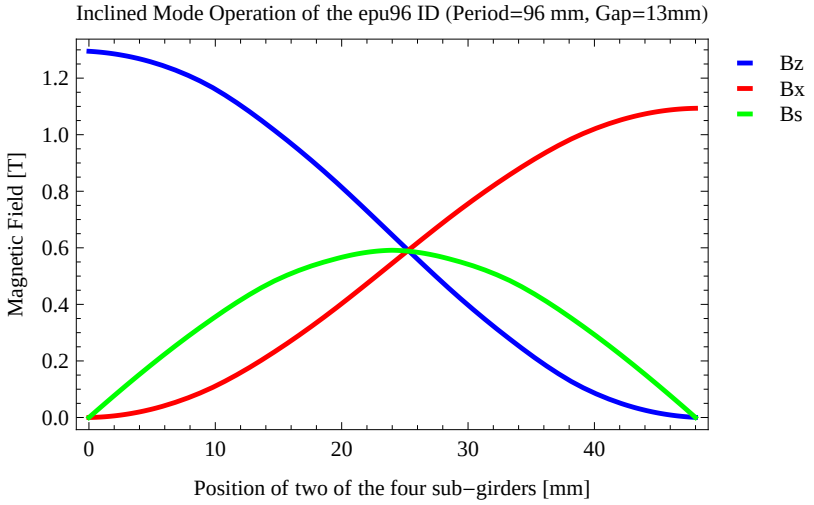

[hb]

Figure 2: Vertical, horizontal, and longitudinal magnetic field for the the epu96 when operating in the inclined mode for different positions for two of the four sub-girders

The following sub-sections will cover four different situations: The epu96 operating in the planar

mode for horizontal polarisation (epu96Plan); The epu96 operating in the helical mode for circular polarisation (epu96Heli),), the epu96operating in the inclined mode for 45 degree polarisation (epu96Incl); and The epu96 operating in the vertical mode for vertical polarisation (epu96Vert).

2.2 Magnet model of the elliptically polarizing undulator epu96Plan

The Radia [2] magnet model of the epu96Plan is shown in Figure 3. The length of the magnet model is 787.992 mm. The magnetic material in the model is NdFeb with a remanence of 1.33 T. Blocks with vertical magnetisation are blue and blocks with horizontal magnetisation are yellow. The block size is 35.x35.x24. mm^3 and there is a 5. mm cut-out in two of the corners of the blocks. The total length of the epu96Plan is 2515.99 mm.

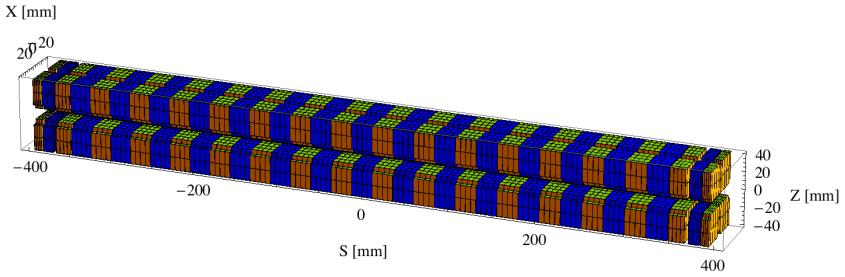

[hb]

Figure 3: Magnetic model of the epu96Plan. The has been modelled with Radia [2]

2.3 Analysis of the magnetic field of the epu96Plan

The effective magnetic fields on axis and the fundamental photon energy of the epu96Plan are shown in Table 6. The higher harmonic contents in the magnetic field of an elliptically polarizing undulator made of permanent magnets is usually small and the effective field has approximately the same strength as the peak field.

Table 6: Effective Fields on axis and Fundamental Photon Energy of the epu96Plan

Undulator Period	96	mm
Undulator Gap	13	mm
Undulator Mode	Planar	
Undulator Phase	0.000	mm
Vertical Peak Field	1.244	T
effective Vertical Field	1.295	T
Kx (from vert. field)	11.611	
Horizontal Peak Field:	0.000	T
effective Horizontal Field	0.000	T
Kz (from hor. field)	0.000	
Photon Energy, Harm.1	0.003	keV
Emitted Power	1.802	kW
Total Length	2516.0	mm

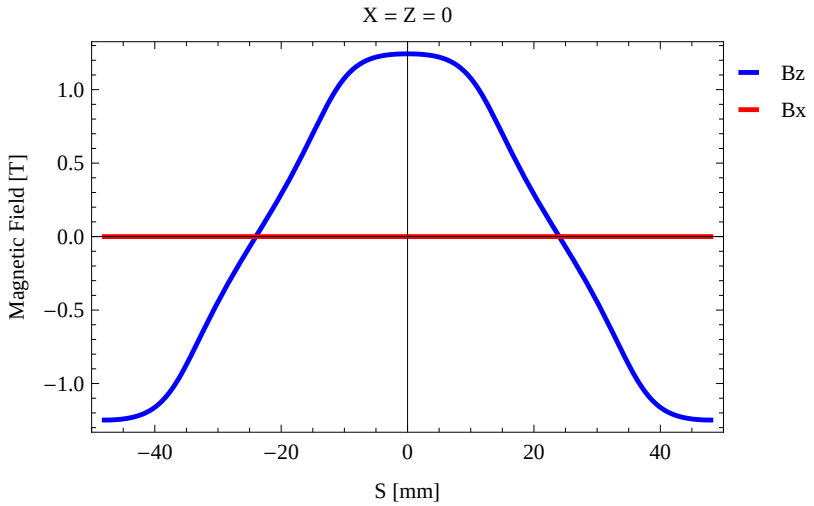

Figure 4: Vertical magnetic field in a central pole of the epu96Plan along the axis, X = Z = 0

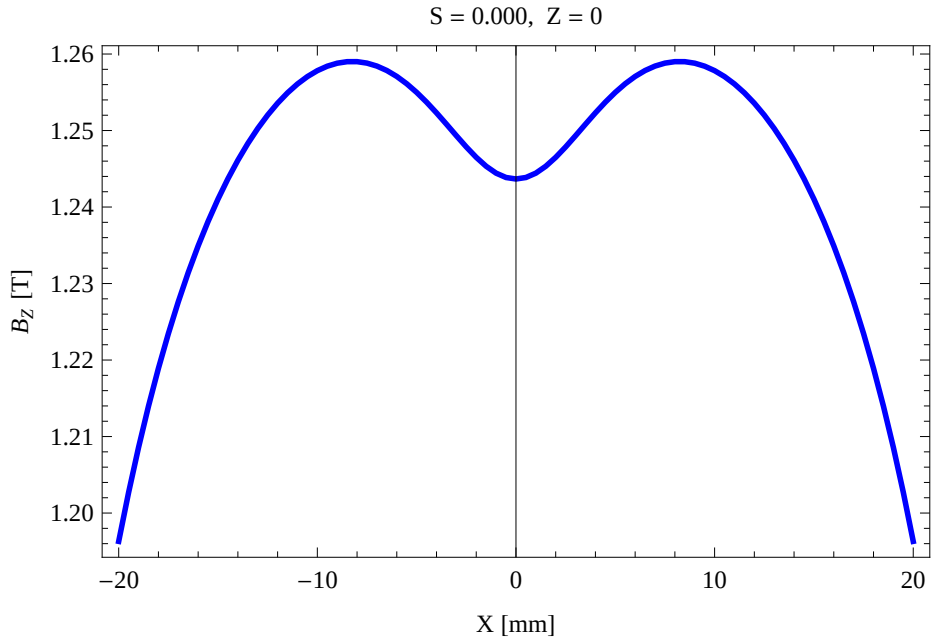

Figure 5: Vertical magnetic field in a central pole of the epu96Plan along the horizontally transverse direction to the axis, S = 0.000, Z = 0

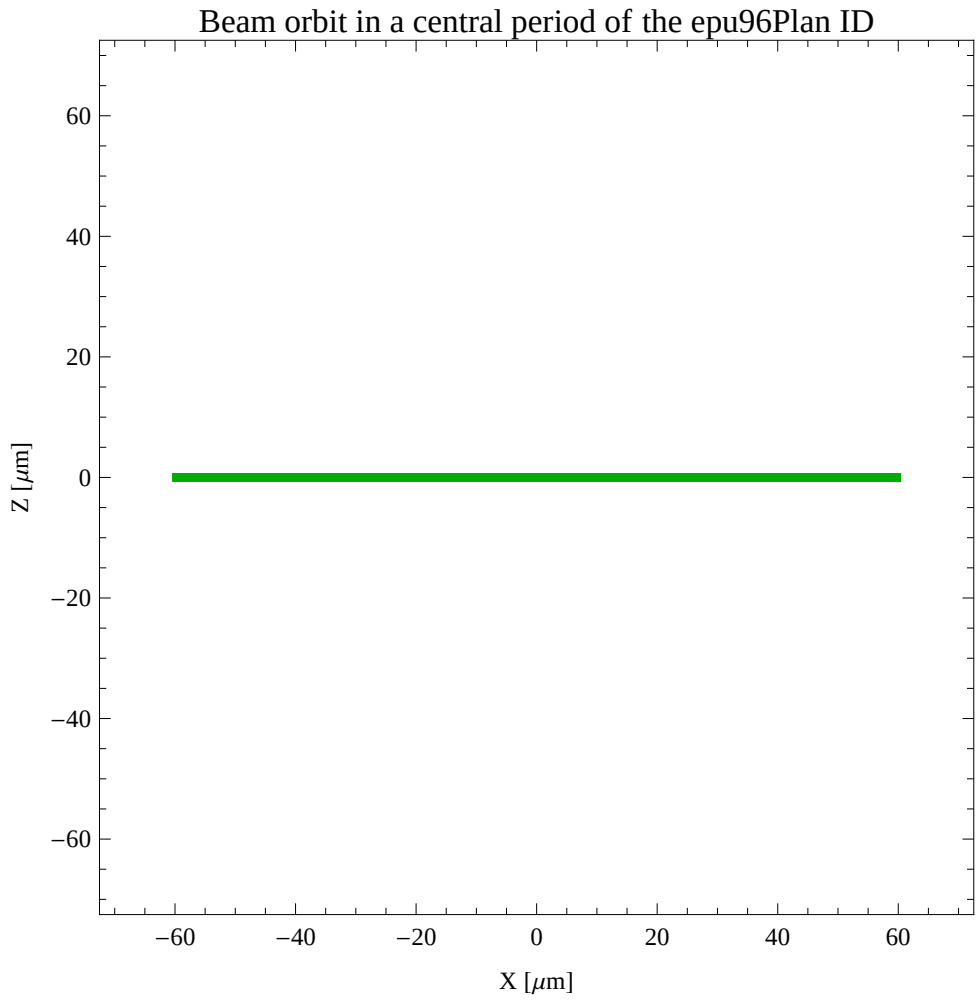

Figure 6: The beam orbit of the electron beam through a central period of the epu96Plan

2.4 Synchrotron radiation from the epu96Plan

The power map of the emitted synchrotron radiation by the epu96Plan, assuming a 0.3 A filament beam with an energy of 1.5 GeV and undulator properties of the synchrotron radiation, is shown in Figure 7. The on-axis power density is 0.532925 kW/mrad^2

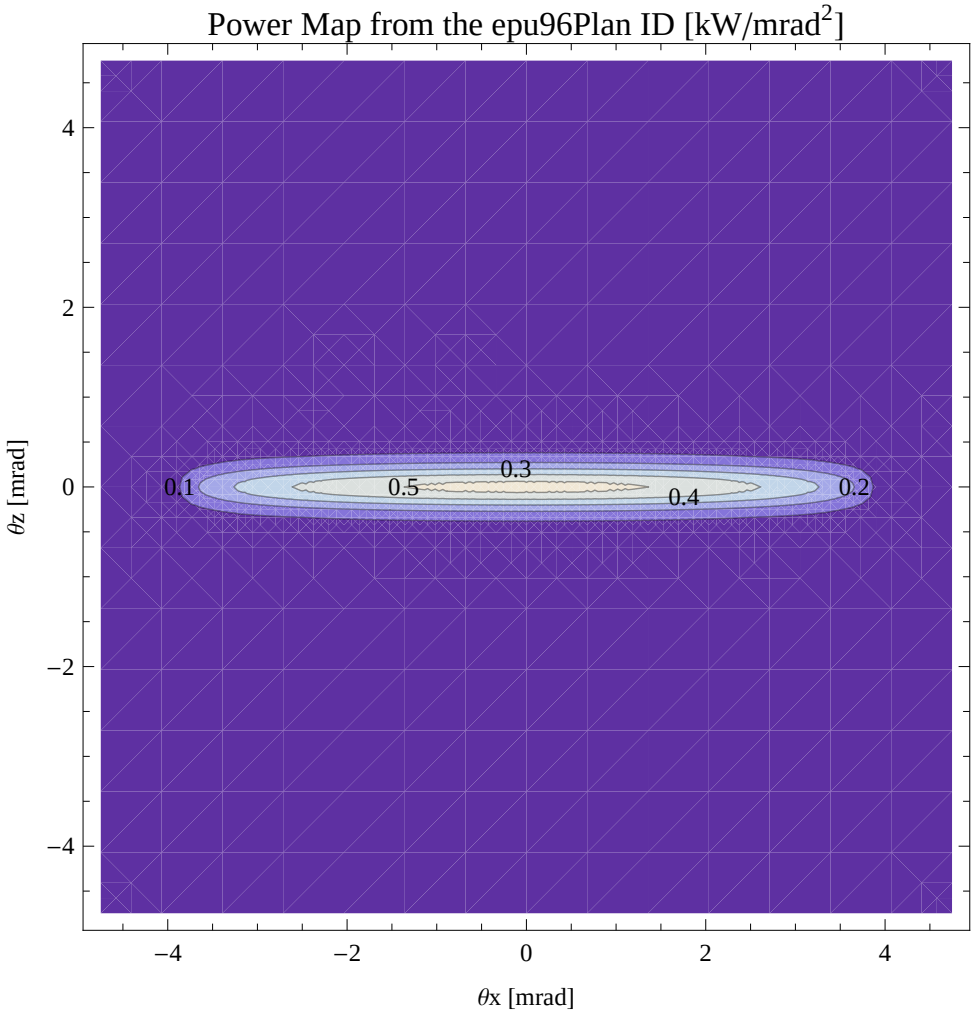

Figure 7: Map of the power distribution of the emitted synchrotron radiation by the epu96Plan

A map of the degree of linear polarisation of the fundamental harmonic of the synchotron radiation emitted by the epu96Plan over the angle of observation is shown in Figure 8.

A map of the degree of 45 degree polarisation of the fundamental harmonic of the synchotron radiation emitted by the epu96Plan over the angle of observation is shown in Figure 9.

A map of the degree of circular polarisation of the fundamental harmonic of the synchotron radiation emitted by the epu96Plan over the angle of observation is shown in Figure 10.

The on axis brilliance at peak energy and the angular spectral flux from the epu96Plan have been calculated with the given beam parameters, which are 0.3 A of stored current, $\beta_H = 5.627$ m, $\varepsilon_H = 5.985$ nmrad, $\beta_V = 2.837$ m, $\varepsilon_V = 59.85$ pmrad, and an energy spread of 0.001.

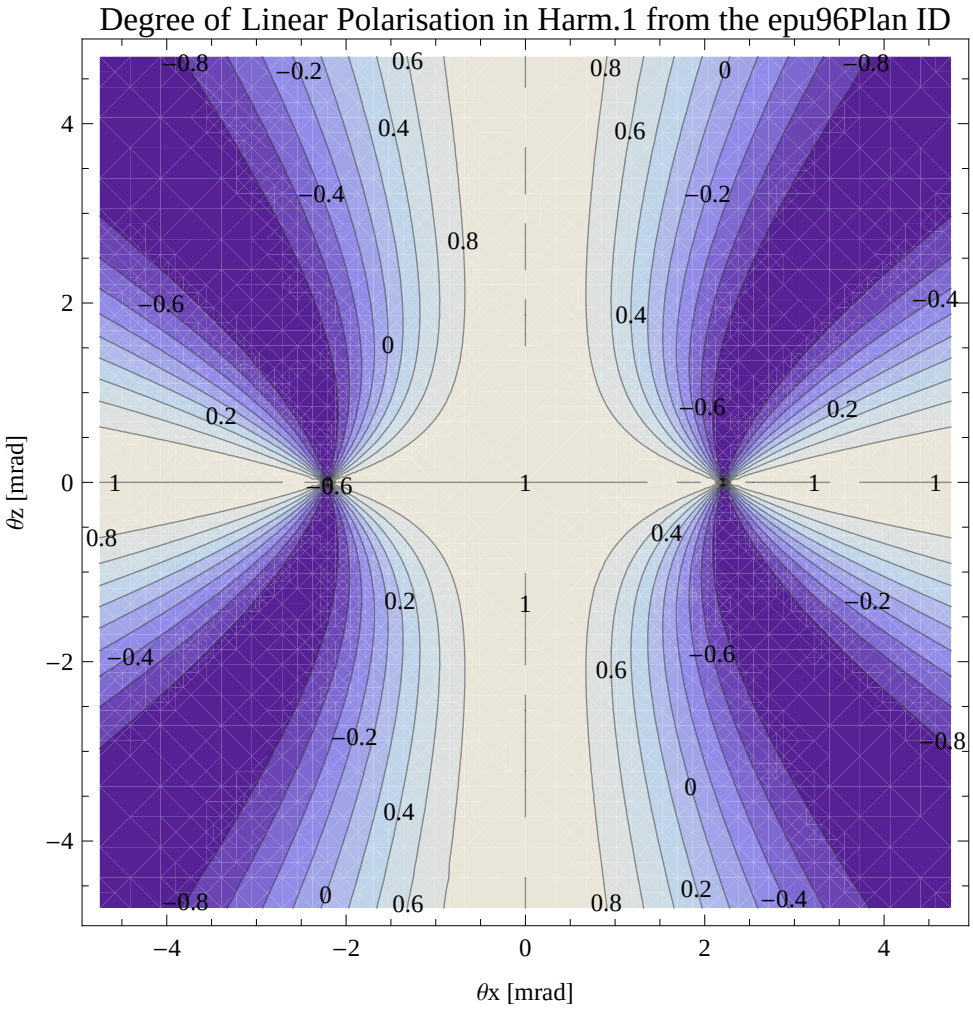

Figure 8: Map of linear polarisation in the fundamental harmonic of the synchotron radiation emitted by the epu96Plan

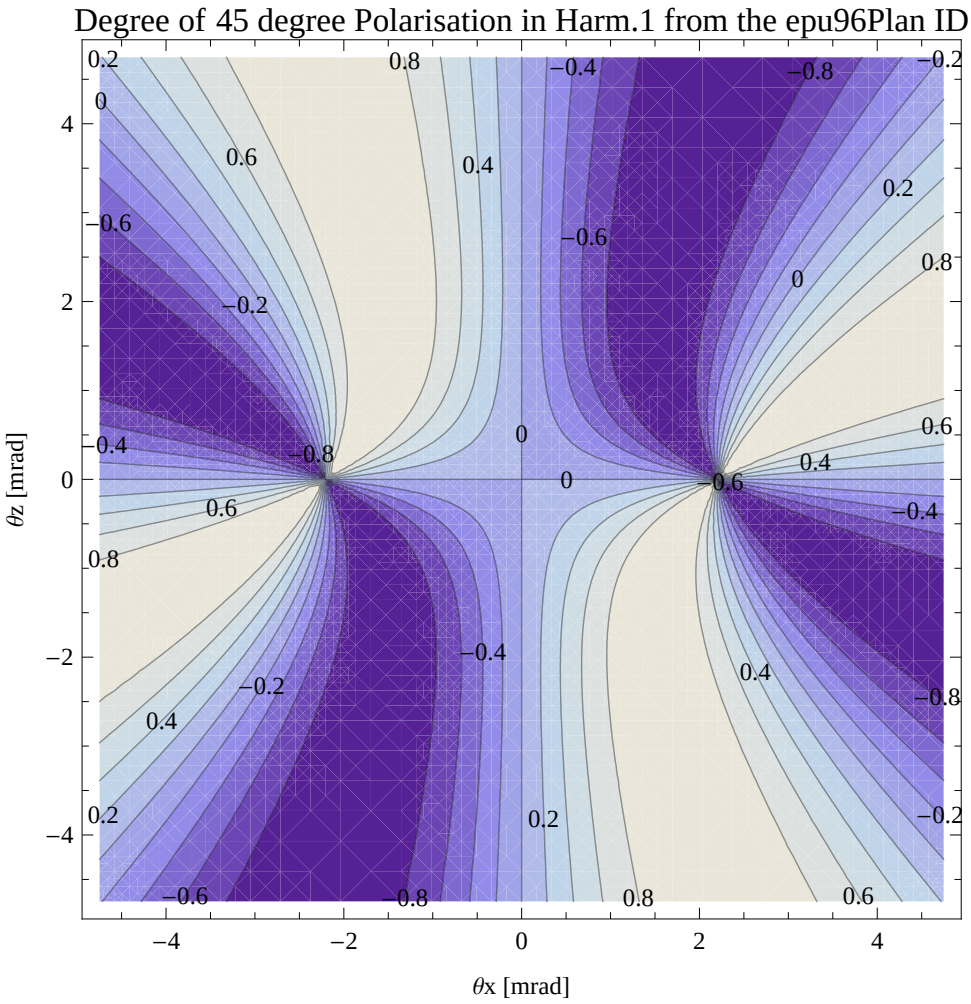

Figure 9: Map of 45 degree polarisation in the fundamental harmonic of the synchotron radiation emitted by the epu96Plan

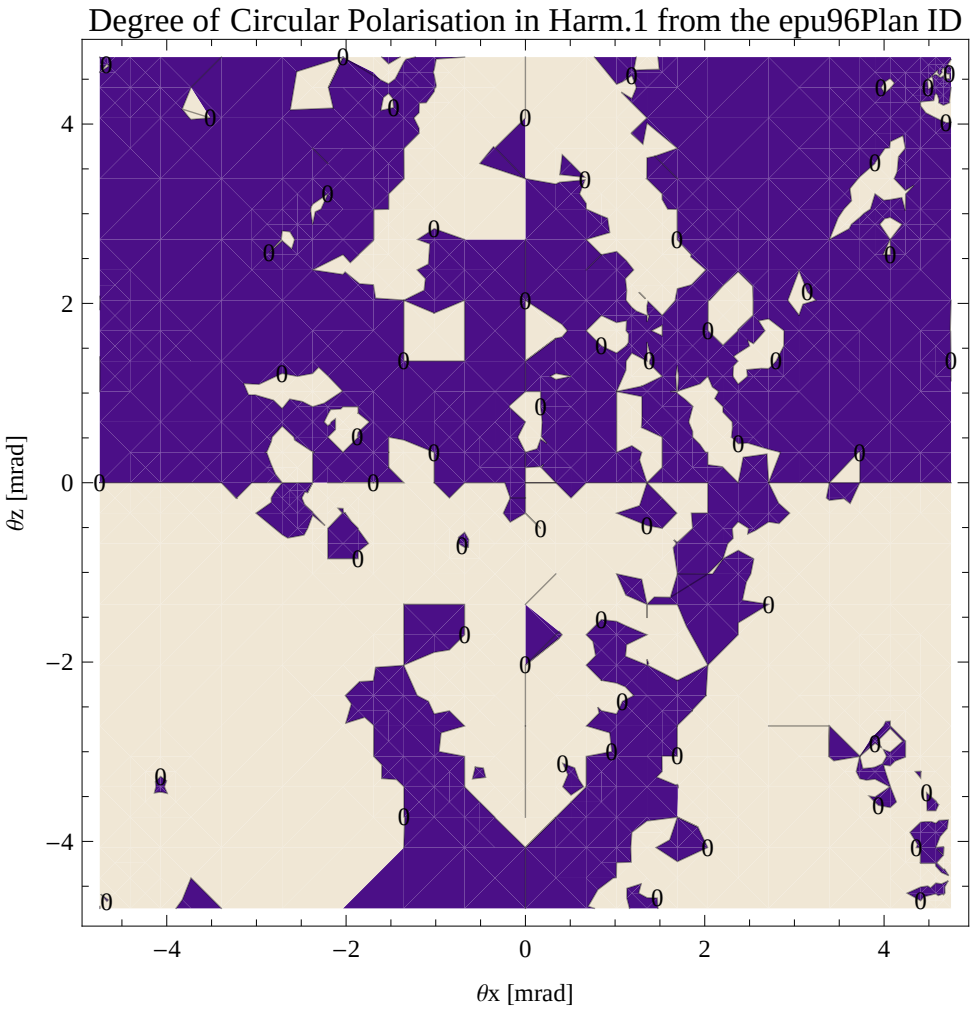

Figure 10: Map of circular polarisation in the fundamental harmonic of the synchotron radiation emitted by the epu96Plan

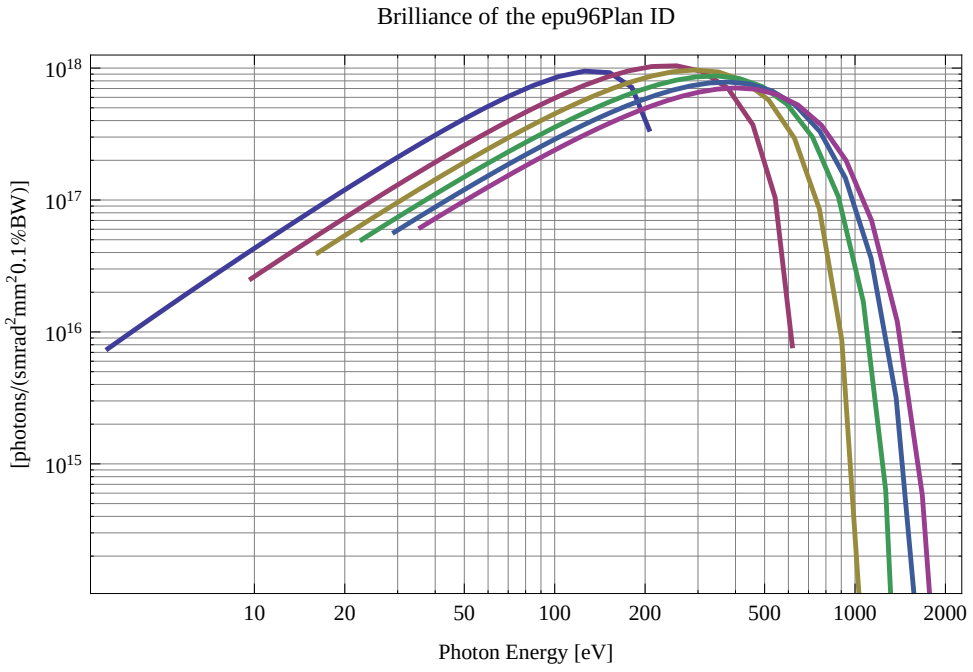

Figure 11: The brilliance at peak energy of the synchotron radiation emitted by the epu96Plan

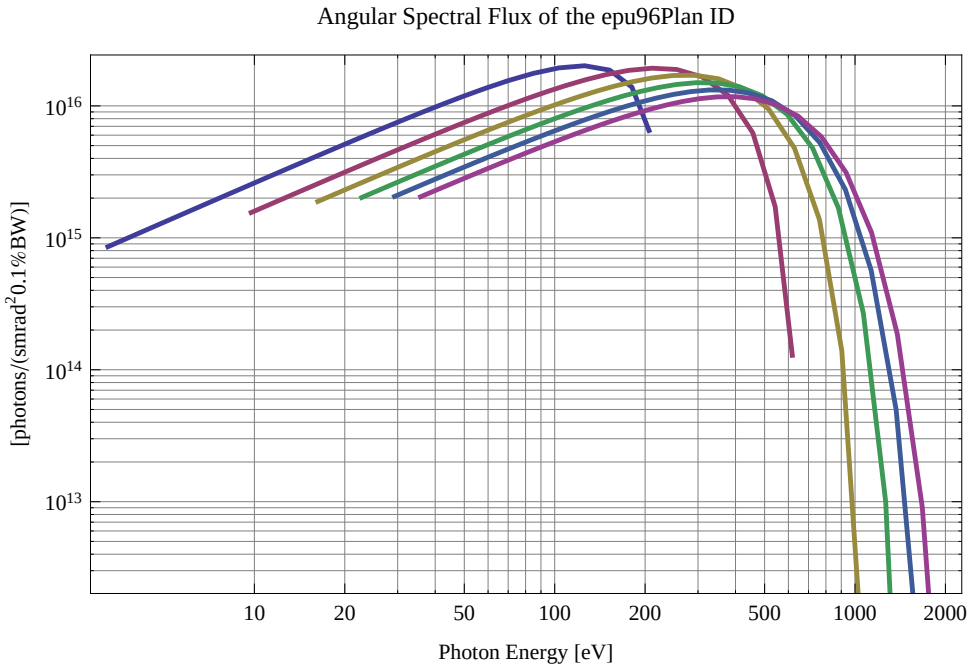

Figure 12: The angular spectral flux of the synchotron radiation emitted by the epu96Plan

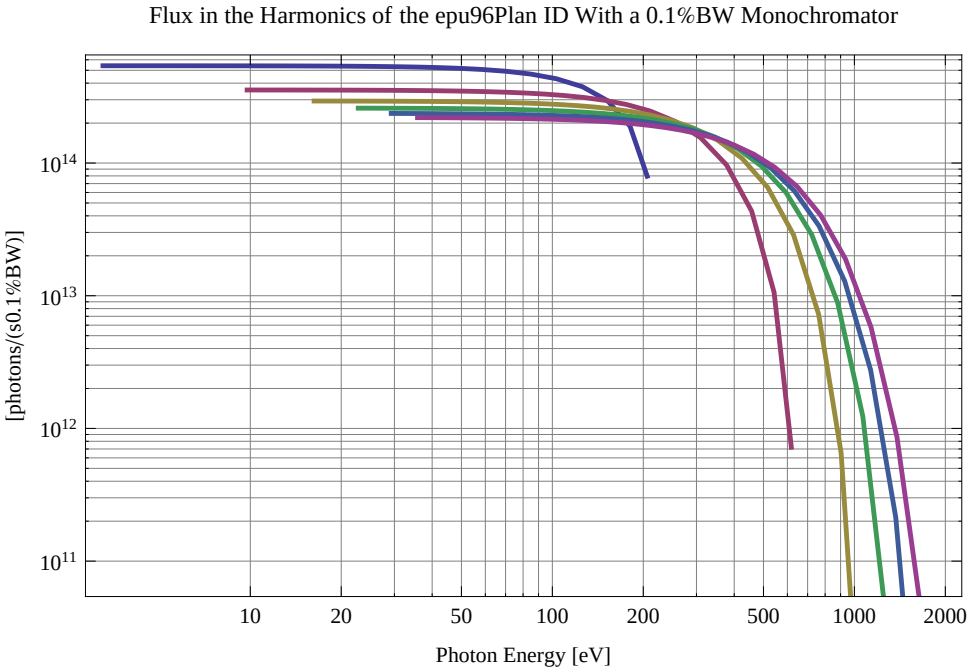

Figure 13: The flux of photons in the harmonics of the emitted synchrotron radiation from the epu96Plan using a 0.1%BW monochromator

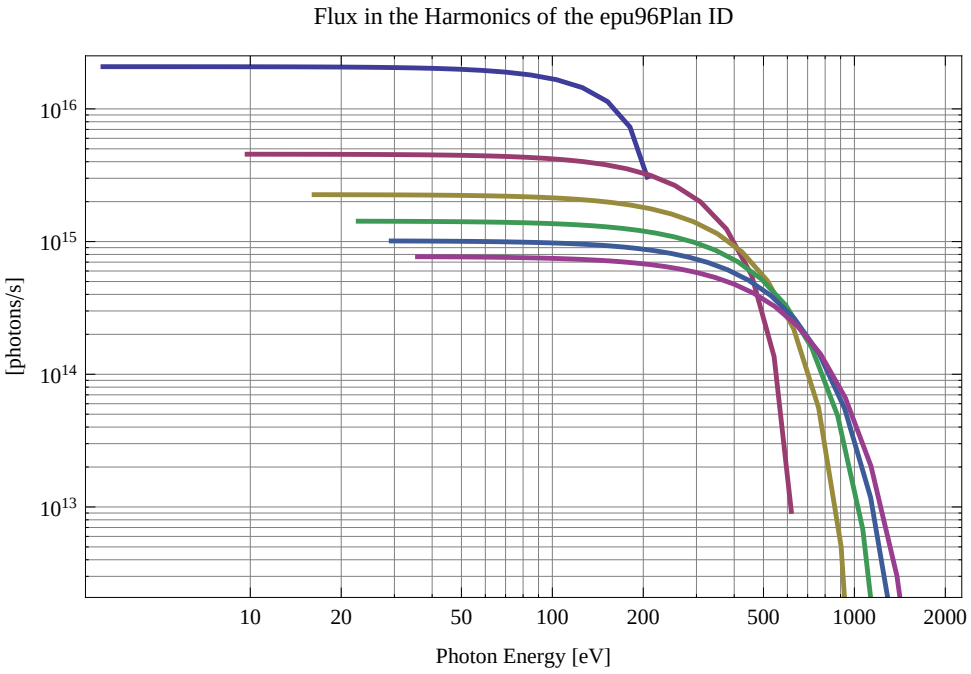

Figure 14: The flux of photons in the harmonics of the emitted synchrotron radiation from the epu96Plan

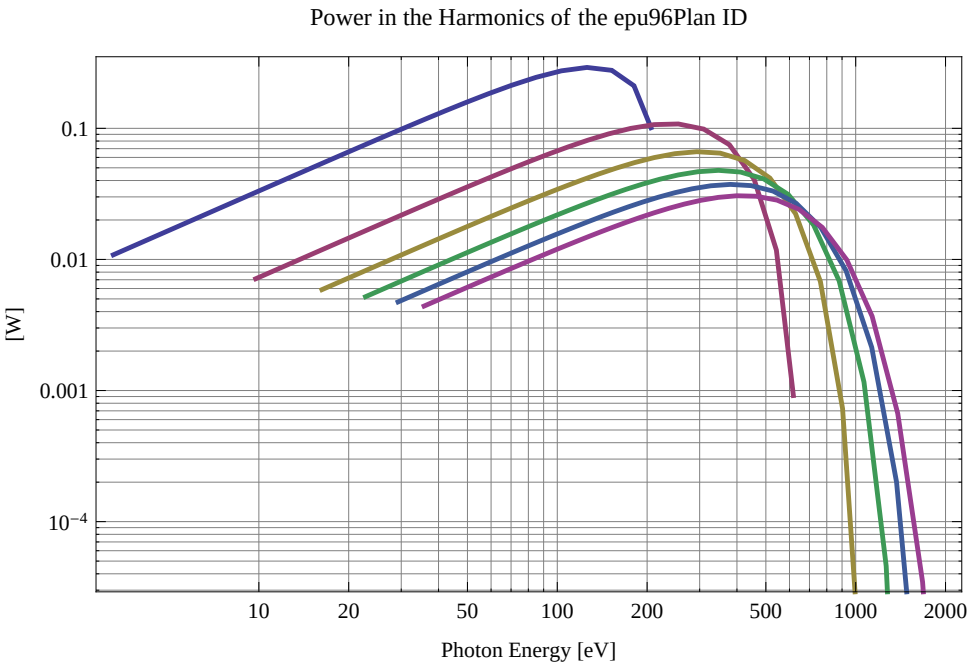

Figure 15: The power in the harmonics of the emitted synchrotron radiation from the epu96Plan

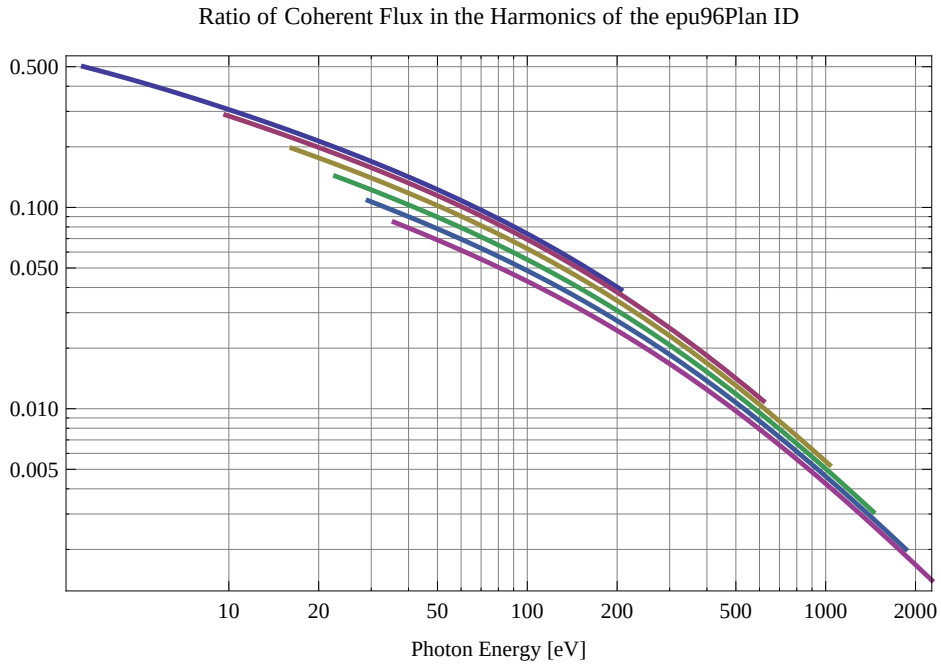

Figure 16: The ratio of coherent flux in the harmonics of the emitted synchrotron radiation from the epu96Plan

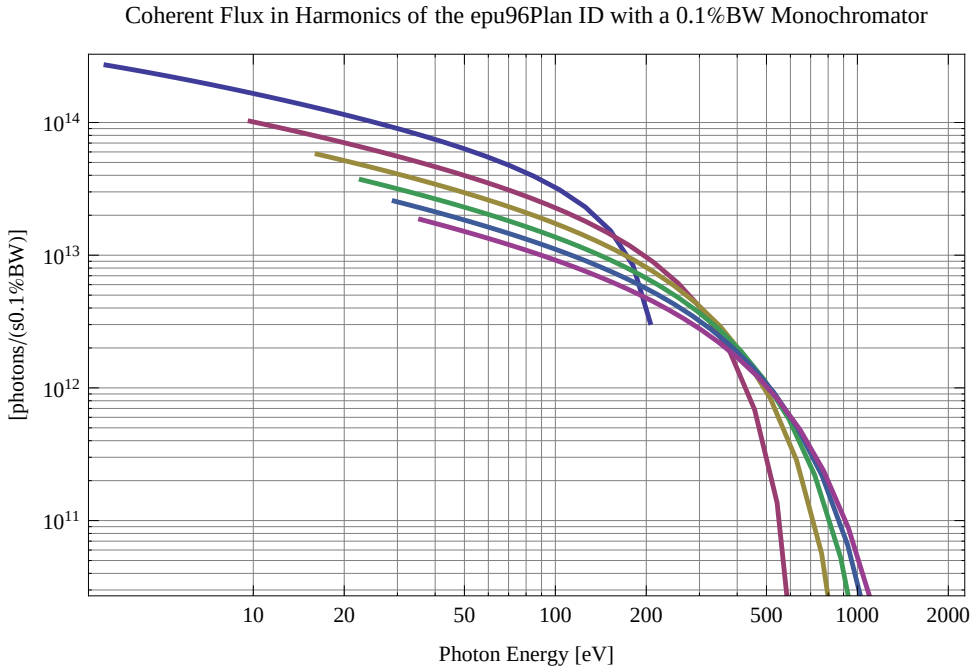

Figure 17: The coherent flux in the harmonics of the epu96Plan using a 0.1%BW Monochromator

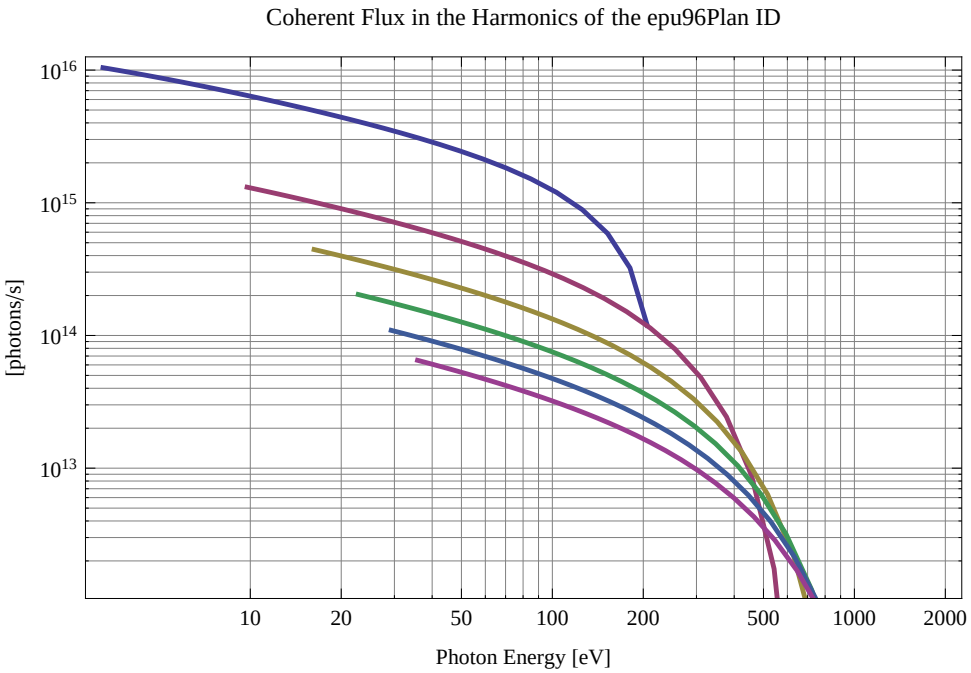

Figure 18: The coherent flux in the harmonics of the epu96Plan

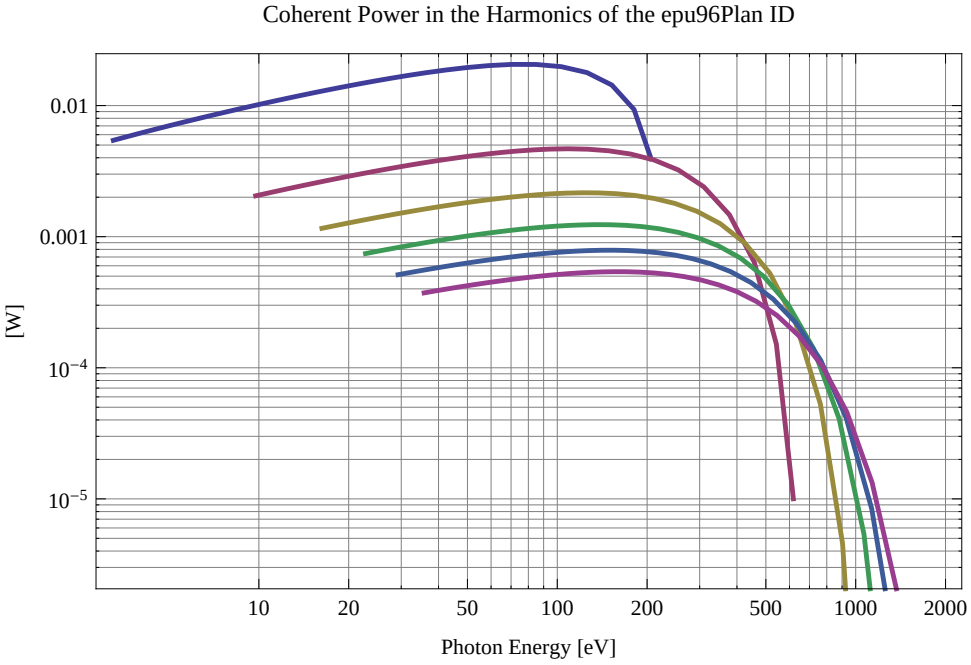

Figure 19: The power of coherent synchrotron radiation in the harmonics of the epu96Plan

The brilliance at peak energy and the angular spectral flux density from the epu96Plan for different harmonics at maximum K-value (11.611) are given in Table 7 and for minimum K-value (0.400) these values are given in Table 8.

Table 7: The brilliance at peak energy and the angular spectral flux density from the epu96Plan for different harmonics at maximum K-value (11.611)

Harmonic	Photon Energy [eV]	Brilliance [Ph./(smrad^{2}mrad^{2}0.1%BW)]	Angular Spectral Flux [Ph./(smrad^{2}0.1%BW)]
1	3.25334	7.46×10^{15}	8.56×10^{14}
3	9.76002	2.53×10^{16}	1.56×10^{15}
5	16.2667	3.98×10^{16}	1.89×10^{15}
7	22.7734	$5. \times 10^{16}$	2.02×10^{15}
9	29.2801	5.71×10^{16}	2.06×10^{15}
11	35.7867	6.19×10^{16}	2.05×10^{15}

Table 8: The brilliance at peak energy and the angular spectral flux density from the epu96Plan for different harmonics at minimum K-value (0.4)

Harmonic	Photon Energy [eV]	Brilliance [Ph./(smrad^{2}mrad^{2}0.1%BW)]	Angular Spectral Flux [Ph./(smrad^{2}0.1%BW)]
1	206.085	3.43×10^{17}	6.5×10^{15}
3	618.255	7.85×10^{15}	1.29×10^{14}
5	1030.43	1.03×10^{14}	1.64×10^{12}
7	1442.6	1.18×10^{12}	1.86×10^{10}
9	1854.77	1.28×10^{10}	2.01×10^{8}
11	2266.94	1.34×10^{8}	2.11×10^{6}

2.5 Influence from the epu96Plan on the optics of the stored beam

Figure 20 shows the focusing potential from the epu96Plan over the beam stay clear aperture of the ring aparture.

Figure 21 shows the kick map in the beam energy independant unit T^2m^2 of the kicks induced by the epu96Plan over the beam stay clear aparture.

Figure 22 shows the induced angular kick on the stored beam from the epu96Plan as a function of the vertical distance to the undulator axis.

Figure 23 shows the induced angular kick on the stored beam from the epu96Plan as a function of the horizontal distance to the undulator axis.

Figure 24 shows tune shift induced by the epu96Plan over the beam stay clear aparture. Note that the tune shift depends on the beam size at the.

Figure 25 shows the induced tune shift from the epu96Plan as a function of the vertical distance to the undulator axis.

Figure 26 shows the induced tune shift from the epu96Plan as a function of the horizontal distance to the undulator axis.

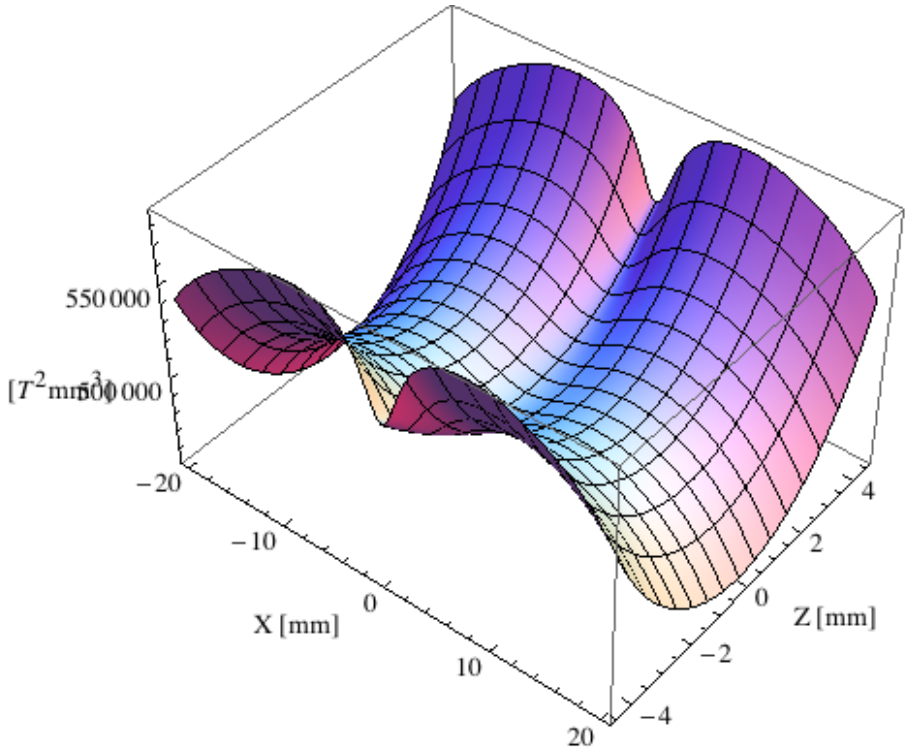

Figure 20: Focusing potential from the epu96Plan over the beam stay clear aparture.

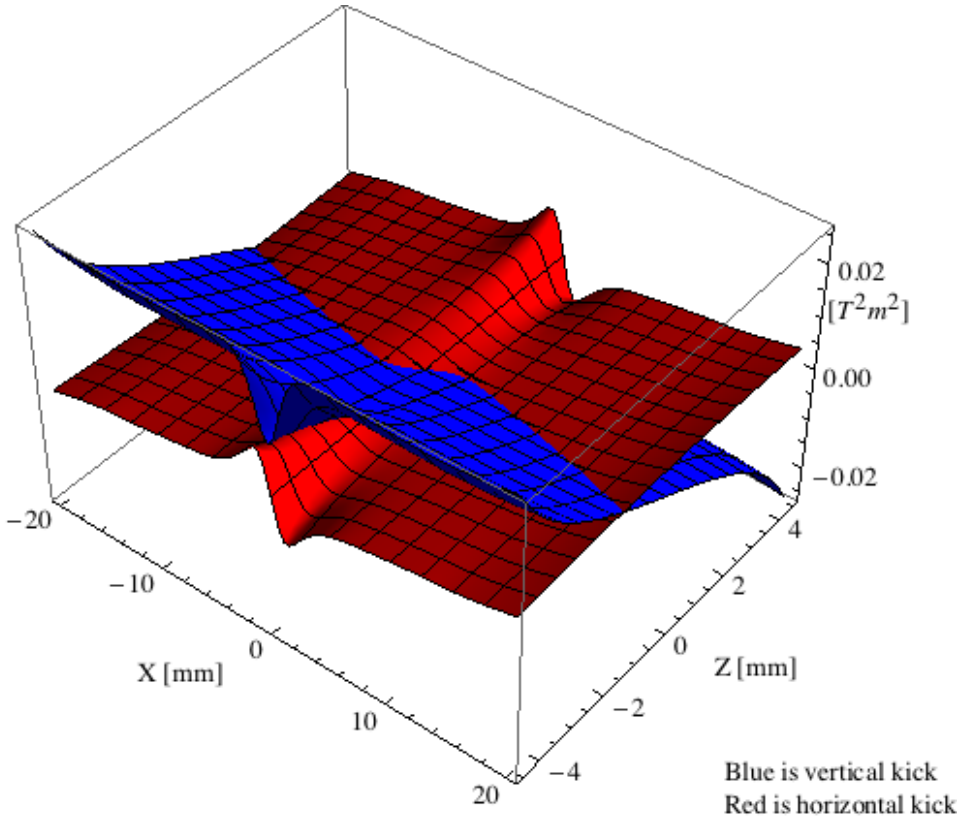

Figure 21: Kick map in the beam energy independant unit T^2m^2 of the kicks induced by the epu96Plan over the beam stay clear aparture.

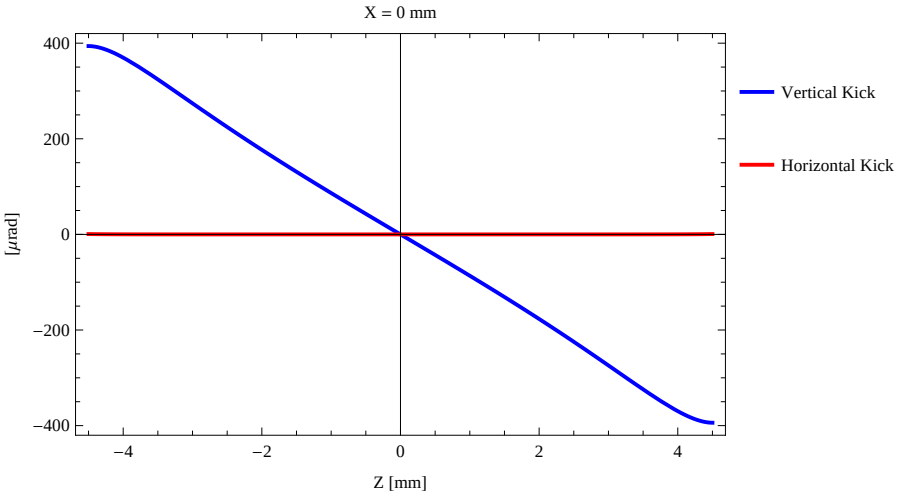

Figure 22: Induced angular kick on the stored beam from the epu96Plan as a function of the vertical distance to the undulator axis.

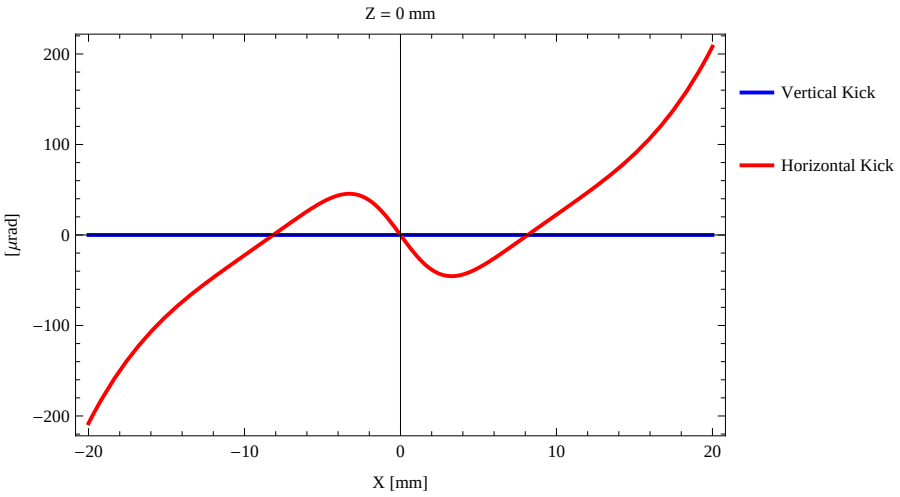

Figure 23: Induced angular kick on the stored beam from the epu96Plan as a function of the horizontal distance to the undulator axis.

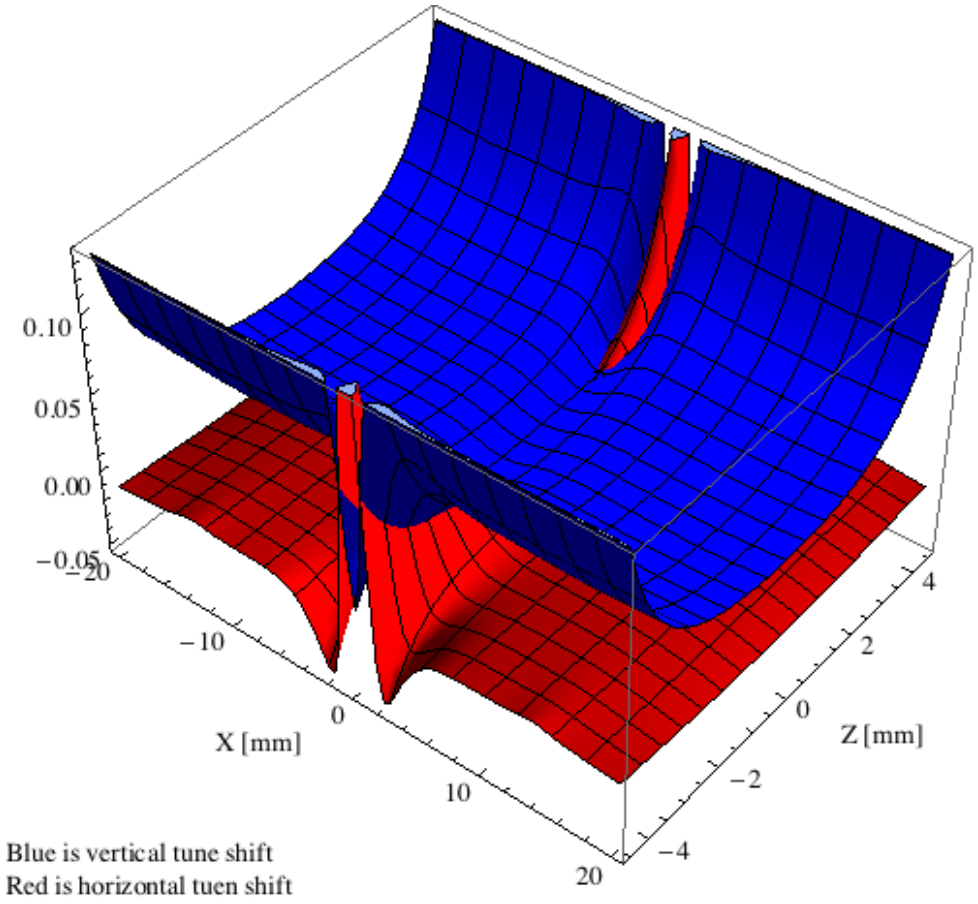

Figure 24: Tune shift induced by the epu96Plan over the beam stay clear aparture.

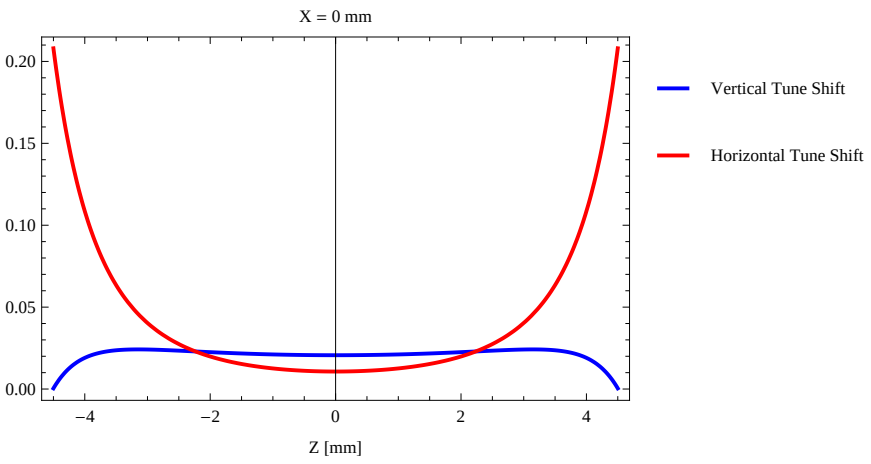

Figure 25: Induced tune shift from the epu96Plan as a function of the vertical distance to the undulator axis.

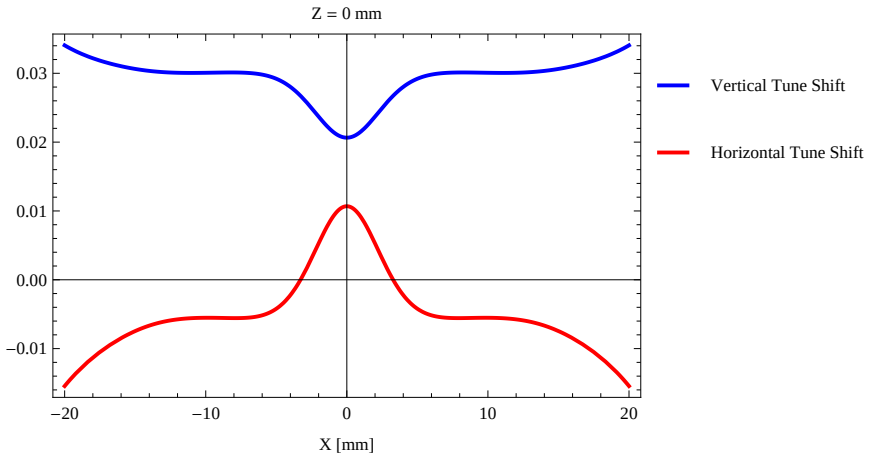

Figure 26: Induced tune shift from the epu96Plan on the stored beam from the as a function of the horizontal distance to the undulator axis.

2.6 Magnet model of the elliptically polarizing undulator epu96Heli

The Radia [2] magnet model of the epu96Heli is shown in Figure 27. The length of the magnet model is 787.992 mm. The magnetic material in the model is NdFeb with a remanence of 1.33 T. Blocks with vertical magnetisation are blue and blocks with horizontal magnetisation are yellow. The block size is 35.x35.x24. mm^3 and there is a 5. mm cut-out in two of the corners of the blocks. The total length of the epu96Heli is 2515.99 mm.

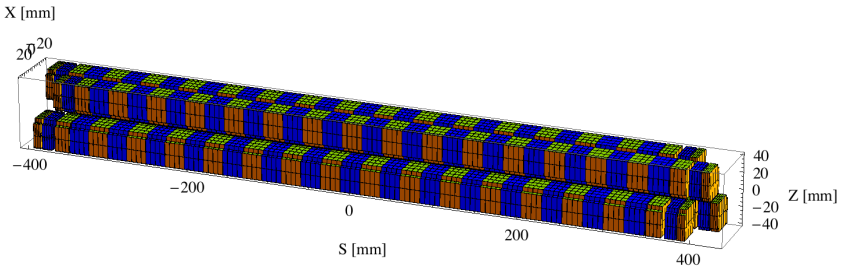

Figure 27: Magnetic model of the epu96Heli. The has been modelled with Radia [2]

2.7 Analysis of the magnetic field of the epu96Heli

The effective magnetic fields on axis and the fundamental photon energy of the epu96Heli are shown in Table 9. The higher harmonic contents in the magnetic field of an elliptically polarizing undulator made of permanent magnets is usually small and the effective field has approximately the same strength as the peak field.

2.8 Synchrotron radiation from the epu96Heli

The power map of the emitted synchrotron radiation by the epu96Heli, assuming a 0.3 A filament beam with an energy of 1.5 GeV and undulator properties of the synchrotron radiation, is shown in Figure 32. The on-axis power density is 0.000064 kW/mrad^2

Table 9: Effective Fields on axis and Fundamental Photon Energy of the epu96Heli

Undulator Period	96	mm
Undulator Gap	13	mm
Undulator Mode	Helical	
Undulator Phase	26.480	mm
Vertical Peak Field	0.846	T
effective Vertical Field	0.832	T
Kx (from vert. field)	7.460	
Horizontal Peak Field:	0.848	T
effective Horizontal Field	0.832	T
Kz (from hor. field)	7.460	
Photon Energy, Harm.1	0.004	keV
Emitted Power	1.488	kW
Total Length	2516.0	mm

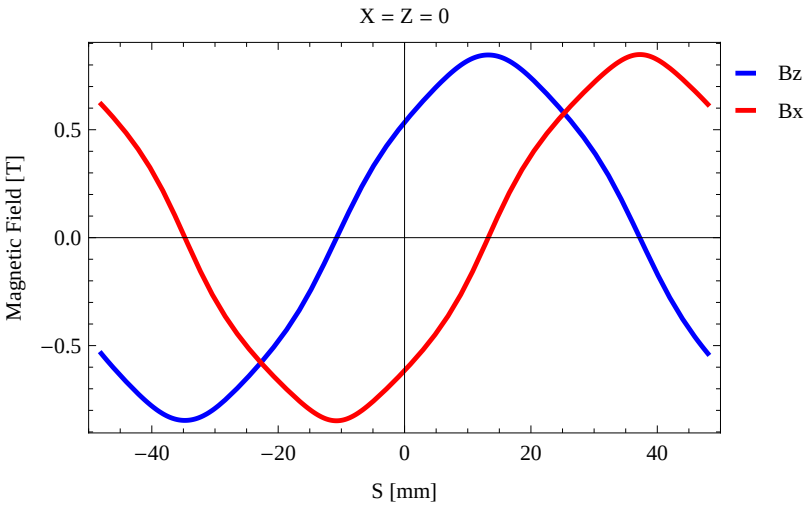

Figure 28: Vertical magnetic field in a central pole of the epu96Heli along the axis, X = Z = 0

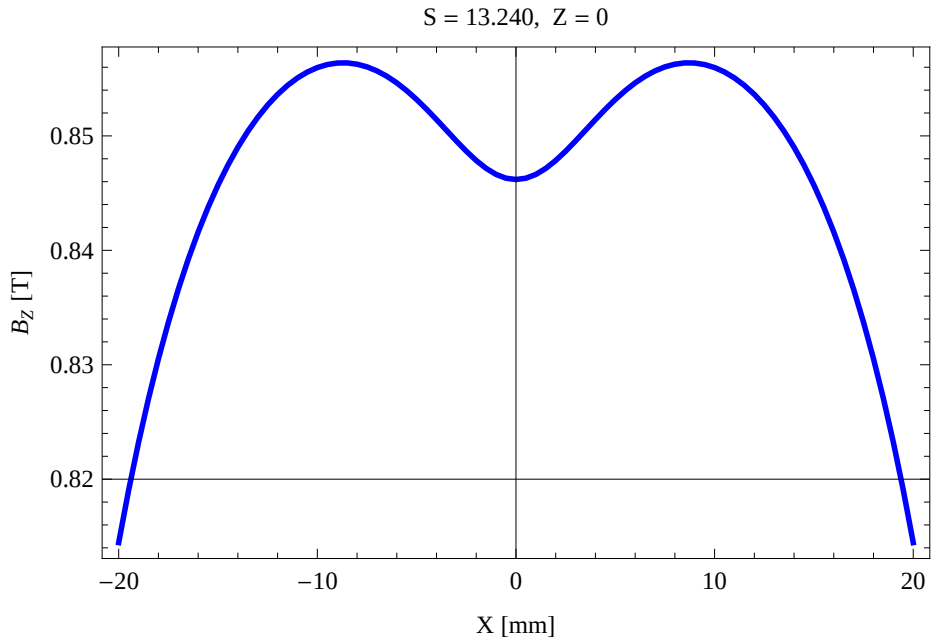

Figure 29: Vertical magnetic field in a central pole of the epu96Heli along the horizontally transverse direction to the axis, S = 13.240, Z = 0

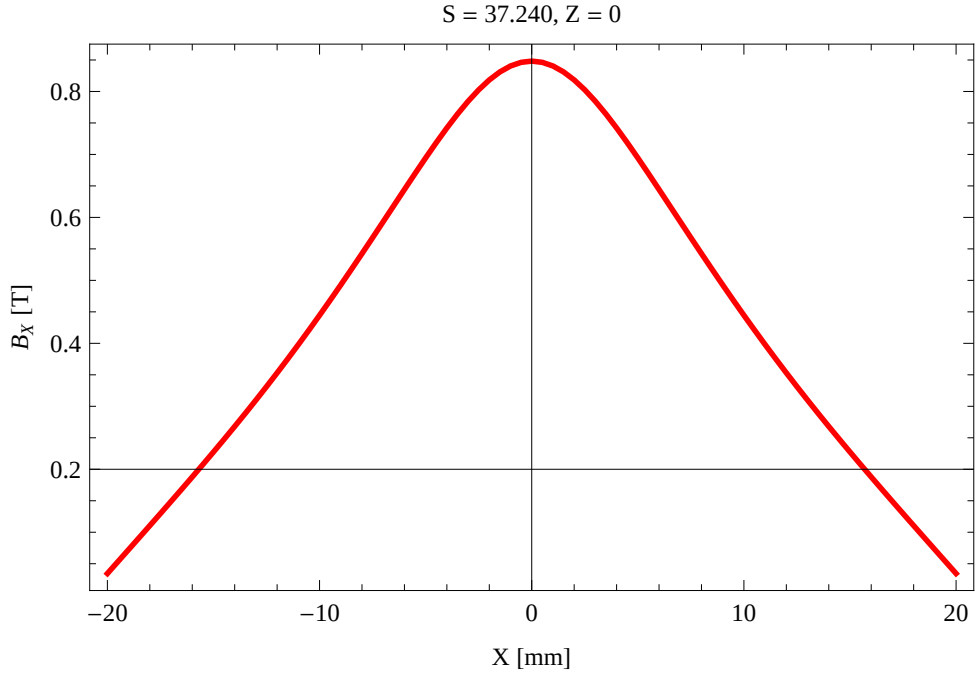

Figure 30: Horizontal magnetic field in a central pole of the epu96Heli along the horizontally transverse direction to the axis, S = 37.240, Z = 0

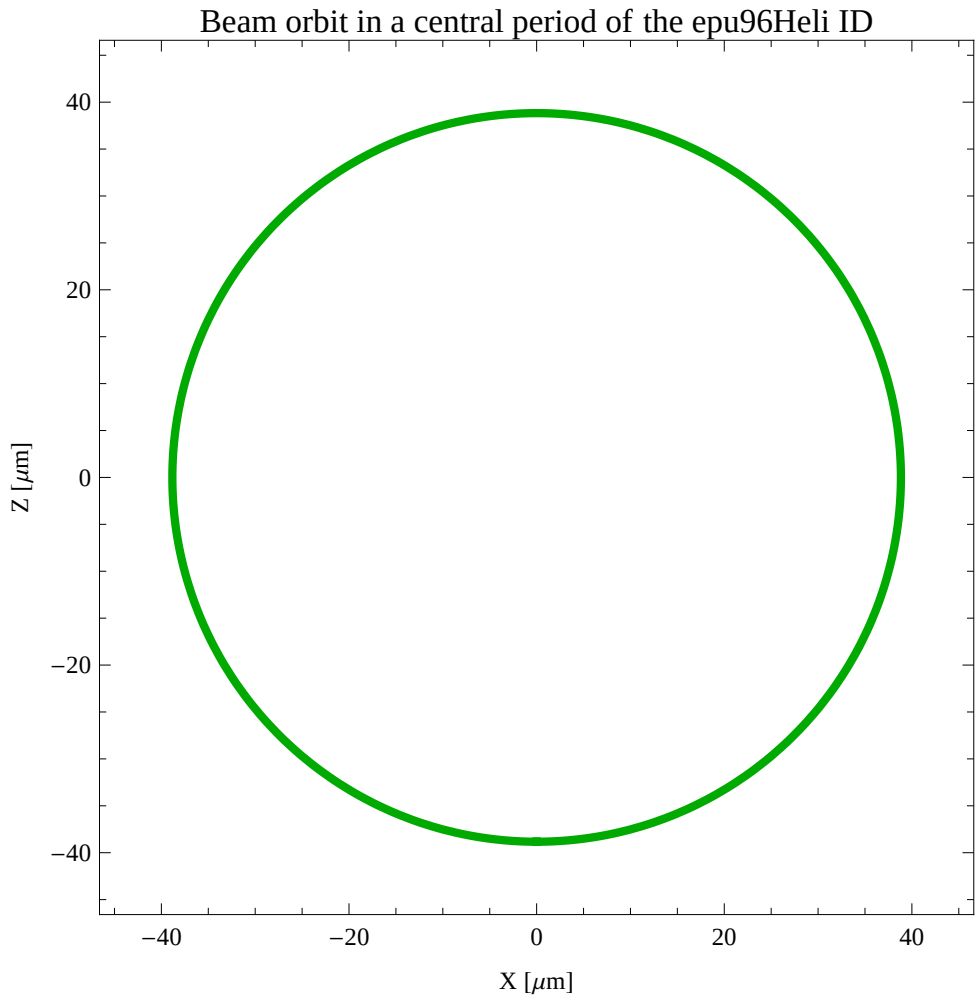

Figure 31: The beam orbit of the electron beam through a central period of the epu96Heli

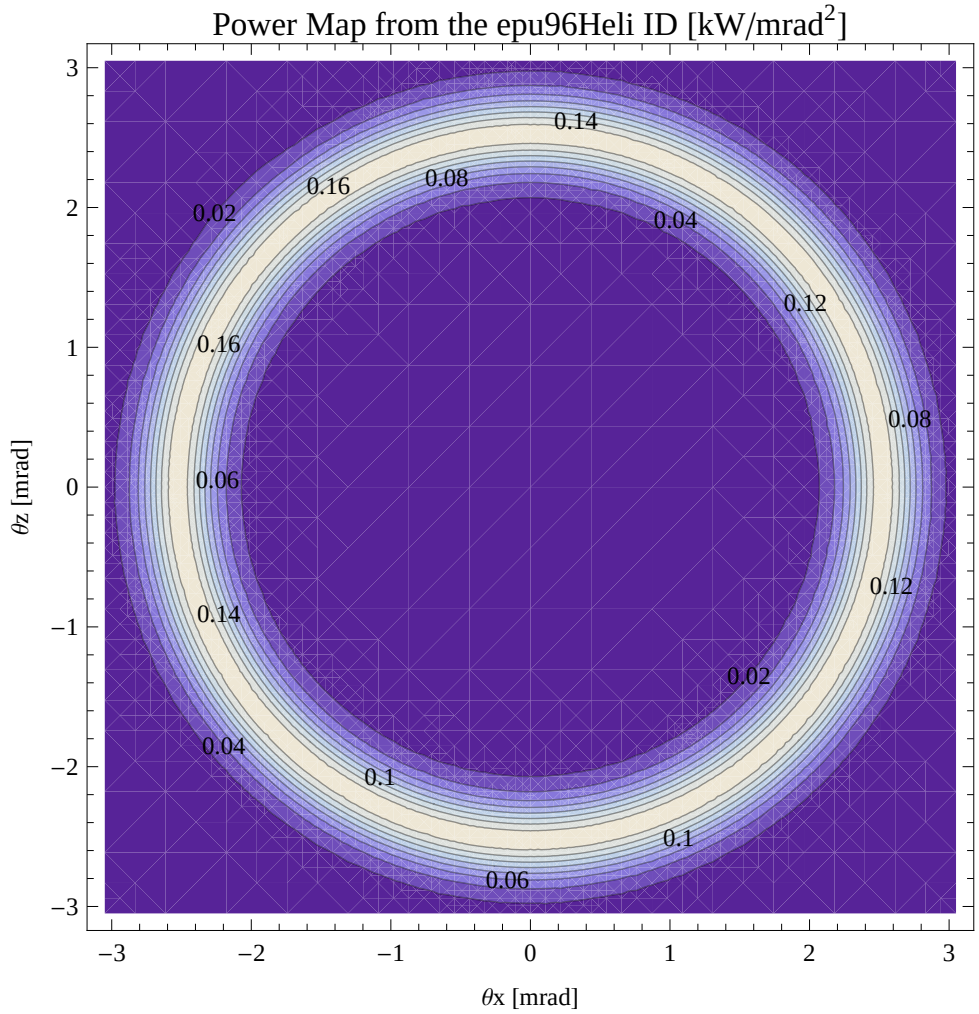

Figure 32: Map of the power distribution of the emitted synchrotron radiation by the epu96Heli

A map of the degree of linear polarisation of the fundamental harmonic of the synchotron radiation emitted by the epu96Heli over the angle of observation is shown in Figure 33.

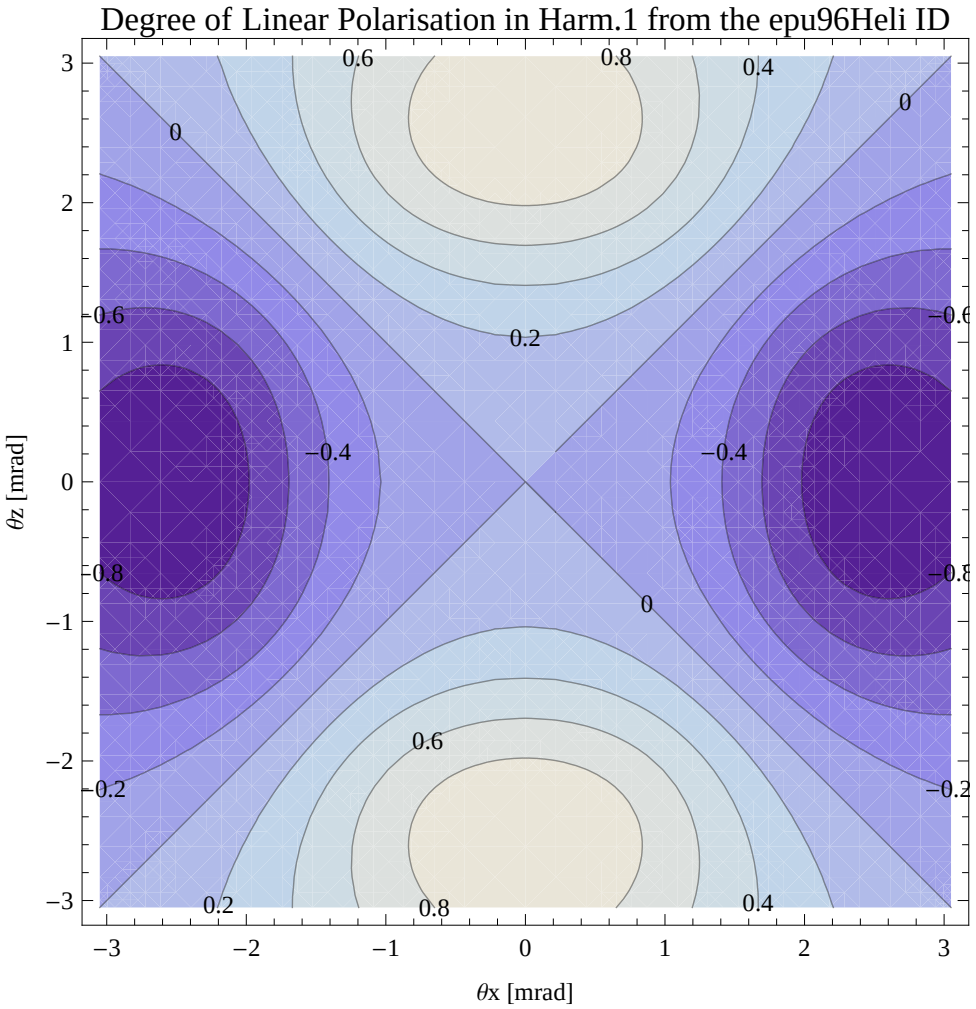

Figure 33: Map of linear polarisation in the fundamental harmonic of the synchotron radiation emitted by the epu96Heli

A map of the degree of 45 degree polarisation of the fundamental harmonic of the synchotron radiation emitted by the epu96Heli over the angle of observation is shown in Figure 34.

A map of the degree of circular polarisation of the fundamental harmonic of the synchotron radiation emitted by the epu96Heli over the angle of observation is shown in Figure 35.

The on axis brilliance at peak energy and the angular spectral flux from the epu96Heli have been calculated with the given beam parameters, which are 0.3 A of stored current, $\beta_H = 5.627$ m, $\varepsilon_H = 5.985$ nmrad, $\beta_V = 2.837$ m, $\varepsilon_V = 59.85$ pmrad, and an energy spread of 0.001.

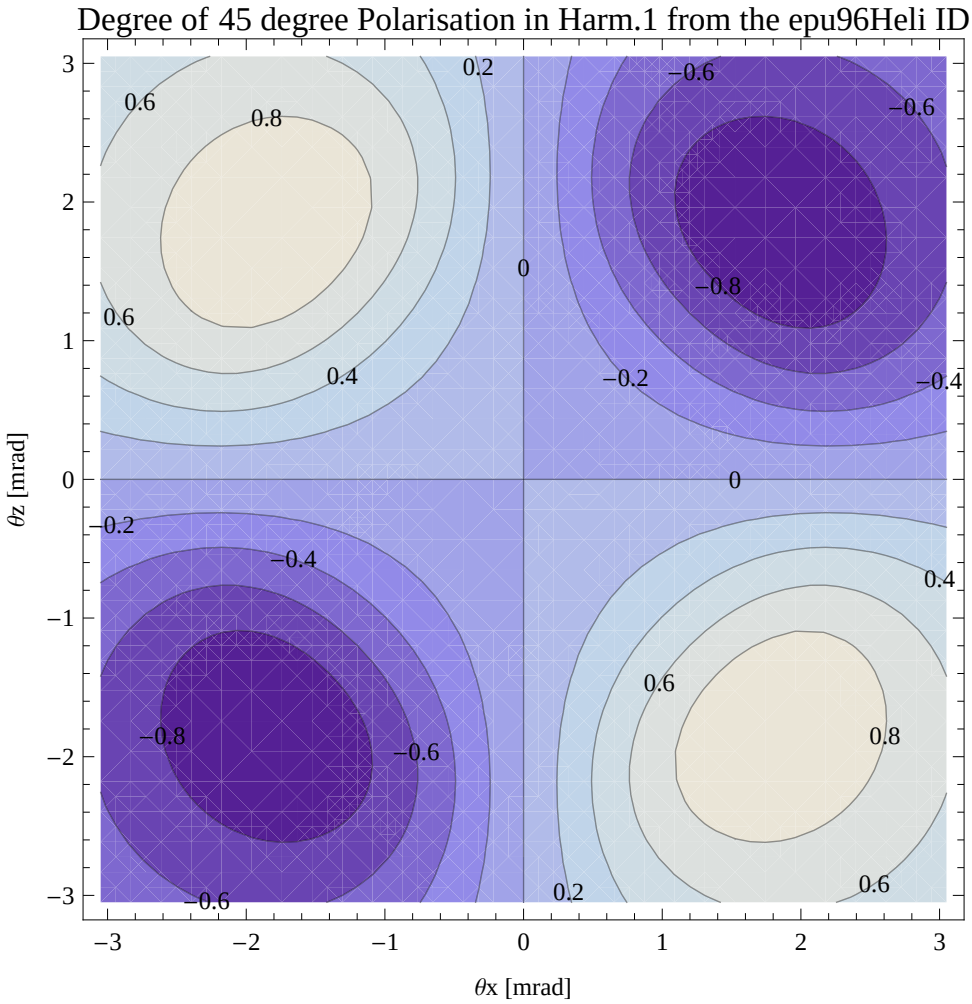

Figure 34: Map of 45 degree polarisation in the fundamental harmonic of the synchotron radiation emitted by the epu96Heli

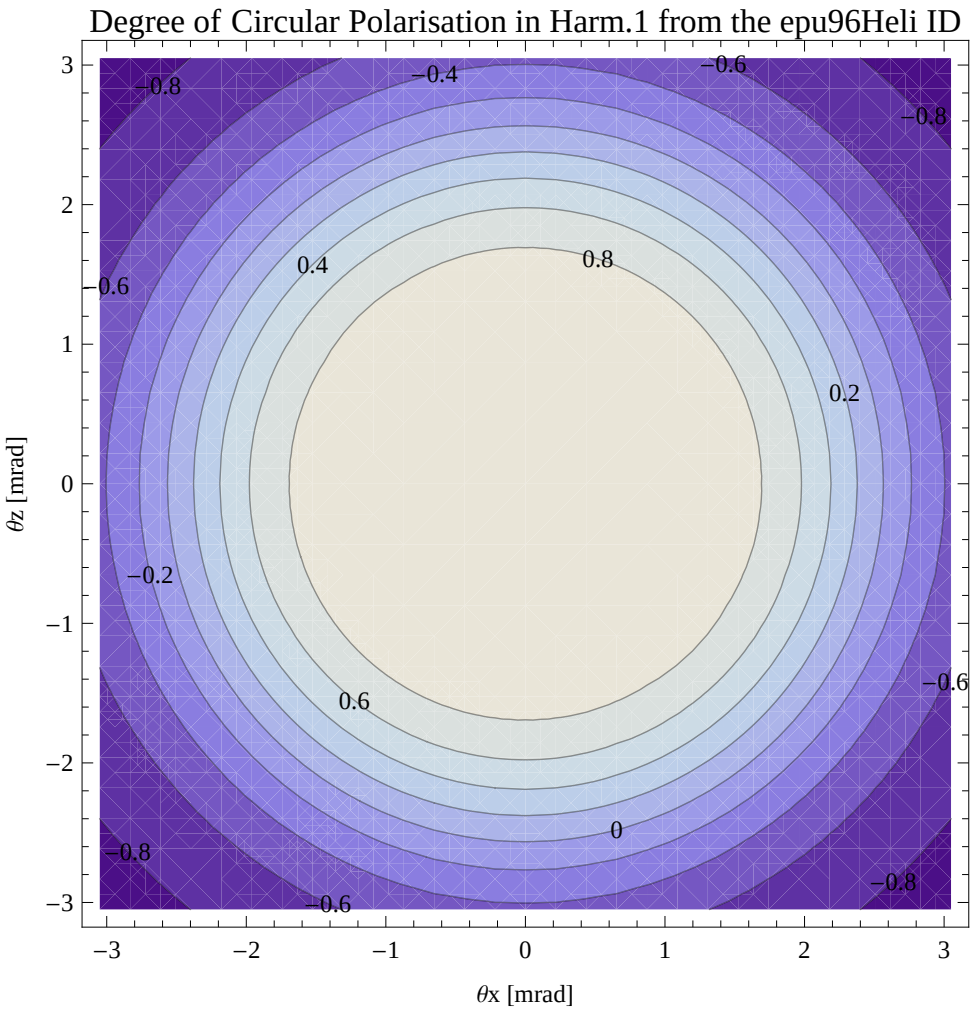

Figure 35: Map of circular polarisation in the fundamental harmonic of the synchotron radiation emitted by the epu96Heli

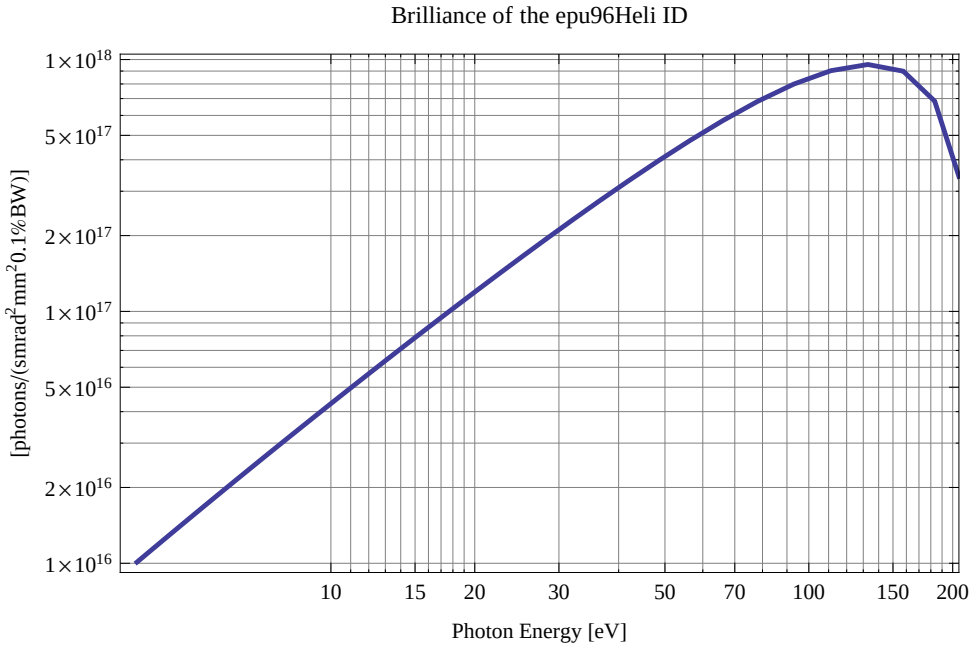

Figure 36: The brilliance at peak energy of the synchotron radiation emitted by the epu96Heli

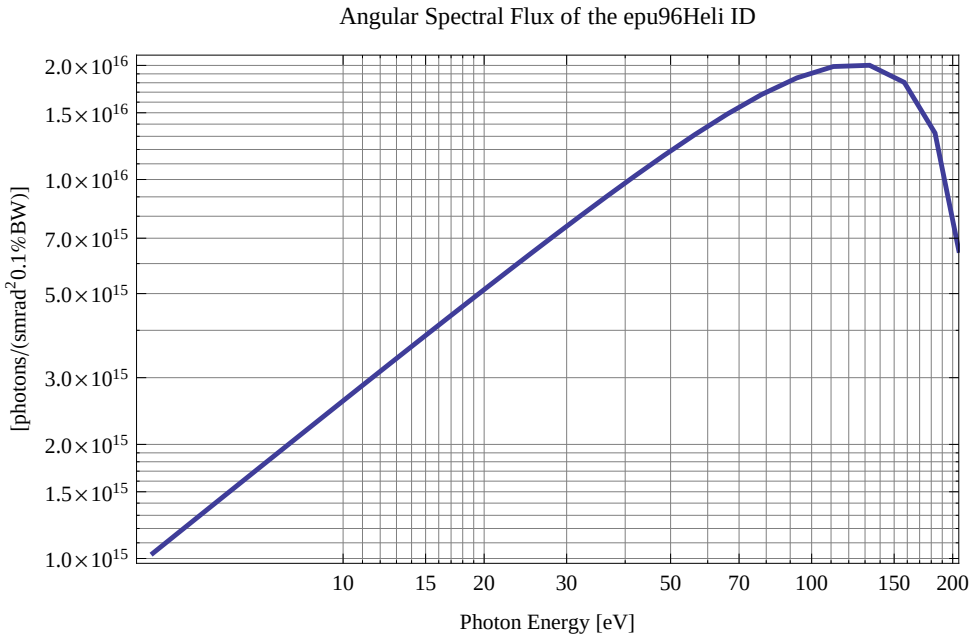

Figure 37: The angular spectral flux of the synchotron radiation emitted by the epu96Heli

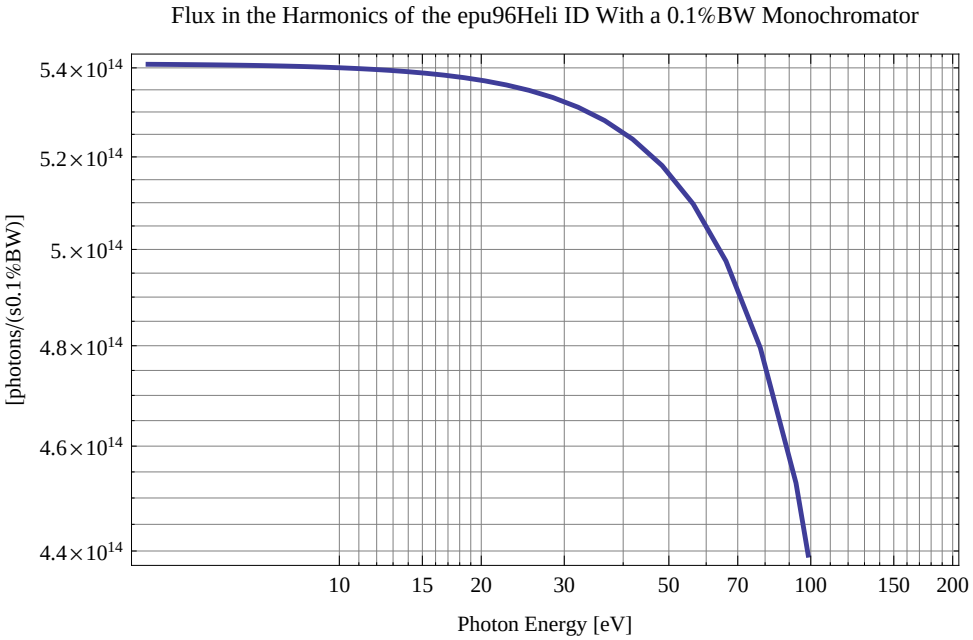

Figure 38: The flux of photons in the harmonics of the emitted synchrotron radiation from the epu96Heli using a 0.1%BW monochromator

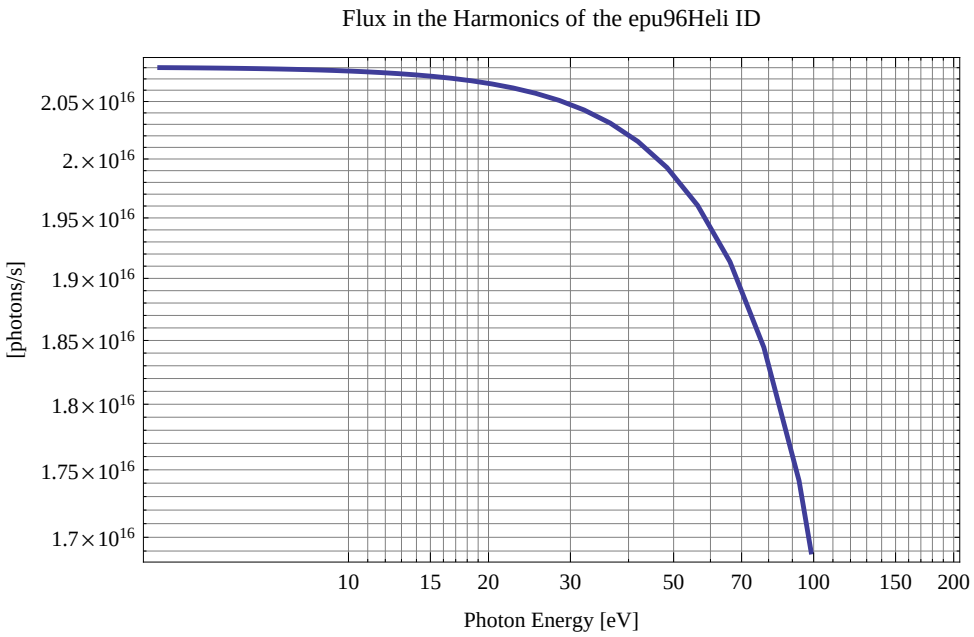

Figure 39: The flux of photons in the harmonics of the emitted synchrotron radiation from the epu96Heli

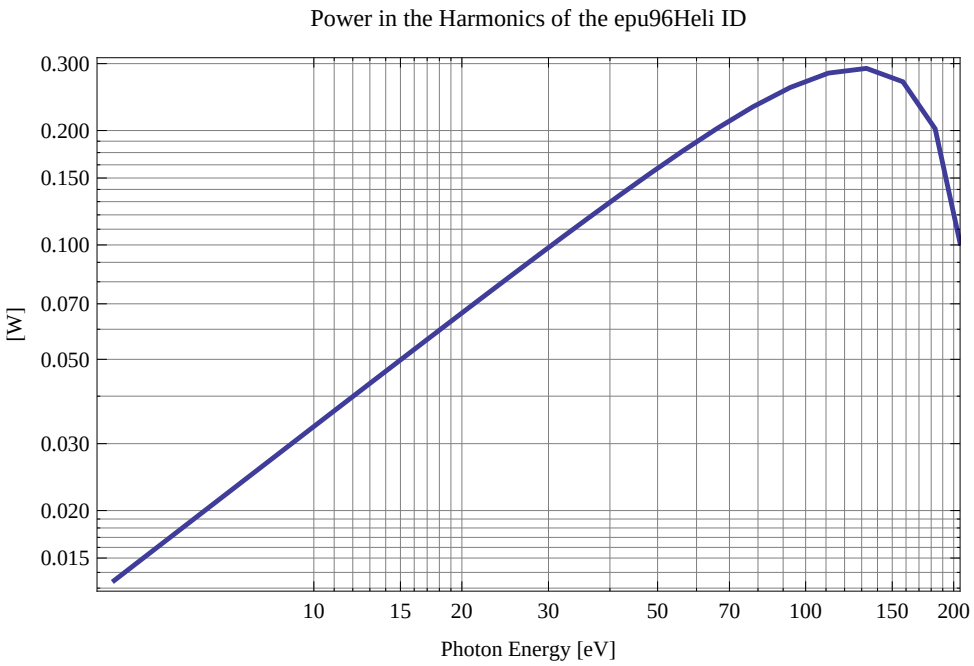

Figure 40: The power in the harmonics of the emitted synchrotron radiation from the epu96Heli

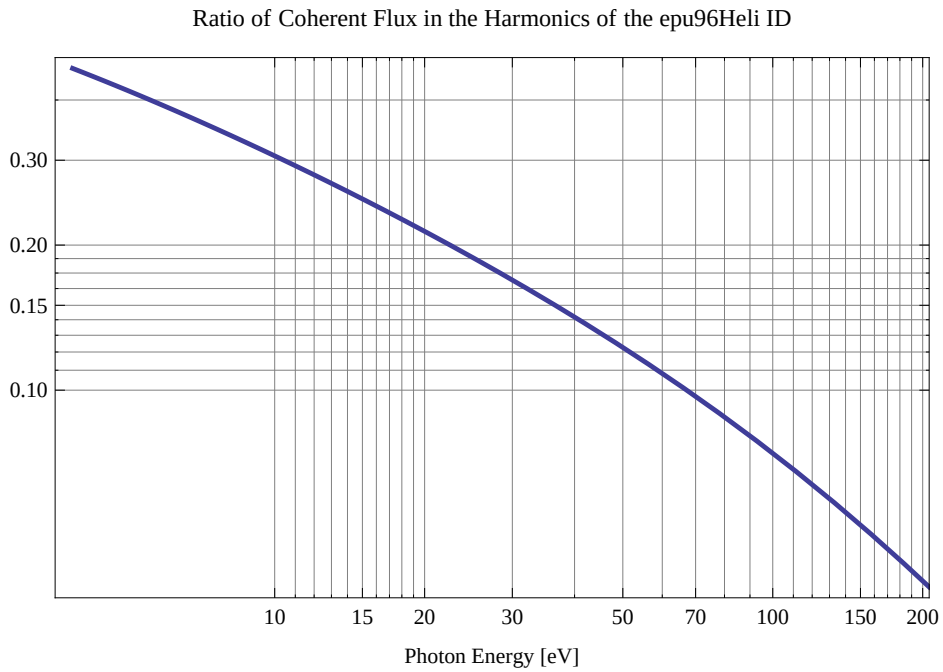

Figure 41: The ratio of coherent flux in the harmonics of the emitted synchrotron radiation from the epu96Heli

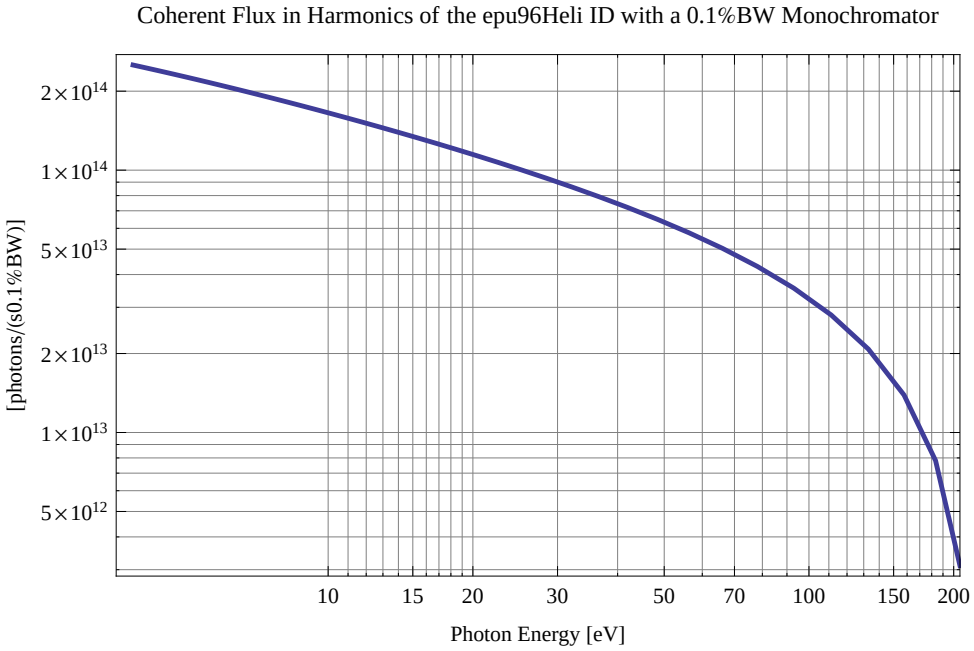

Figure 42: The coherent flux in the harmonics of the epu96Heli using a 0.1%BW Monochromator

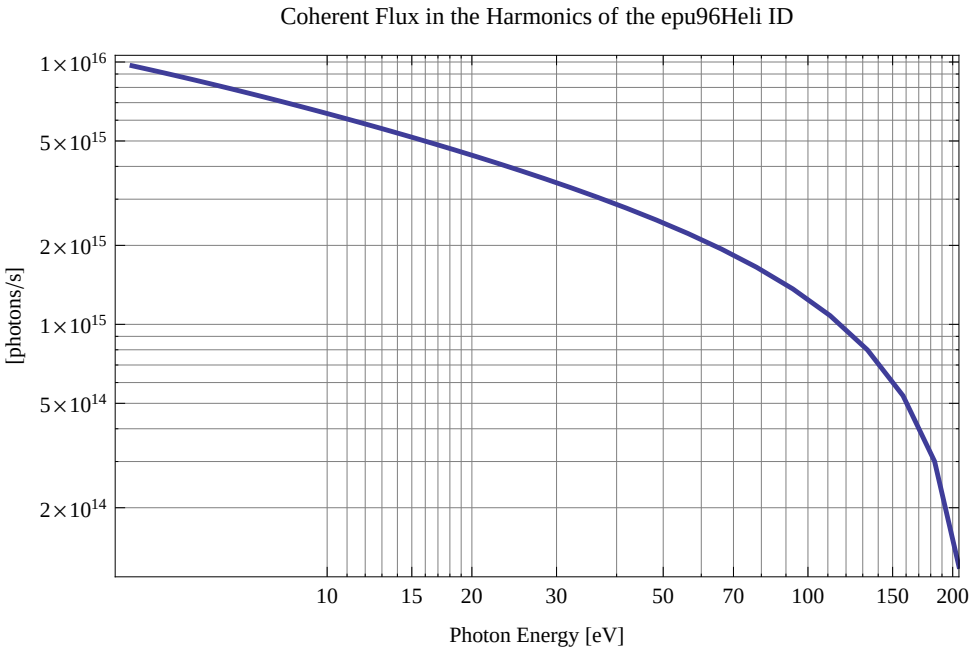

Figure 43: The coherent flux in the harmonics of the epu96Heli

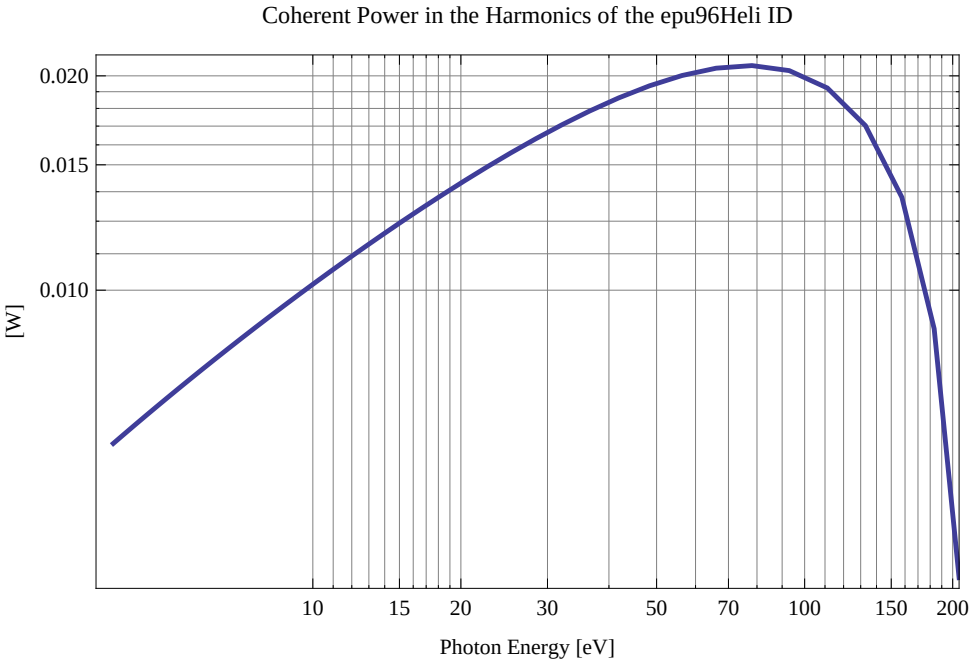

Figure 44: The power of coherent synchrotron radiation in the harmonics of the epu96Heli

The brilliance at peak energy and the angular spectral flux density from the epu96Heli for different harmonics at maximum K-value (10.550) are given in Table 10 and for minimum K-value (0.400) these values are given in Table 11.

Table 10: The brilliance at peak energy and the angular spectral flux density from the epu96Heli for different harmonics at maximum K-value (10.550)

Harmonic	Photon Energy [eV]	Brilliance [Ph./(smrad^{2}mrad^{2}0.1%BW)]	Angular Spectral Flux [Ph./(smrad^{2}0.1%BW)]
1	3.92874	1.01×10^{16}	1.03×10^{15}

Table 11: The brilliance at peak energy and the angular spectral flux density from the epu96Heli for different harmonics at minimum K-value (0.4)

Harmonic	Photon Energy [eV]	Brilliance [Ph./(smrad^{2}mrad^{2}0.1%BW)]	Angular Spectral Flux [Ph./(smrad^{2}0.1%BW)]
1	206.085	3.43×10^{17}	6.5×10^{15}

2.9 Influence from the epu96Heli on the optics of the stored beam

Figure 45 shows the focusing potential from the epu96Heli over the beam stay clear aperture of the ring aparture.

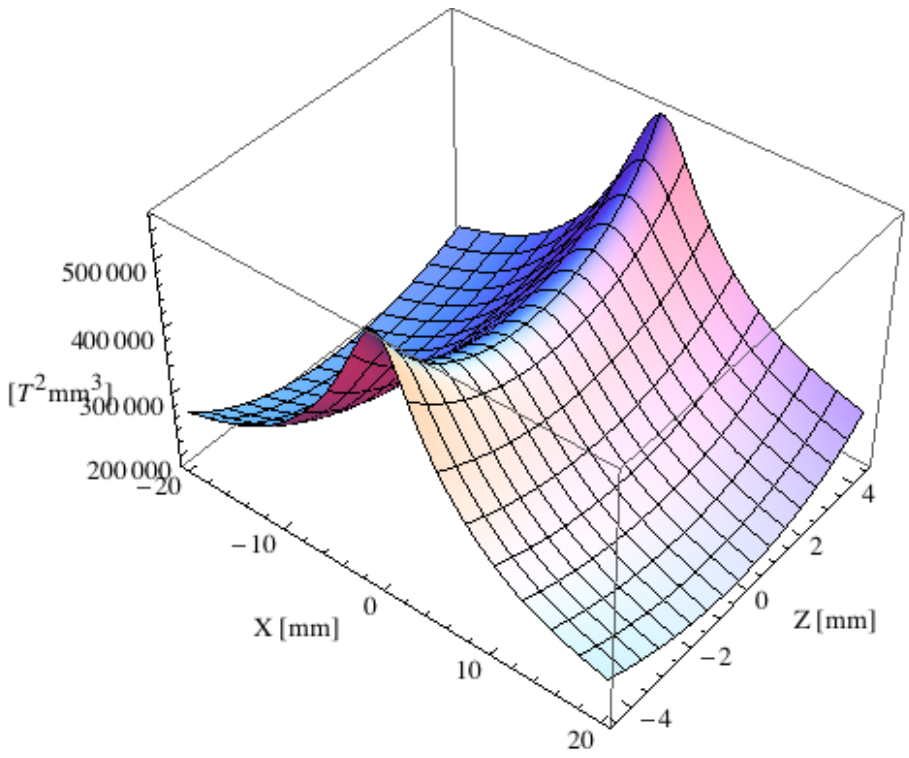

Figure 45: Focusing potential from the epu96Heli over the beam stay clear aparture.

Figure 46 shows the kick map in the beam energy independant unit T^2m^2 of the kicks induced by the epu96Heli over the beam stay clear aparture.

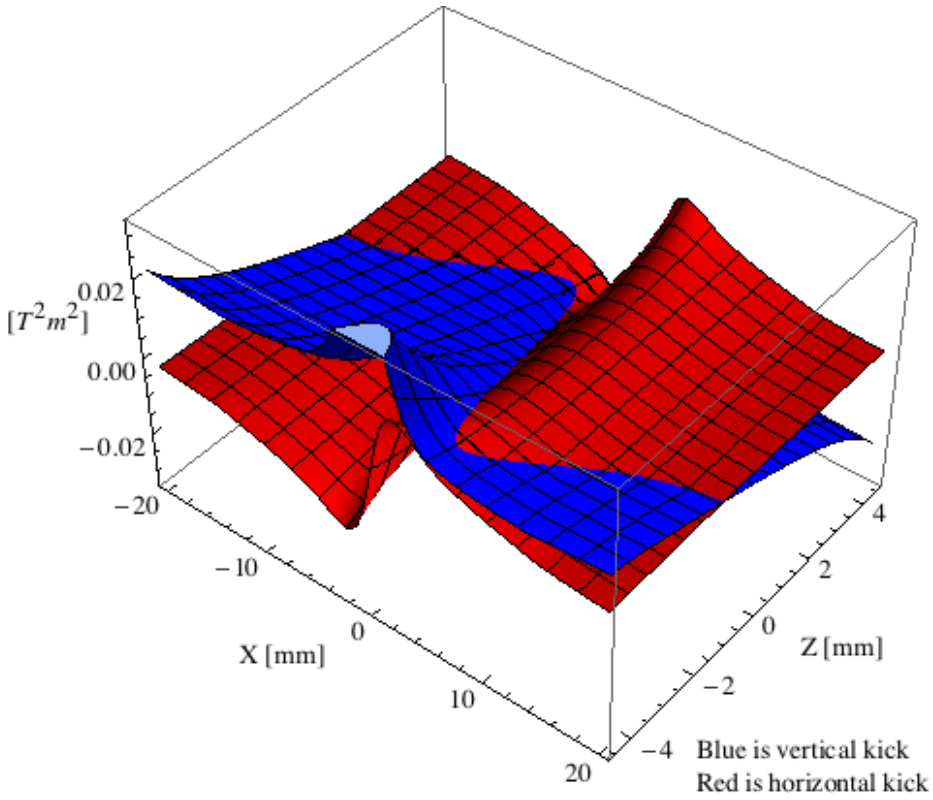

Figure 46: Kick map in the beam energy independant unit T^2m^2 of the kicks induced by the epu96Heli over the beam stay clear aparture.

Figure 47 shows the induced angular kick on the stored beam from the epu96Heli as a function of the vertical distance to the undulator axis.

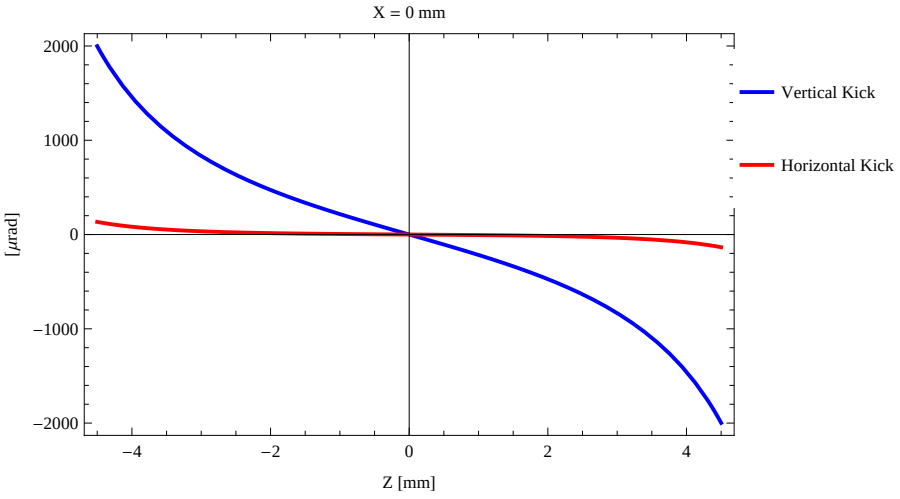

Figure 47: Induced angular kick on the stored beam from the epu96Heli as a function of the vertical distance to the undulator axis.

Figure 48 shows the induced angular kick on the stored beam from the epu96Heli as a function of the horizontal distance to the undulator axis.

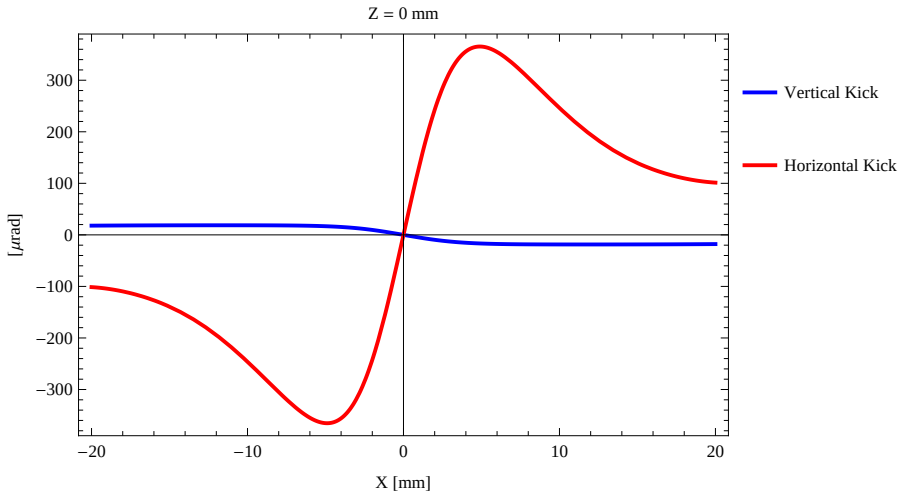

Figure 48: Induced angular kick on the stored beam from the epu96Heli as a function of the horizontal distance to the undulator axis.

Figure 49 shows tune shift induced by the epu96Heli over the beam stay clear aparture. Note that the tune shift depends on the beam size at the.

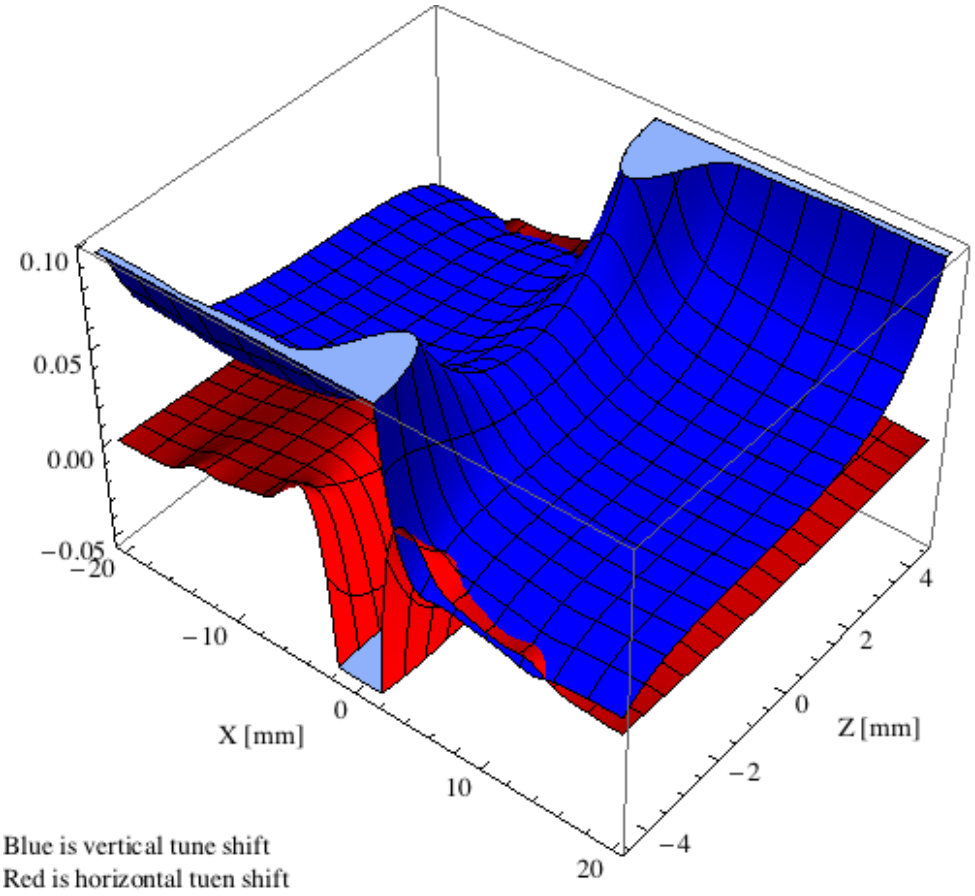

Figure 49: Tune shift induced by the epu96Heli over the beam stay clear aparture.

Figure 50 shows the induced tune shift from the epu96Heli as a function of the vertical distance to the undulator axis.

Figure 51 shows the induced tune shift from the epu96Heli as a function of the horizontal distance

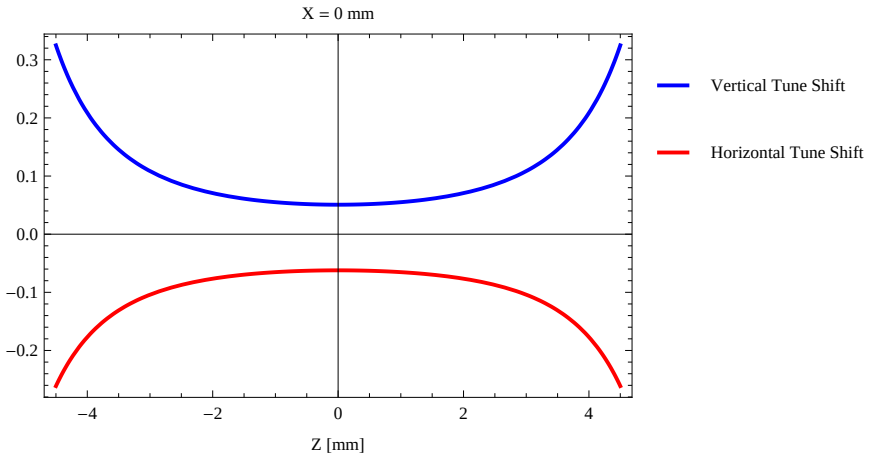

Figure 50: Induced tune shift from the epu96Heli as a function of the vertical distance to the undulator axis.

to the undulator axis.

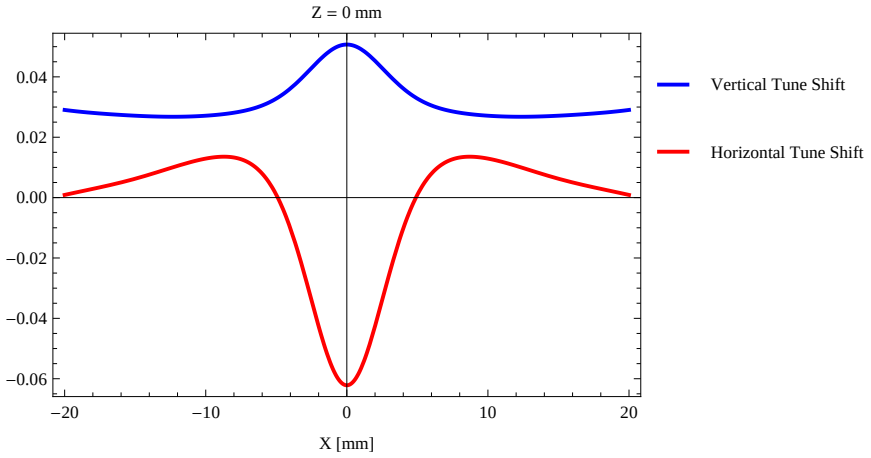

Figure 51: Induced tune shift from the epu96Heli on the stored beam from the as a function of the horizontal distance to the undulator axis.

2.10 Magnet model of the elliptically polarizing undulator epu96Incl

The Radia [2] magnet model of the epu96Incl is shown in Figure 52. The length of the magnet model is 787.992 mm. The magnetic material in the model is NdFeb with a remanence of 1.33 T. Blocks with vertical magnetisation are blue and blocks with horizontal magnetisation are yellow. The block size is 35.x35.x24. mm^3 and there is a 5. mm cut-out in two of the corners of the blocks. The total length of the epu96Incl is 2515.99 mm.

2.11 Analysis of the magnetic field of the epu96Incl

The effective magnetic fields on axis and the fundamental photon energy of the epu96Incl are shown in Table 12. The higher harmonic contents in the magnetic field of an elliptically polarizing undulator made of permanent magnets is usually small and the effective field has approximately the same strength as the peak field.

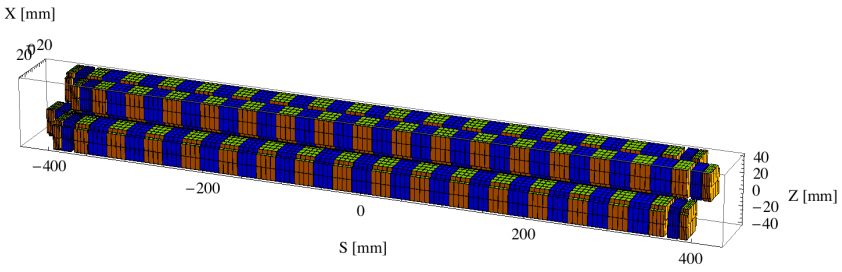

Figure 52: Magnetic model of the epu96Incl. The has been modelled with Radia [2]

Table 12: Effective Fields on axis and Fundamental Photon Energy of the epu96Incl

Undulator Period	96	mm
Undulator Gap	13	mm
Undulator Mode	Inclined	
Undulator Phase	25.266	mm
Vertical Peak Field	0.577	T
effective Vertical Field	0.590	T
Kx (from vert. field)	5.290	
Horizontal Peak Field:	−0.578	T
effective Horizontal Field	0.592	T
Kz (from hor. field)	5.308	
Photon Energy, Harm.1	0.008	keV
Emitted Power	0.751	kW
Total Length	2516.0	mm

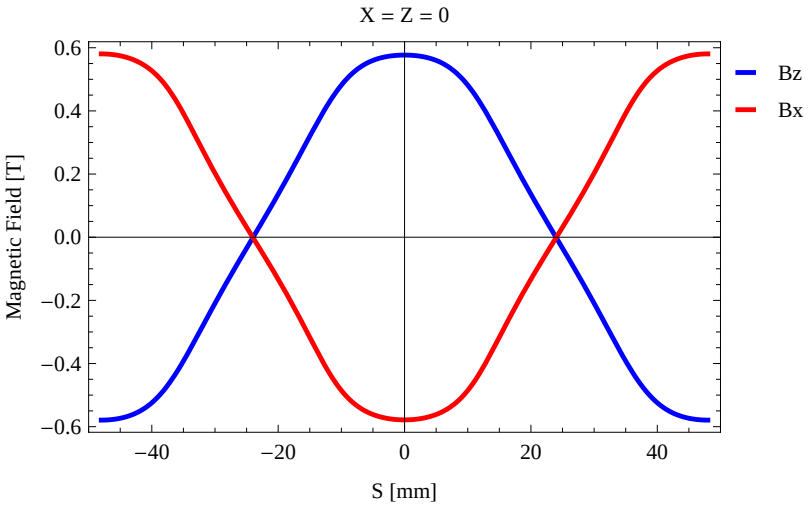

Figure 53: Vertical magnetic field in a central pole of the epu96Incl along the axis, X = Z = 0

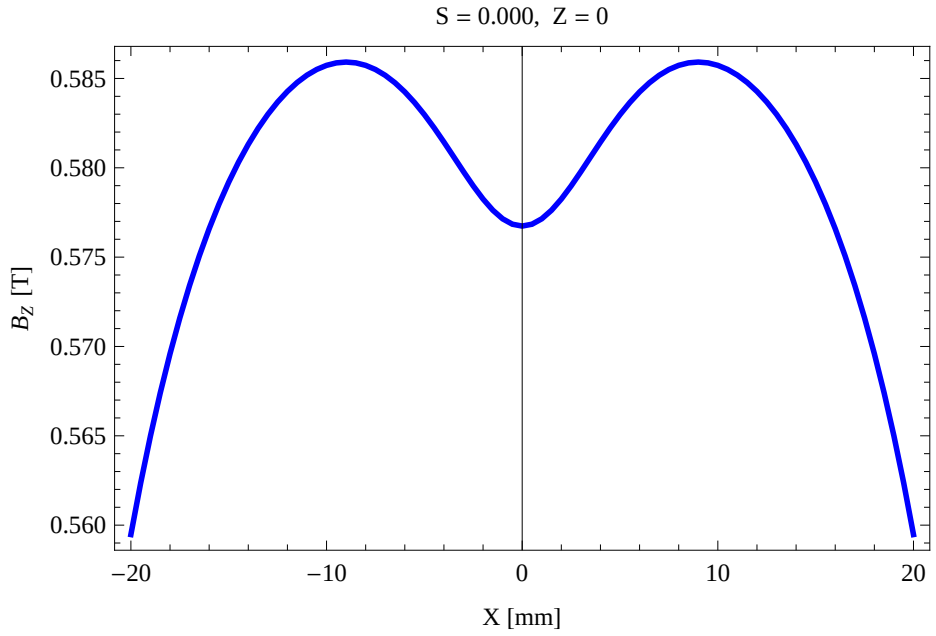

Figure 54: Vertical magnetic field in a central pole of the epu96Incl along the horizontally transverse direction to the axis, S = 0.000, Z = 0

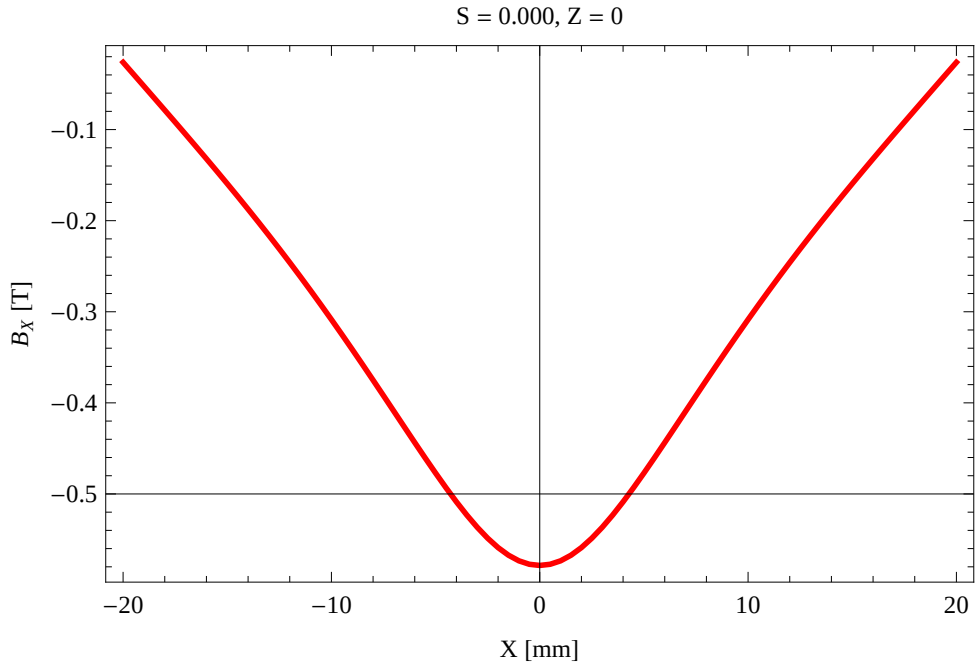

Figure 55: Horizontal magnetic field in a central pole of the epu96Incl along the horizontally transverse direction to the axis, S = 0.000, Z = 0

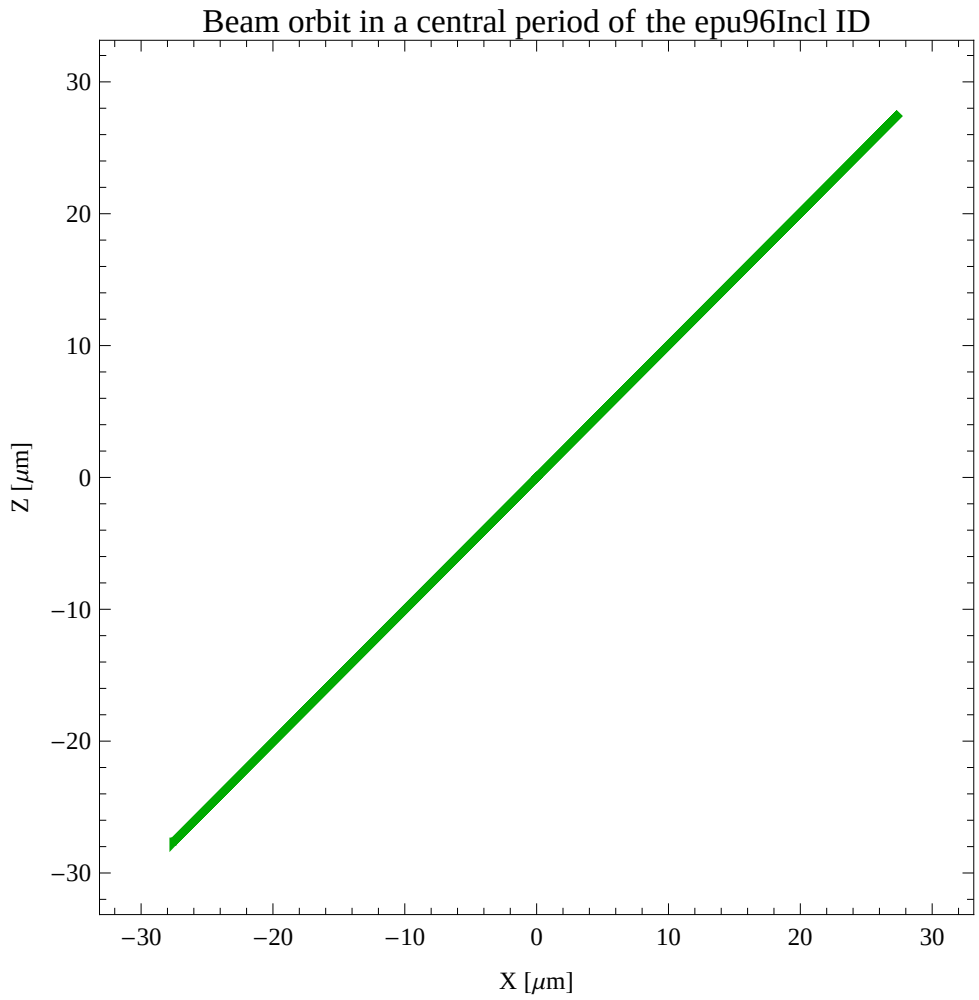

Figure 56: The beam orbit of the electron beam through a central period of the epu96Incl

2.12 Synchrotron radiation from the epu96Incl

The power map of the emitted synchrotron radiation by the epu96Incl, assuming a 0.3 A filament beam with an energy of 1.5 GeV and undulator properties of the synchrotron radiation, is shown in Figure 57. The on-axis power density is 0.343688 kW/mrad^2

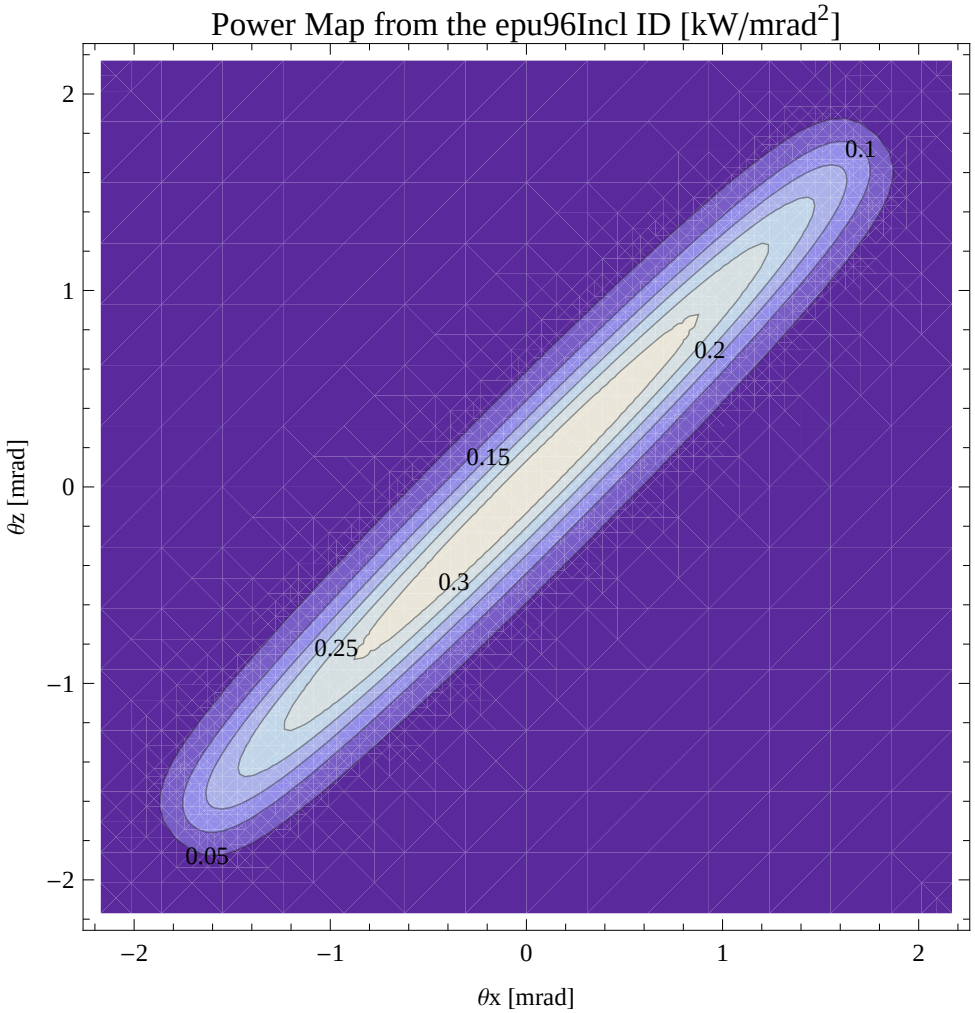

Figure 57: Map of the power distribution of the emitted synchrotron radiation by the epu96Incl

A map of the degree of linear polarisation of the fundamental harmonic of the synchotron radiation emitted by the epu96Incl over the angle of observation is shown in Figure 58.

A map of the degree of 45 degree polarisation of the fundamental harmonic of the synchotron radiation emitted by the epu96Incl over the angle of observation is shown in Figure 59.

A map of the degree of circular polarisation of the fundamental harmonic of the synchotron radiation emitted by the epu96Incl over the angle of observation is shown in Figure 60.

The on axis brilliance at peak energy and the angular spectral flux from the epu96Incl have been calculated with the given beam parameters, which are 0.3 A of stored current, $\beta_H = 5.627$ m, $\varepsilon_H = 5.985$ nmrad, $\beta_V = 2.837$ m, $\varepsilon_V = 59.85$ pmrad, and an energy spread of 0.001.

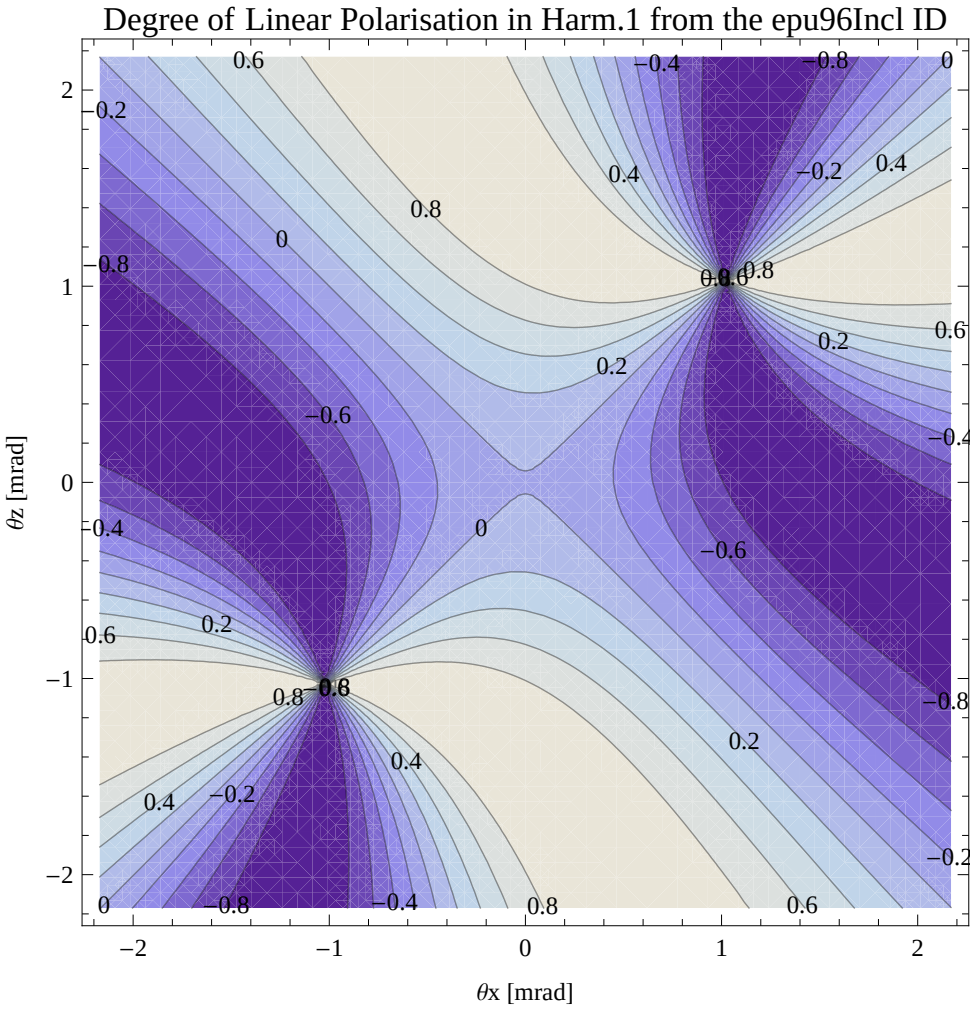

Figure 58: Map of linear polarisation in the fundamental harmonic of the synchotron radiation emitted by the epu96Incl

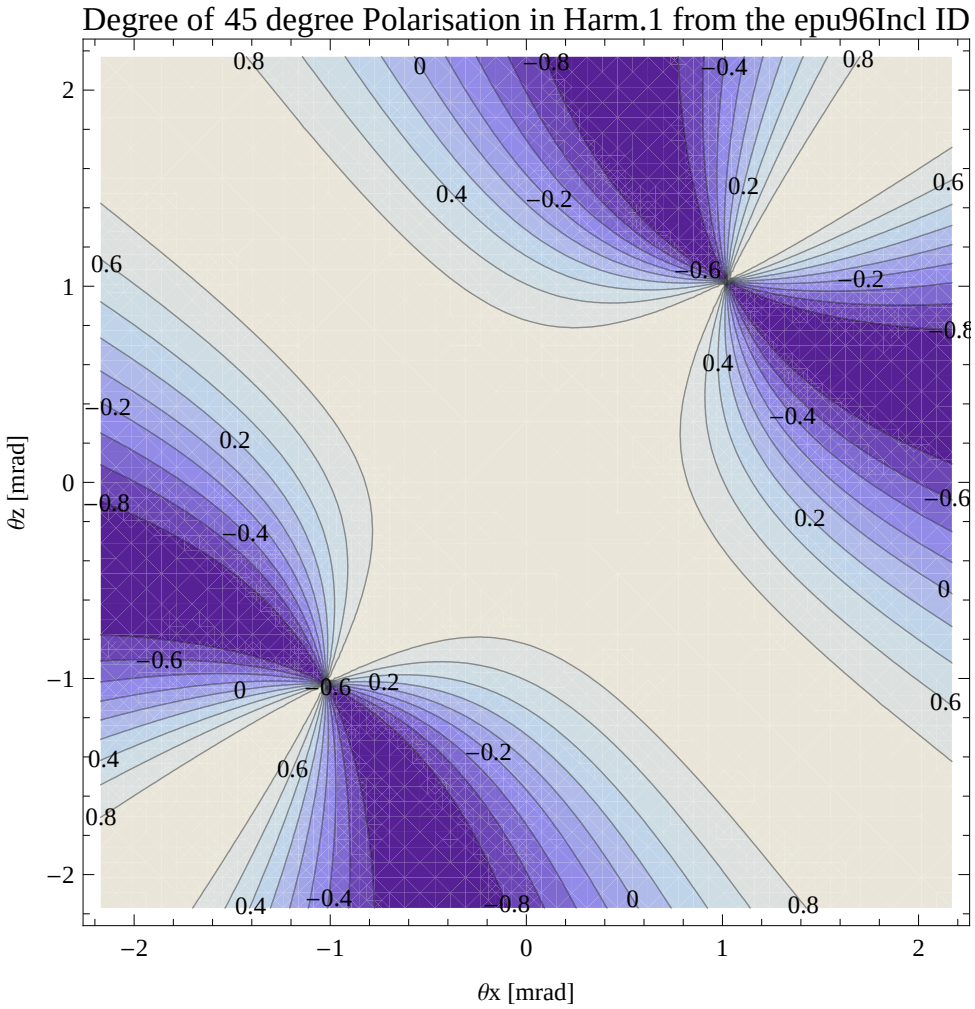

Figure 59: Map of 45 degree polarisation in the fundamental harmonic of the synchotron radiation emitted by the epu96Incl

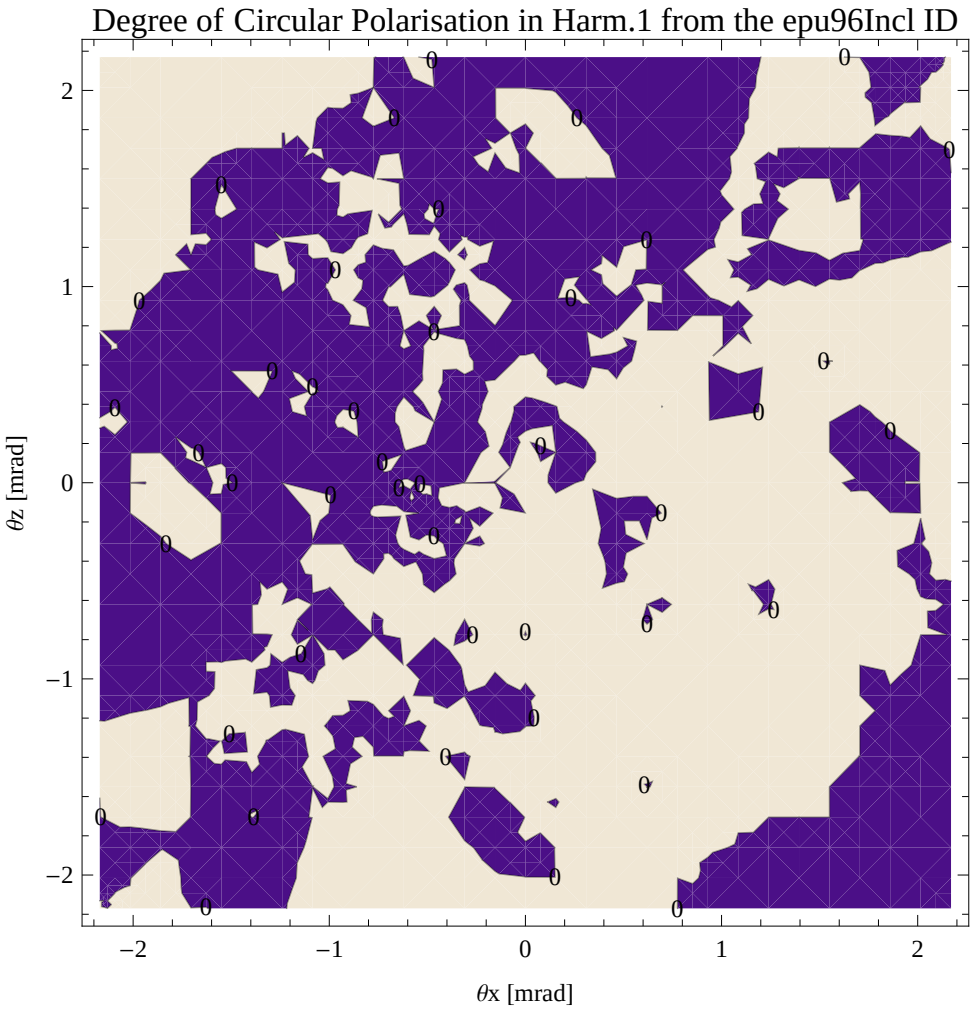

Figure 60: Map of circular polarisation in the fundamental harmonic of the synchotron radiation emitted by the epu96Incl

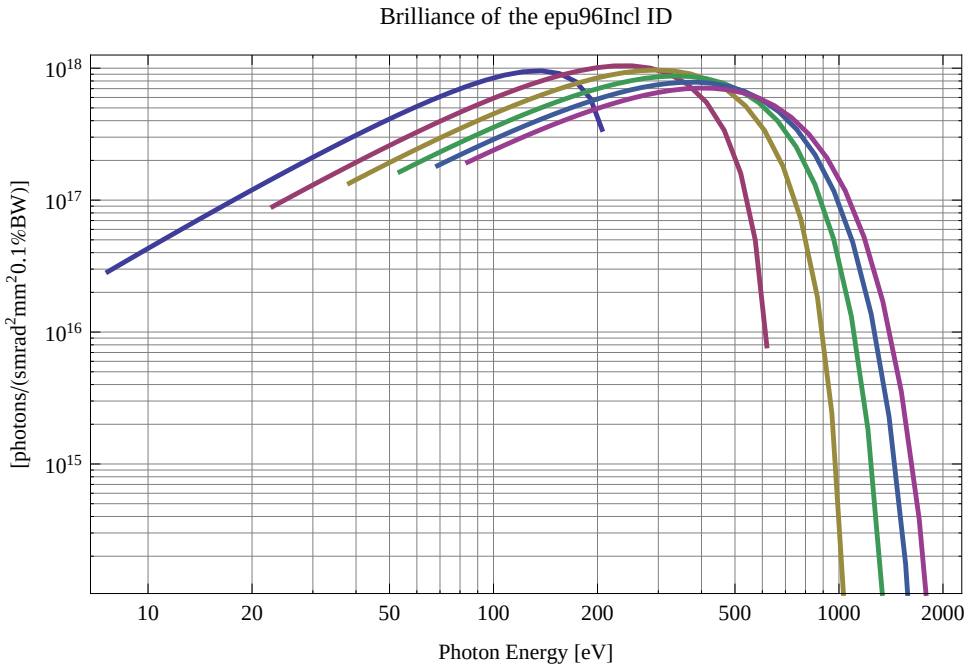

Figure 61: The brilliance at peak energy of the synchotron radiation emitted by the epu96Incl

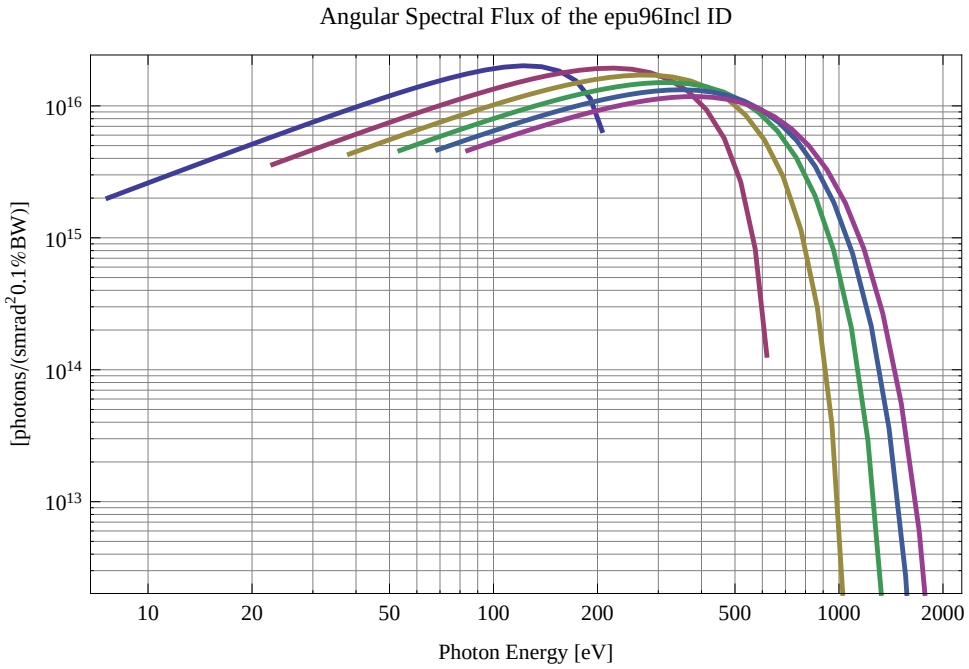

Figure 62: The angular spectral flux of the synchotron radiation emitted by the epu96Incl

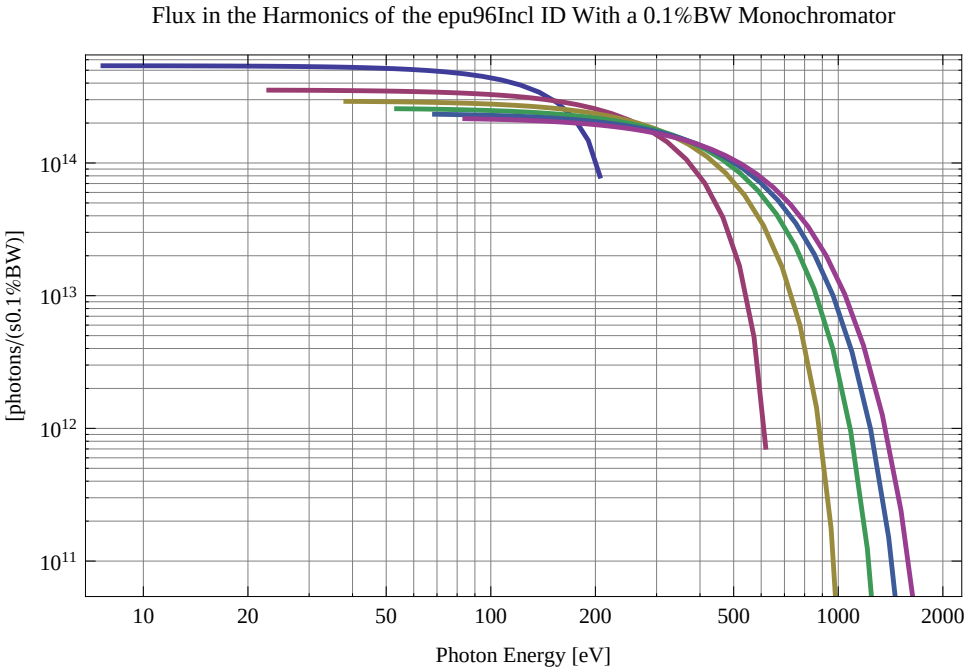

Figure 63: The flux of photons in the harmonics of the emitted synchrotron radiation from the epu96Incl using a 0.1%BW monochromator

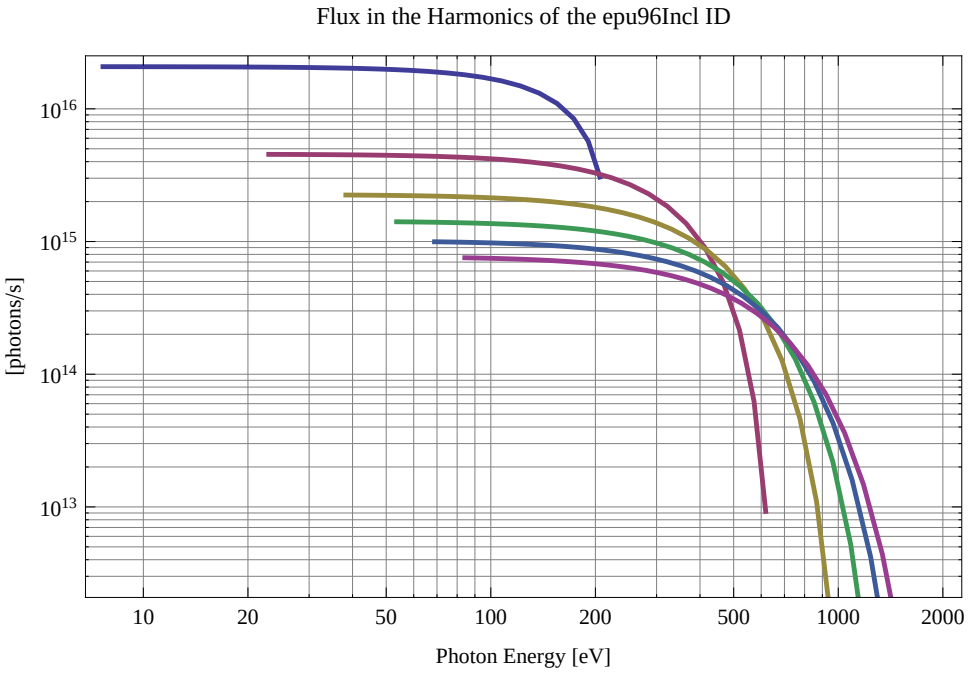

Figure 64: The flux of photons in the harmonics of the emitted synchrotron radiation from the epu96Incl

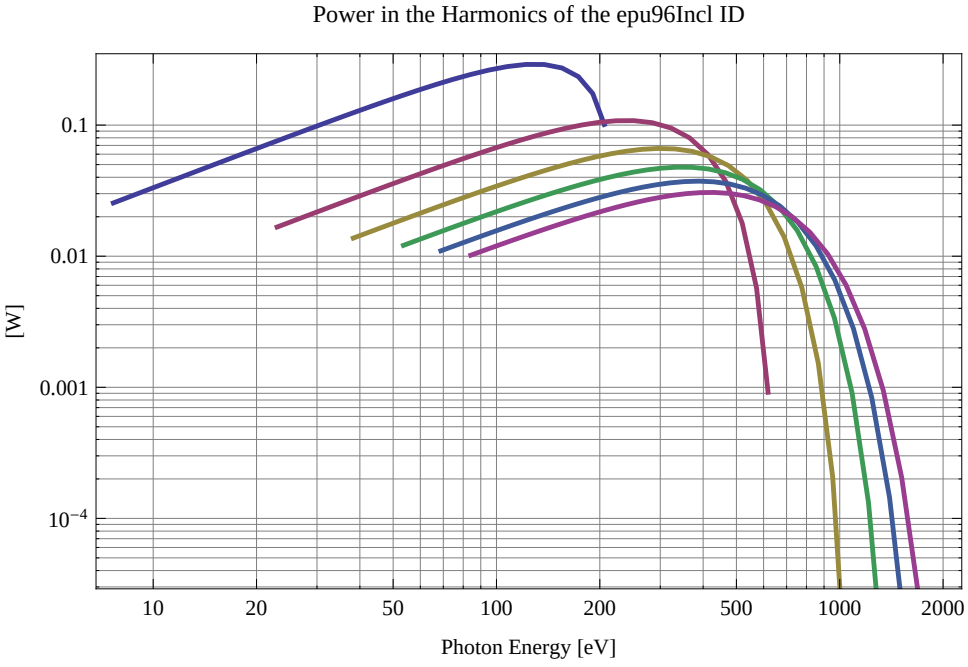

Figure 65: The power in the harmonics of the emitted synchrotron radiation from the epu96Incl

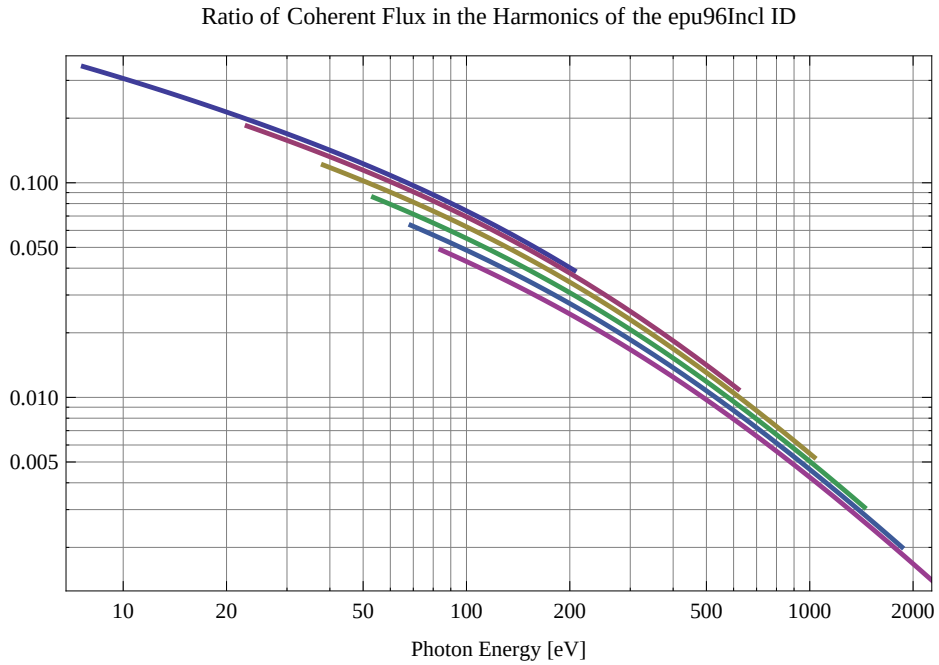

Figure 66: The ratio of coherent flux in the harmonics of the emitted synchrotron radiation from the epu96Incl

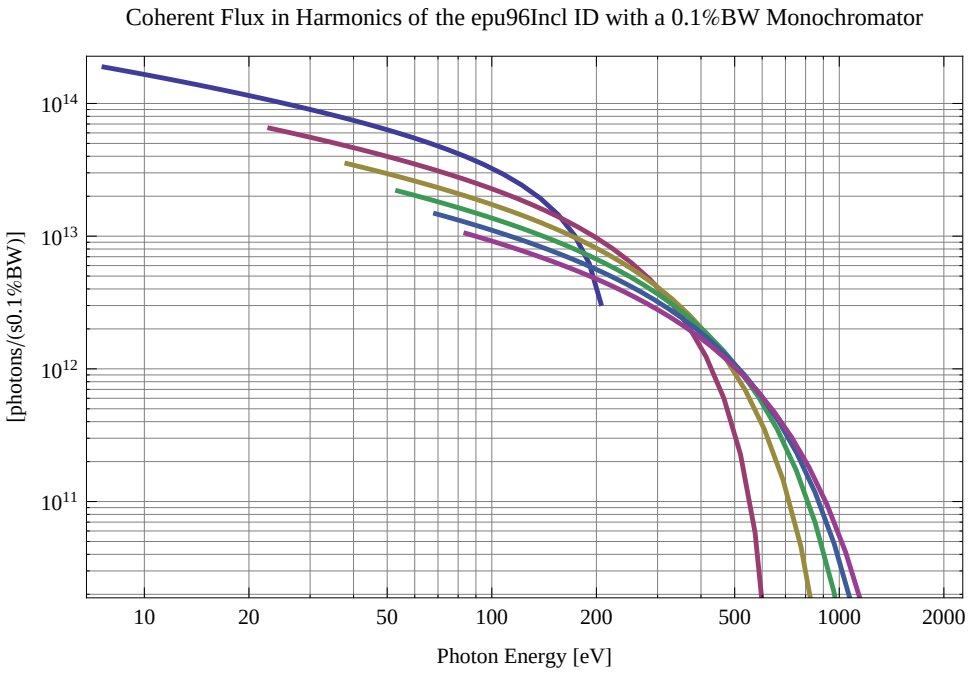

Figure 67: The coherent flux in the harmonics of the epu96Incl using a 0.1%BW Monochromator

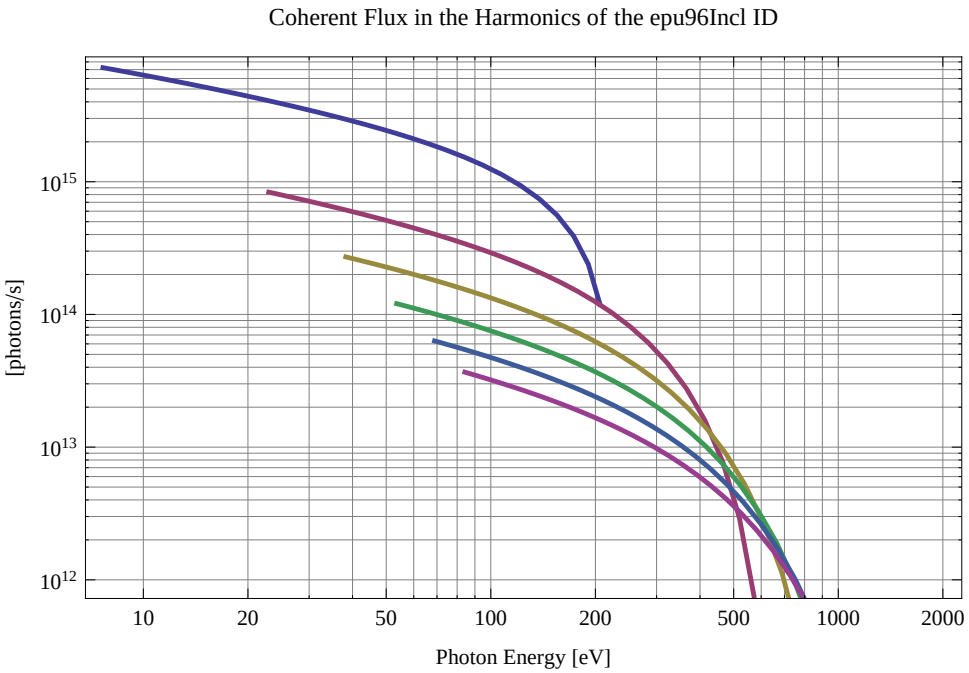

Figure 68: The coherent flux in the harmonics of the epu96Incl

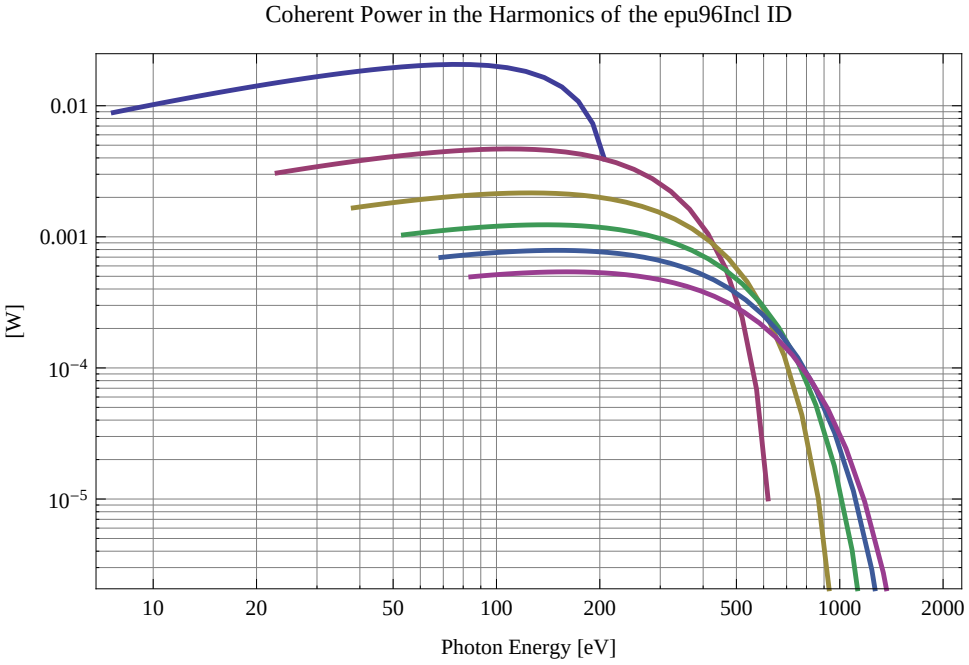

Figure 69: The power of coherent synchrotron radiation in the harmonics of the epu96Incl

The brilliance at peak energy and the angular spectral flux density from the epu96Incl for different harmonics at maximum K-value (7.494) are given in Table 13 and for minimum K-value (0.400) these values are given in Table 14.

Table 13: The brilliance at peak energy and the angular spectral flux density from the epu96Incl for different harmonics at maximum K-value (7.494)

Harmonic	Photon Energy [eV]	Brilliance [Ph./(smrad^{2}mrad^{2}0.1%BW)]	Angular Spectral Flux [Ph./(smrad^{2}0.1%BW)]
1	7.65352	2.87×10^{16}	$2. \times 10^{15}$
3	22.9606	8.93×10^{16}	3.59×10^{15}
5	38.2676	1.34×10^{17}	4.31×10^{15}
7	53.5746	1.64×10^{17}	4.59×10^{15}
9	68.8817	1.82×10^{17}	4.64×10^{15}
11	84.1887	1.94×10^{17}	4.59×10^{15}

Table 14: The brilliance at peak energy and the angular spectral flux density from the epu96Incl for different harmonics at minimum K-value (0.4)

Harmonic	Photon Energy [eV]	Brilliance [Ph./(smrad^{2}mrad^{2}0.1%BW)]	Angular Spectral Flux [Ph./(smrad^{2}0.1%BW)]
1	206.085	3.43×10^{17}	6.5×10^{15}
3	618.255	7.85×10^{15}	1.29×10^{14}
5	1030.43	1.03×10^{14}	1.64×10^{12}
7	1442.6	1.18×10^{12}	1.86×10^{10}
9	1854.77	1.28×10^{10}	2.01×10^{8}
11	2266.94	1.34×10^{8}	2.11×10^{6}

2.13 Influence from the epu96Incl on the optics of the stored beam

Figure 70 shows the focusing potential from the epu96Incl over the beam stay clear aperture of the ring aparture.

Figure 71 shows the kick map in the beam energy independant unit T^2m^2 of the kicks induced by the epu96Incl over the beam stay clear aparture.

Figure 72 shows the induced angular kick on the stored beam from the epu96Incl as a function of the vertical distance to the undulator axis.

Figure 73 shows the induced angular kick on the stored beam from the epu96Incl as a function of the horizontal distance to the undulator axis.

Figure 74 shows tune shift induced by the epu96Incl over the beam stay clear aparture. Note that the tune shift depends on the beam size at the.

Figure 75 shows the induced tune shift from the epu96Incl as a function of the vertical distance to the undulator axis.

Figure 76 shows the induced tune shift from the epu96Incl as a function of the horizontal distance to the undulator axis.

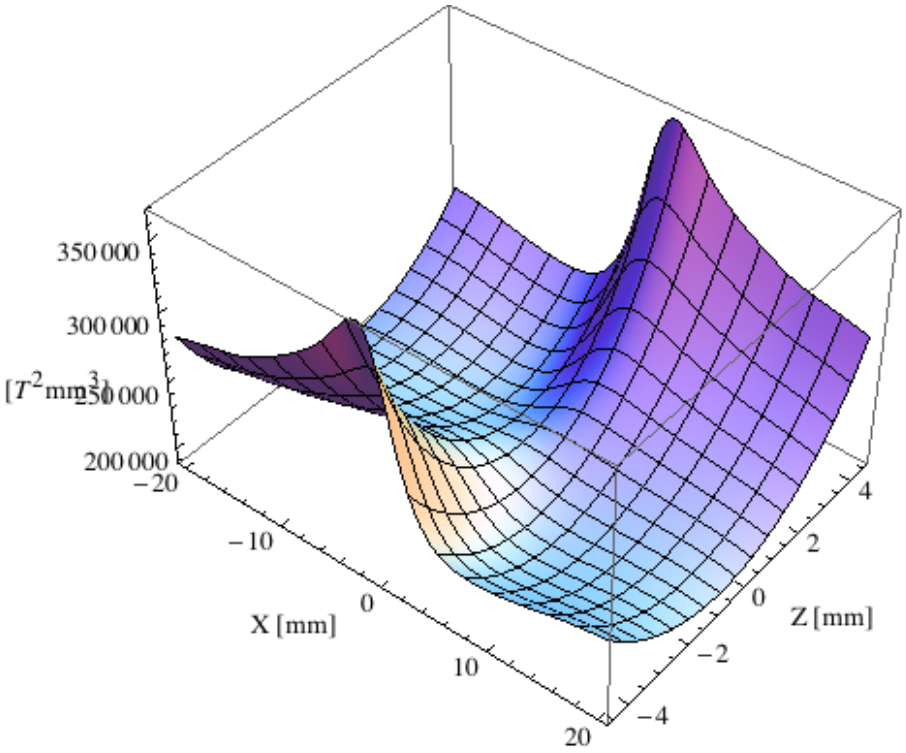

Figure 70: Focusing potential from the epu96Incl over the beam stay clear aparture.

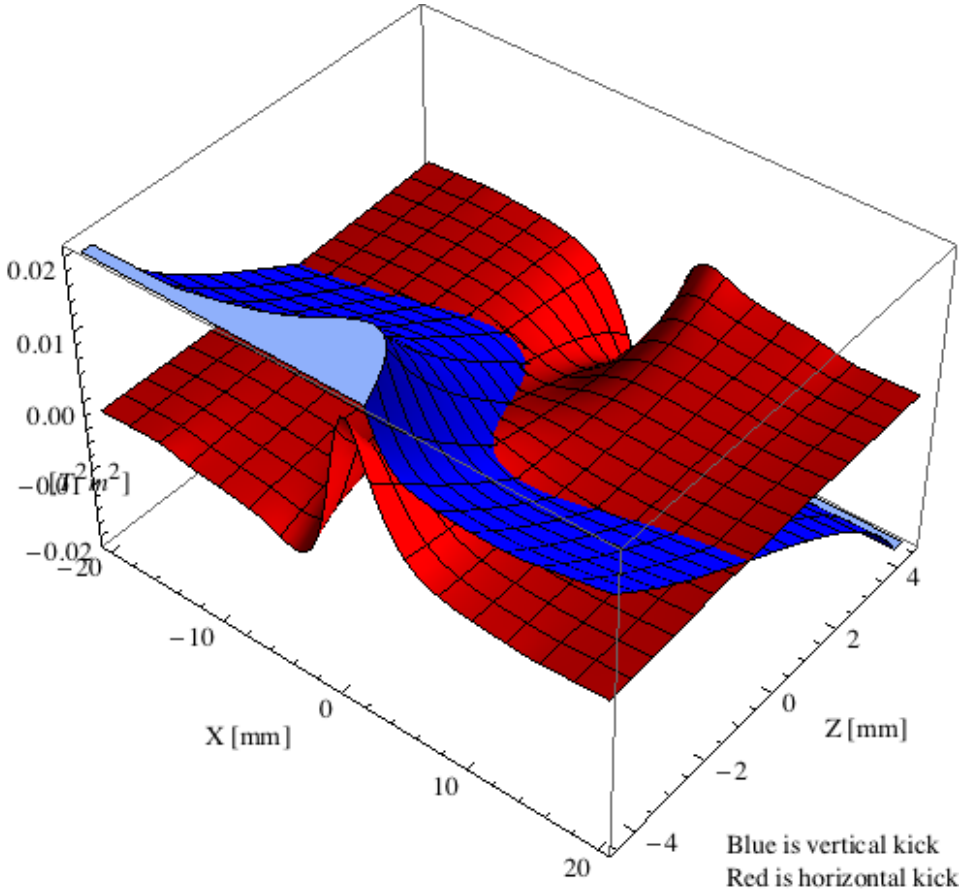

Figure 71: Kick map in the beam energy independant unit T^2m^2 of the kicks induced by the epu96Incl over the beam stay clear aparture.

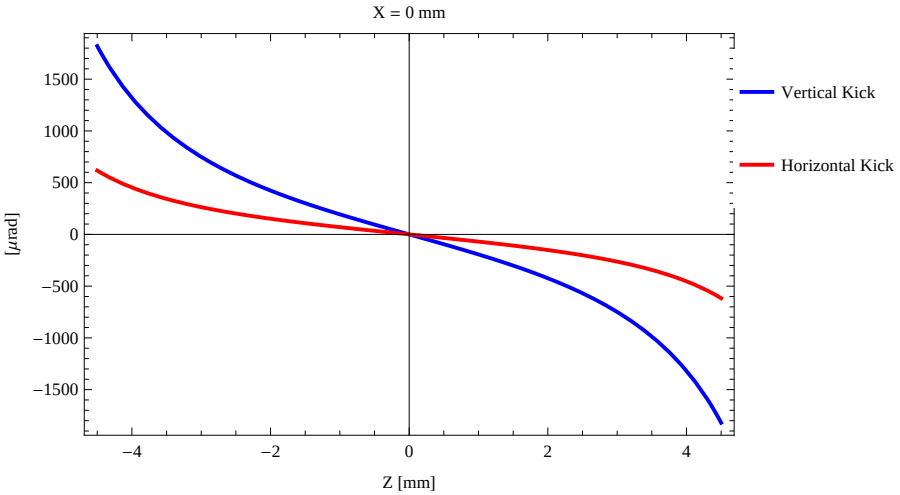

Figure 72: Induced angular kick on the stored beam from the epu96Incl as a function of the vertical distance to the undulator axis.

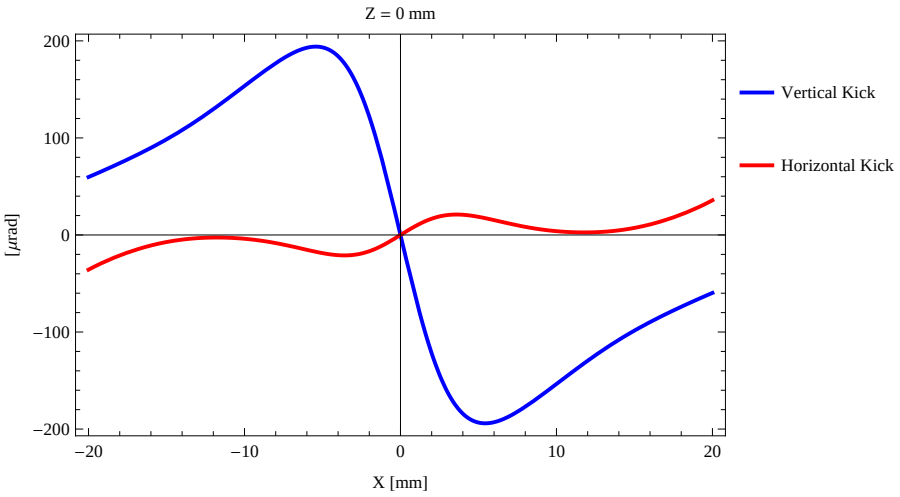

Figure 73: Induced angular kick on the stored beam from the epu96Incl as a function of the horizontal distance to the undulator axis.

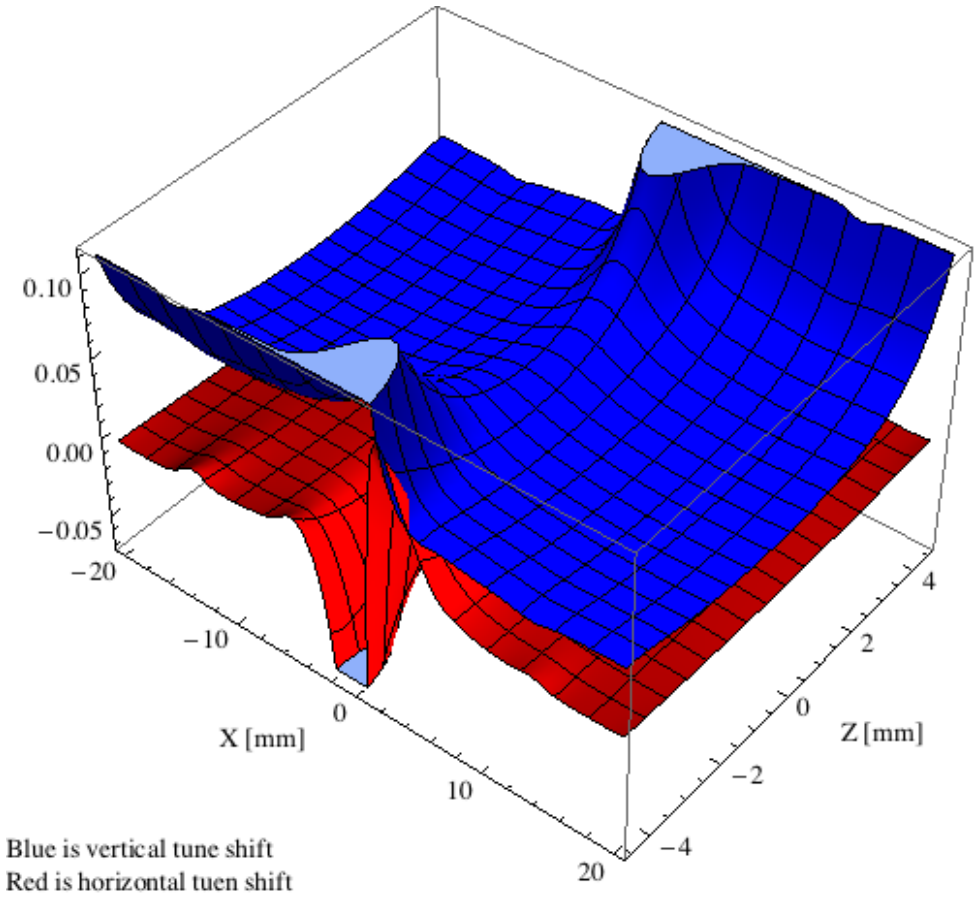

Figure 74: Tune shift induced by the epu96Incl over the beam stay clear aparture.

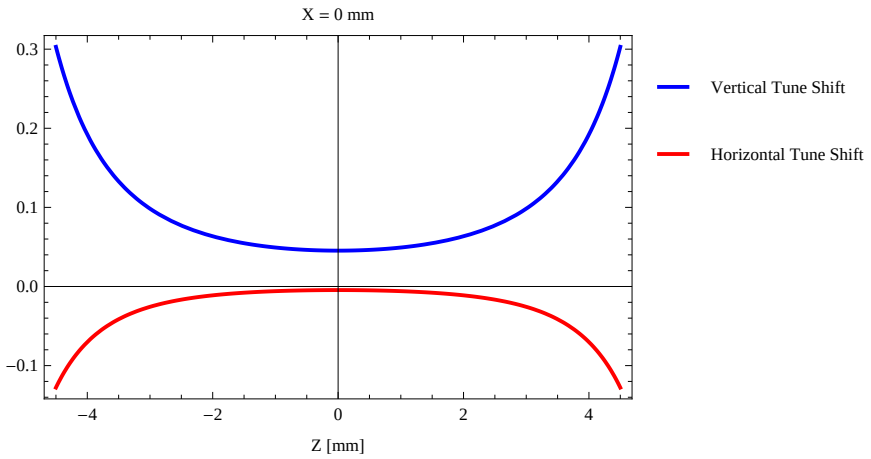

Figure 75: Induced tune shift from the epu96Incl as a function of the vertical distance to the undulator axis.

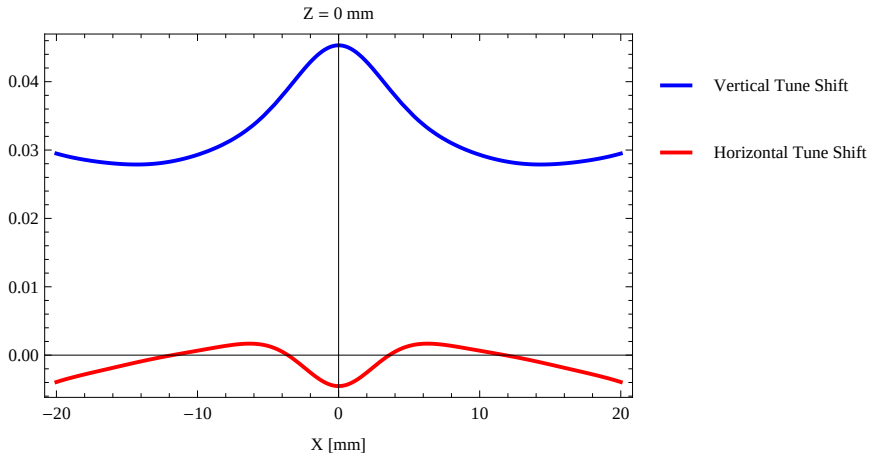

Figure 76: Induced tune shift from the epu96Incl on the stored beam from the as a function of the horizontal distance to the undulator axis.

2.14 Magnet model of the elliptically polarizing undulator epu96Vert

The Radia [2] magnet model of the epu96Vert is shown in Figure 77. The length of the magnet model is 787.992 mm. The magnetic material in the model is NdFeb with a remanence of 1.33 T. Blocks with vertical magnetisation are blue and blocks with horizontal magnetisation are yellow. The block size is 35.x35.x24. mm^3 and there is a 5. mm cut-out in two of the corners of the blocks. The total length of the epu96Vert is 2515.99 mm.

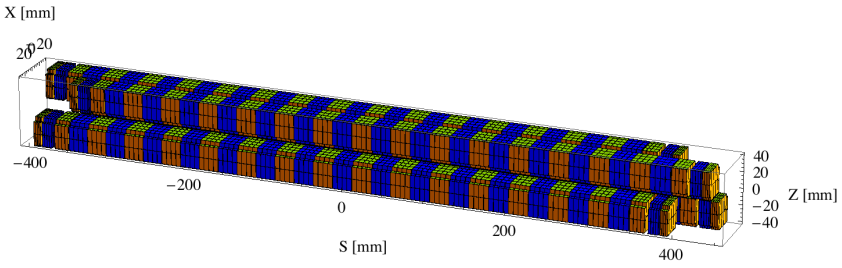

Figure 77: Magnetic model of the epu96Vert. The has been modelled with Radia [2]

2.15 Analysis of the magnetic field of the epu96Vert

The effective magnetic fields on axis and the fundamental photon energy of the epu96Vert are shown in Table 15. The higher harmonic contents in the magnetic field of an elliptically polarizing undulator made of permanent magnets is usually small and the effective field has approximately the same strength as the peak field.

2.16 Synchrotron radiation from the epu96Vert

The power map of the emitted synchrotron radiation by the epu96Vert, assuming a 0.3 A filament beam with an energy of 1.5 GeV and undulator properties of the synchrotron radiation, is shown in Figure 81. The on-axis power density is 0.449698 kW/mrad^2

Table 15: Effective Fields on axis and Fundamental Photon Energy of the epu96Vert

Undulator Period	96	mm
Undulator Gap	13	mm
Undulator Mode	Vertical	
Undulator Phase	48.000	mm
Vertical Peak Field	0.000	T
effective Vertical Field	0.000	T
Kx (from vert. field)	0.000	
Horizontal Peak Field:	1.085	T
effective Horizontal Field	1.093	T
Kz (from hor. field)	9.800	
Photon Energy, Harm.1	0.005	keV
Emitted Power	1.284	kW
Total Length	2516.0	mm

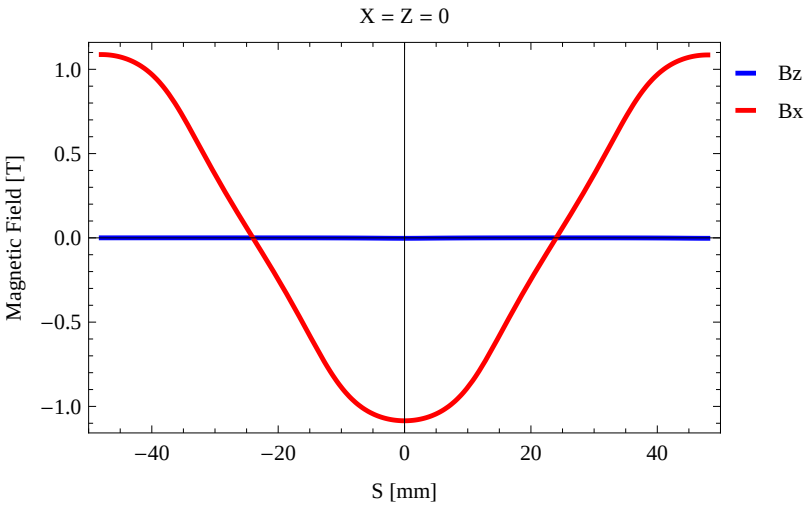

Figure 78: Vertical magnetic field in a central pole of the epu96Vert along the axis, X = Z = 0

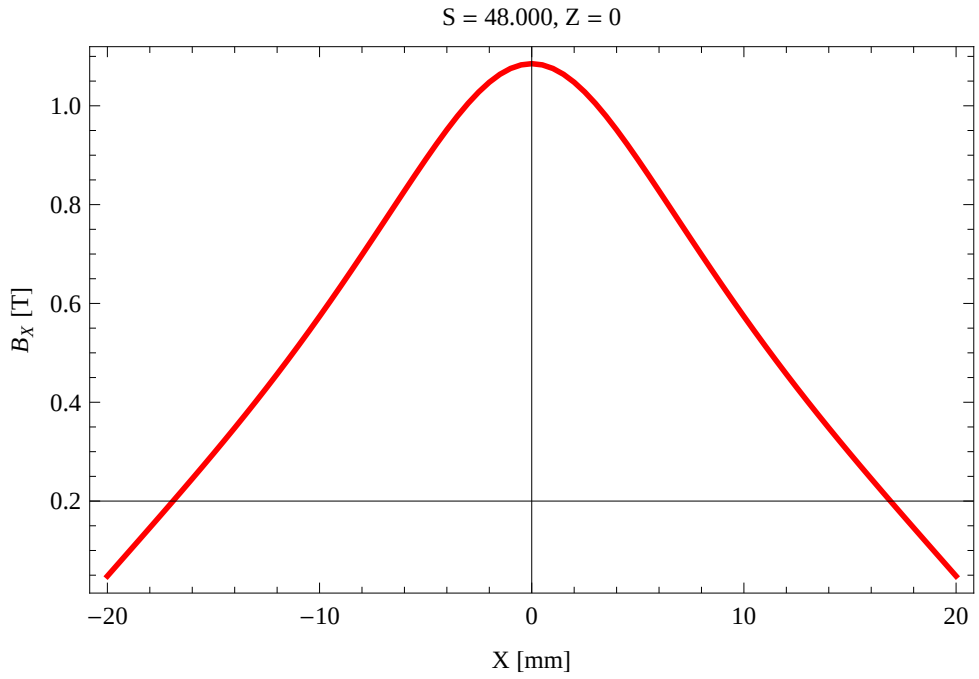

Figure 79: Horizontal magnetic field in a central pole of the epu96Vert along the horizontally transverse direction to the axis, S = 48.000, Z = 0

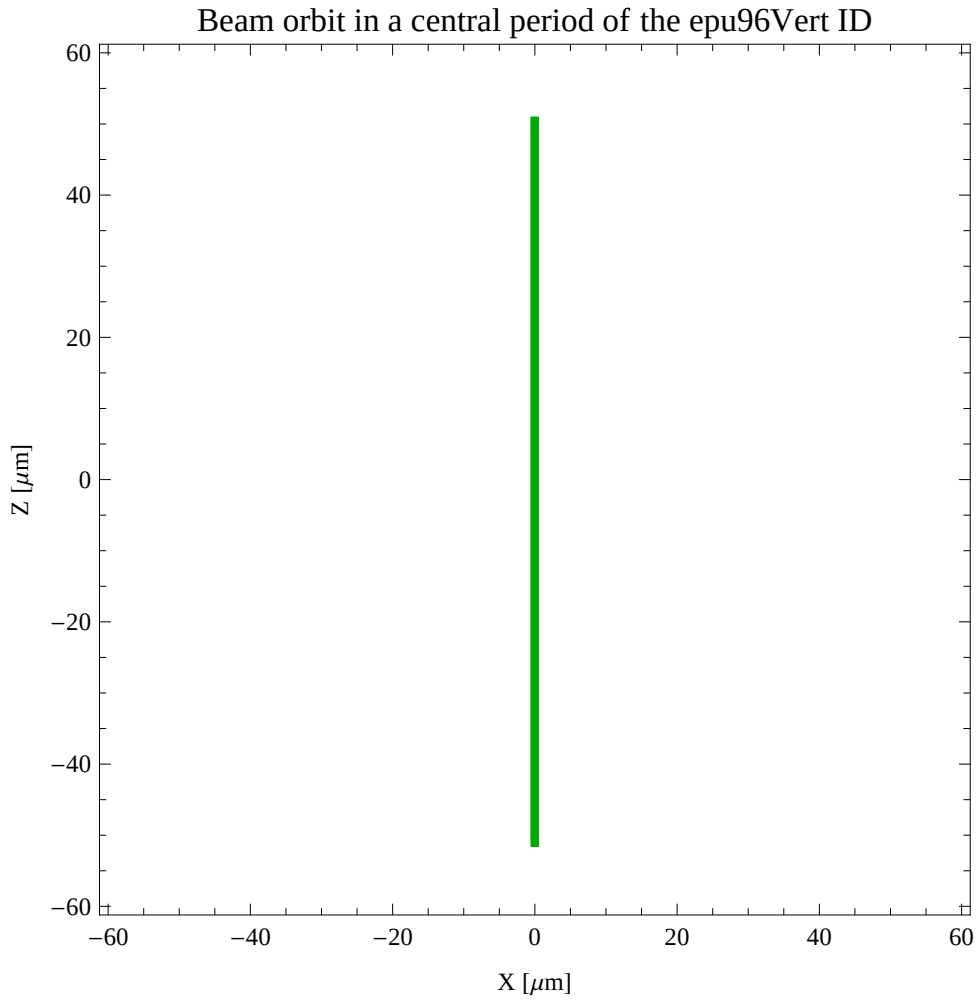

Figure 80: The beam orbit of the electron beam through a central period of the epu96Vert

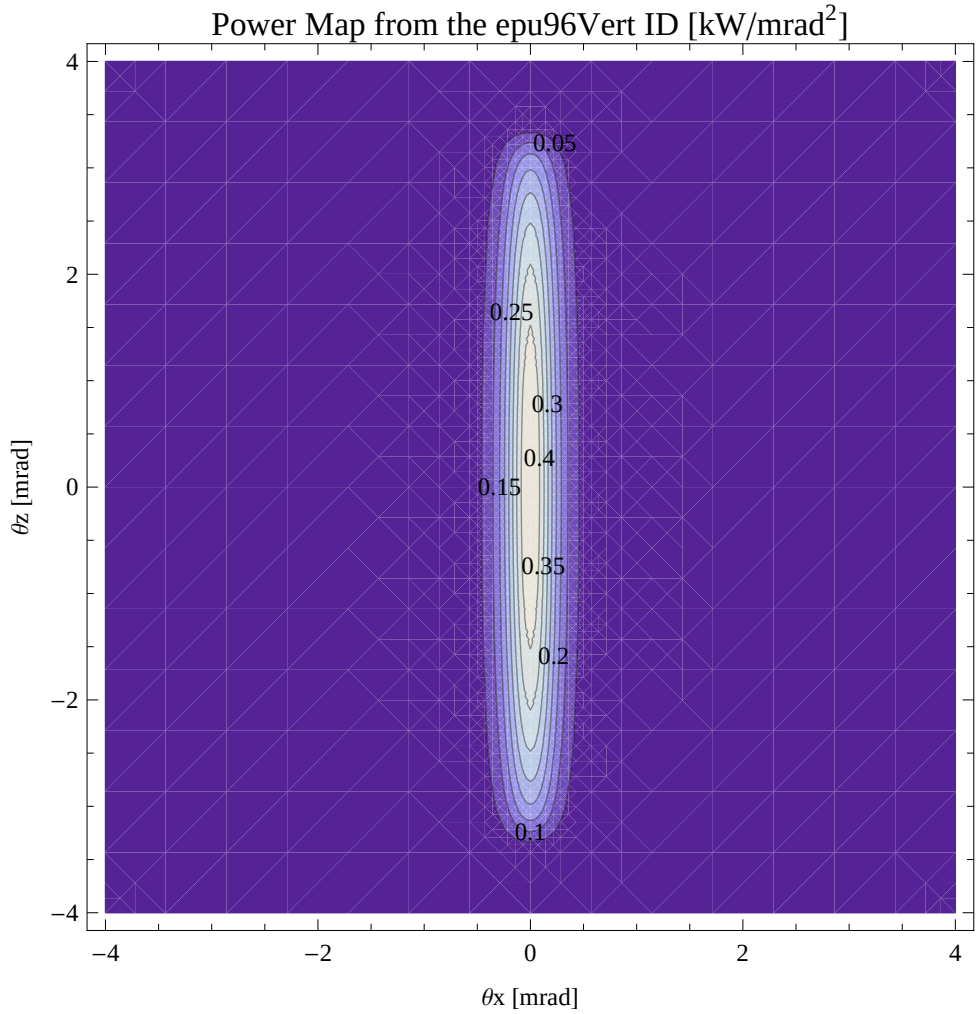

Figure 81: Map of the power distribution of the emitted synchrotron radiation by the epu96Vert

A map of the degree of linear polarisation of the fundamental harmonic of the synchotron radiation emitted by the epu96Vert over the angle of observation is shown in Figure 82.

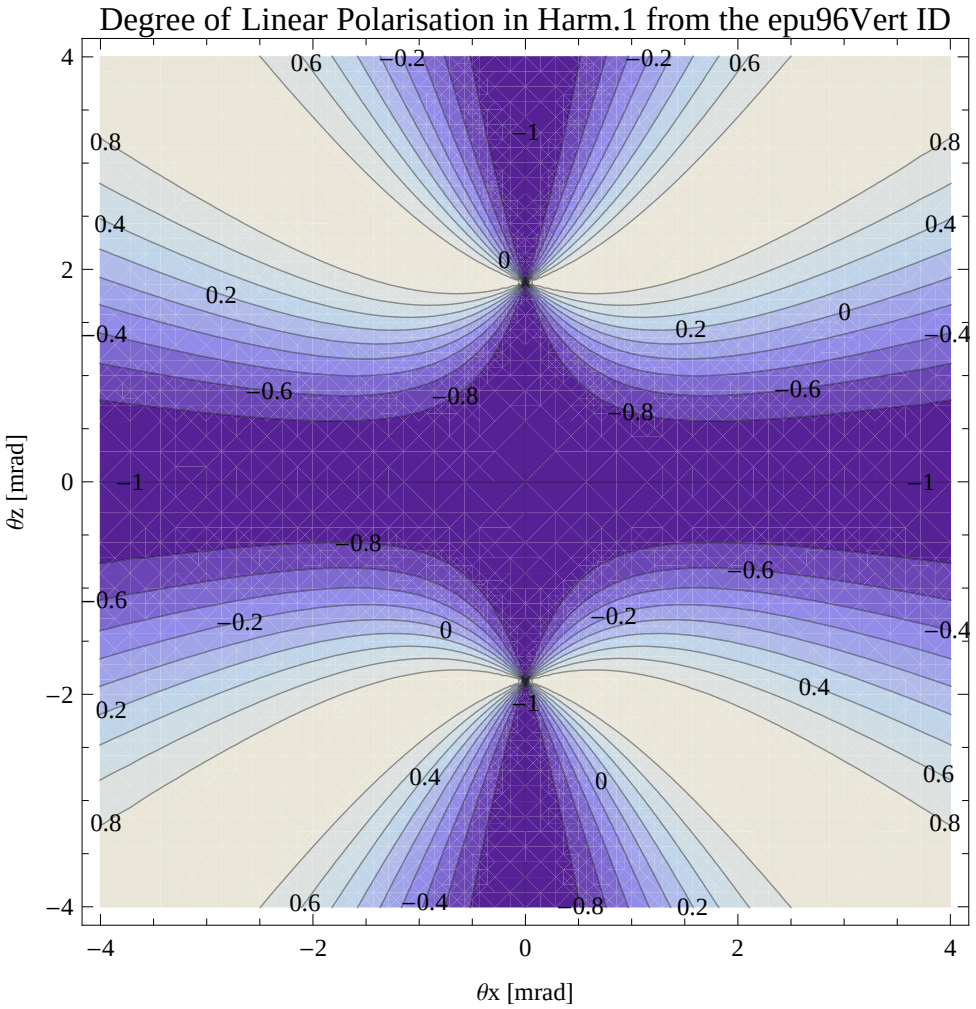

Figure 82: Map of linear polarisation in the fundamental harmonic of the synchotron radiation emitted by the epu96Vert

A map of the degree of 45 degree polarisation of the fundamental harmonic of the synchotron radiation emitted by the epu96Vert over the angle of observation is shown in Figure 83.

A map of the degree of circular polarisation of the fundamental harmonic of the synchotron radiation emitted by the epu96Vert over the angle of observation is shown in Figure 84.

The on axis brilliance at peak energy and the angular spectral flux from the epu96Vert have been calculated with the given beam parameters, which are 0.3 A of stored current, $\beta_H = 5.627$ m, $\varepsilon_H = 5.985$ nmrad, $\beta_V = 2.837$ m, $\varepsilon_V = 59.85$ pmrad, and an energy spread of 0.001.

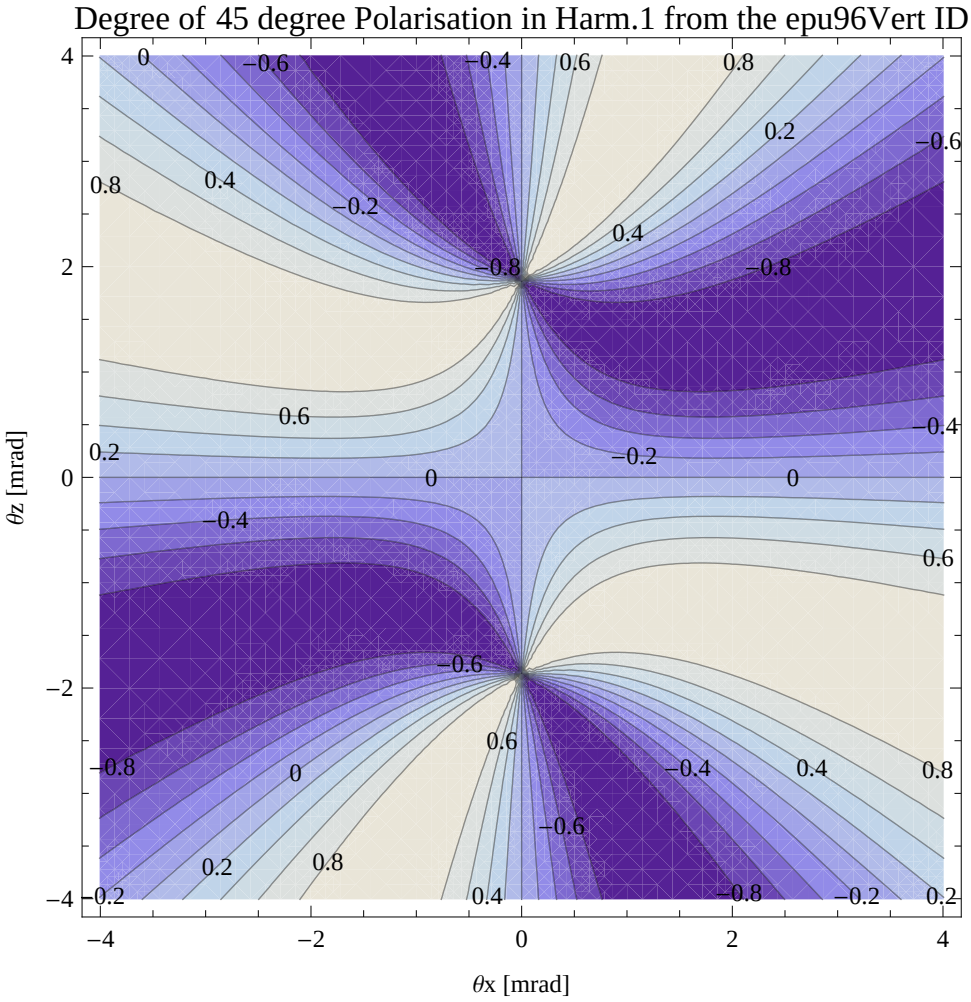

Figure 83: Map of 45 degree polarisation in the fundamental harmonic of the synchotron radiation emitted by the epu96Vert

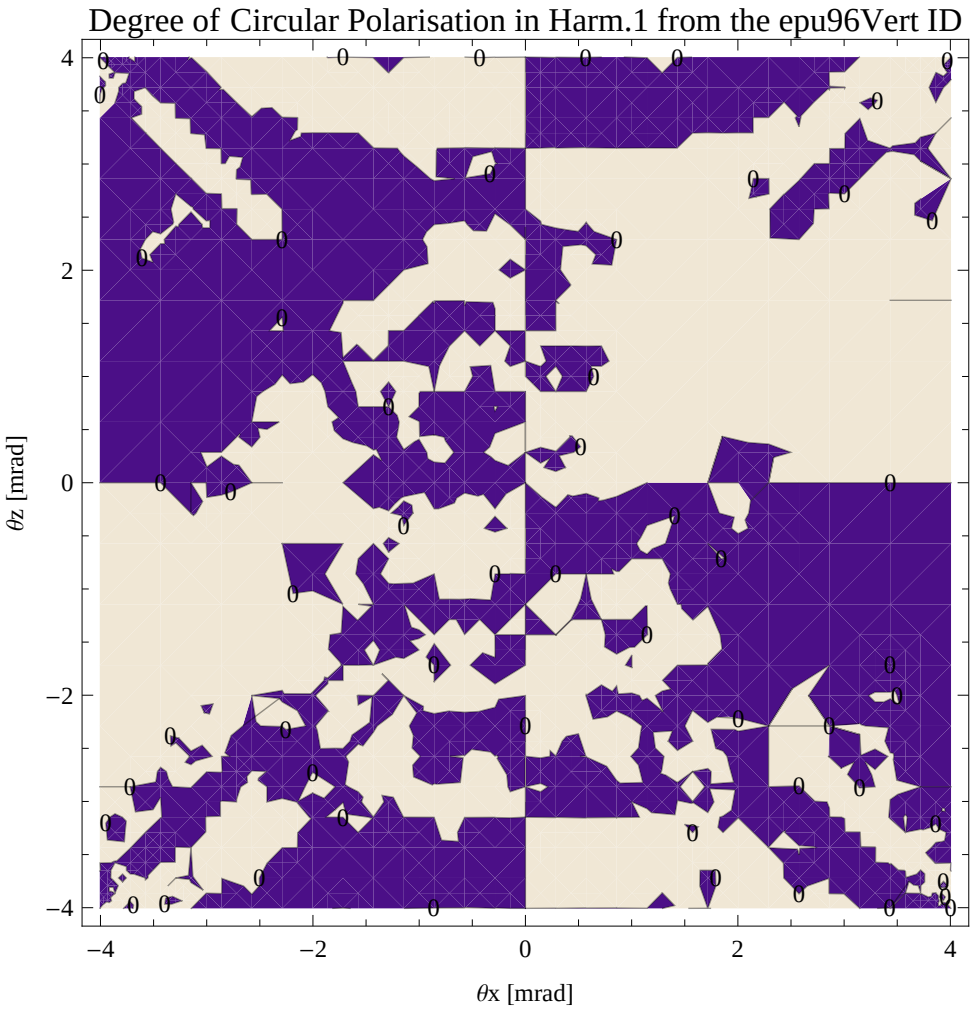

Figure 84: Map of circular polarisation in the fundamental harmonic of the synchotron radiation emitted by the epu96Vert

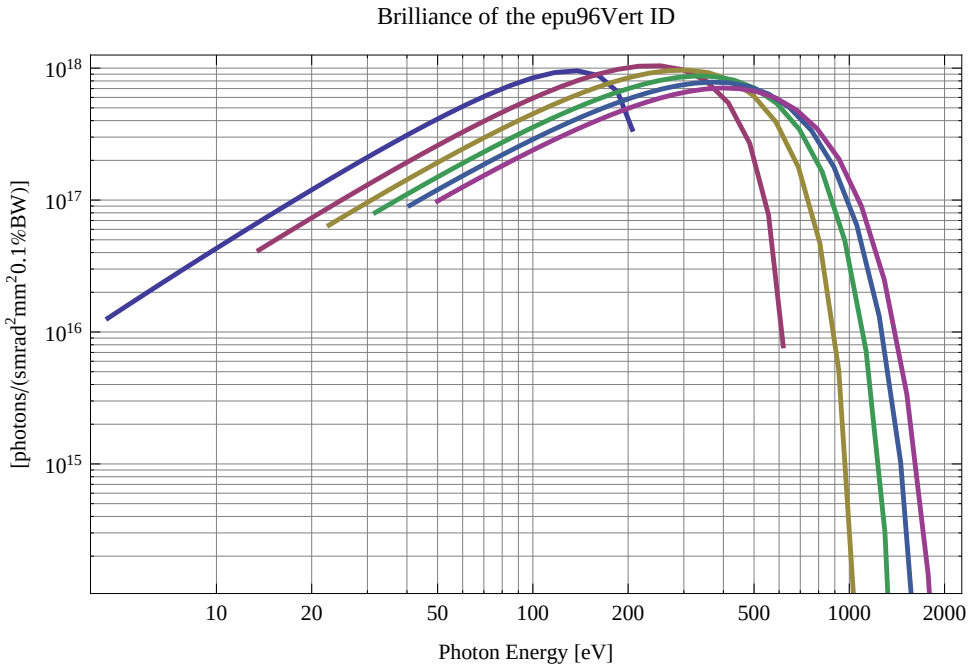

Figure 85: The brilliance at peak energy of the synchotron radiation emitted by the epu96Vert

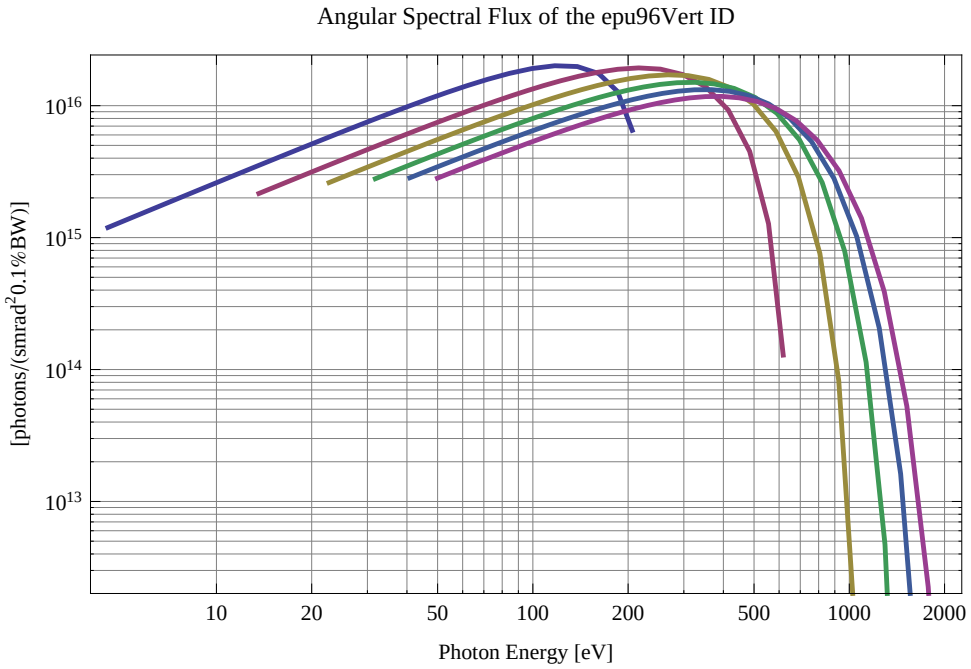

Figure 86: The angular spectral flux of the synchotron radiation emitted by the epu96Vert

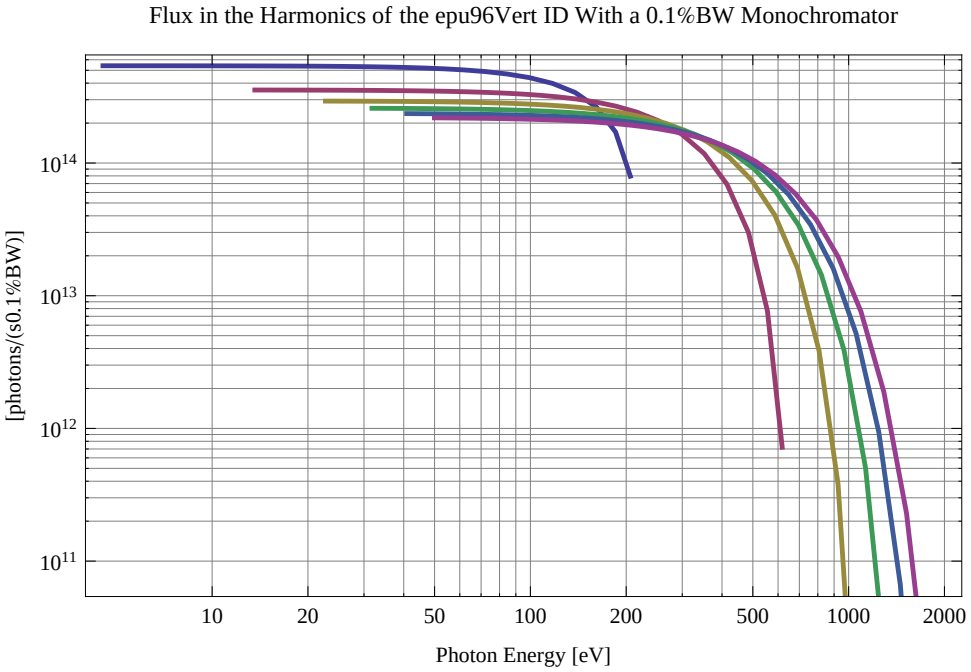

Figure 87: The flux of photons in the harmonics of the emitted synchrotron radiation from the epu96Vert using a 0.1%BW monochromator

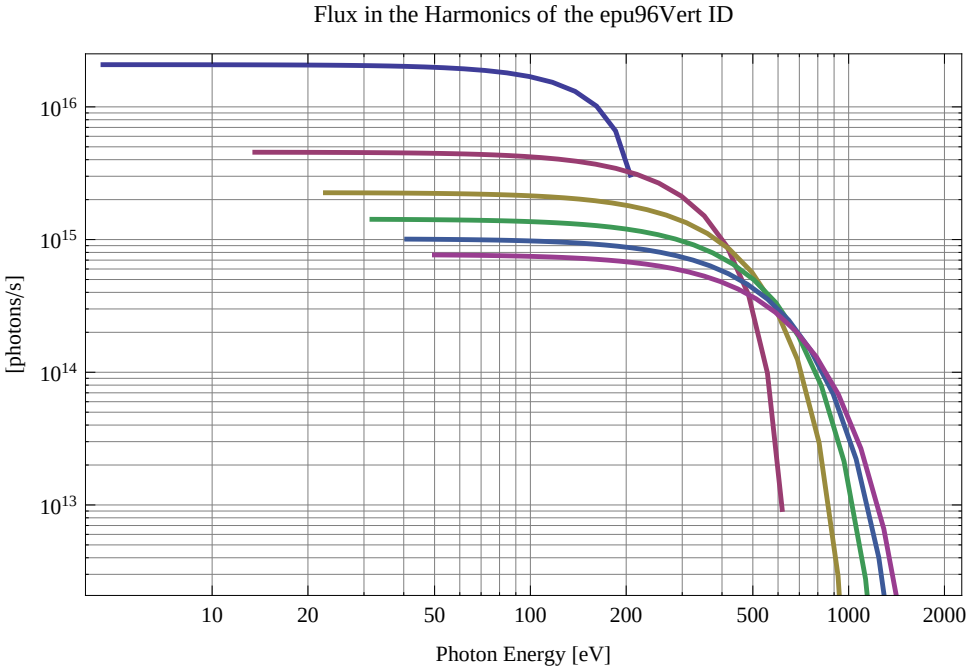

Figure 88: The flux of photons in the harmonics of the emitted synchrotron radiation from the epu96Vert

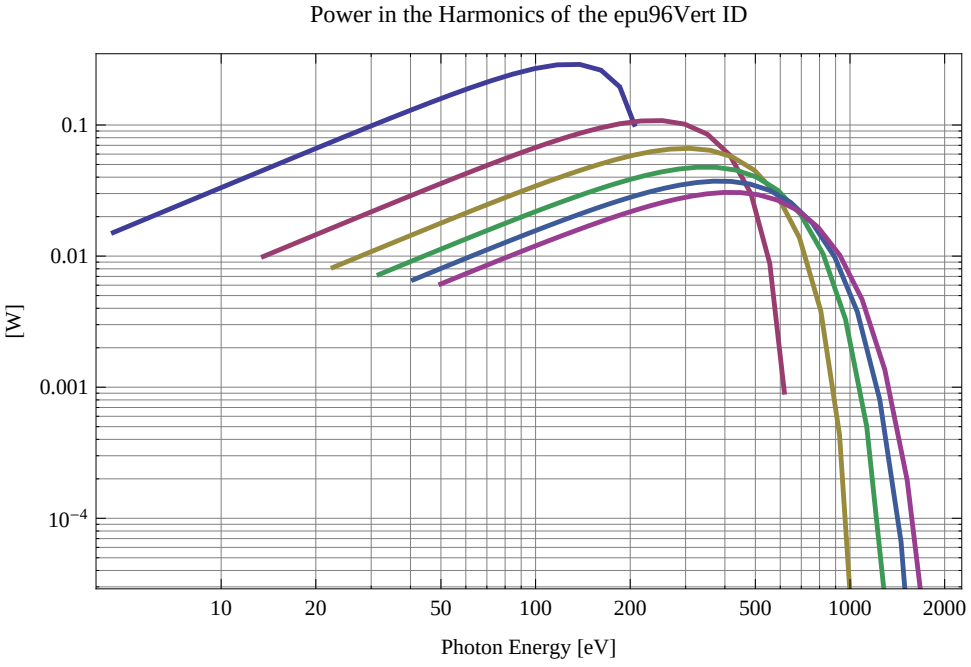

Figure 89: The power in the harmonics of the emitted synchrotron radiation from the epu96Vert

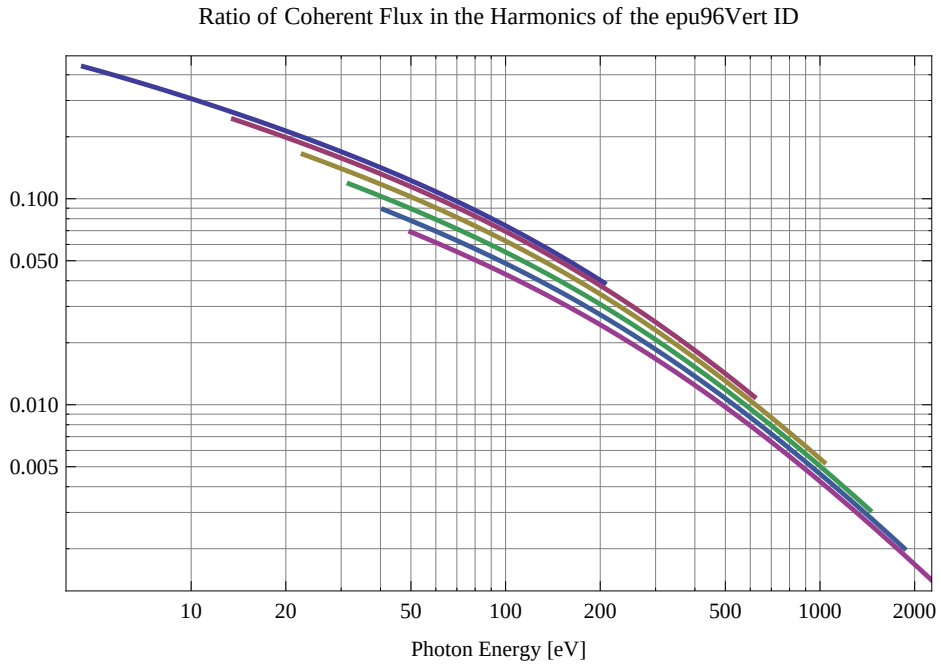

Figure 90: The ratio of coherent flux in the harmonics of the emitted synchrotron radiation from the epu96Vert

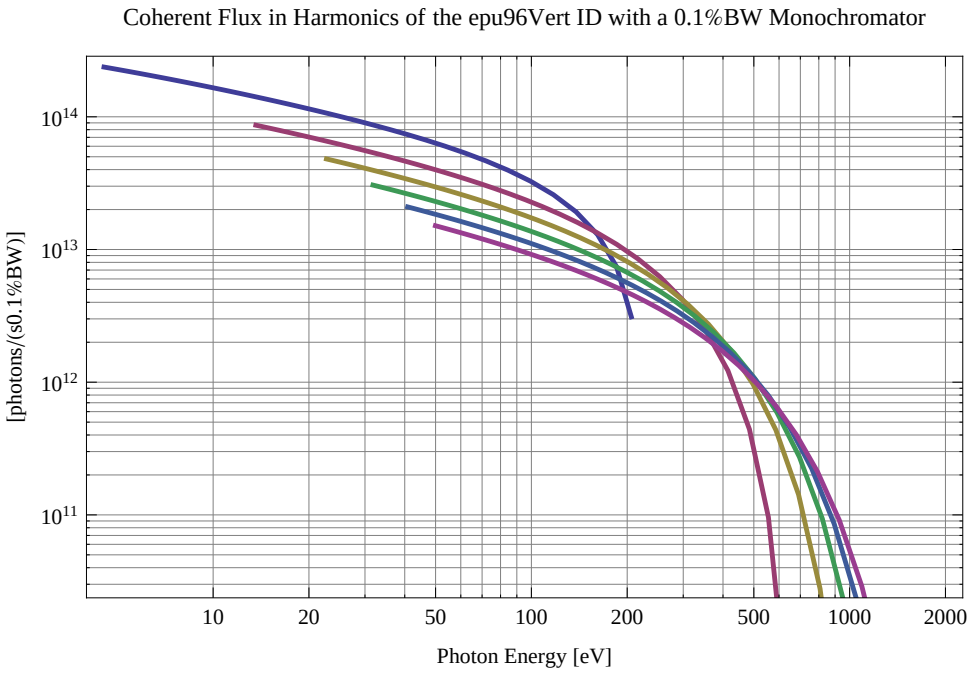

Figure 91: The coherent flux in the harmonics of the epu96Vert using a 0.1%BW Monochromator

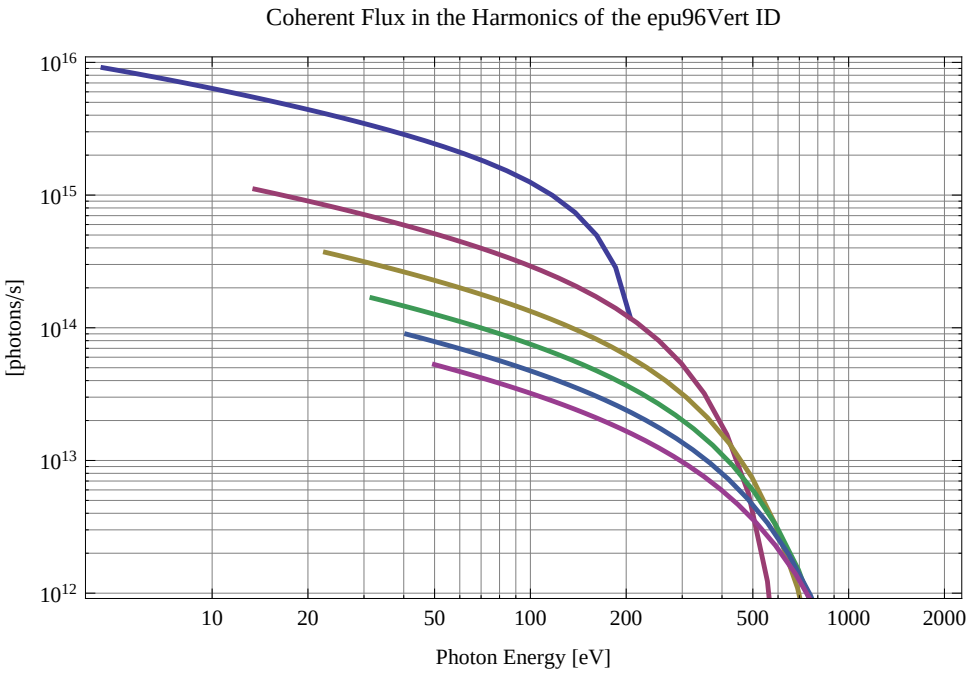

Figure 92: The coherent flux in the harmonics of the epu96Vert

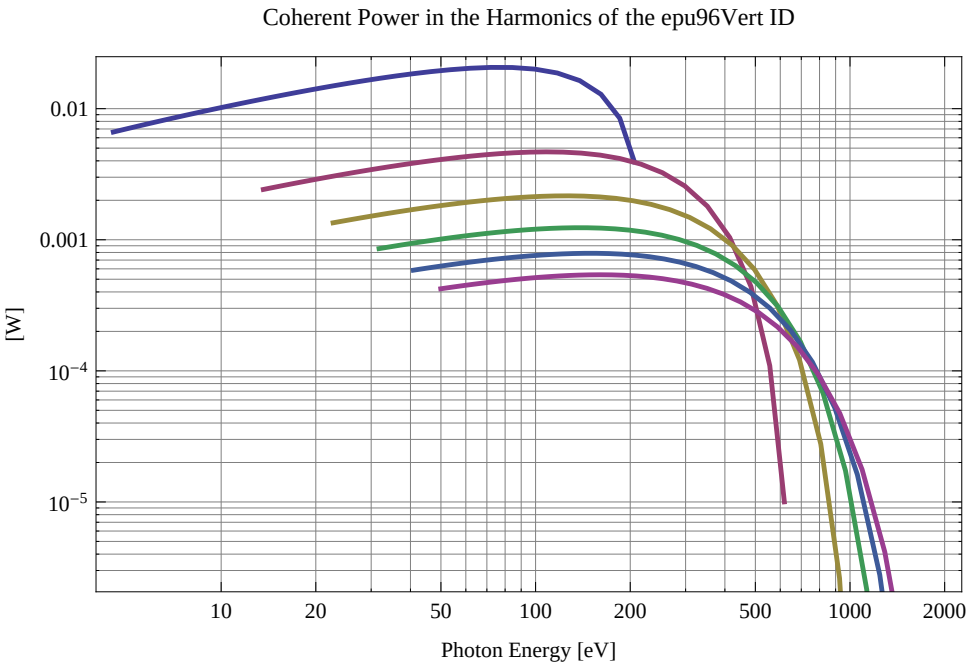

Figure 93: The power of coherent synchrotron radiation in the harmonics of the epu96Vert

The brilliance at peak energy and the angular spectral flux density from the epu96Vert for different harmonics at maximum K-value (9.800) are given in Table 16 and for minimum K-value (0.400) these values are given in Table 17.

Table 16: The brilliance at peak energy and the angular spectral flux density from the epu96Vert for different harmonics at maximum K-value (9.800)

Harmonic	Photon Energy [eV]	Brilliance [Ph./(smrad^{2}mrad^{2}0.1%BW)]	Angular Spectral Flux [Ph./(smrad^{2}0.1%BW)]
1	4.54018	1.27×10^{16}	1.19×10^{15}
3	13.6205	4.17×10^{16}	2.16×10^{15}
5	22.7009	6.46×10^{16}	2.61×10^{15}
7	31.7813	8.04×10^{16}	2.79×10^{15}
9	40.8616	9.1×10^{16}	2.84×10^{15}
11	49.942	9.81×10^{16}	2.82×10^{15}

Table 17: The brilliance at peak energy and the angular spectral flux density from the epu96Vert for different harmonics at minimum K-value (0.4)

Harmonic	Photon Energy [eV]	Brilliance [Ph./(smrad^{2}mrad^{2}0.1%BW)]	Angular Spectral Flux [Ph./(smrad^{2}0.1%BW)]
1	206.085	3.43×10^{17}	6.5×10^{15}
3	618.255	7.85×10^{15}	1.29×10^{14}
5	1030.43	1.03×10^{14}	1.64×10^{12}
7	1442.6	1.18×10^{12}	1.86×10^{10}
9	1854.77	1.28×10^{10}	2.01×10^{8}
11	2266.94	1.34×10^{8}	2.11×10^{6}

2.17 Influence from the epu96Vert on the optics of the stored beam

Figure 94 shows the focusing potential from the epu96Vert over the beam stay clear aperture of the ring aparture.

Figure 95 shows the kick map in the beam energy independant unit T^2m^2 of the kicks induced by the epu96Vert over the beam stay clear aparture.

Figure 96 shows the induced angular kick on the stored beam from the epu96Vert as a function of the vertical distance to the undulator axis.

Figure 97 shows the induced angular kick on the stored beam from the epu96Vert as a function of the horizontal distance to the undulator axis.

Figure 98 shows tune shift induced by the epu96Vert over the beam stay clear aparture. Note that the tune shift depends on the beam size at the.

Figure 99 shows the induced tune shift from the epu96Vert as a function of the vertical distance to the undulator axis.

Figure 100 shows the induced tune shift from the epu96Vert as a function of the horizontal distance to the undulator axis.

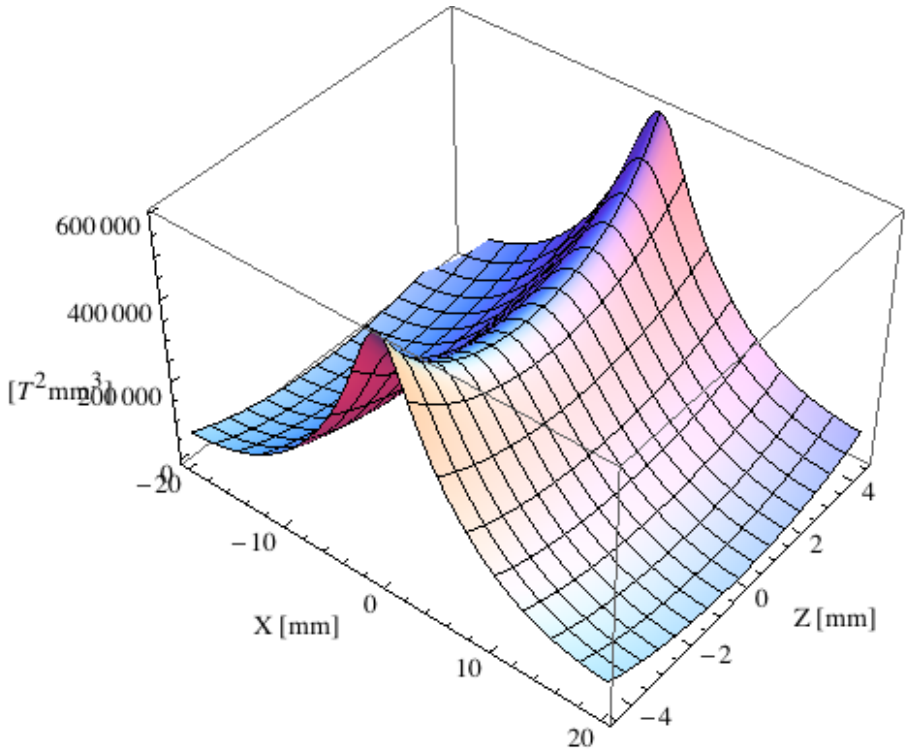

Figure 94: Focusing potential from the epu96Vert over the beam stay clear aparture.

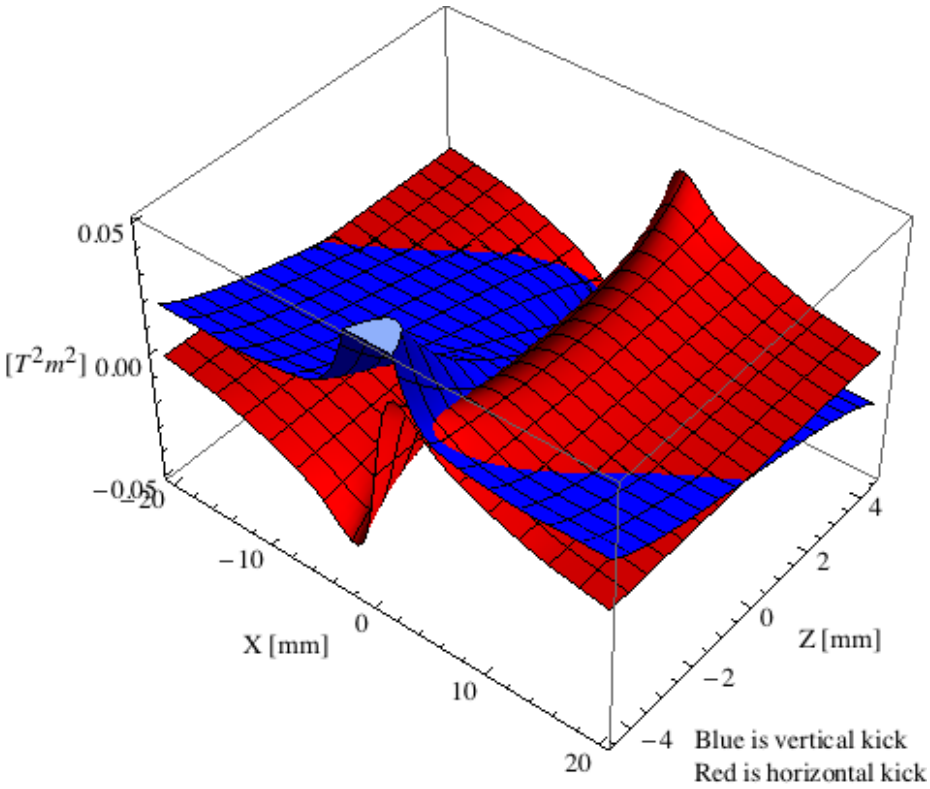

Figure 95: Kick map in the beam energy independant unit T^2m^2 of the kicks induced by the epu96Vert over the beam stay clear aparture.

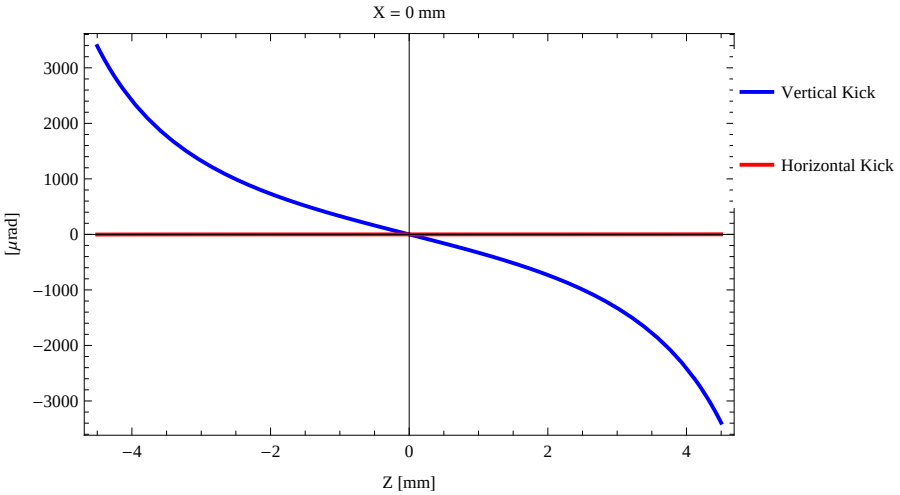

Figure 96: Induced angular kick on the stored beam from the epu96Vert as a function of the vertical distance to the undulator axis.

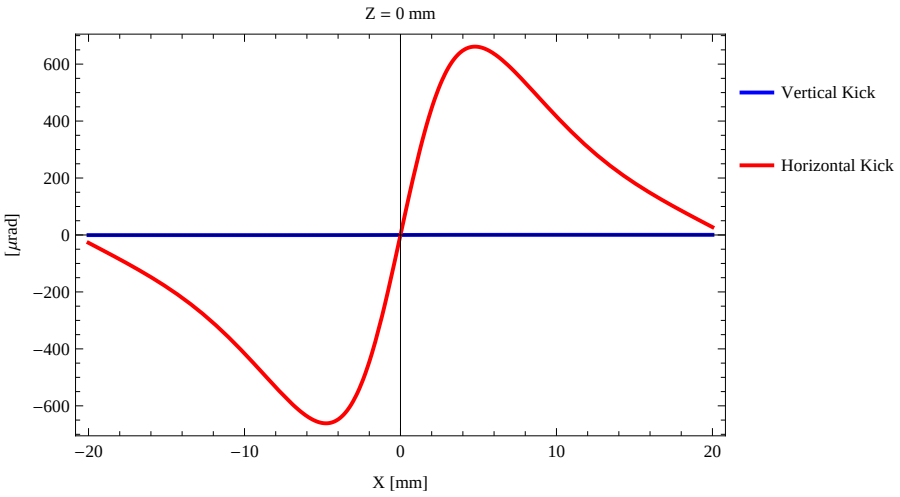

Figure 97: Induced angular kick on the stored beam from the epu96Vert as a function of the horizontal distance to the undulator axis.

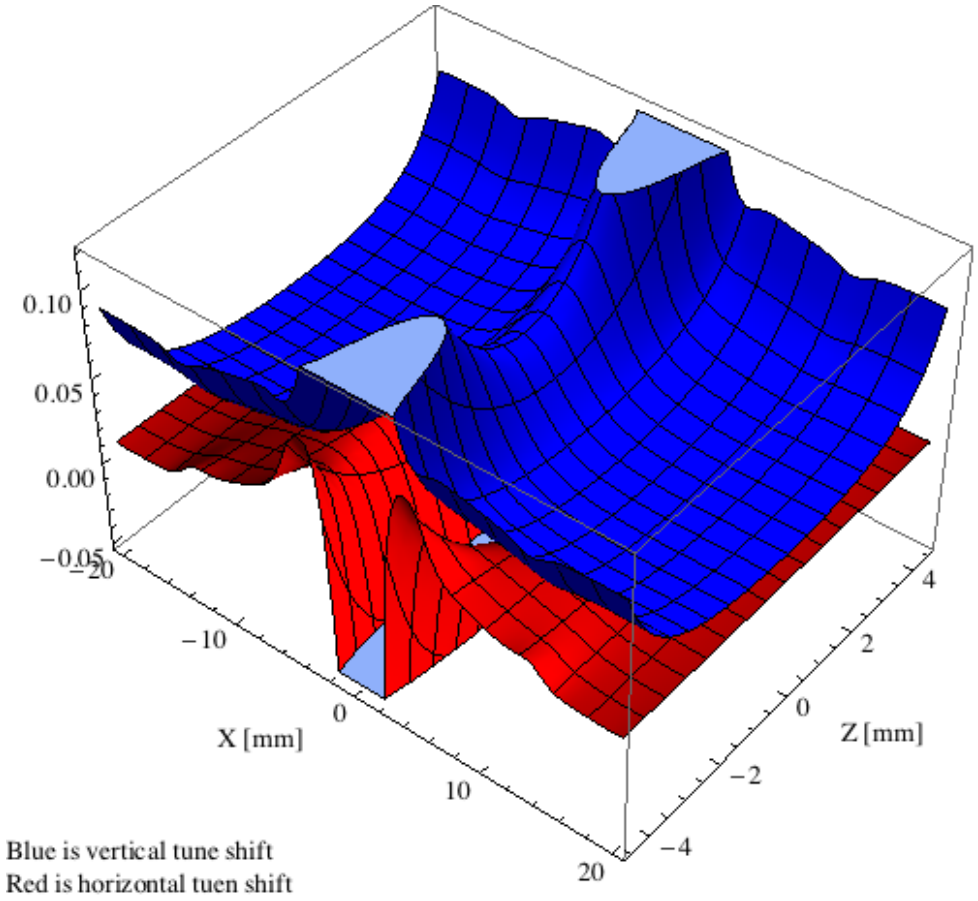

Figure 98: Tune shift induced by the epu96Vert over the beam stay clear aparture.

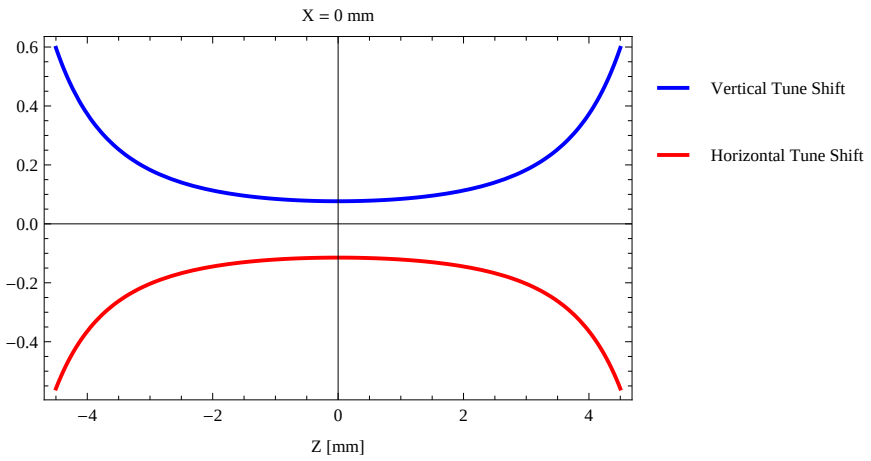

Figure 99: Induced tune shift from the epu96Vert as a function of the vertical distance to the undulator axis.

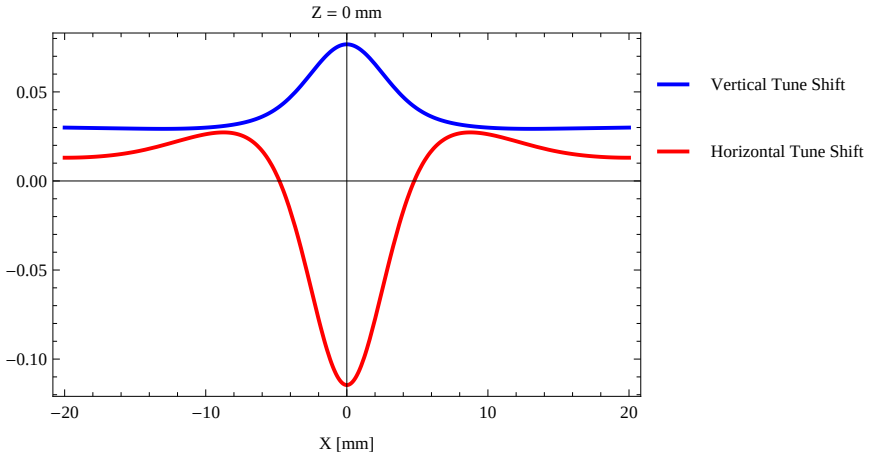

Figure 100: Induced tune shift from the epu96Vert on the stored beam from the as a function of the horizontal distance to the undulator axis.

3 The elliptically polarizing undulator epu90

3.1 Modes of operation in the elliptically polarizing undulator epu90

Horizontal polarisation of the emitted synchrotron radiation from the epu90 (Period=90 mm, Gap=13mm) is found in the planar mode when there is no movement of the sub-girders.

Circular polarisation is found in the elliptical mode of operation for a symmetric sub-grider movement of 25.071 mm. Figure 101 shows the vertical and horizontal magnetic field for the epu90 when operating in the helical mode.

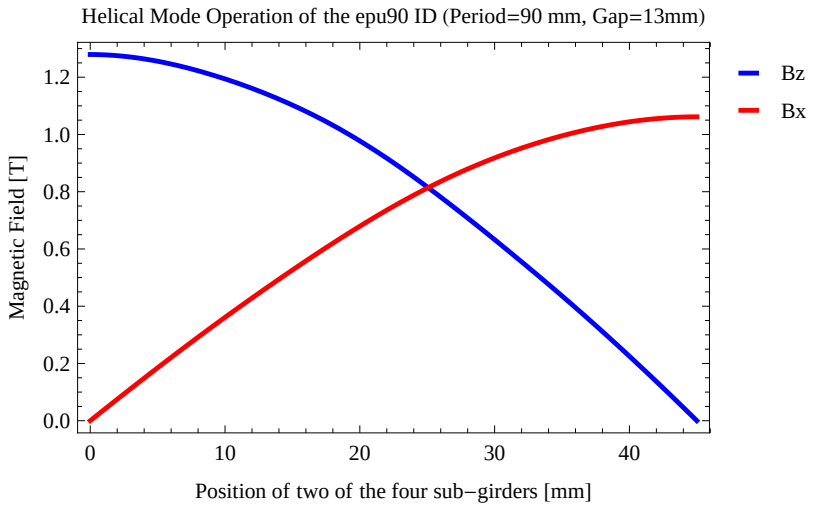

Figure 101: Vertical and horizontal magnetic field for the the epu90 when operating in the helical mode for different positions for two of the four sub-girders

45 degree polarisation is found in the inclined mode of operation for an assymetric sub-grider movement of 23.8073 mm. Figure 102 shows the vertical and horizontal magnetic field for the epu90 when operating in the inclined mode.

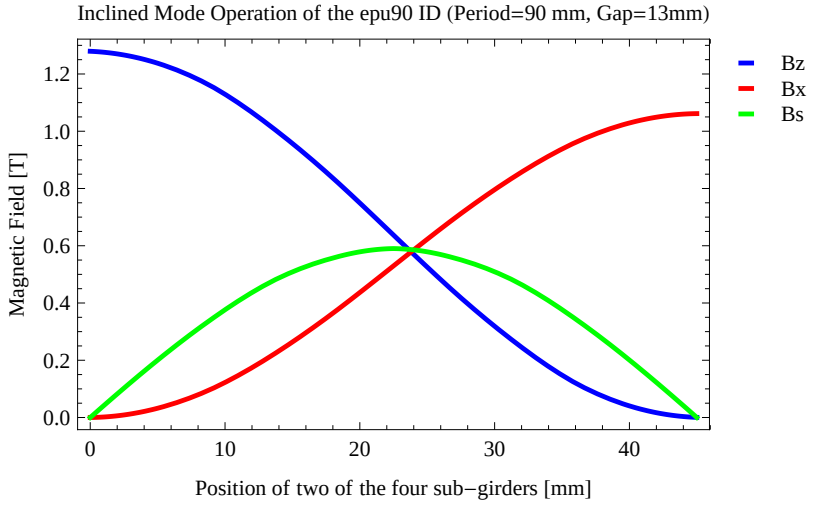

Figure 102: Vertical, horizontal, and longitudinal magnetic field for the the epu90 when operating in the inclined mode for different positions for two of the four sub-girders

The following sub-sections will cover four different situations: The epu90 operating in the planar

mode for horizontal polarisation (epu90Plan); The epu90 operating in the helical mode for circular polarisation (epu90Heli),), the epu90operating in the inclined mode for 45 degree polarisation (epu90Incl); and The epu90 operating in the vertical mode for vertical polarisation (epu90Vert).

3.2 Magnet model of the elliptically polarizing undulator epu90Plan

The Radia [2] magnet model of the epu90Plan is shown in Figure 103. The length of the magnet model is 739.68 mm. The magnetic material in the model is NdFeb with a remanence of 1.33 T. Blocks with vertical magnetisation are blue and blocks with horizontal magnetisation are yellow. The block size is 35.x35.x22.5 mm^3 and there is a 5. mm cut-out in two of the corners of the blocks. The total length of the epu90Plan is 2539.68 mm.

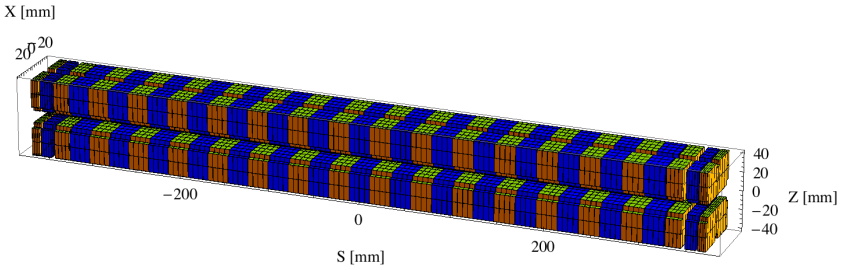

Figure 103: Magnetic model of the epu90Plan. The has been modelled with Radia [2]

3.3 Analysis of the magnetic field of the epu90Plan

The effective magnetic fields on axis and the fundamental photon energy of the epu90Plan are shown in Table 18. The higher harmonic contents in the magnetic field of an elliptically polarizing undulator made of permanent magnets is usually small and the effective field has approximately the same strength as the peak field.

Table 18: Effective Fields on axis and Fundamental Photon Energy of the epu90Plan

Undulator Period	90	mm
Undulator Gap	13	mm
Undulator Mode	Planar	
Undulator Phase	0.000	mm
Vertical Peak Field	1.235	T
effective Vertical Field	1.279	T
Kx (from vert. field)	10.751	
Horizontal Peak Field:	0.000	T
effective Horizontal Field	0.000	T
Kz (from hor. field)	0.000	
Photon Energy, Harm.1	0.004	keV
Emitted Power	1.774	kW
Total Length	2539.7	mm

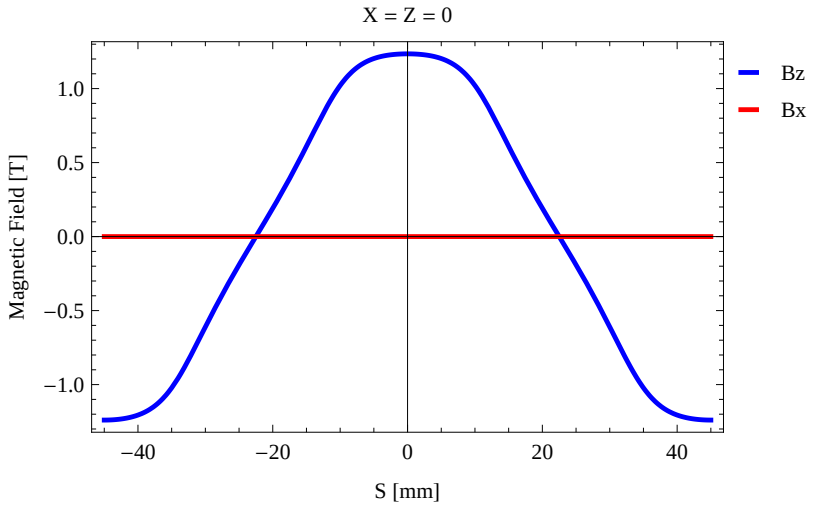

Figure 104: Vertical magnetic field in a central pole of the epu90Plan along the axis, X = Z = 0

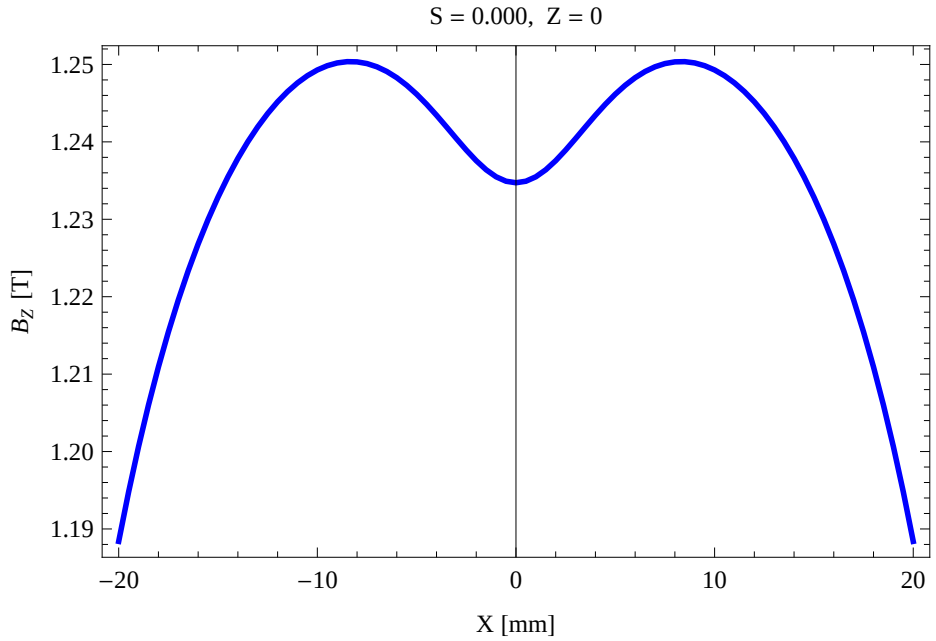

Figure 105: Vertical magnetic field in a central pole of the epu90Plan along the horizontally transverse direction to the axis, S = 0.000, Z = 0

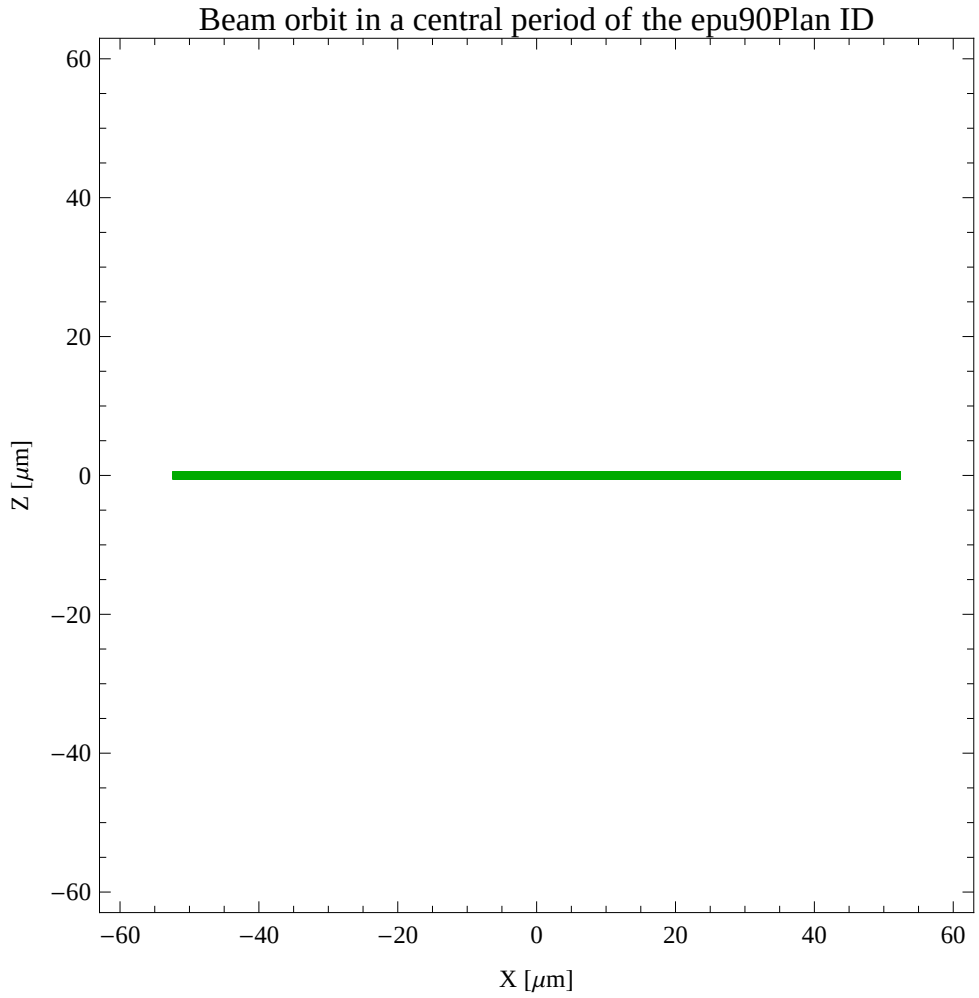

Figure 106: The beam orbit of the electron beam through a central period of the epu90Plan

3.4 Synchrotron radiation from the epu90Plan

The power map of the emitted synchrotron radiation by the epu90Plan, assuming a 0.3 A filament beam with an energy of 1.5 GeV and undulator properties of the synchrotron radiation, is shown in Figure 107. The on-axis power density is 0.568397 kW/mrad^2

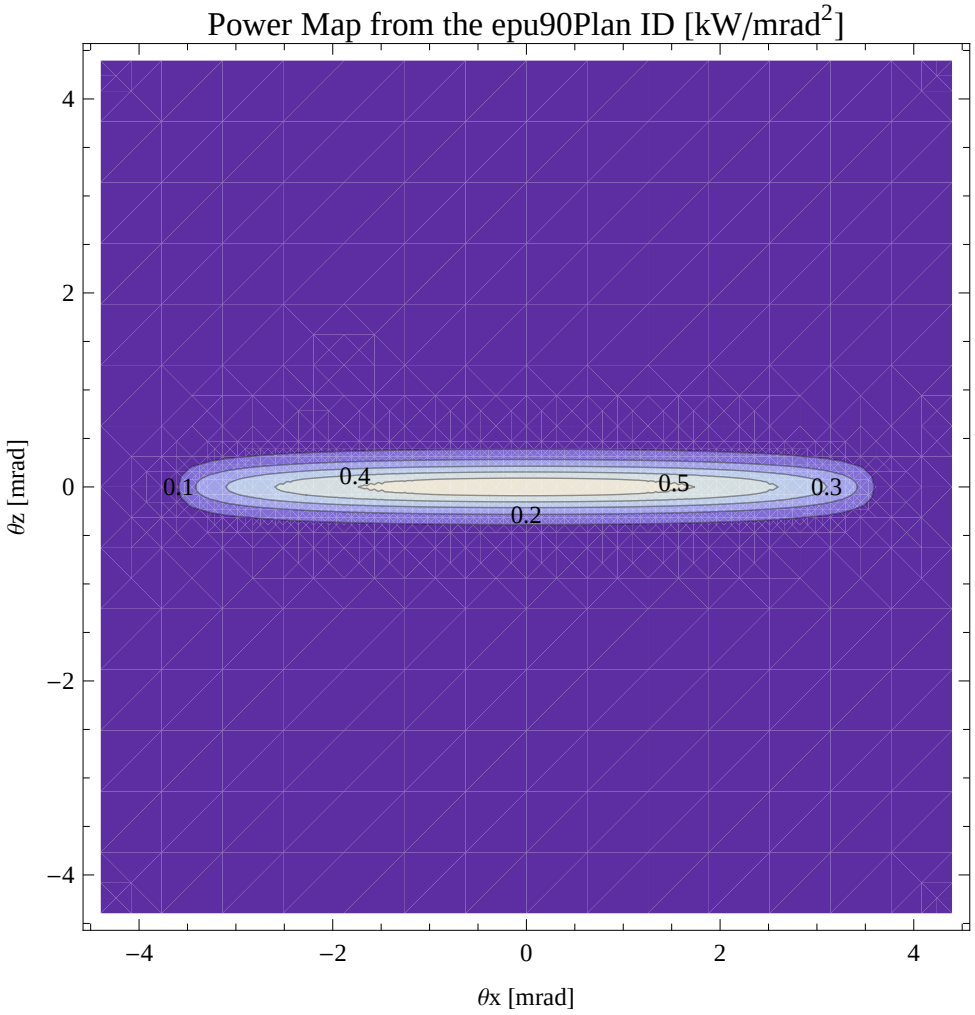

Figure 107: Map of the power distribution of the emitted synchrotron radiation by the epu90Plan

A map of the degree of linear polarisation of the fundamental harmonic of the synchotron radiation emitted by the epu90Plan over the angle of observation is shown in Figure 108.

A map of the degree of 45 degree polarisation of the fundamental harmonic of the synchotron radiation emitted by the epu90Plan over the angle of observation is shown in Figure 109.

A map of the degree of circular polarisation of the fundamental harmonic of the synchotron radiation emitted by the epu90Plan over the angle of observation is shown in Figure 110.

The on axis brilliance at peak energy and the angular spectral flux from the epu90Plan have been calculated with the given beam parameters, which are 0.3 A of stored current, $\beta_H = 5.627$ m, $\varepsilon_H = 5.985$ nmrad, $\beta_V = 2.837$ m, $\varepsilon_V = 59.85$ pmrad, and an energy spread of 0.001.

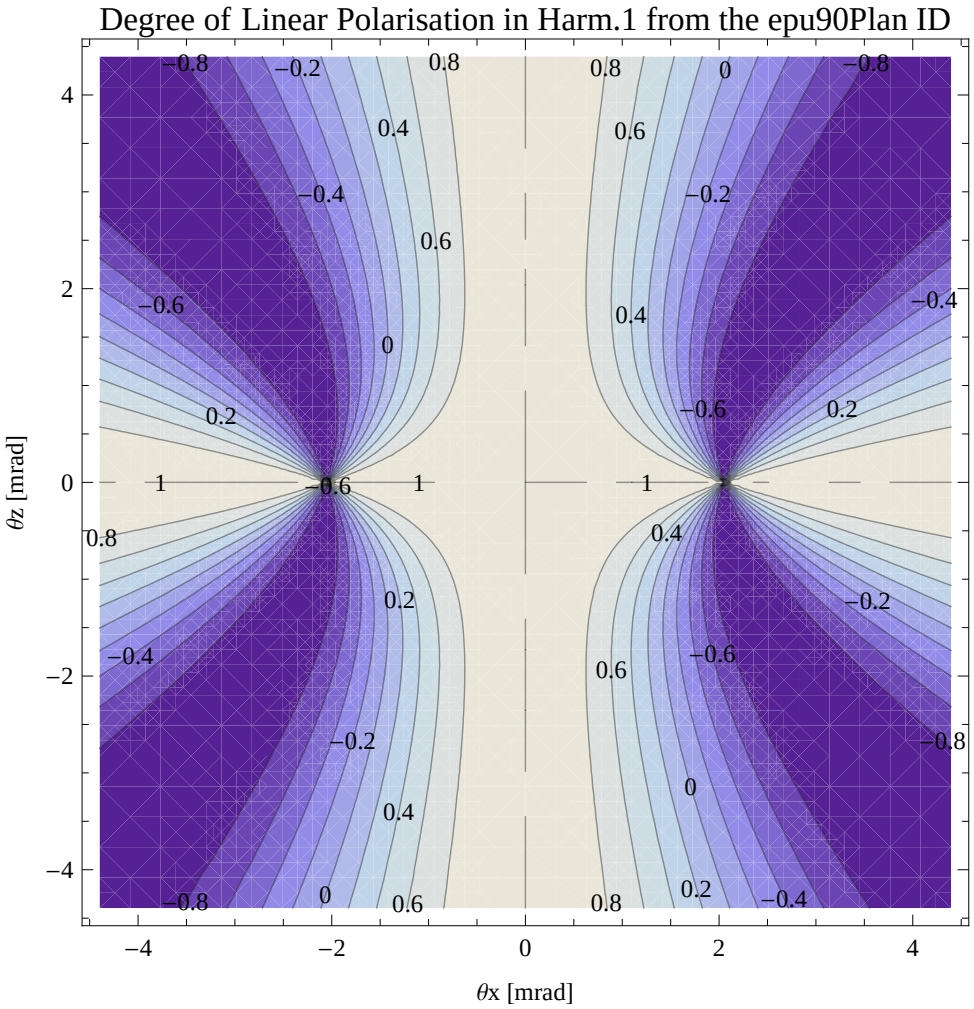

Figure 108: Map of linear polarisation in the fundamental harmonic of the synchotron radiation emitted by the epu90Plan

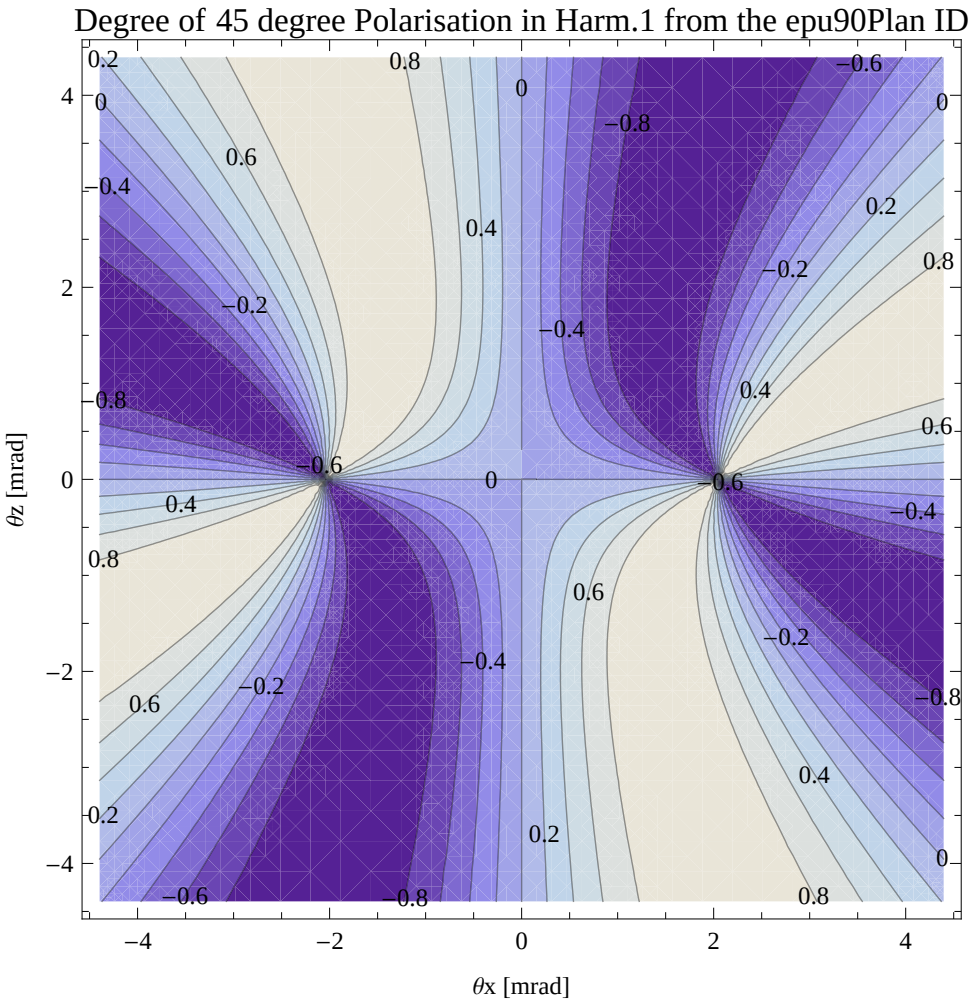

Figure 109: Map of 45 degree polarisation in the fundamental harmonic of the synchotron radiation emitted by the epu90Plan

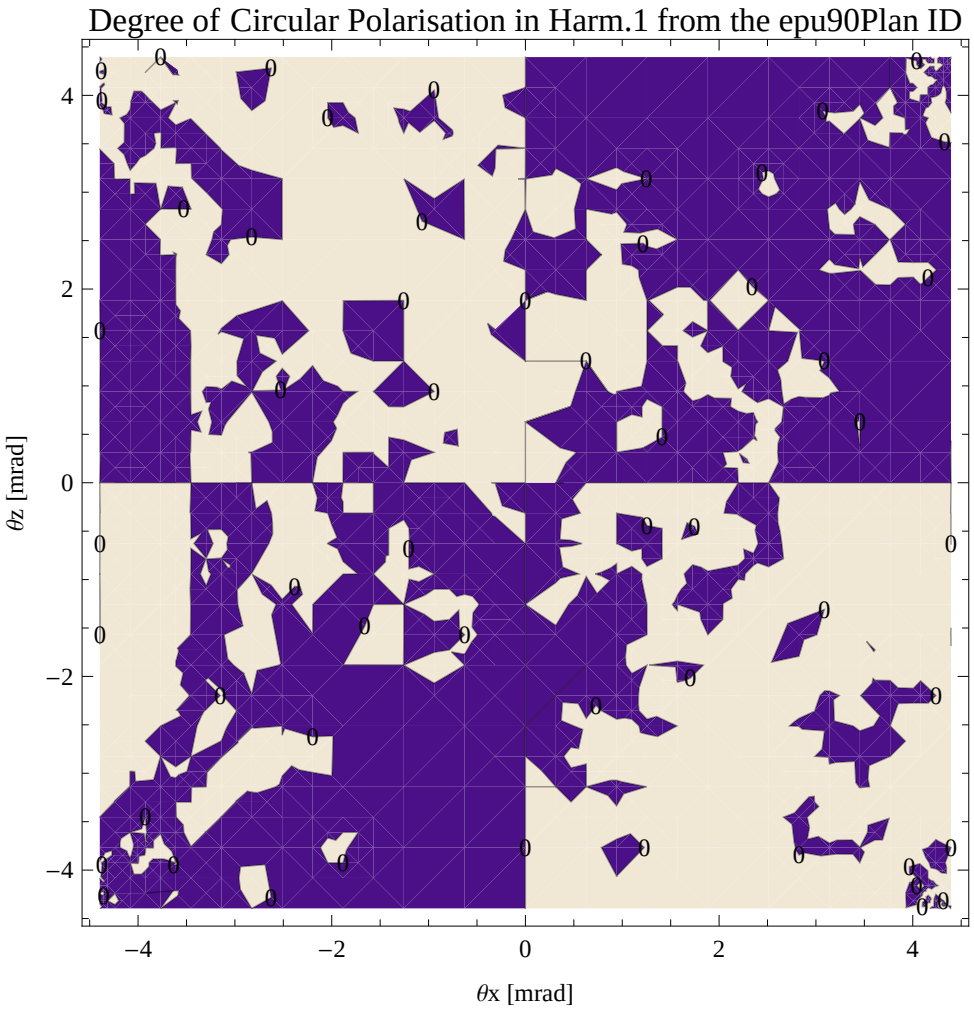

Figure 110: Map of circular polarisation in the fundamental harmonic of the synchotron radiation emitted by the epu90Plan

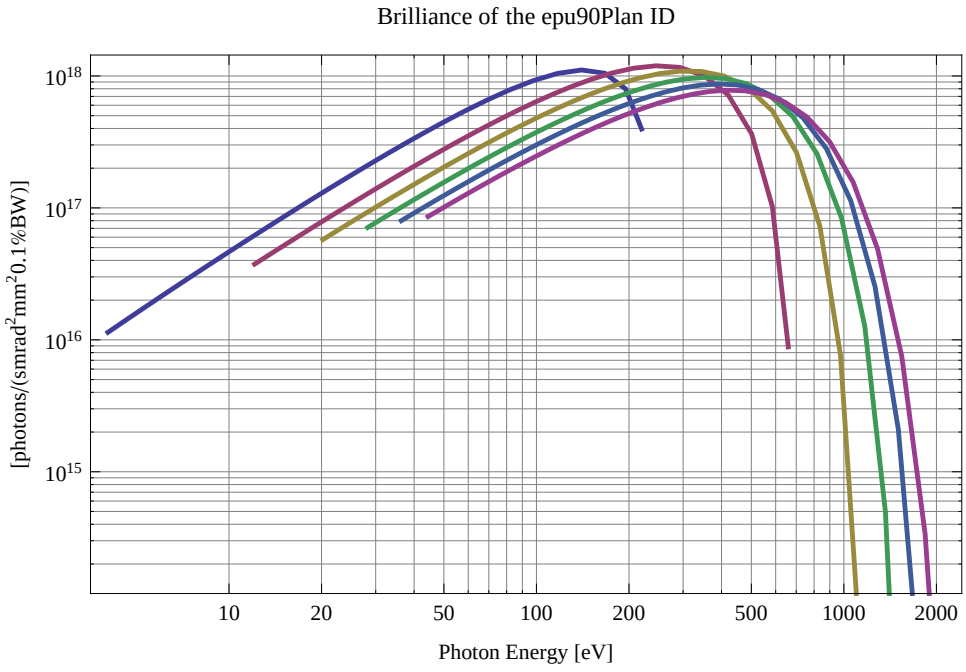

Figure 111: The brilliance at peak energy of the synchotron radiation emitted by the epu90Plan

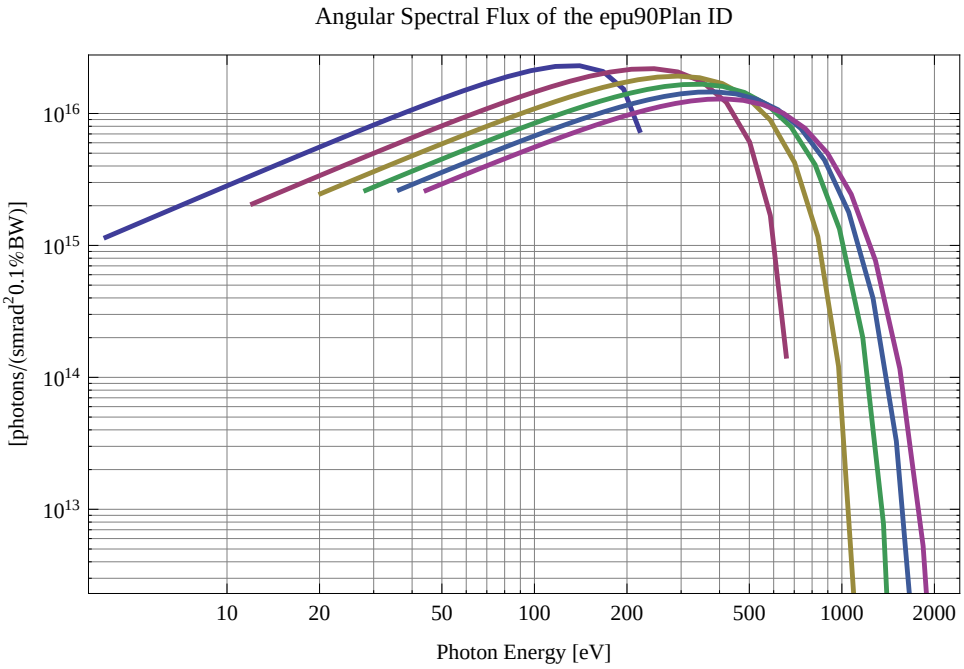

Figure 112: The angular spectral flux of the synchotron radiation emitted by the epu90Plan

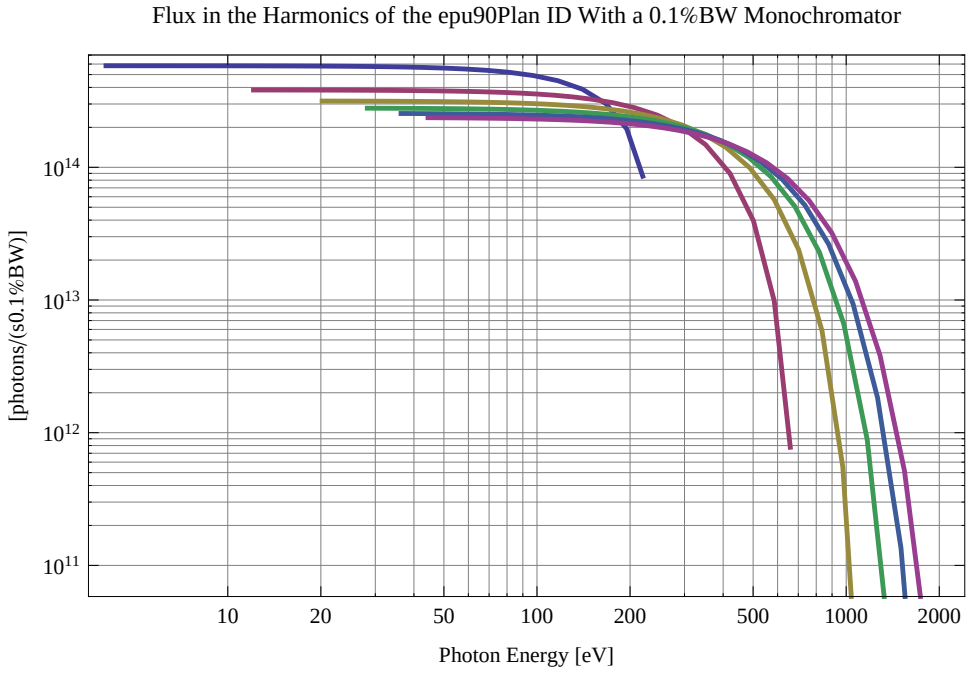

Figure 113: The flux of photons in the harmonics of the emitted synchrotron radiation from the epu90Plan using a 0.1%BW monochromator

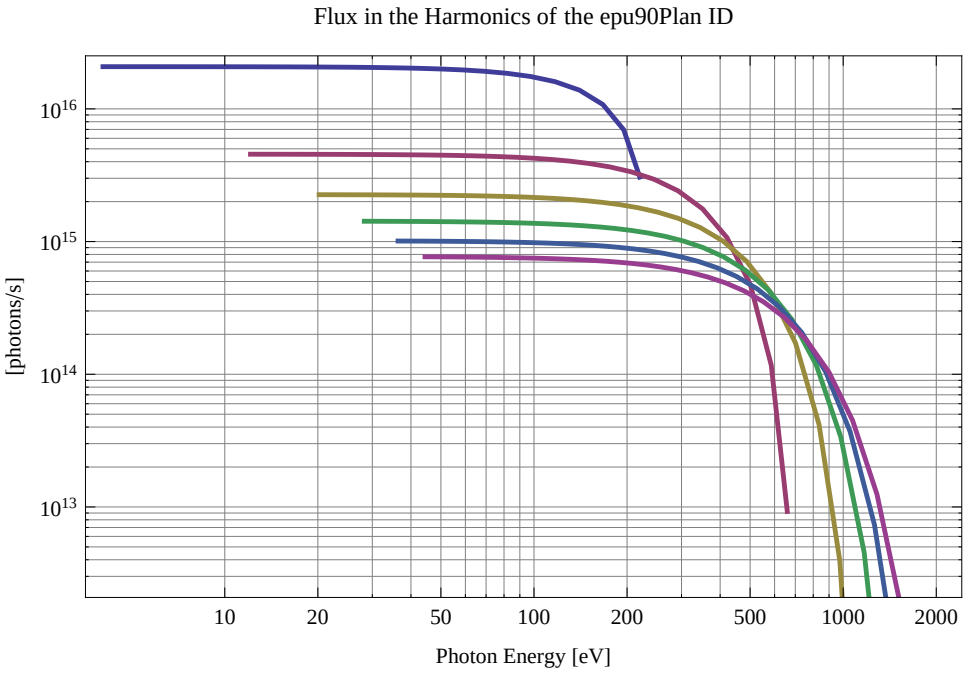

Figure 114: The flux of photons in the harmonics of the emitted synchrotron radiation from the epu90Plan

Figure 115: The power in the harmonics of the emitted synchrotron radiation from the epu90Plan

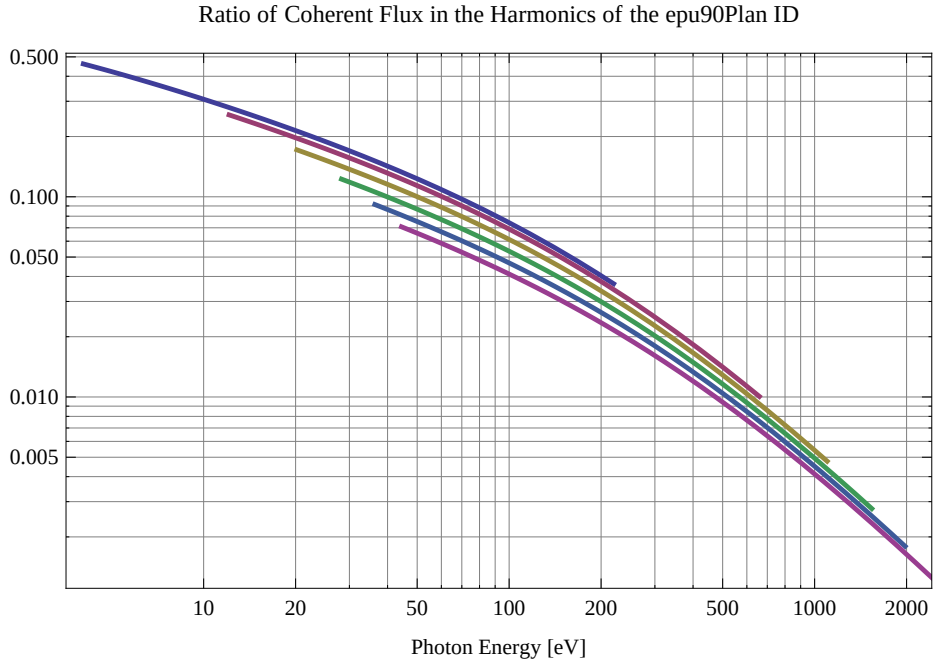

Figure 116: The ratio of coherent flux in the harmonics of the emitted synchrotron radiation from the epu90Plan

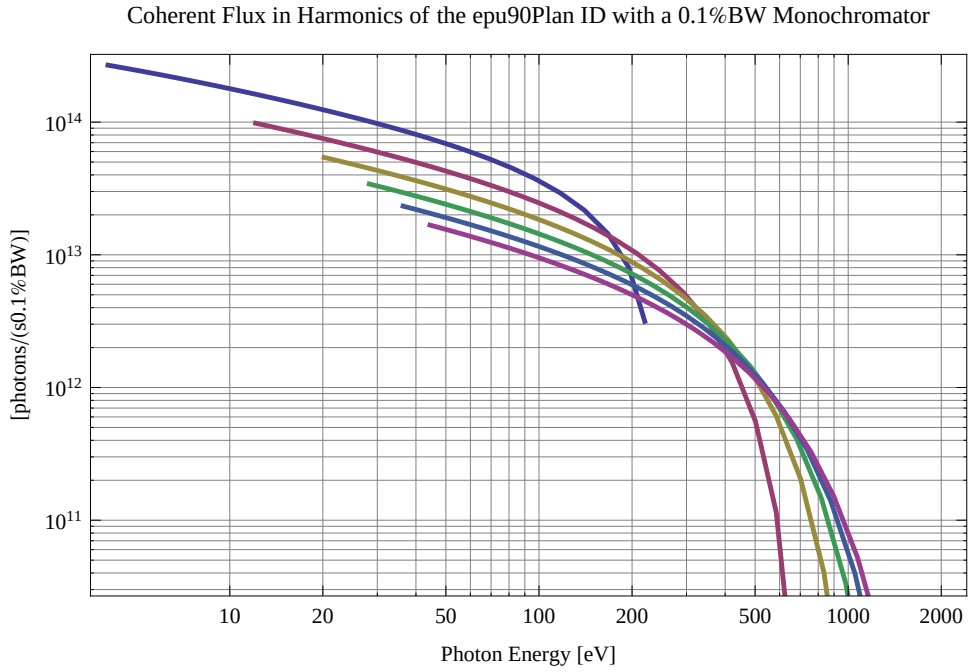

Figure 117: The coherent flux in the harmonics of the epu90Plan using a 0.1%BW Monochromator

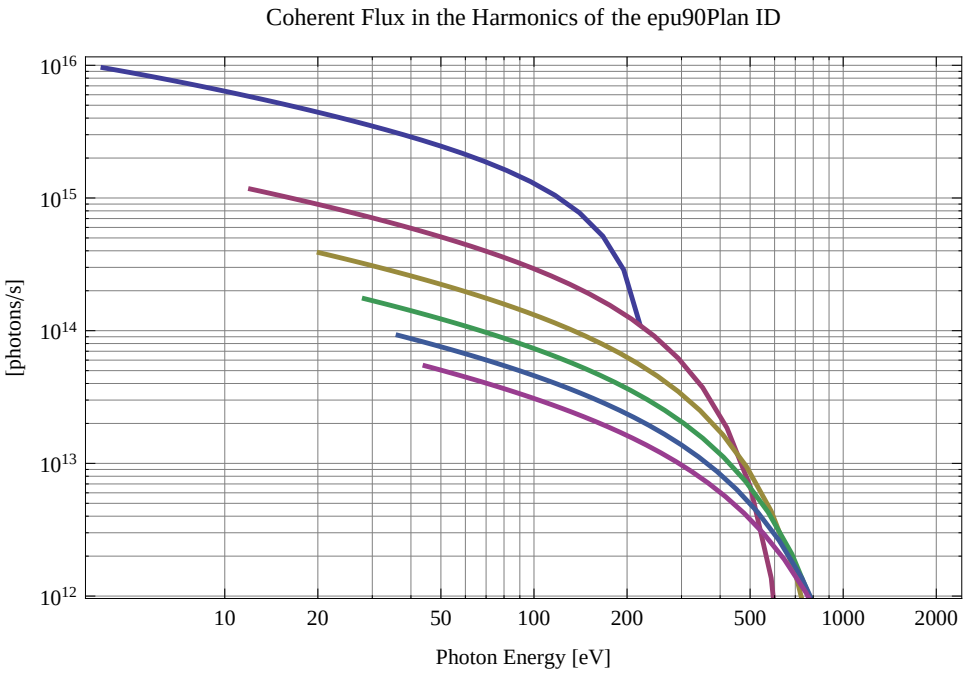

Figure 118: The coherent flux in the harmonics of the epu90Plan

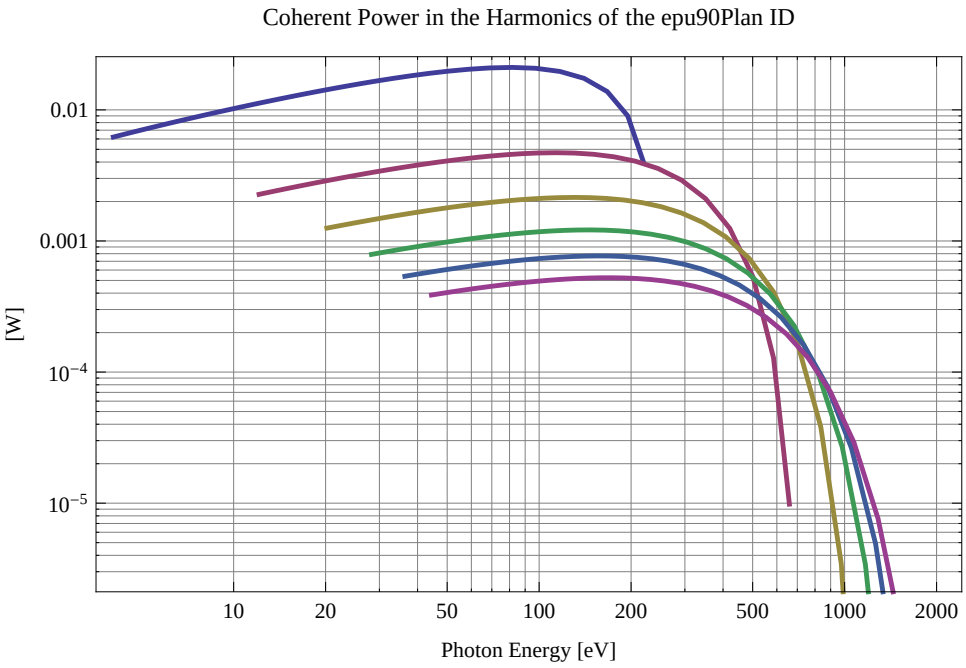

Figure 119: The power of coherent synchrotron radiation in the harmonics of the epu90Plan

The brilliance at peak energy and the angular spectral flux density from the epu90Plan for different harmonics at maximum K-value (10.751) are given in Table 19 and for minimum K-value (0.400) these values are given in Table 20.

Table 19: The brilliance at peak energy and the angular spectral flux density from the epu90Plan for different harmonics at maximum K-value (10.751)

Harmonic	Photon Energy [eV]	Brilliance [Ph./(smrad^{2}mrad^{2}0.1%BW)]	Angular Spectral Flux [Ph./(smrad^{2}0.1%BW)]
1	4.03793	1.14×10^{16}	1.15×10^{15}
3	12.1138	3.75×10^{16}	2.07×10^{15}
5	20.1897	5.75×10^{16}	2.47×10^{15}
7	28.2655	7.11×10^{16}	2.61×10^{15}
9	36.3414	$8. \times 10^{16}$	2.64×10^{15}
11	44.4173	8.6×10^{16}	2.61×10^{15}

Table 20: The brilliance at peak energy and the angular spectral flux density from the epu90Plan for different harmonics at minimum K-value (0.4)

Harmonic	Photon Energy [eV]	Brilliance [Ph./(smrad^{2}mrad^{2}0.1%BW)]	Angular Spectral Flux [Ph./(smrad^{2}0.1%BW)]
1	219.824	3.96×10^{17}	7.43×10^{15}
3	659.472	8.84×10^{15}	1.45×10^{14}
5	1099.12	1.15×10^{14}	1.83×10^{12}
7	1538.77	1.3×10^{12}	2.05×10^{10}
9	1978.42	1.4×10^{10}	2.2×10^{8}
11	2418.06	1.47×10^{8}	2.3×10^{6}

3.5 Influence from the epu90Plan on the optics of the stored beam

Figure 120 shows the focusing potential from the epu90Plan over the beam stay clear aperture of the ring aparture.

Figure 121 shows the kick map in the beam energy independant unit T^2m^2 of the kicks induced by the epu90Plan over the beam stay clear aparture.

Figure 122 shows the induced angular kick on the stored beam from the epu90Plan as a function of the vertical distance to the undulator axis.

Figure 123 shows the induced angular kick on the stored beam from the epu90Plan as a function of the horizontal distance to the undulator axis.

Figure 124 shows tune shift induced by the epu90Plan over the beam stay clear aparture. Note that the tune shift depends on the beam size at the.

Figure 125 shows the induced tune shift from the epu90Plan as a function of the vertical distance to the undulator axis.

Figure 126 shows the induced tune shift from the epu90Plan as a function of the horizontal distance to the undulator axis.

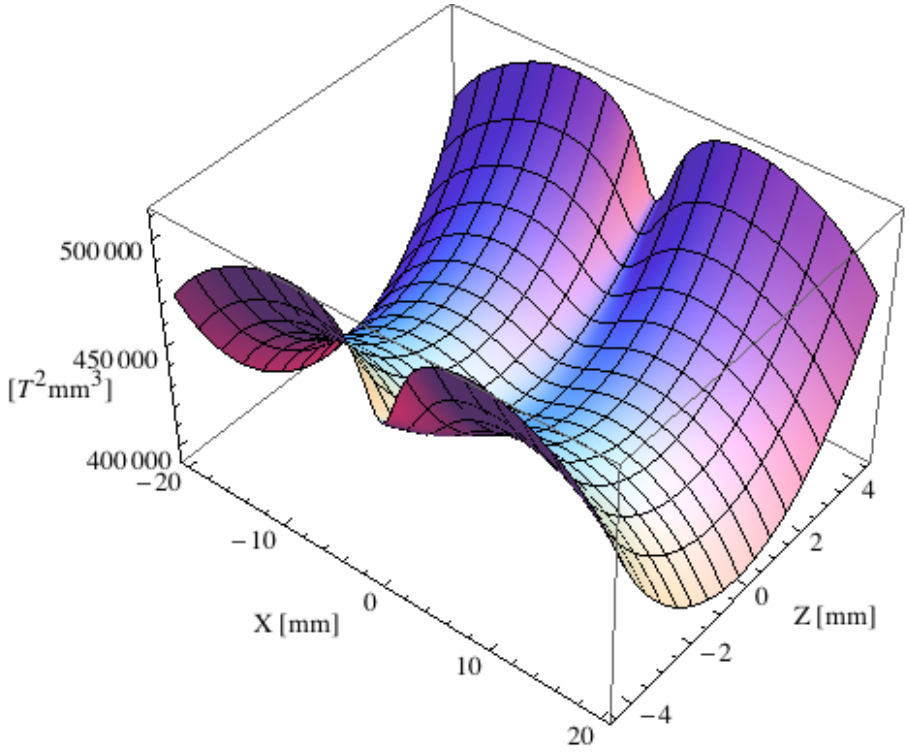

Figure 120: Focusing potential from the epu90Plan over the beam stay clear aparture.

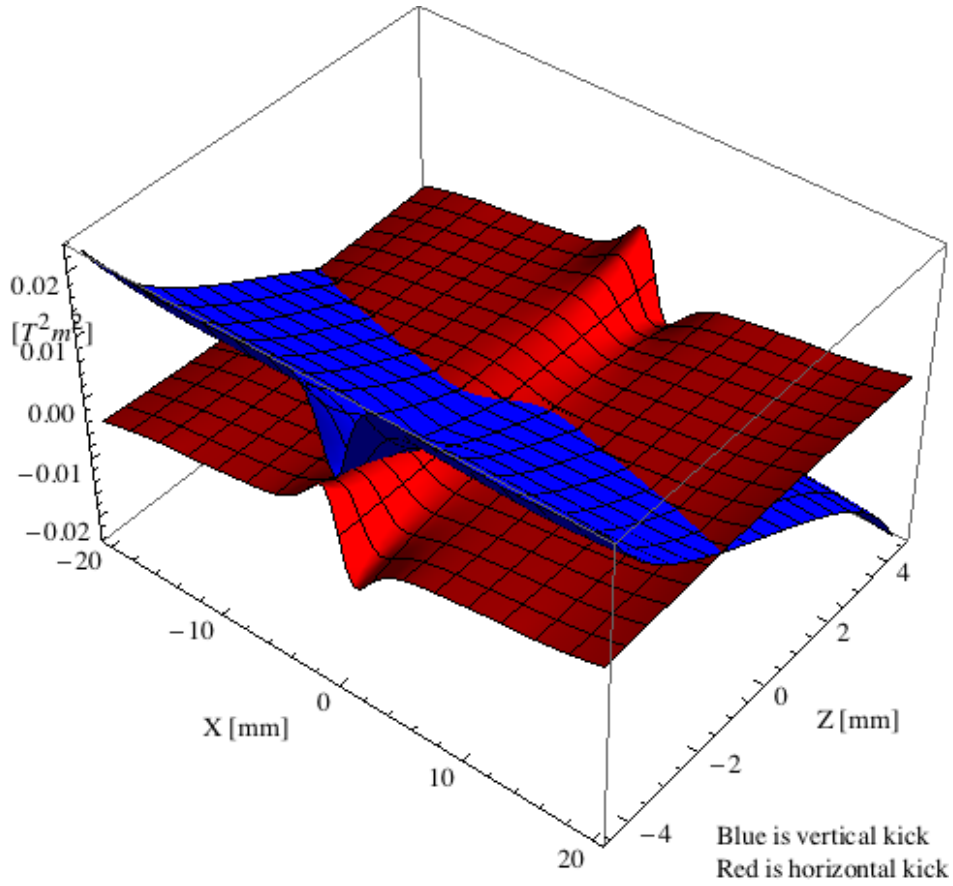

Figure 121: Kick map in the beam energy independant unit T^2m^2 of the kicks induced by the epu90Plan over the beam stay clear aparture.

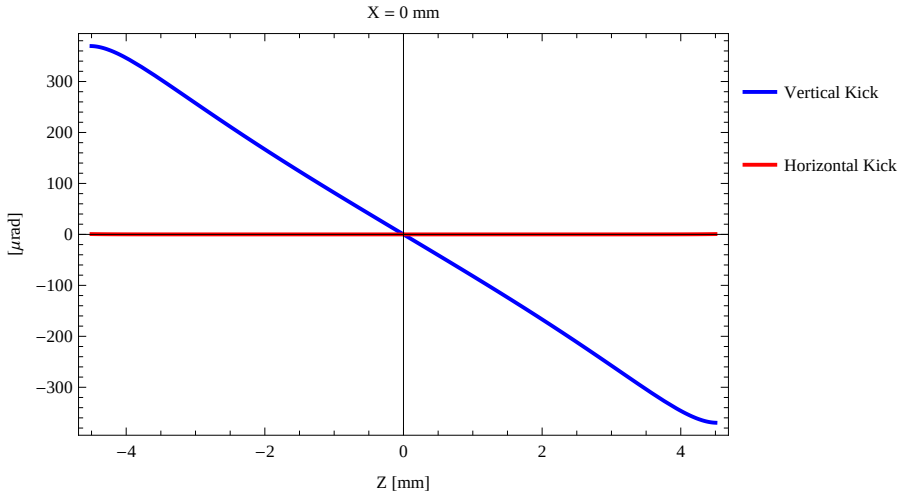

Figure 122: Induced angular kick on the stored beam from the epu90Plan as a function of the vertical distance to the undulator axis.

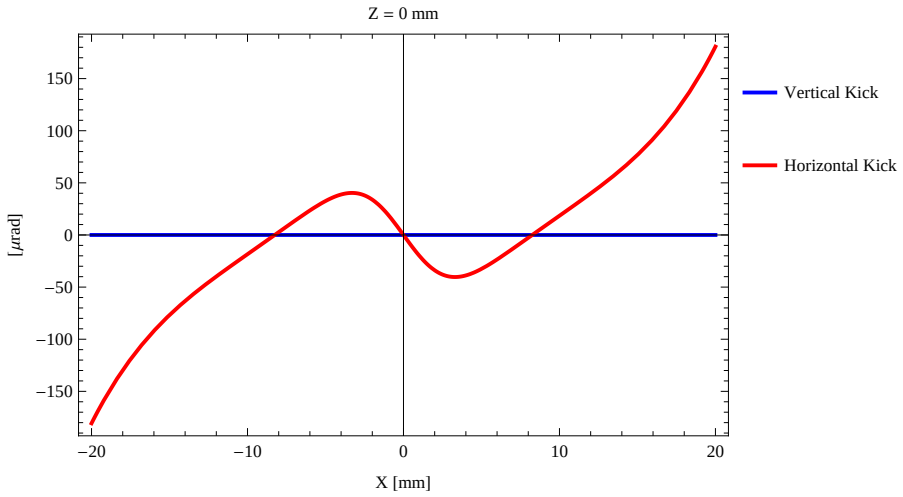

Figure 123: Induced angular kick on the stored beam from the epu90Plan as a function of the horizontal distance to the undulator axis.

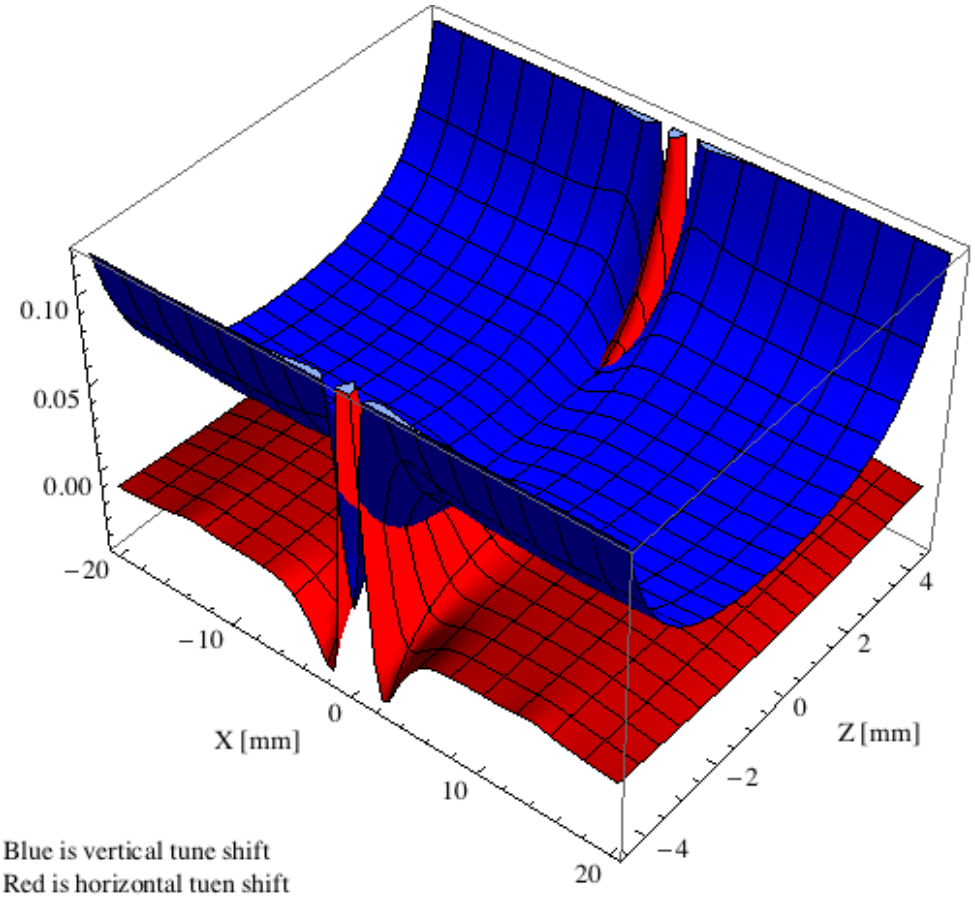

Figure 124: Tune shift induced by the epu90Plan over the beam stay clear aparture.

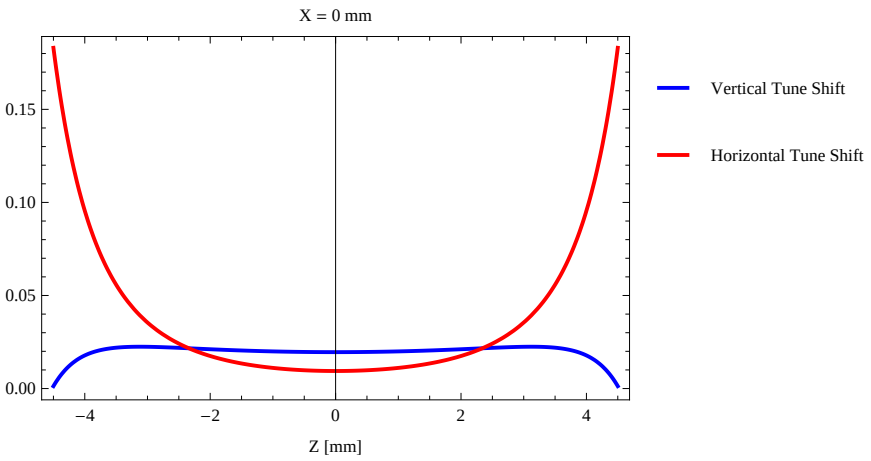

Figure 125: Induced tune shift from the epu90Plan as a function of the vertical distance to the undulator axis.

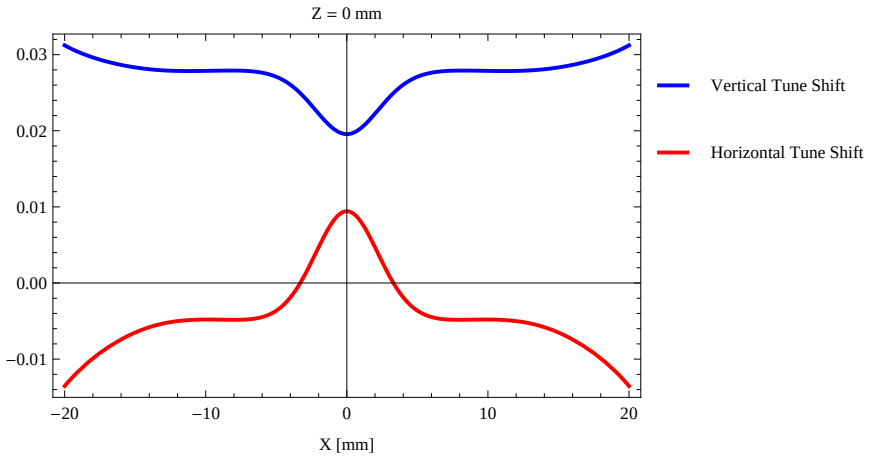

Figure 126: Induced tune shift from the epu90Plan on the stored beam from the as a function of the horizontal distance to the undulator axis.

3.6 Magnet model of the elliptically polarizing undulator epu90Heli

The Radia [2] magnet model of the epu90Heli is shown in Figure 127. The length of the magnet model is 739.68 mm. The magnetic material in the model is NdFeb with a remanence of 1.33 T. Blocks with vertical magnetisation are blue and blocks with horizontal magnetisation are yellow. The block size is 35.x35.x22.5 mm^3 and there is a 5. mm cut-out in two of the corners of the blocks. The total length of the epu90Heli is 2539.68 mm.

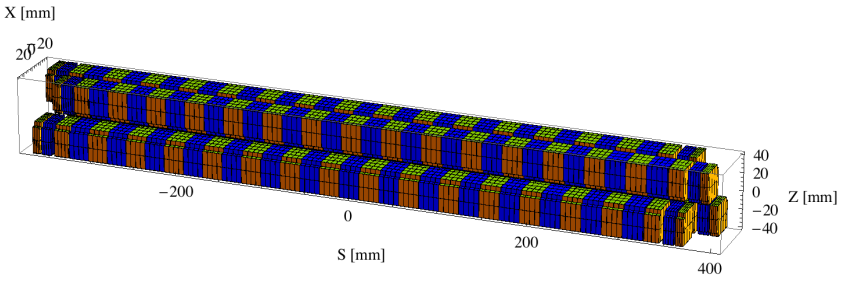

Figure 127: Magnetic model of the epu90Heli. The has been modelled with Radia [2]

3.7 Analysis of the magnetic field of the epu90Heli

The effective magnetic fields on axis and the fundamental photon energy of the epu90Heli are shown in Table 21. The higher harmonic contents in the magnetic field of an elliptically polarizing undulator made of permanent magnets is usually small and the effective field has approximately the same strength as the peak field.

3.8 Synchrotron radiation from the epu90Heli

The power map of the emitted synchrotron radiation by the epu90Heli, assuming a 0.3 A filament beam with an energy of 1.5 GeV and undulator properties of the synchrotron radiation, is shown in Figure 132. The on-axis power density is 0.000104 $kW/mrad^2$

Table 21: Effective Fields on axis and Fundamental Photon Energy of the epu90Heli

Undulator Period	90	mm
Undulator Gap	13	mm
Undulator Mode	Helical	
Undulator Phase	25.071	mm
Vertical Peak Field	0.824	T
effective Vertical Field	0.814	T
Kx (from vert. field)	6.842	
Horizontal Peak Field:	0.828	T
effective Horizontal Field	0.814	T
Kz (from hor. field)	6.842	
Photon Energy, Harm.1	0.005	keV
Emitted Power	1.437	kW
Total Length	2539.7	mm

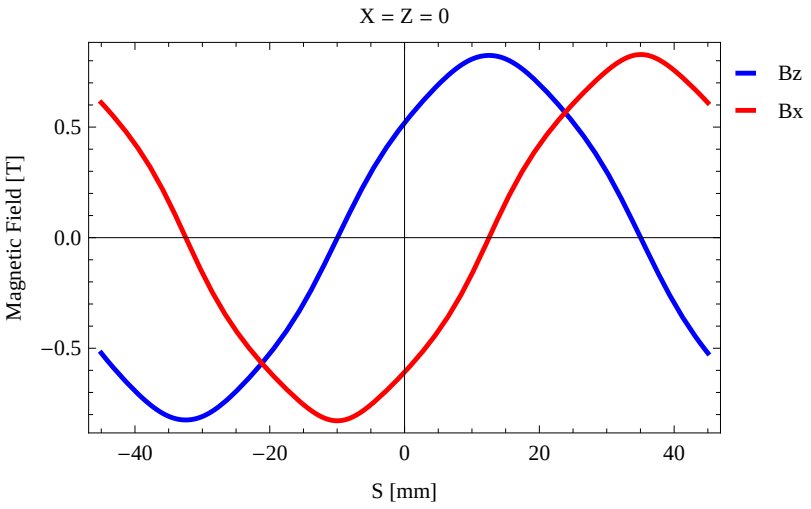

Figure 128: Vertical magnetic field in a central pole of the epu90Heli along the axis, X = Z = 0

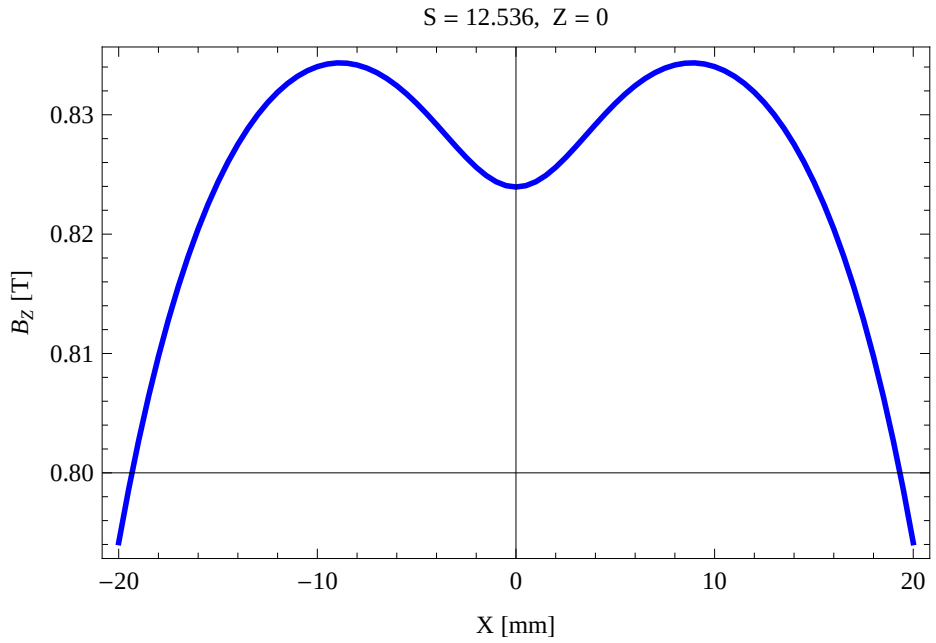

Figure 129: Vertical magnetic field in a central pole of the epu90Heli along the horizontally transverse direction to the axis, S = 12.536, Z = 0

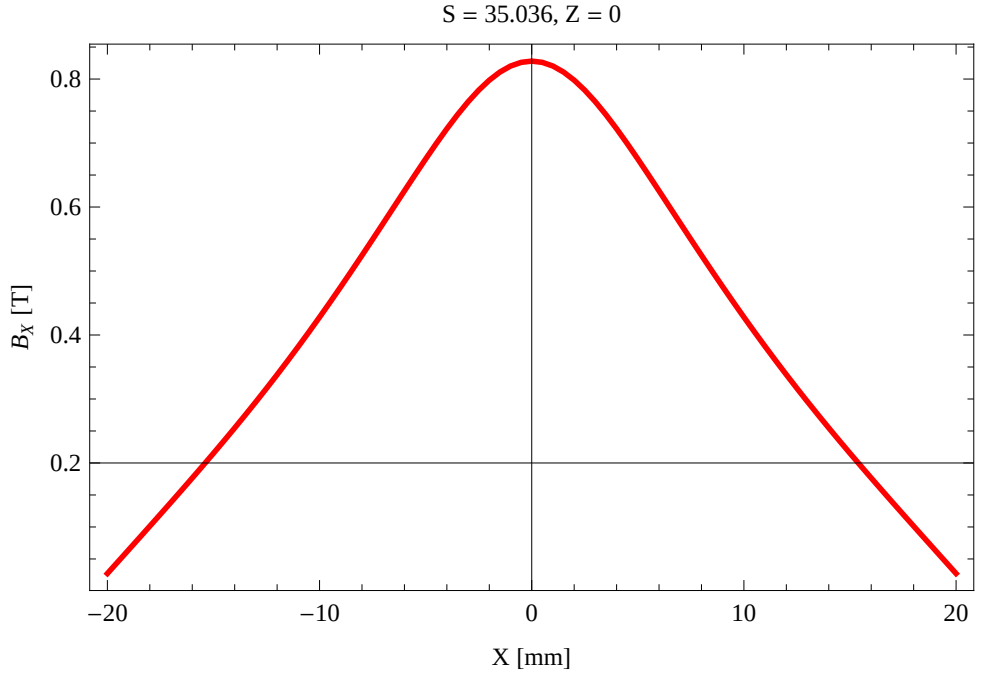

Figure 130: Horizontal magnetic field in a central pole of the epu90Heli along the horizontally transverse direction to the axis, S = 35.036, Z = 0

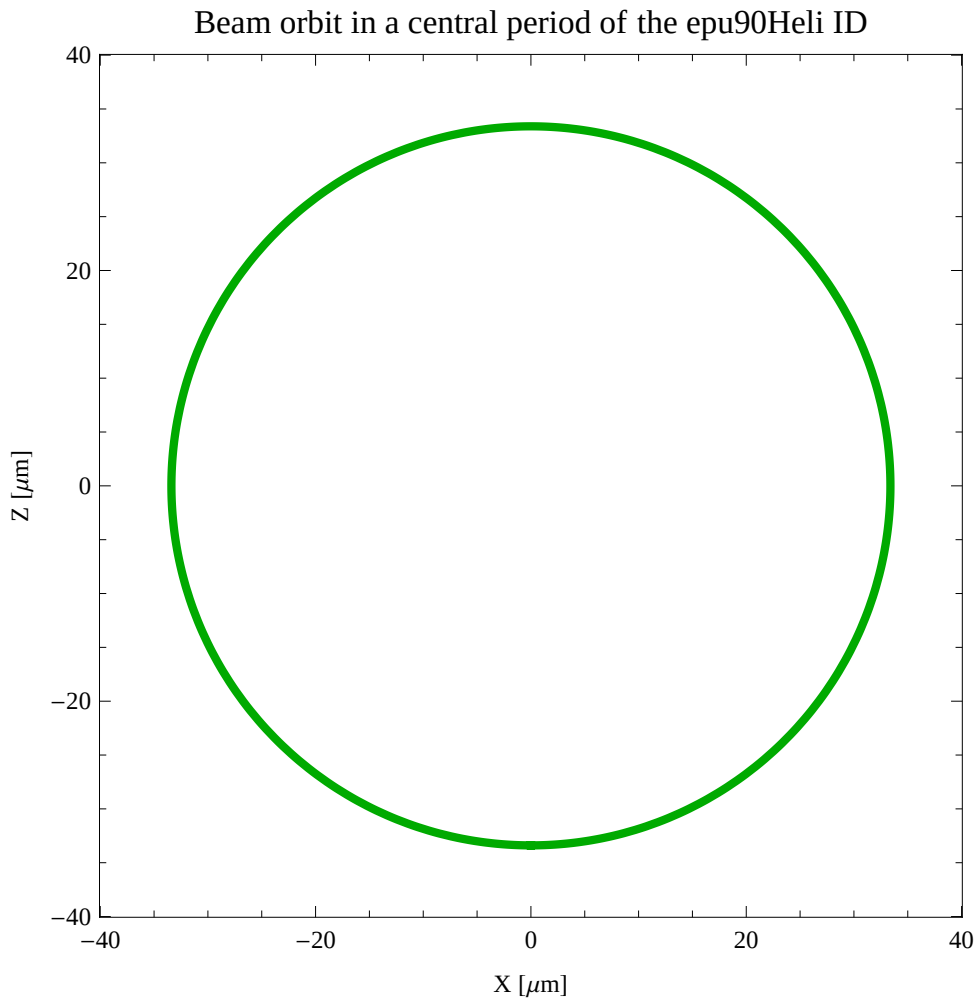

Figure 131: The beam orbit of the electron beam through a central period of the epu90Heli

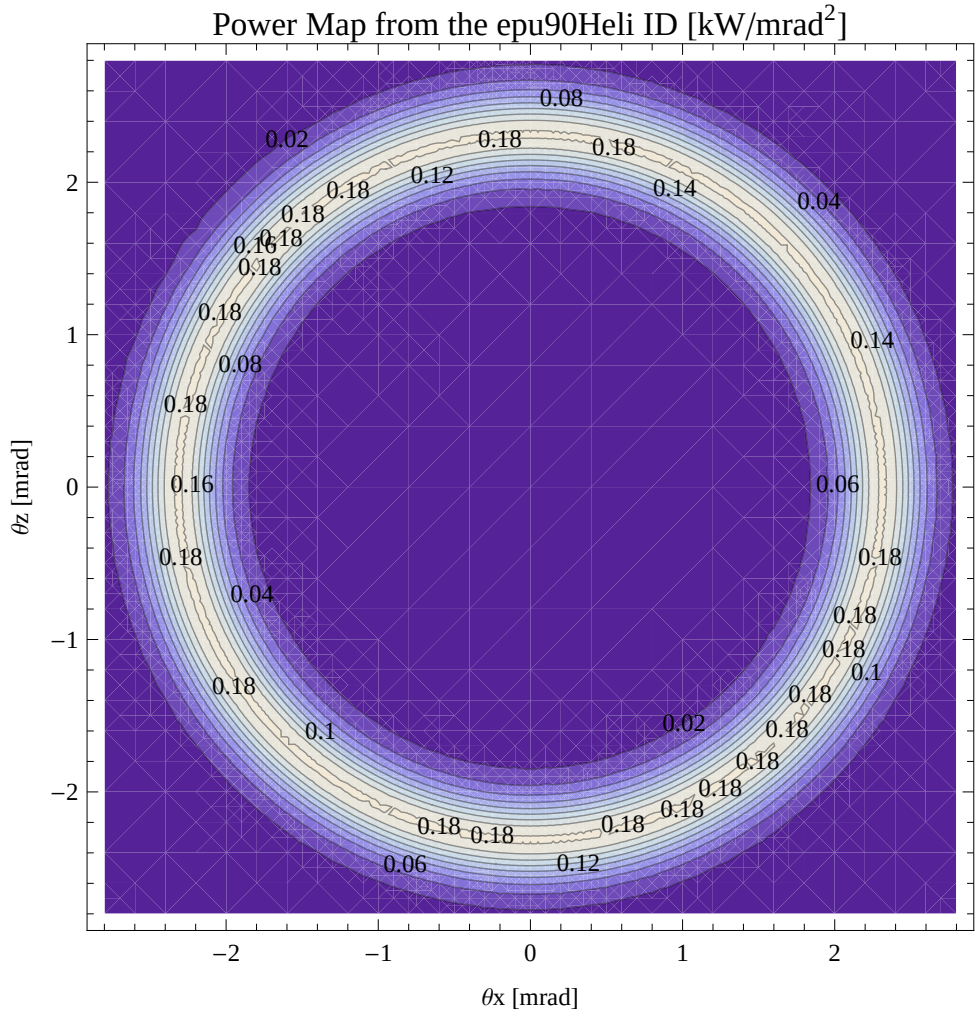

Figure 132: Map of the power distribution of the emitted synchrotron radiation by the epu90Heli

A map of the degree of linear polarisation of the fundamental harmonic of the synchotron radiation emitted by the epu90Heli over the angle of observation is shown in Figure 133.

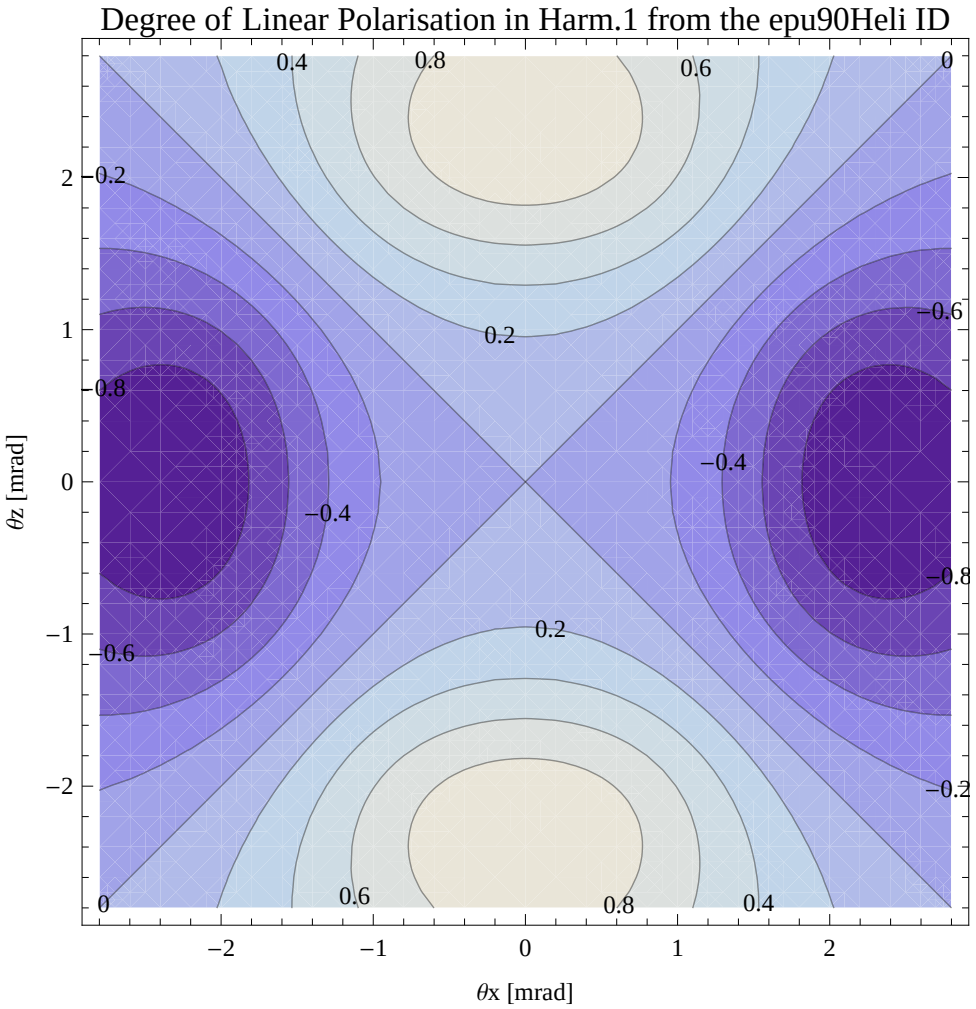

Figure 133: Map of linear polarisation in the fundamental harmonic of the synchotron radiation emitted by the epu90Heli

A map of the degree of 45 degree polarisation of the fundamental harmonic of the synchotron radiation emitted by the epu90Heli over the angle of observation is shown in Figure 134.

A map of the degree of circular polarisation of the fundamental harmonic of the synchotron radiation emitted by the epu90Heli over the angle of observation is shown in Figure 135.

The on axis brilliance at peak energy and the angular spectral flux from the epu90Heli have been calculated with the given beam parameters, which are 0.3 A of stored current, $\beta_H = 5.627$ m, $\varepsilon_H = 5.985$ nmrad, $\beta_V = 2.837$ m, $\varepsilon_V = 59.85$ pmrad, and an energy spread of 0.001.

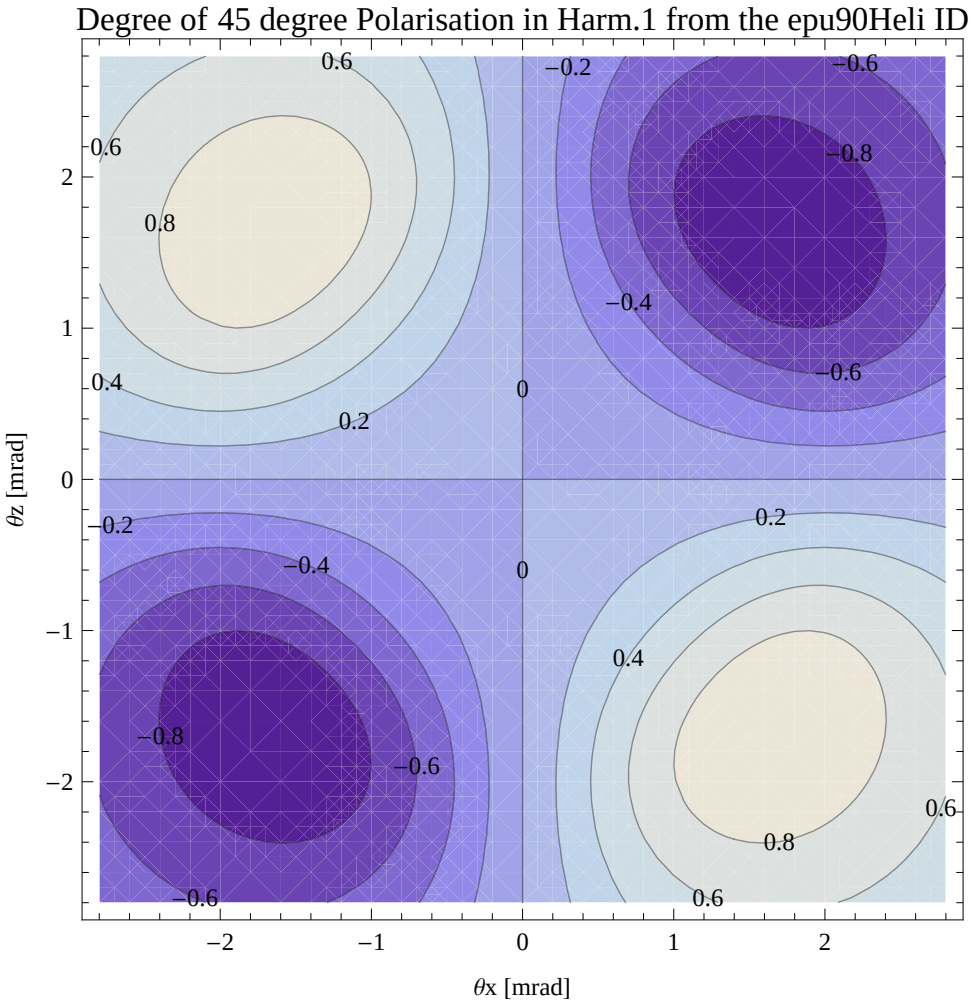

Figure 134: Map of 45 degree polarisation in the fundamental harmonic of the synchotron radiation emitted by the epu90Heli

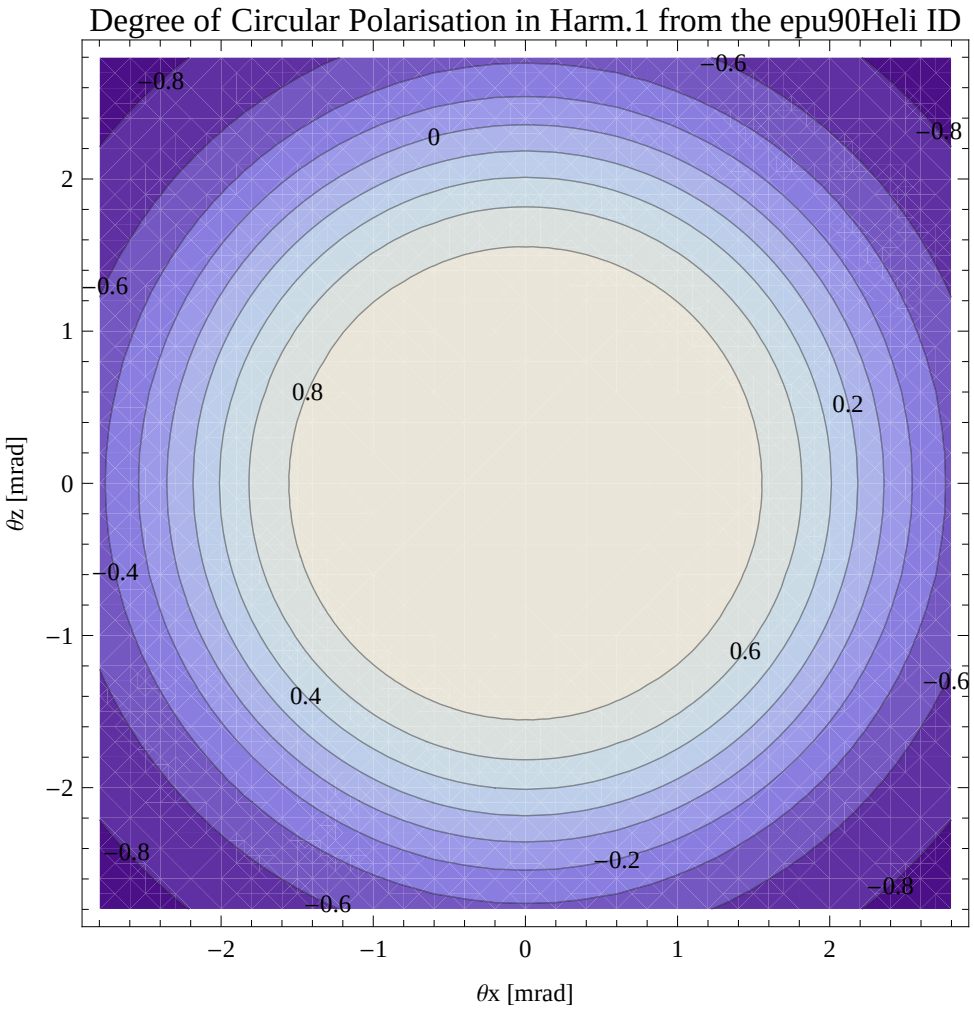

Figure 135: Map of circular polarisation in the fundamental harmonic of the synchotron radiation emitted by the epu90Heli

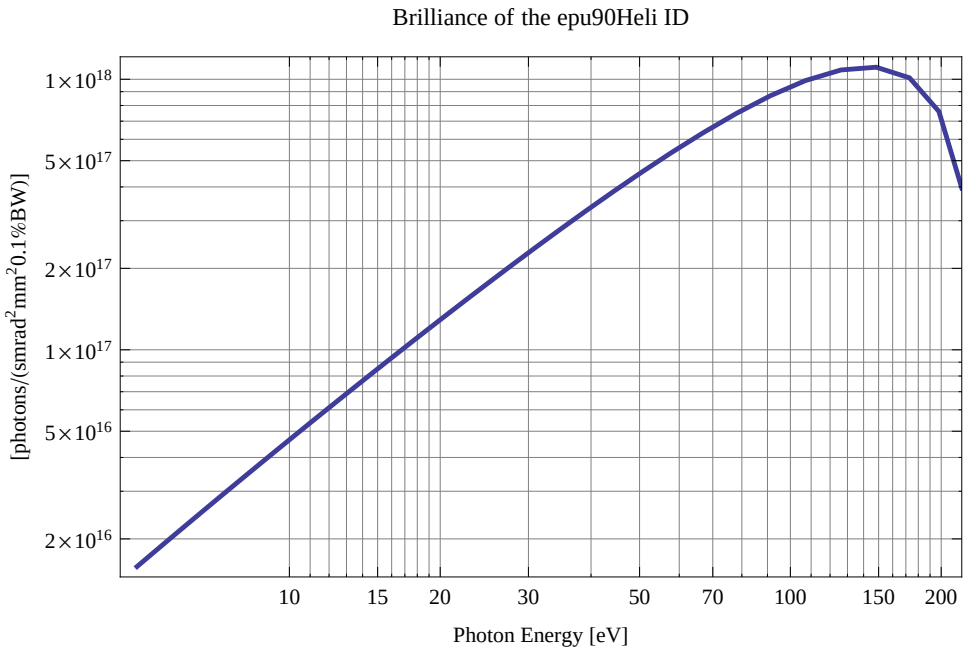

Figure 136: The brilliance at peak energy of the synchotron radiation emitted by the epu90Heli

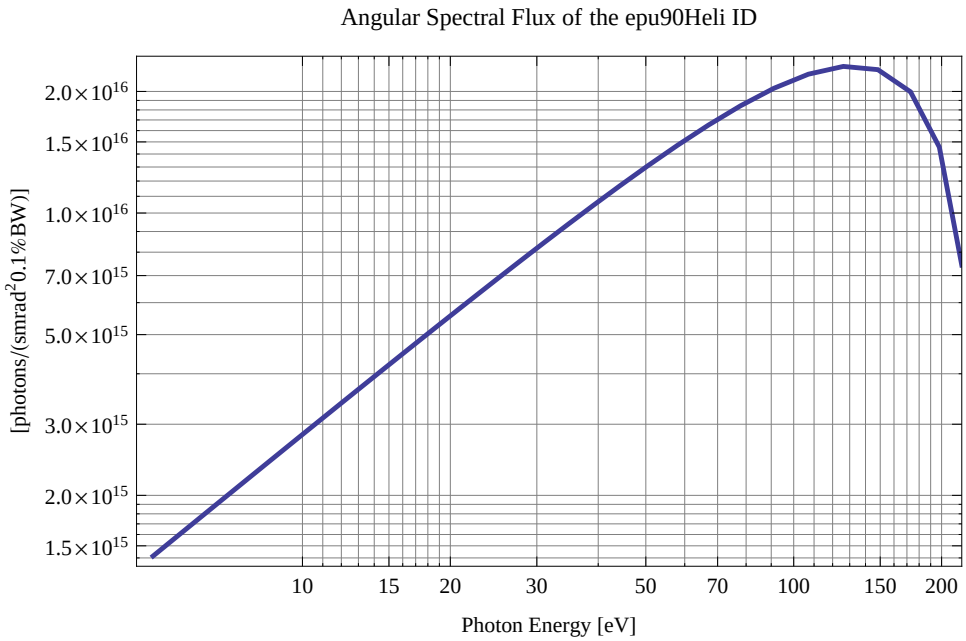

Figure 137: The angular spectral flux of the synchotron radiation emitted by the epu90Heli

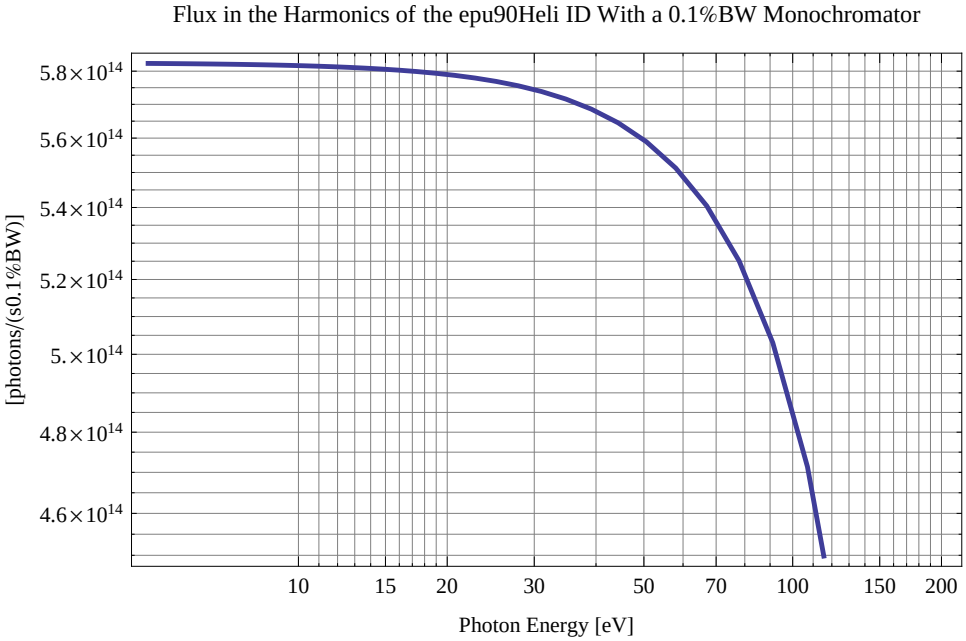

Figure 138: The flux of photons in the harmonics of the emitted synchrotron radiation from the epu90Heli using a 0.1%BW monochromator

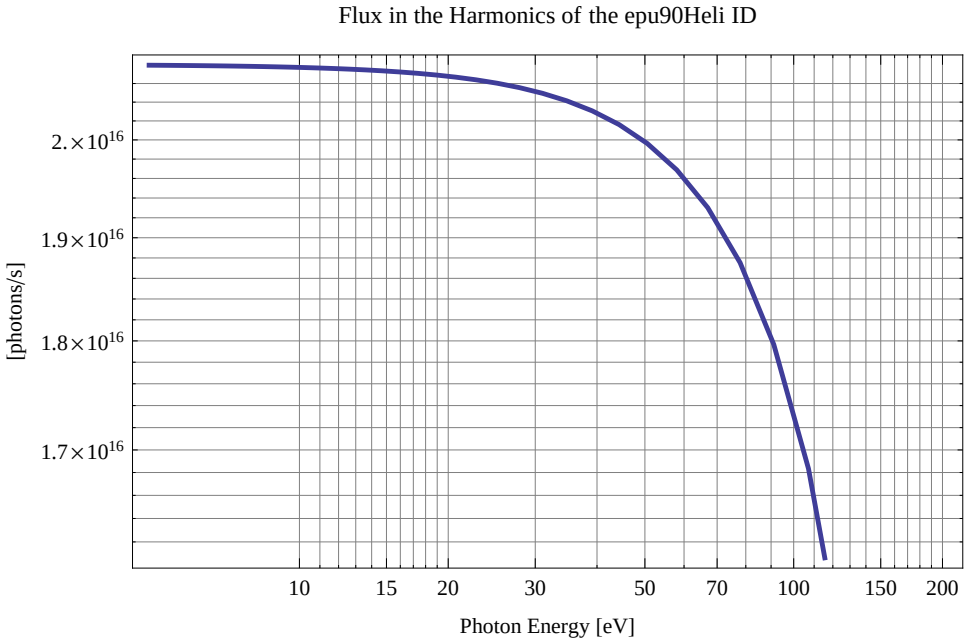

Figure 139: The flux of photons in the harmonics of the emitted synchrotron radiation from the epu90Heli

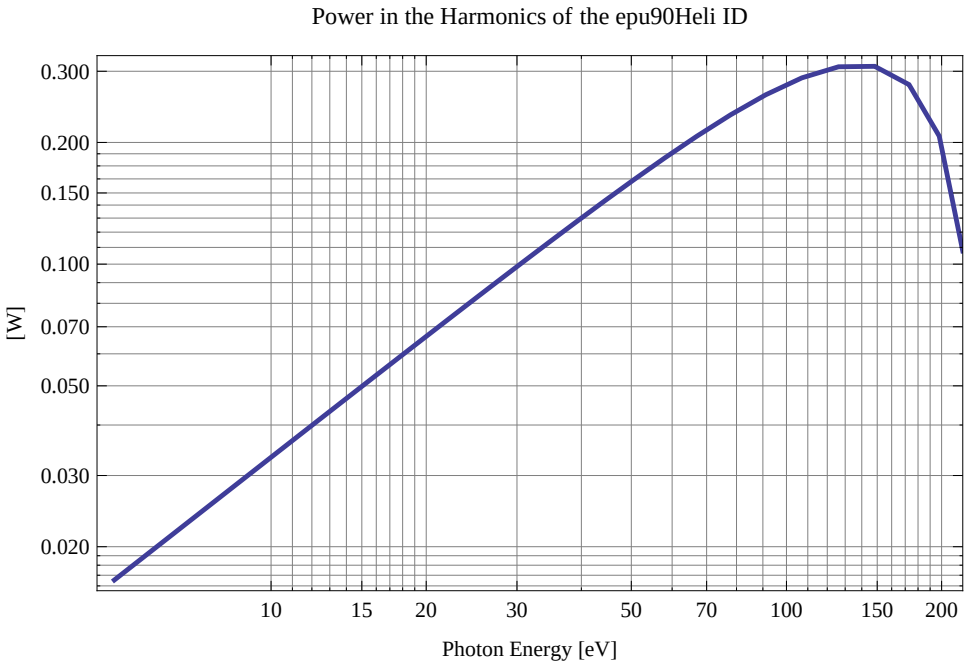

Figure 140: The power in the harmonics of the emitted synchrotron radiation from the epu90Heli

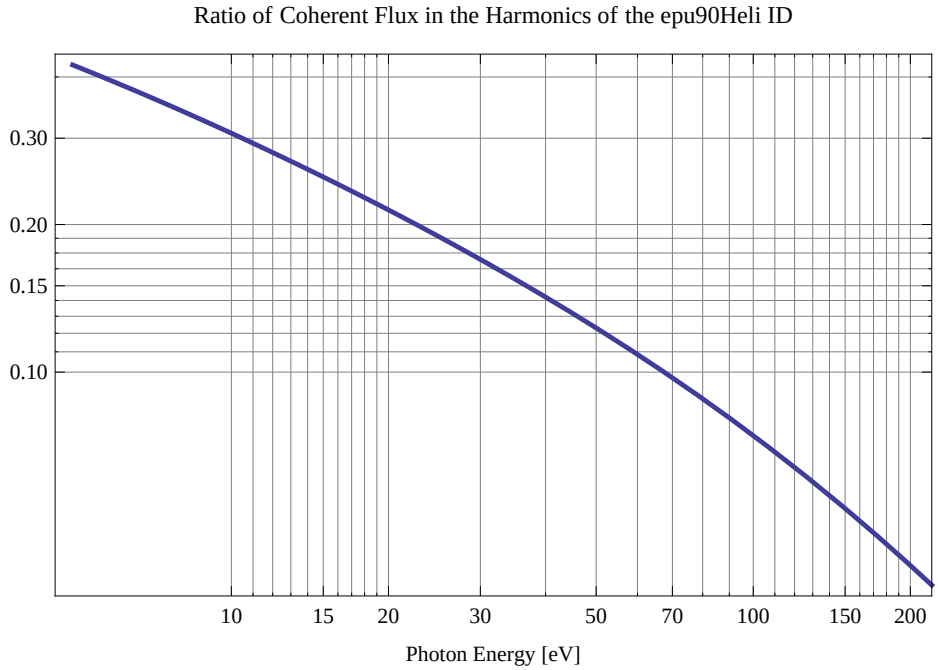

Figure 141: The ratio of coherent flux in the harmonics of the emitted synchrotron radiation from the epu90Heli

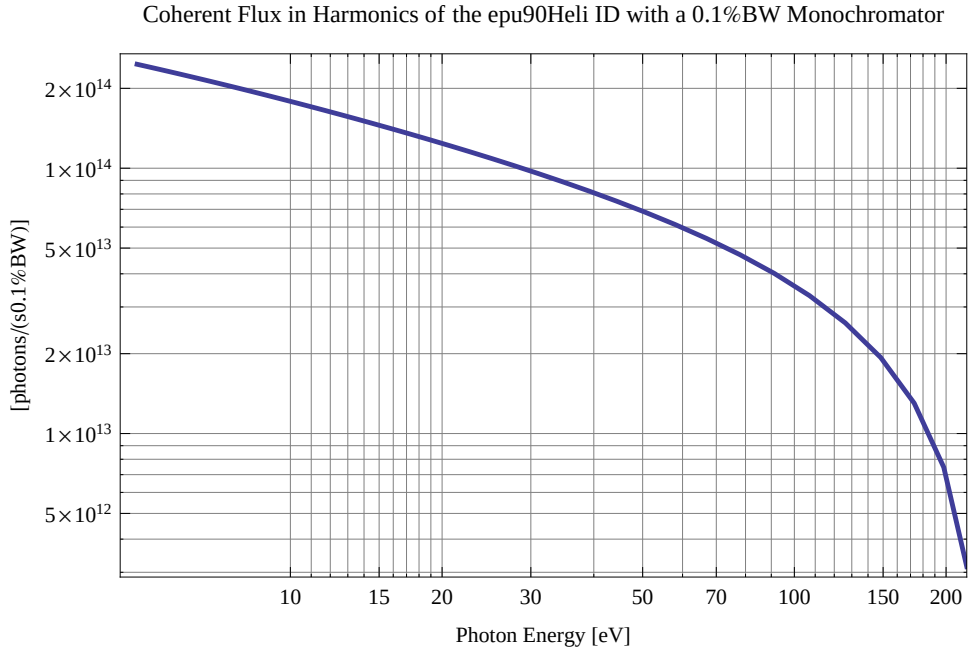

Figure 142: The coherent flux in the harmonics of the epu90Heli using a 0.1%BW Monochromator

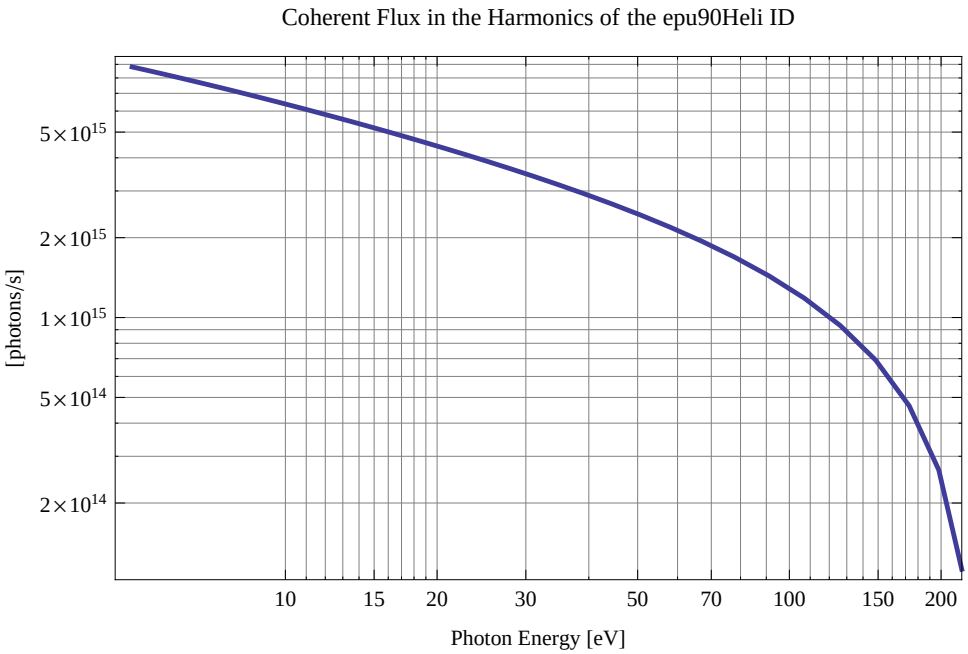

Figure 143: The coherent flux in the harmonics of the epu90Heli

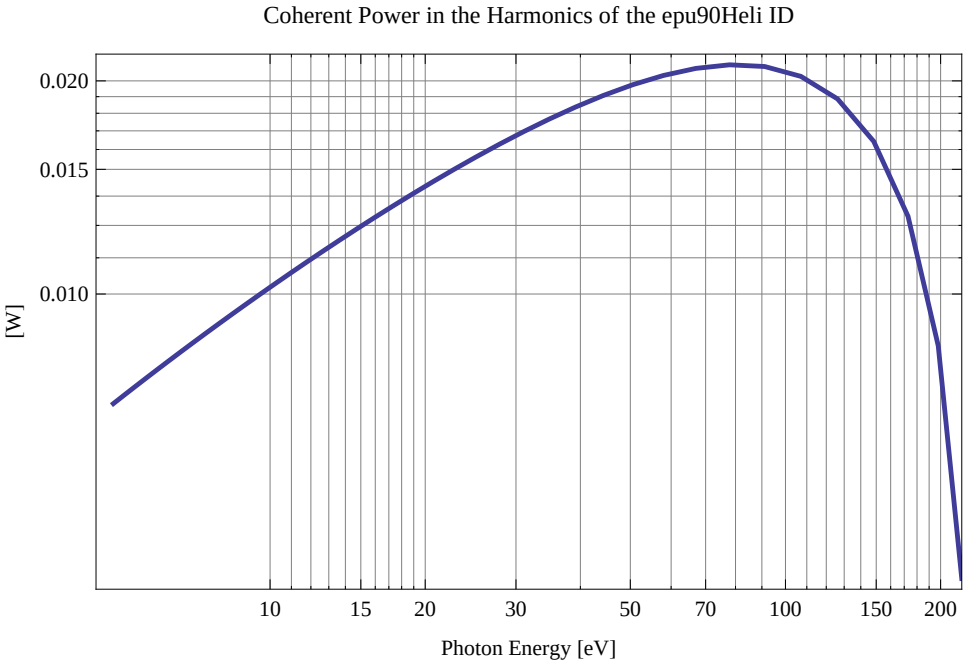

Figure 144: The power of coherent synchrotron radiation in the harmonics of the epu90Heli

The brilliance at peak energy and the angular spectral flux density from the epu90Heli for different harmonics at maximum K-value (9.677) are given in Table 22 and for minimum K-value (0.400) these values are given in Table 23.

Table 22: The brilliance at peak energy and the angular spectral flux density from the epu90Heli for different harmonics at maximum K-value (9.677)

Harmonic	Photon Energy [eV]	Brilliance [Ph./(smrad^{2}mrad^{2}0.1%BW)]	Angular Spectral Flux [Ph./(smrad^{2}0.1%BW)]
1	4.9647	1.58×10^{16}	1.41×10^{15}

Table 23: The brilliance at peak energy and the angular spectral flux density from the epu90Heli for different harmonics at minimum K-value (0.4)

Harmonic	Photon Energy [eV]	Brilliance [Ph./(smrad^{2}mrad^{2}0.1%BW)]	Angular Spectral Flux [Ph./(smrad^{2}0.1%BW)]
1	219.824	3.96×10^{17}	7.43×10^{15}

3.9 Influence from the epu90Heli on the optics of the stored beam

Figure 145 shows the focusing potential from the epu90Heli over the beam stay clear aperture of the ring aparture.

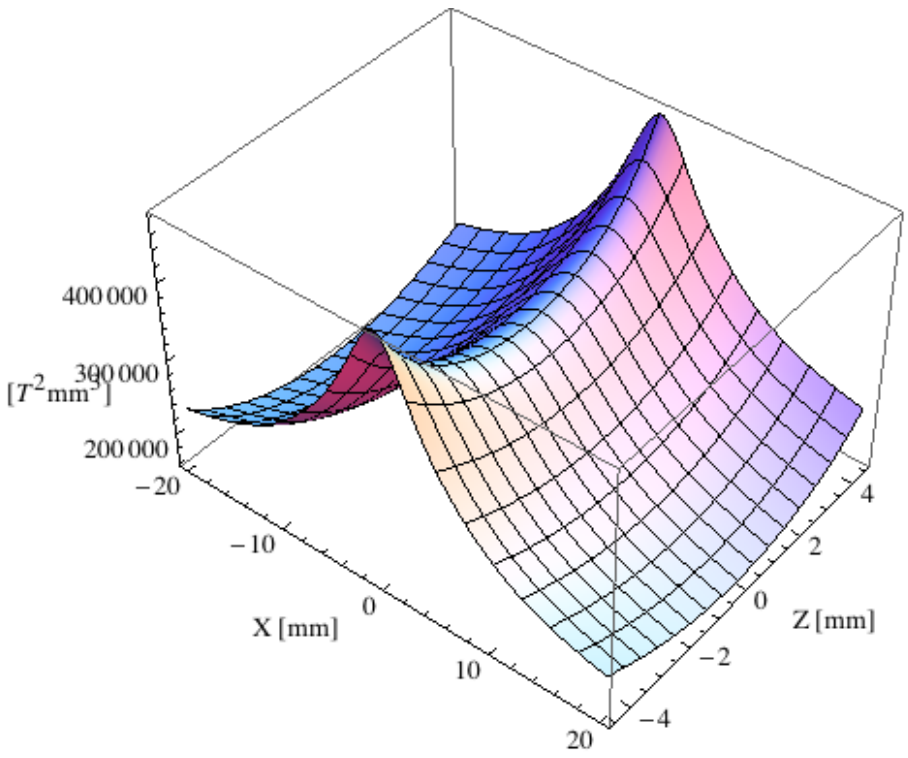

Figure 145: Focusing potential from the epu90Heli over the beam stay clear aparture.

Figure 146 shows the kick map in the beam energy independant unit T^2m^2 of the kicks induced by the epu90Heli over the beam stay clear aparture.

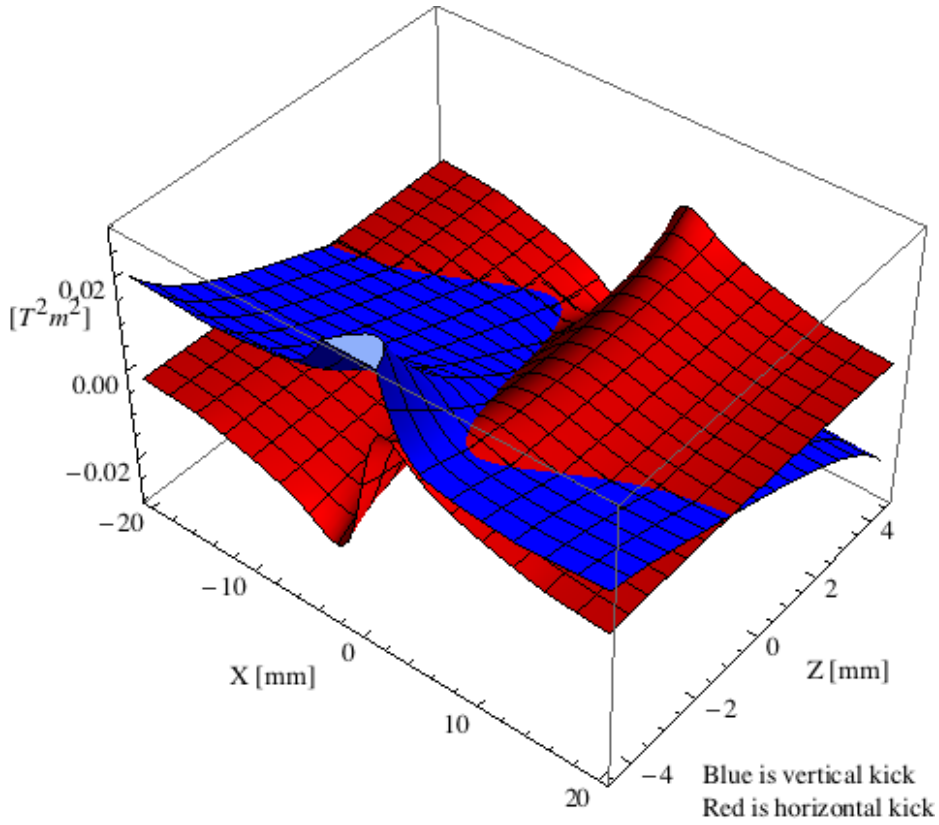

Figure 146: Kick map in the beam energy independant unit T^2m^2 of the kicks induced by the epu90Heli over the beam stay clear aparture.

Figure 147 shows the induced angular kick on the stored beam from the epu90Heli as a function of the vertical distance to the undulator axis.

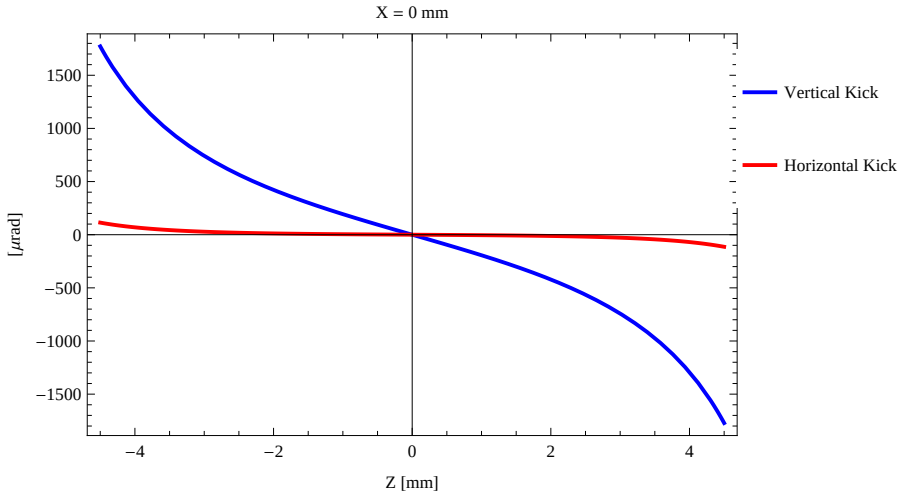

Figure 147: Induced angular kick on the stored beam from the epu90Heli as a function of the vertical distance to the undulator axis.

Figure 148 shows the induced angular kick on the stored beam from the epu90Heli as a function of the horizontal distance to the undulator axis.

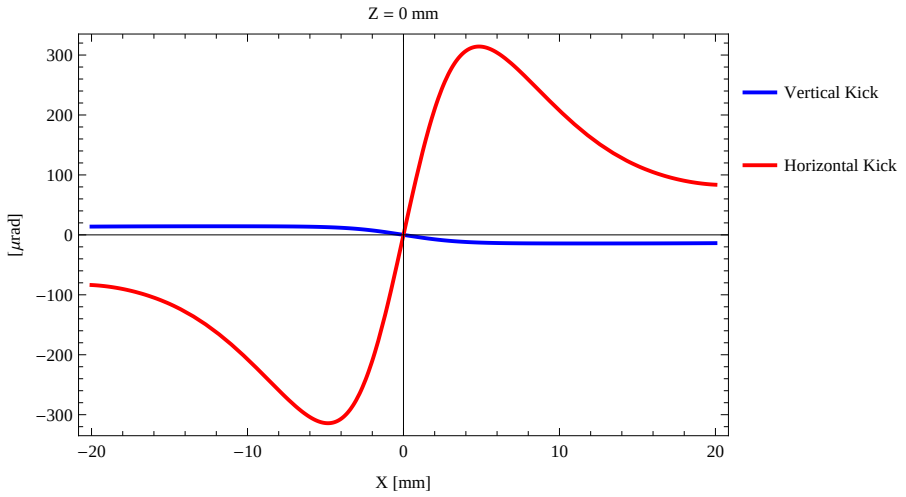

Figure 148: Induced angular kick on the stored beam from the epu90Heli as a function of the horizontal distance to the undulator axis.

Figure 149 shows tune shift induced by the epu90Heli over the beam stay clear aparture. Note that the tune shift depends on the beam size at the.

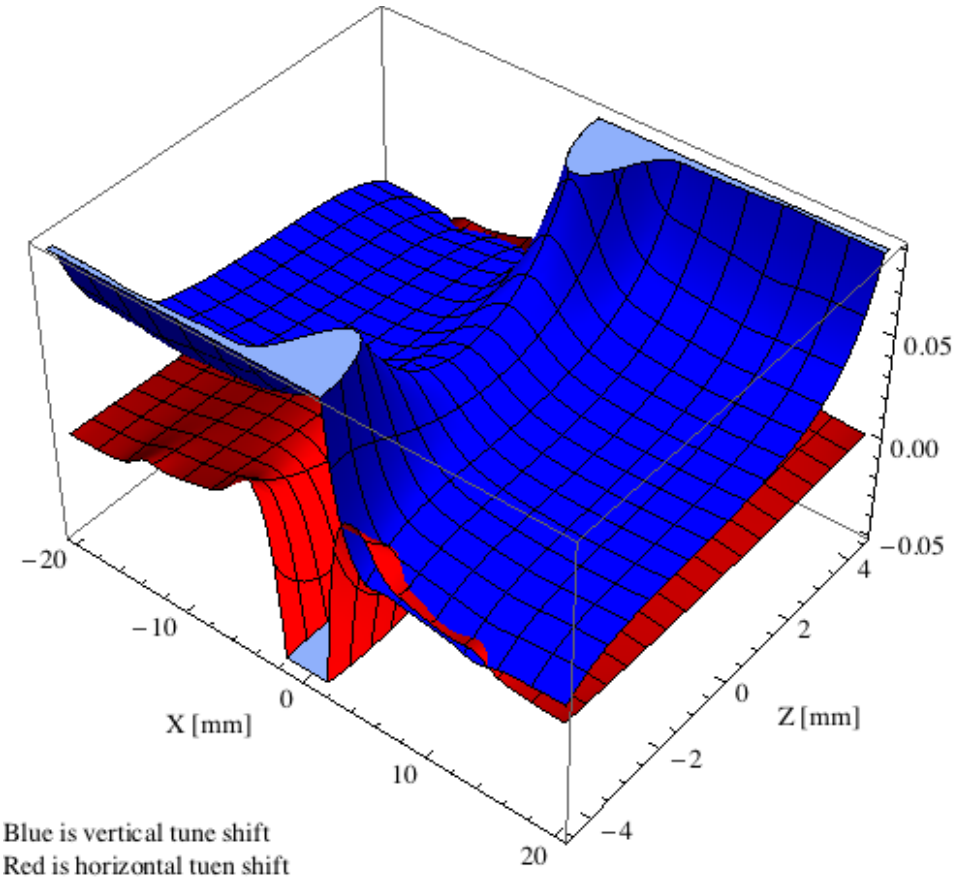

Figure 149: Tune shift induced by the epu90Heli over the beam stay clear aparture.

Figure 150 shows the induced tune shift from the epu90Heli as a function of the vertical distance to the undulator axis.

Figure 151 shows the induced tune shift from the epu90Heli as a function of the horizontal

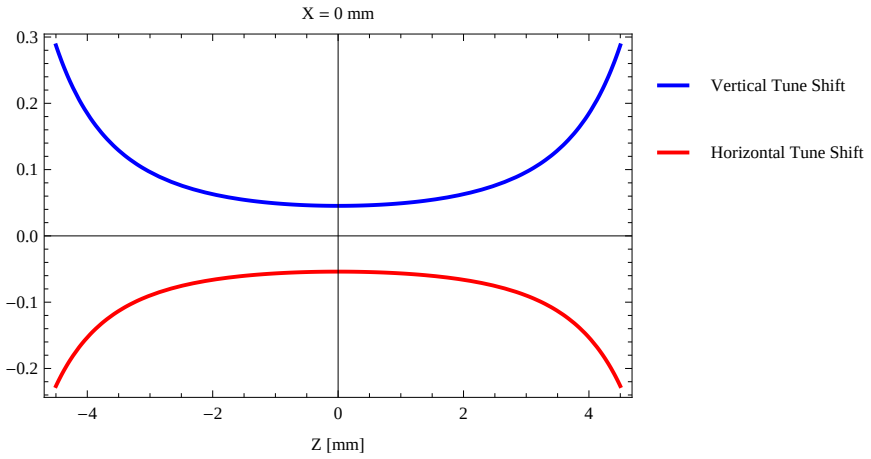

Figure 150: Induced tune shift from the epu90Heli as a function of the vertical distance to the undulator axis.

distance to the undulator axis.

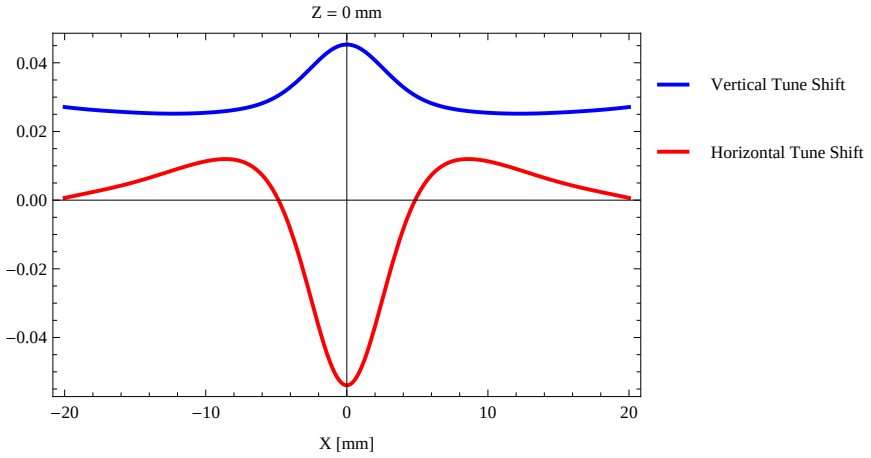

Figure 151: Induced tune shift from the epu90Heli on the stored beam from the as a function of the horizontal distance to the undulator axis.

3.10 Magnet model of the elliptically polarizing undulator epu90Incl

The Radia [2] magnet model of the epu90Incl is shown in Figure 152. The length of the magnet model is 739.68 mm. The magnetic material in the model is NdFeb with a remanence of 1.33 T. Blocks with vertical magnetisation are blue and blocks with horizontal magnetisation are yellow. The block size is 35.x35.x22.5 mm^3 and there is a 5. mm cut-out in two of the corners of the blocks. The total length of the epu90Incl is 2539.68 mm.

3.11 Analysis of the magnetic field of the epu90Incl

The effective magnetic fields on axis and the fundamental photon energy of the epu90Incl are shown in Table 24. The higher harmonic contents in the magnetic field of an elliptically polarizing undulator made of permanent magnets is usually small and the effective field has approximately the same strength as the peak field.

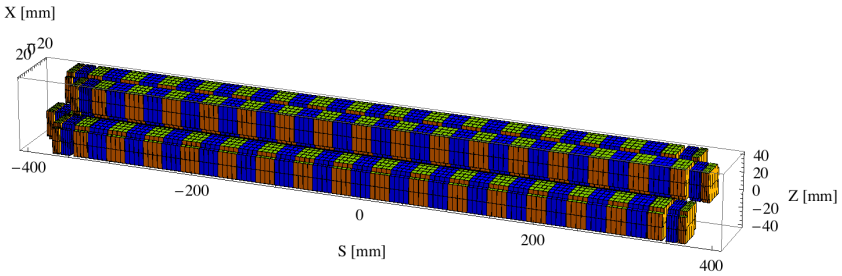

Figure 152: Magnetic model of the epu90Incl. The has been modelled with Radia [2]

Table 24: Effective Fields on axis and Fundamental Photon Energy of the epu90Incl

Undulator Period	90	mm
Undulator Gap	13	mm
Undulator Mode	Inclined	
Undulator Phase	23.807	mm
Vertical Peak Field	0.567	T
effective Vertical Field	0.577	T
Kx (from vert. field)	4.850	
Horizontal Peak Field:	−0.567	T
effective Horizontal Field	0.579	T
Kz (from hor. field)	4.867	
Photon Energy, Harm.1	0.010	keV
Emitted Power	0.725	kW
Total Length	2539.7	mm

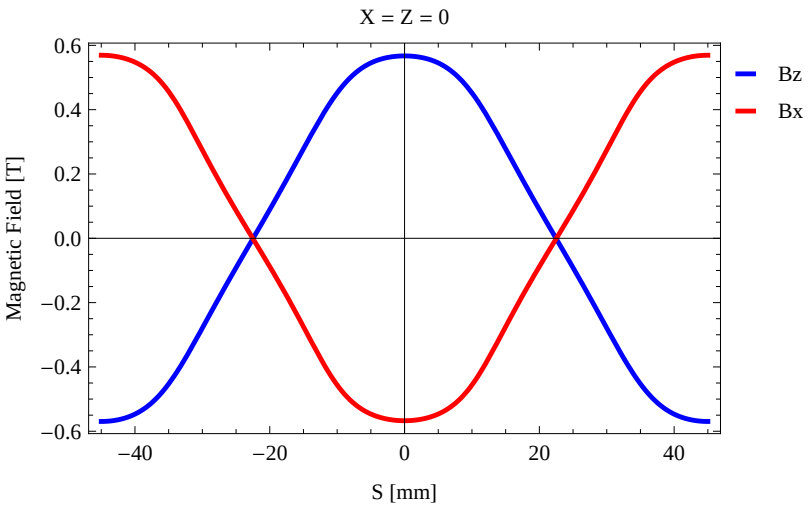

Figure 153: Vertical magnetic field in a central pole of the epu90Incl along the axis, X = Z = 0

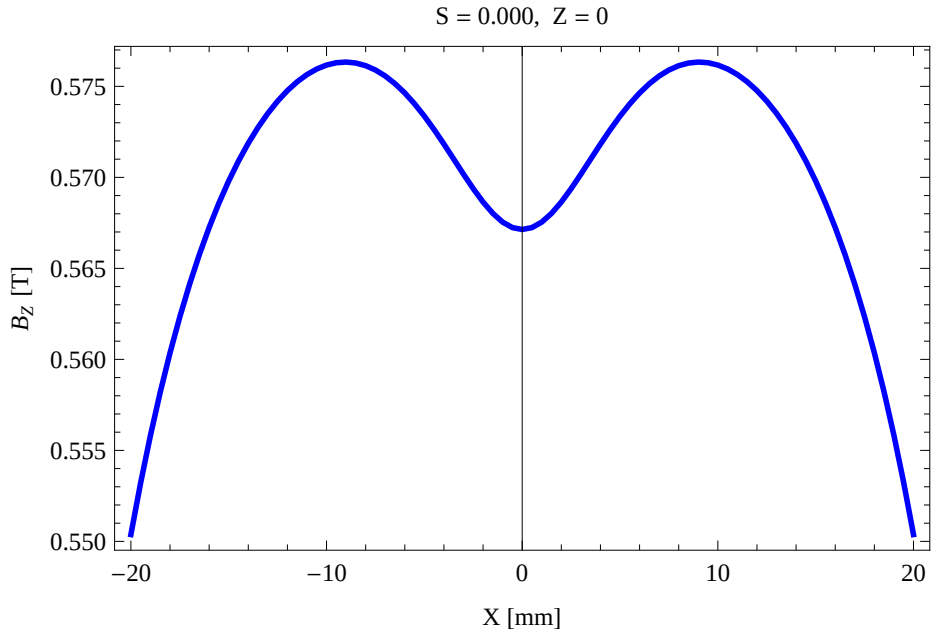

Figure 154: Vertical magnetic field in a central pole of the epu90Incl along the horizontally transverse direction to the axis, S = 0.000, Z = 0

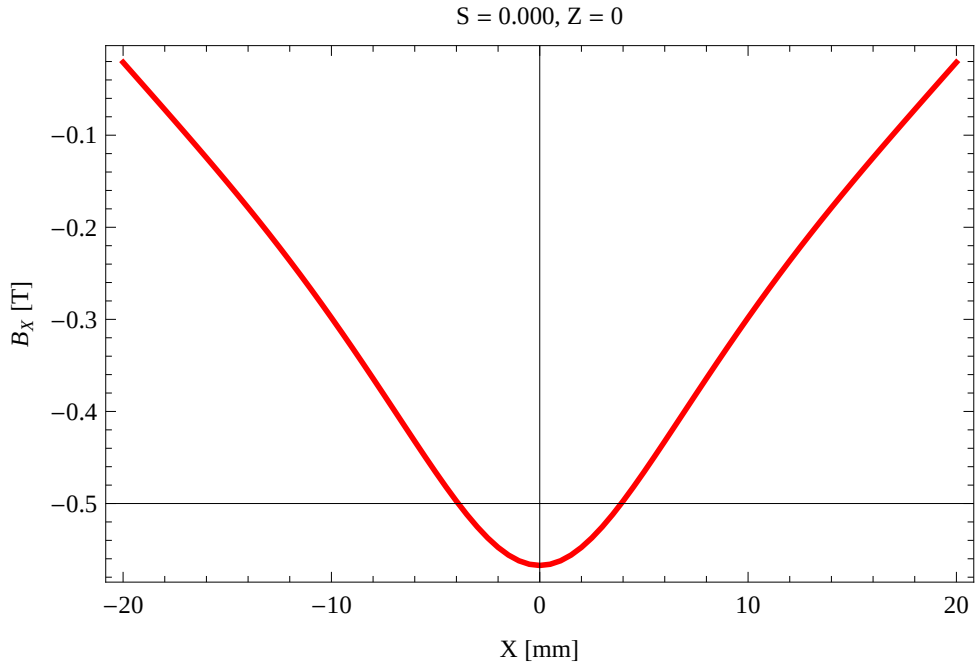

Figure 155: Horizontal magnetic field in a central pole of the epu90Incl along the horizontally transverse direction to the axis, S = 0.000, Z = 0

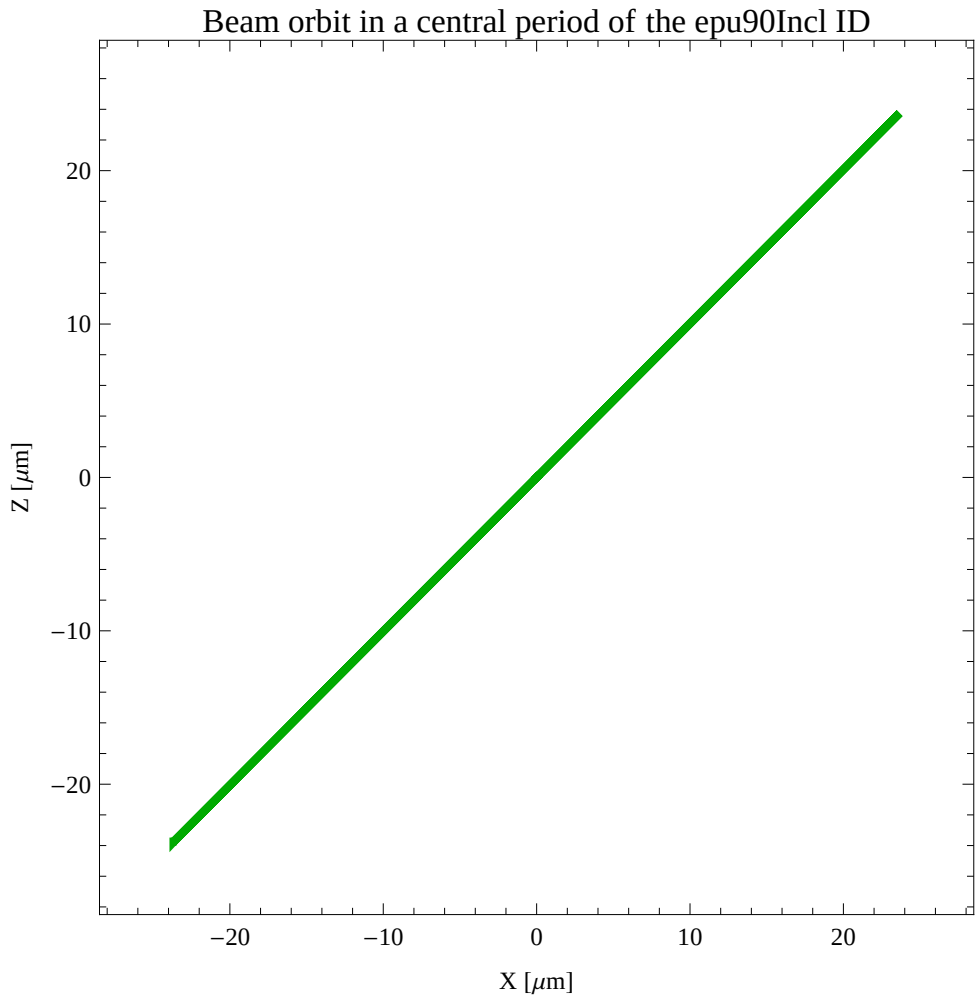

Figure 156: The beam orbit of the electron beam through a central period of the epu90Incl

3.12 Synchrotron radiation from the epu90Incl

The power map of the emitted synchrotron radiation by the epu90Incl, assuming a 0.3 A filament beam with an energy of 1.5 GeV and undulator properties of the synchrotron radiation, is shown in Figure 157. The on-axis power density is 0.362926 kW/mrad^2

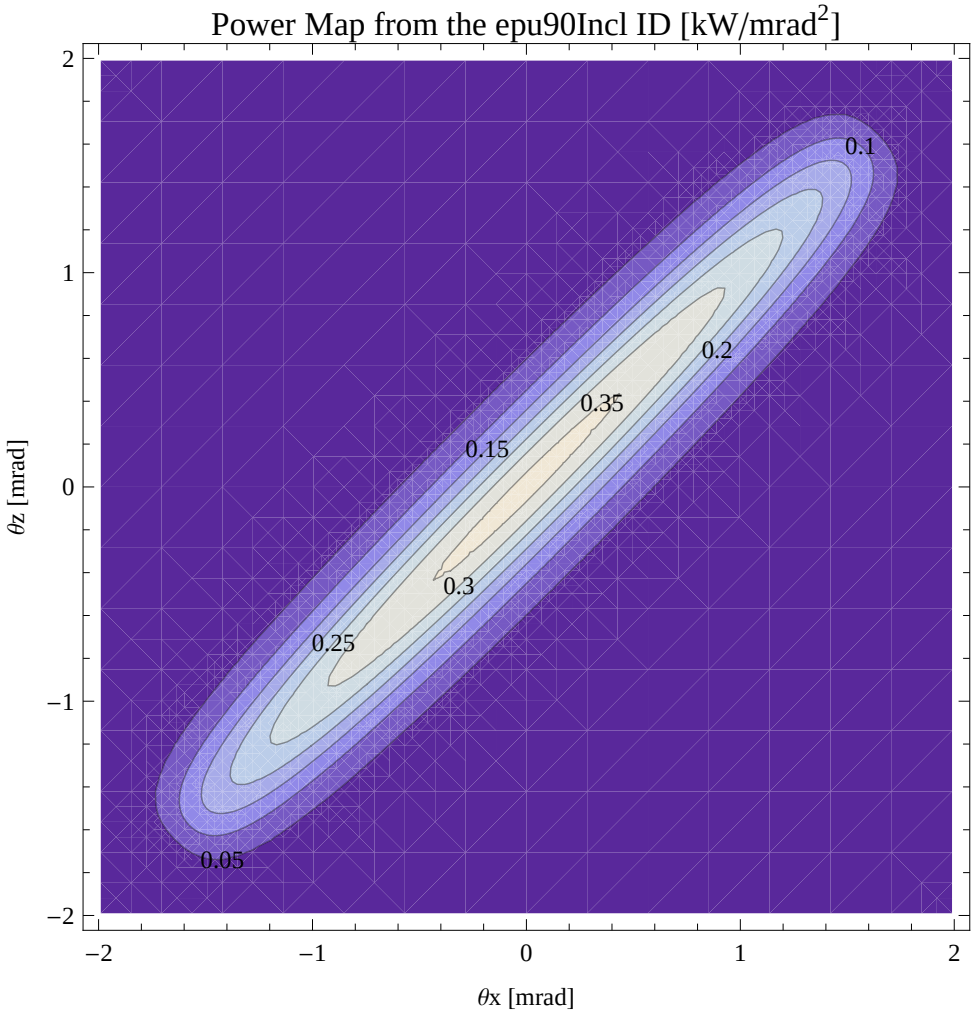

Figure 157: Map of the power distribution of the emitted synchrotron radiation by the epu90Incl

A map of the degree of linear polarisation of the fundamental harmonic of the synchotron radiation emitted by the epu90Incl over the angle of observation is shown in Figure 158.

A map of the degree of 45 degree polarisation of the fundamental harmonic of the synchotron radiation emitted by the epu90Incl over the angle of observation is shown in Figure 159.

A map of the degree of circular polarisation of the fundamental harmonic of the synchotron radiation emitted by the epu90Incl over the angle of observation is shown in Figure 160.

The on axis brilliance at peak energy and the angular spectral flux from the epu90Incl have been calculated with the given beam parameters, which are 0.3 A of stored current, $\beta_H = 5.627$ m, $\varepsilon_H = 5.985$ nmrad, $\beta_V = 2.837$ m, $\varepsilon_V = 59.85$ pmrad, and an energy spread of 0.001.

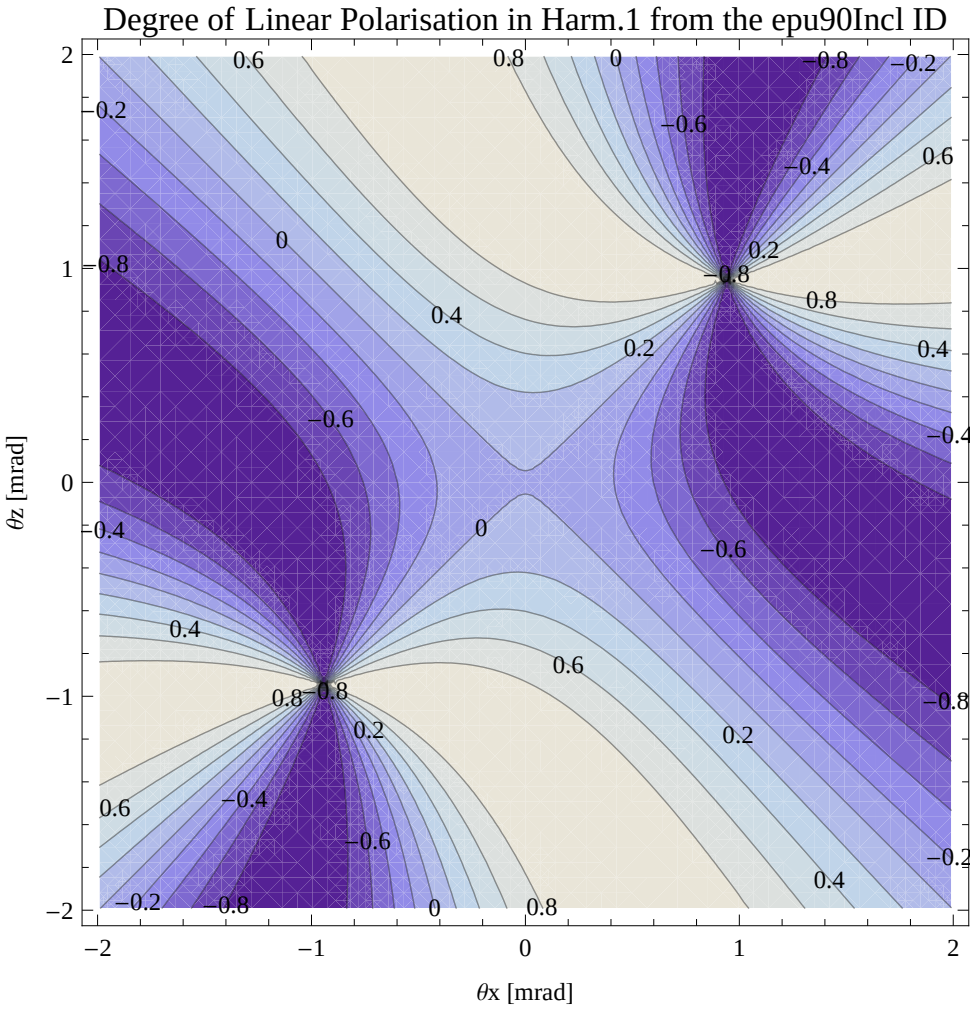

Figure 158: Map of linear polarisation in the fundamental harmonic of the synchotron radiation emitted by the epu90Incl

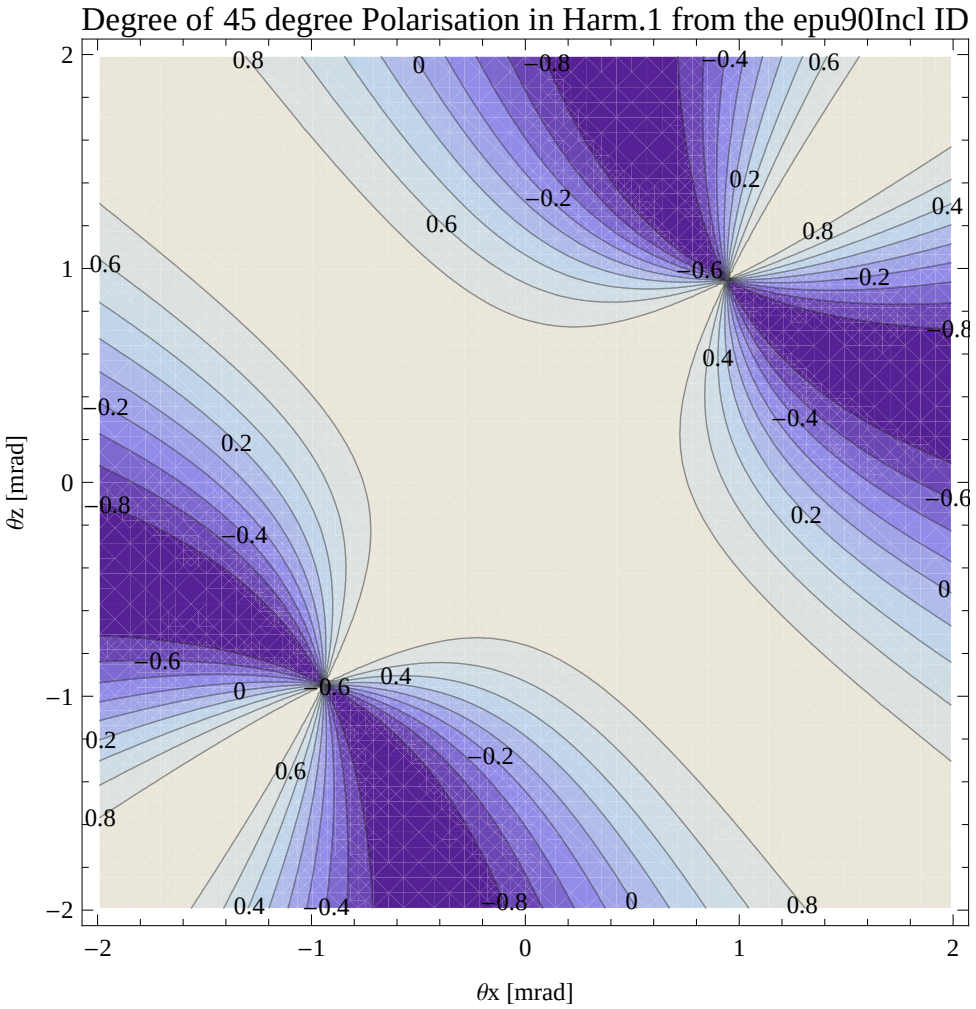

Figure 159: Map of 45 degree polarisation in the fundamental harmonic of the synchotron radiation emitted by the epu90Incl

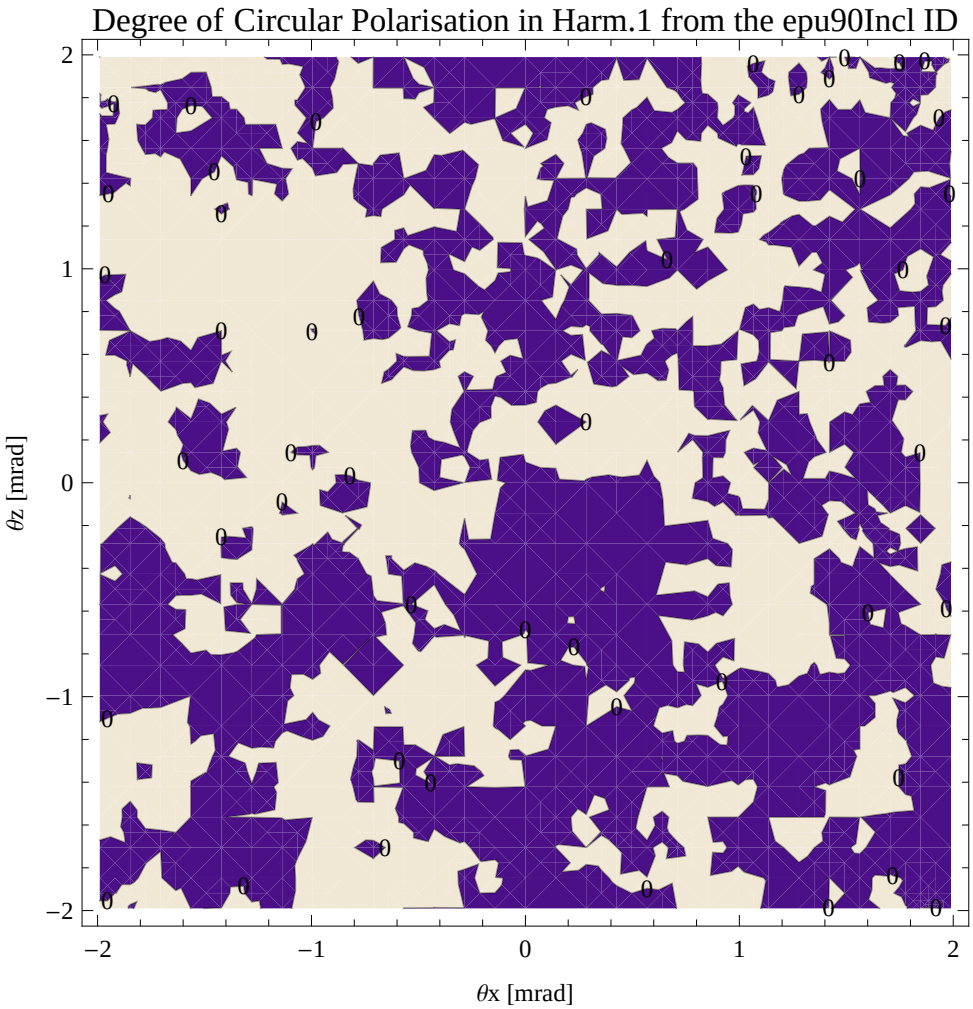

Figure 160: Map of circular polarisation in the fundamental harmonic of the synchotron radiation emitted by the epu90Incl

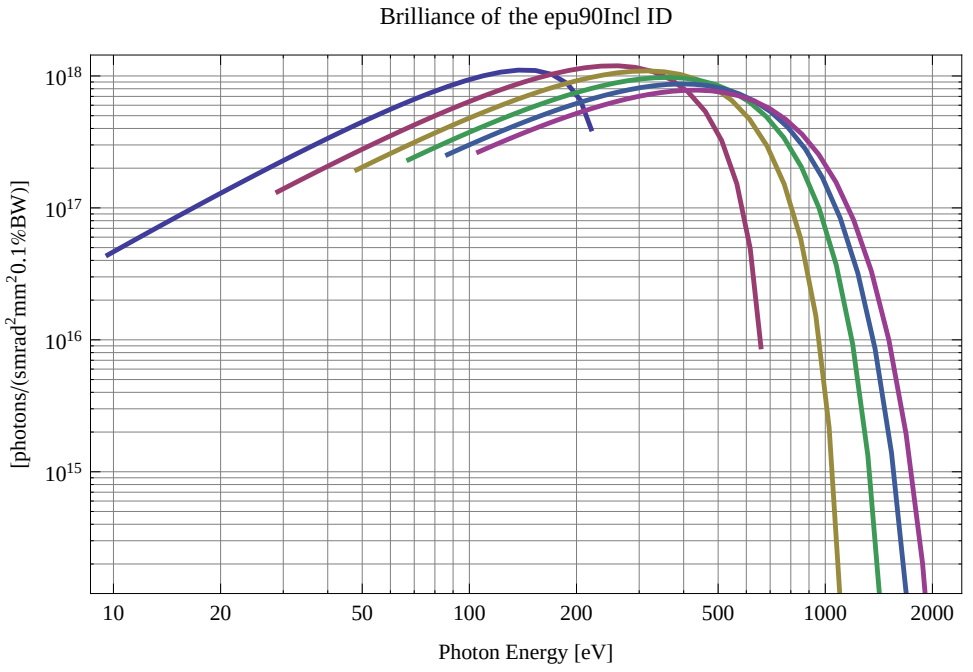

Figure 161: The brilliance at peak energy of the synchotron radiation emitted by the epu90Incl

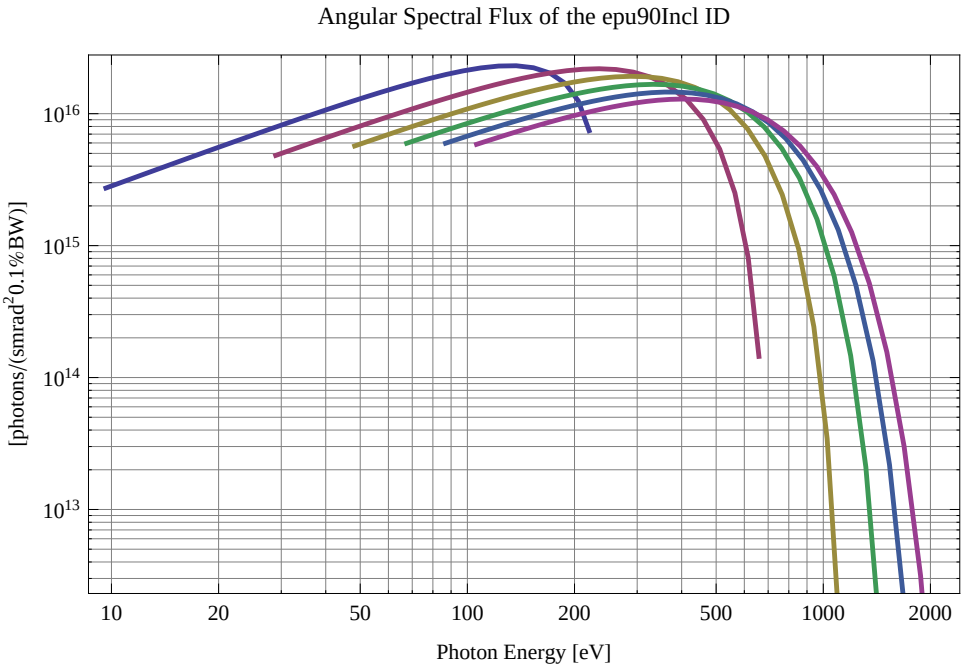

Figure 162: The angular spectral flux of the synchotron radiation emitted by the epu90Incl

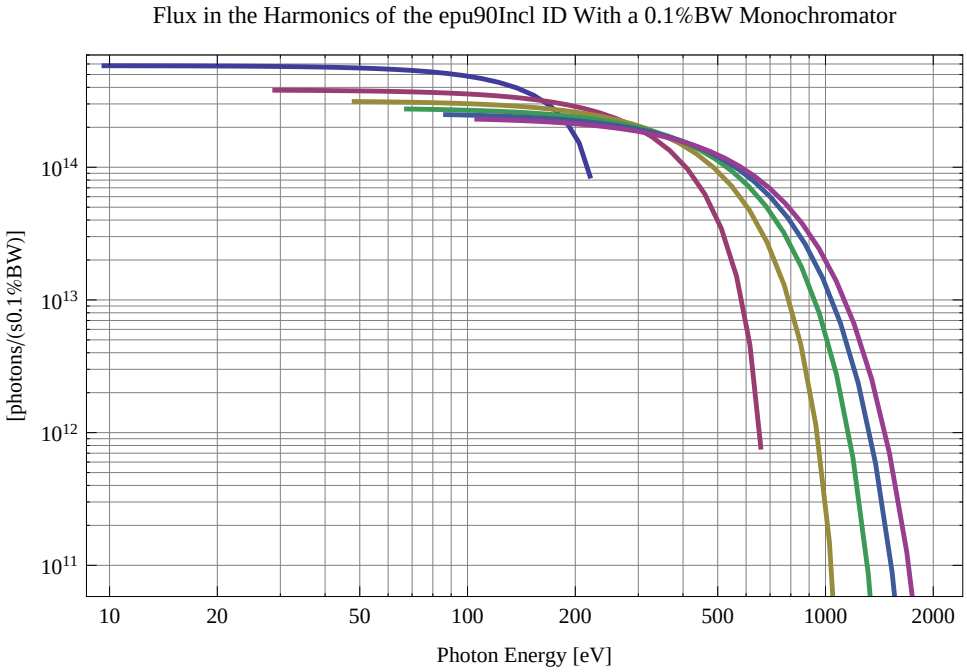

Figure 163: The flux of photons in the harmonics of the emitted synchrotron radiation from the epu90Incl using a 0.1%BW monochromator

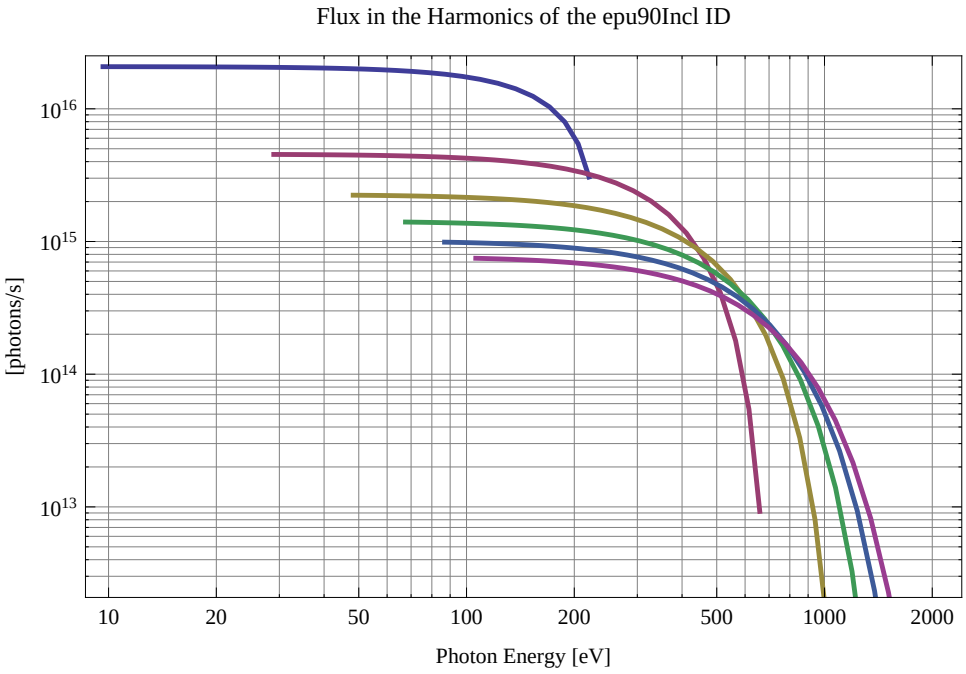

Figure 164: The flux of photons in the harmonics of the emitted synchrotron radiation from the epu90Incl

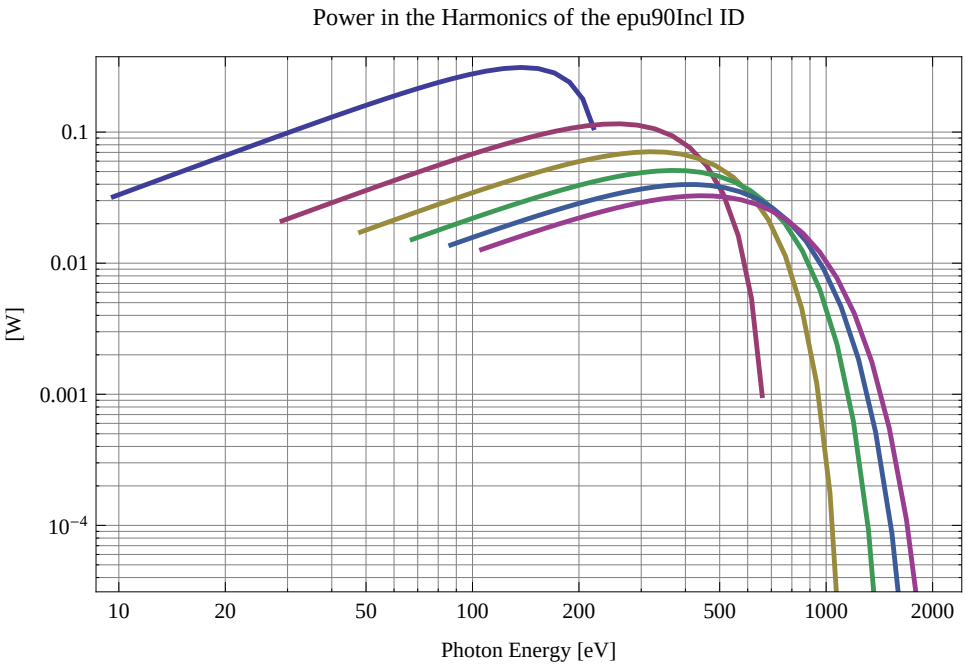

Figure 165: The power in the harmonics of the emitted synchrotron radiation from the epu90Incl

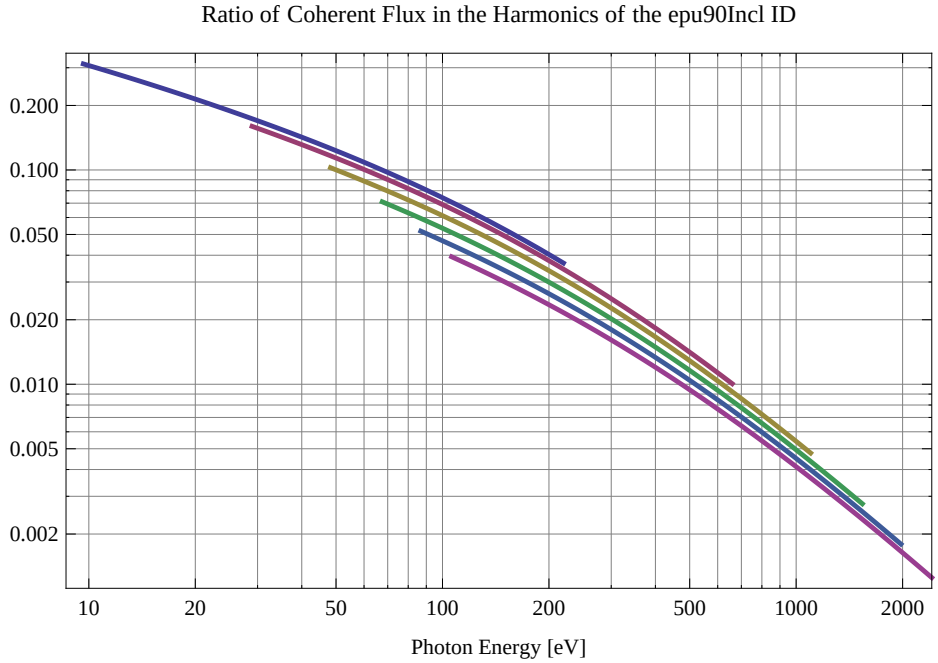

Figure 166: The ratio of coherent flux in the harmonics of the emitted synchrotron radiation from the epu90Incl

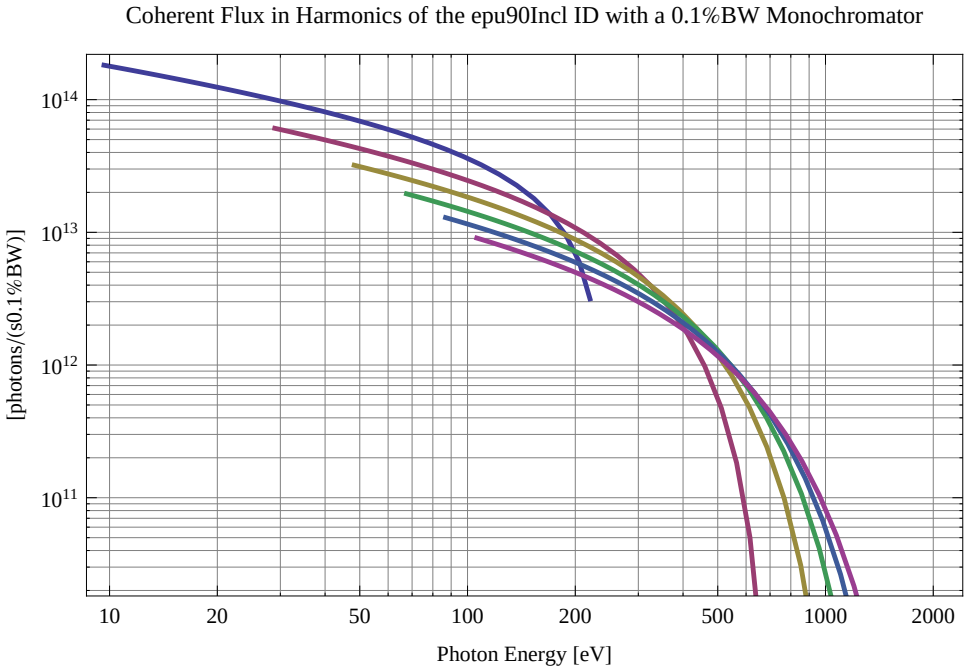

Figure 167: The coherent flux in the harmonics of the epu90Incl using a 0.1%BW Monochromator

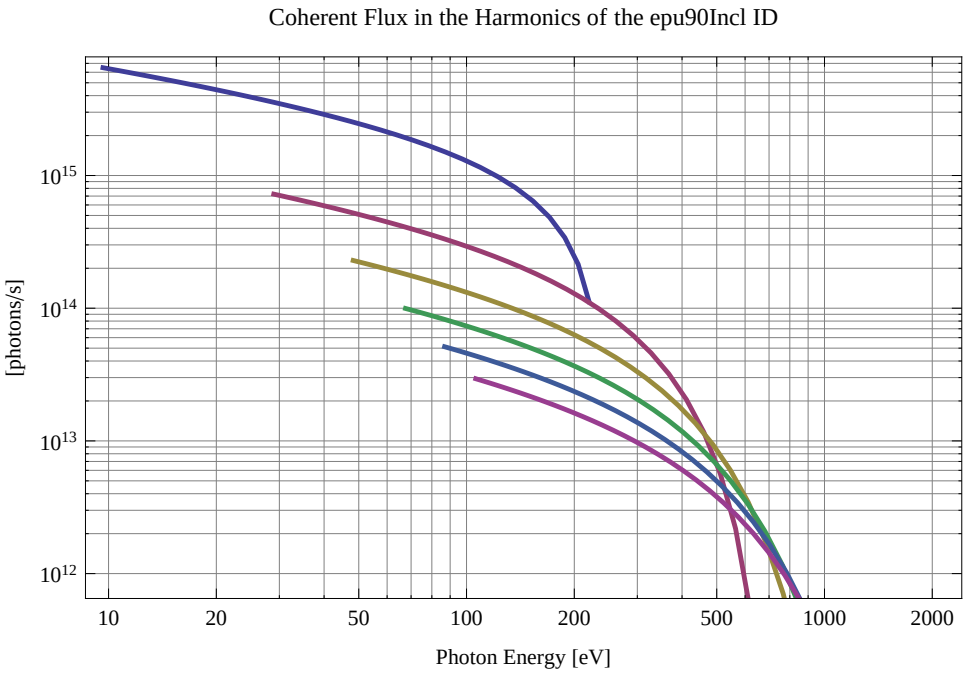

Figure 168: The coherent flux in the harmonics of the epu90Incl

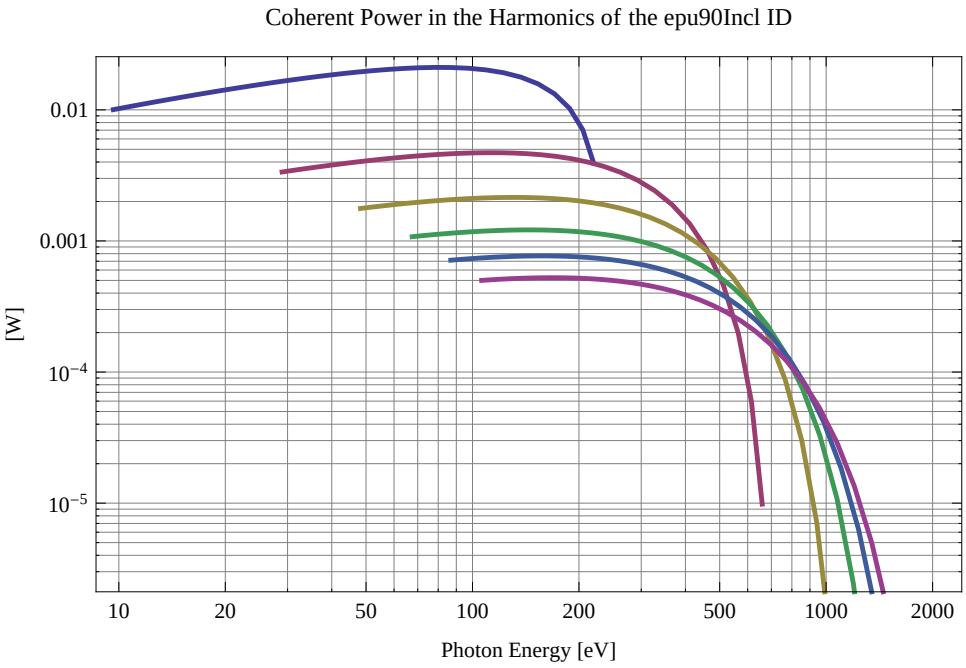

Figure 169: The power of coherent synchrotron radiation in the harmonics of the epu90Incl

The brilliance at peak energy and the angular spectral flux density from the epu90Incl for different harmonics at maximum K-value (6.871) are given in Table 25 and for minimum K-value (0.400) these values are given in Table 26.

Table 25: The brilliance at peak energy and the angular spectral flux density from the epu90Incl for different harmonics at maximum K-value (6.871)

Harmonic	Photon Energy [eV]	Brilliance [Ph./(smrad^{2}mrad^{2}0.1%BW)]	Angular Spectral Flux [Ph./(smrad^{2}0.1%BW)]
1	9.64817	4.4×10^{16}	2.73×10^{15}
3	28.9445	1.33×10^{17}	4.83×10^{15}
5	48.2409	1.94×10^{17}	5.69×10^{15}
7	67.5372	2.32×10^{17}	5.97×10^{15}
9	86.8336	2.53×10^{17}	5.97×10^{15}
11	106.13	2.66×10^{17}	5.86×10^{15}

Table 26: The brilliance at peak energy and the angular spectral flux density from the epu90Incl for different harmonics at minimum K-value (0.4)

Harmonic	Photon Energy [eV]	Brilliance [Ph./(smrad^{2}mrad^{2}0.1%BW)]	Angular Spectral Flux [Ph./(smrad^{2}0.1%BW)]
1	219.824	3.96×10^{17}	7.43×10^{15}
3	659.472	8.84×10^{15}	1.45×10^{14}
5	1099.12	1.15×10^{14}	1.83×10^{12}
7	1538.77	1.3×10^{12}	2.05×10^{10}
9	1978.42	1.4×10^{10}	2.2×10^{8}
11	2418.06	1.47×10^{8}	2.3×10^{6}

3.13 Influence from the epu90Incl on the optics of the stored beam

Figure 170 shows the focusing potential from the epu90Incl over the beam stay clear aperture of the ring aparture.

Figure 171 shows the kick map in the beam energy independant unit T^2m^2 of the kicks induced by the epu90Incl over the beam stay clear aparture.

Figure 172 shows the induced angular kick on the stored beam from the epu90Incl as a function of the vertical distance to the undulator axis.

Figure 173 shows the induced angular kick on the stored beam from the epu90Incl as a function of the horizontal distance to the undulator axis.

Figure 174 shows tune shift induced by the epu90Incl over the beam stay clear aparture. Note that the tune shift depends on the beam size at the.

Figure 175 shows the induced tune shift from the epu90Incl as a function of the vertical distance to the undulator axis.

Figure 176 shows the induced tune shift from the epu90Incl as a function of the horizontal distance to the undulator axis.

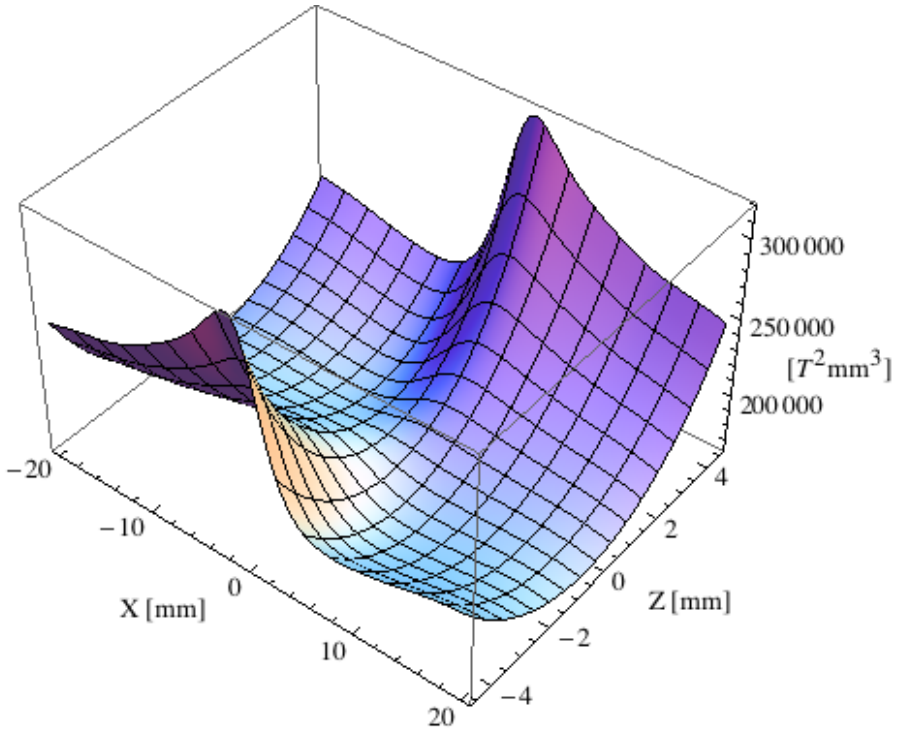

Figure 170: Focusing potential from the epu90Incl over the beam stay clear aparture.

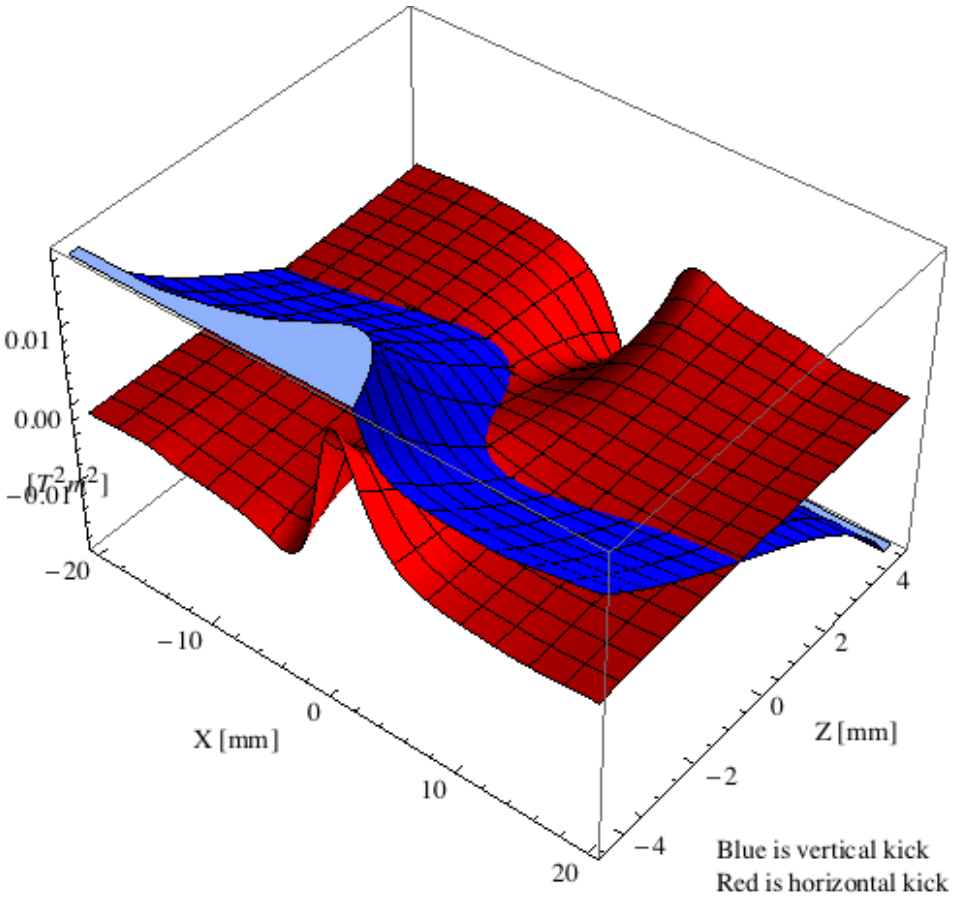

Figure 171: Kick map in the beam energy independant unit T^2m^2 of the kicks induced by the epu90Incl over the beam stay clear aparture.

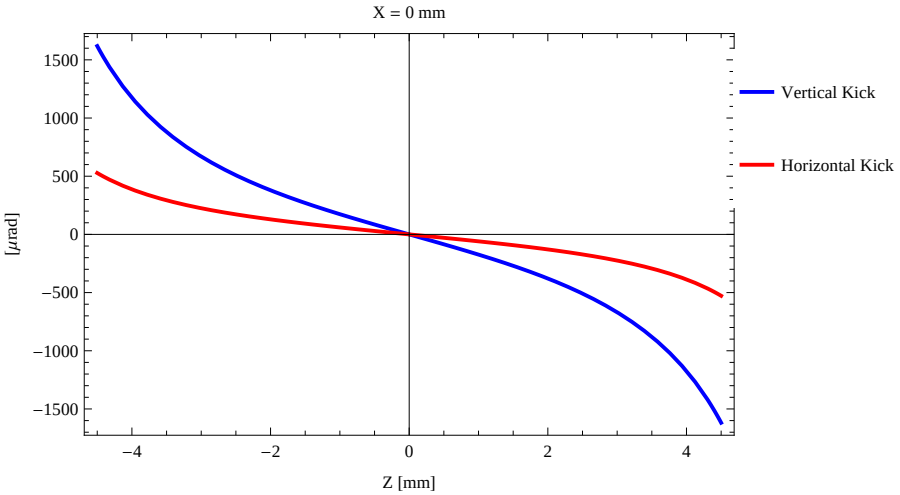

Figure 172: Induced angular kick on the stored beam from the epu90Incl as a function of the vertical distance to the undulator axis.

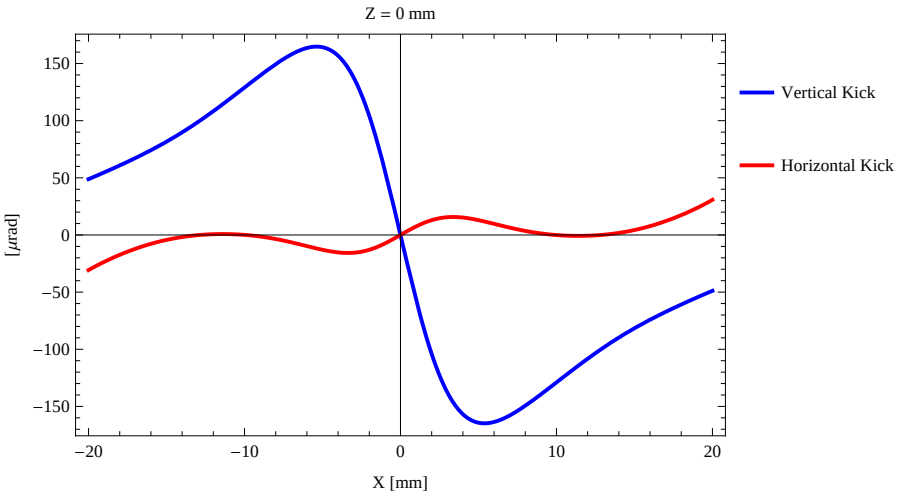

Figure 173: Induced angular kick on the stored beam from the epu90Incl as a function of the horizontal distance to the undulator axis.

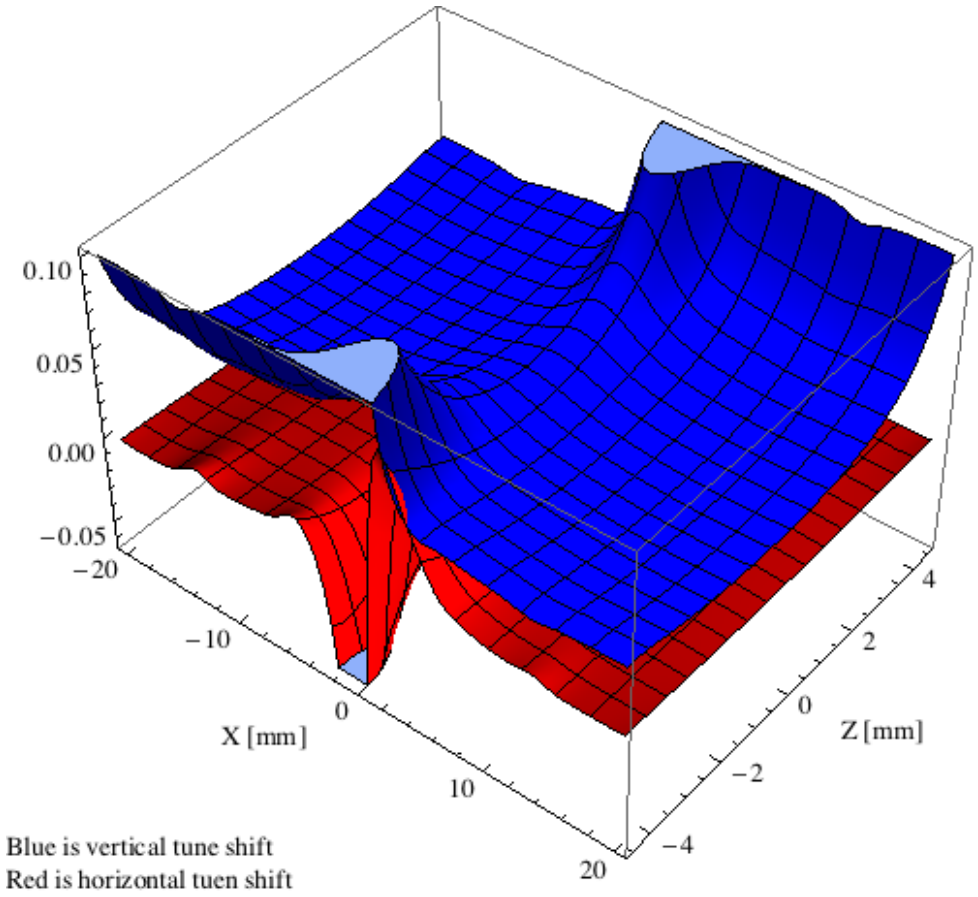

Figure 174: Tune shift induced by the epu90Incl over the beam stay clear aparture.

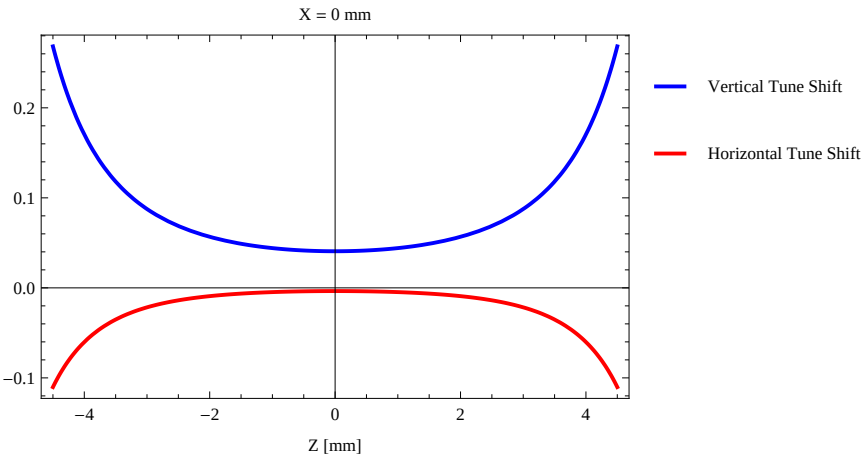

Figure 175: Induced tune shift from the epu90Incl as a function of the vertical distance to the undulator axis.

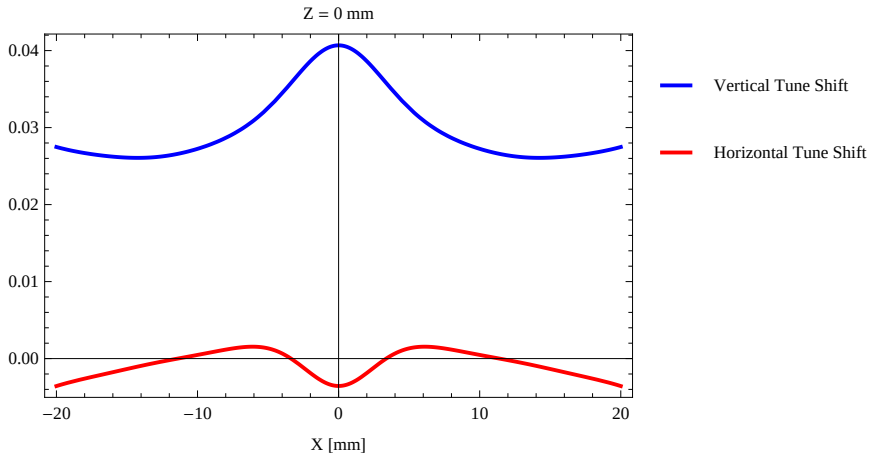

Figure 176: Induced tune shift from the epu90Incl on the stored beam from the as a function of the horizontal distance to the undulator axis.

3.14 Magnet model of the elliptically polarizing undulator epu90Vert

The Radia [2] magnet model of the epu90Vert is shown in Figure 177. The length of the magnet model is 739.68 mm. The magnetic material in the model is NdFeb with a remanence of 1.33 T. Blocks with vertical magnetisation are blue and blocks with horizontal magnetisation are yellow. The block size is 35.x35.x22.5 mm^3 and there is a 5. mm cut-out in two of the corners of the blocks. The total length of the epu90Vert is 2539.68 mm.

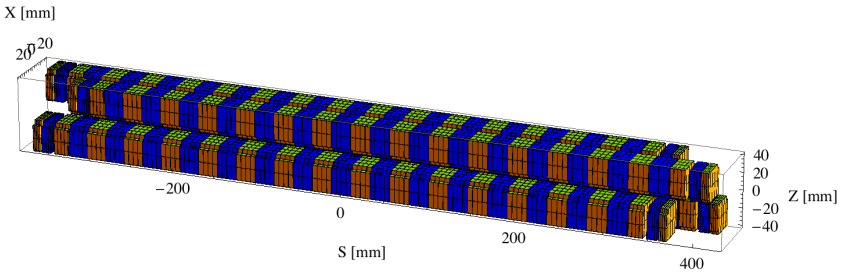

Figure 177: Magnetic model of the epu90Vert. The has been modelled with Radia [2]

3.15 Analysis of the magnetic field of the epu90Vert

The effective magnetic fields on axis and the fundamental photon energy of the epu90Vert are shown in Table 27. The higher harmonic contents in the magnetic field of an elliptically polarizing undulator made of permanent magnets is usually small and the effective field has approximately the same strength as the peak field.

3.16 Synchrotron radiation from the epu90Vert

The power map of the emitted synchrotron radiation by the epu90Vert, assuming a 0.3 A filament beam with an energy of 1.5 GeV and undulator properties of the synchrotron radiation, is shown in Figure 181. The on-axis power density is 0.471824 $kW/mrad^2$

Table 27: Effective Fields on axis and Fundamental Photon Energy of the epu90Vert

Undulator Period	90	mm
Undulator Gap	13	mm
Undulator Mode	Vertical	
Undulator Phase	45.000	mm
Vertical Peak Field	0.000	T
effective Vertical Field	0.000	T
Kx (from vert. field)	0.000	
Horizontal Peak Field:	1.055	T
effective Horizontal Field	1.062	T
Kz (from hor. field)	8.927	
Photon Energy, Harm.1	0.006	keV
Emitted Power	1.223	kW
Total Length	2539.7	mm

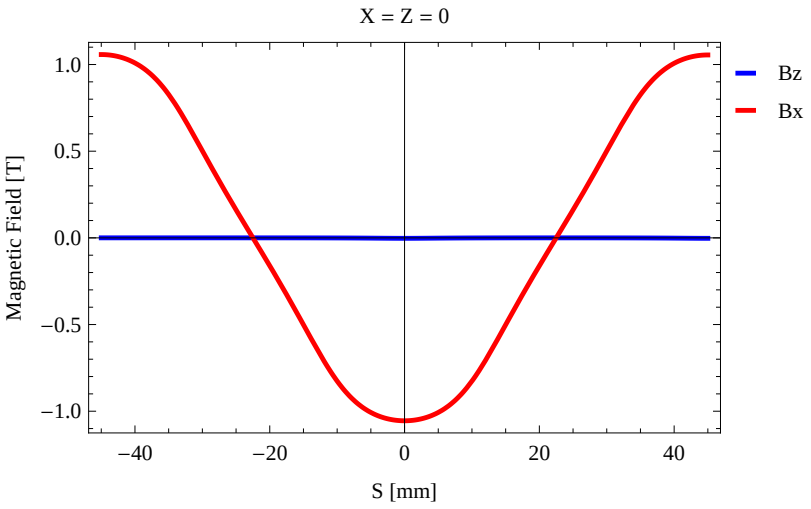

Figure 178: Vertical magnetic field in a central pole of the epu90Vert along the axis, X = Z = 0

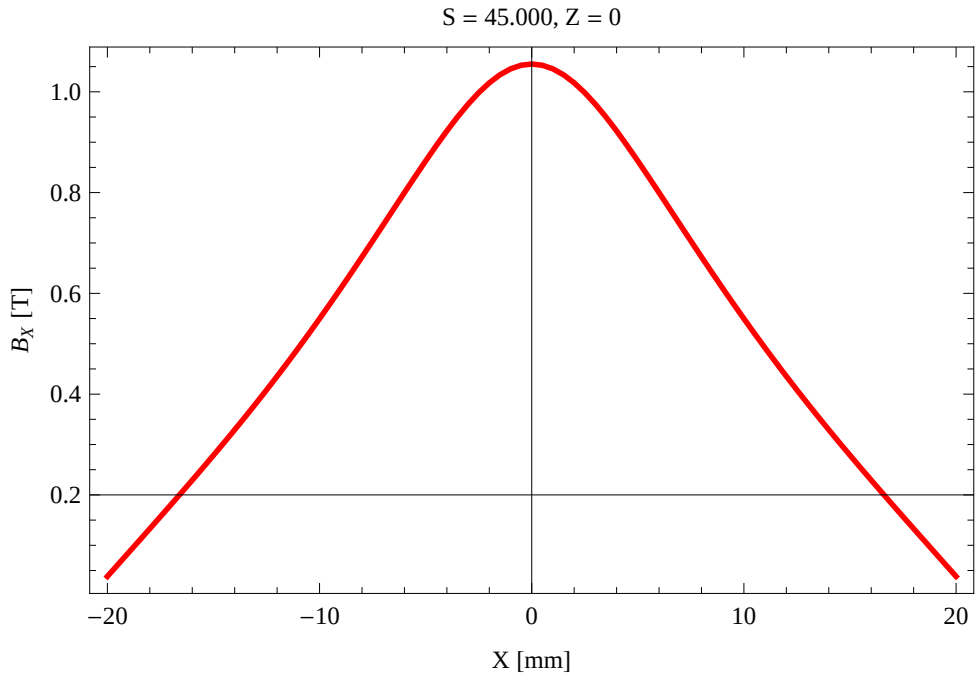

Figure 179: Horizontal magnetic field in a central pole of the epu90Vert along the horizontally transverse direction to the axis, S = 45.000, Z = 0

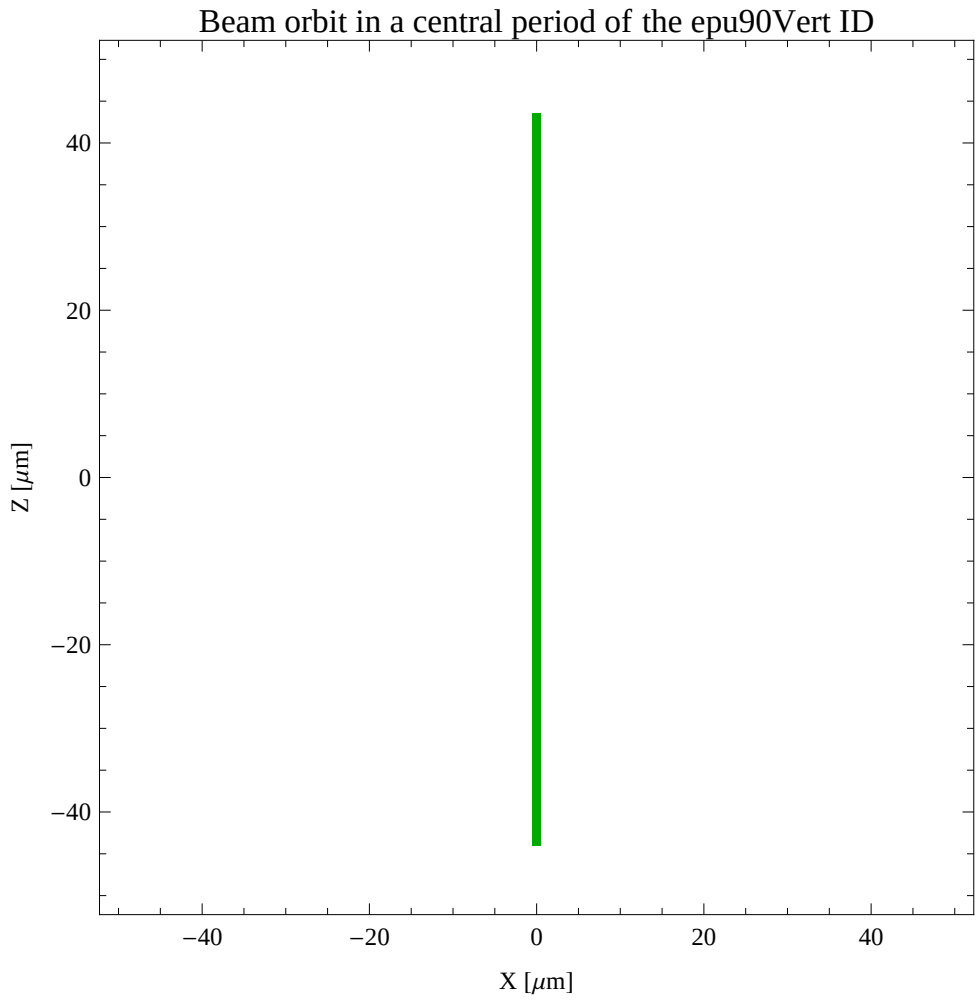

Figure 180: The beam orbit of the electron beam through a central period of the epu90Vert

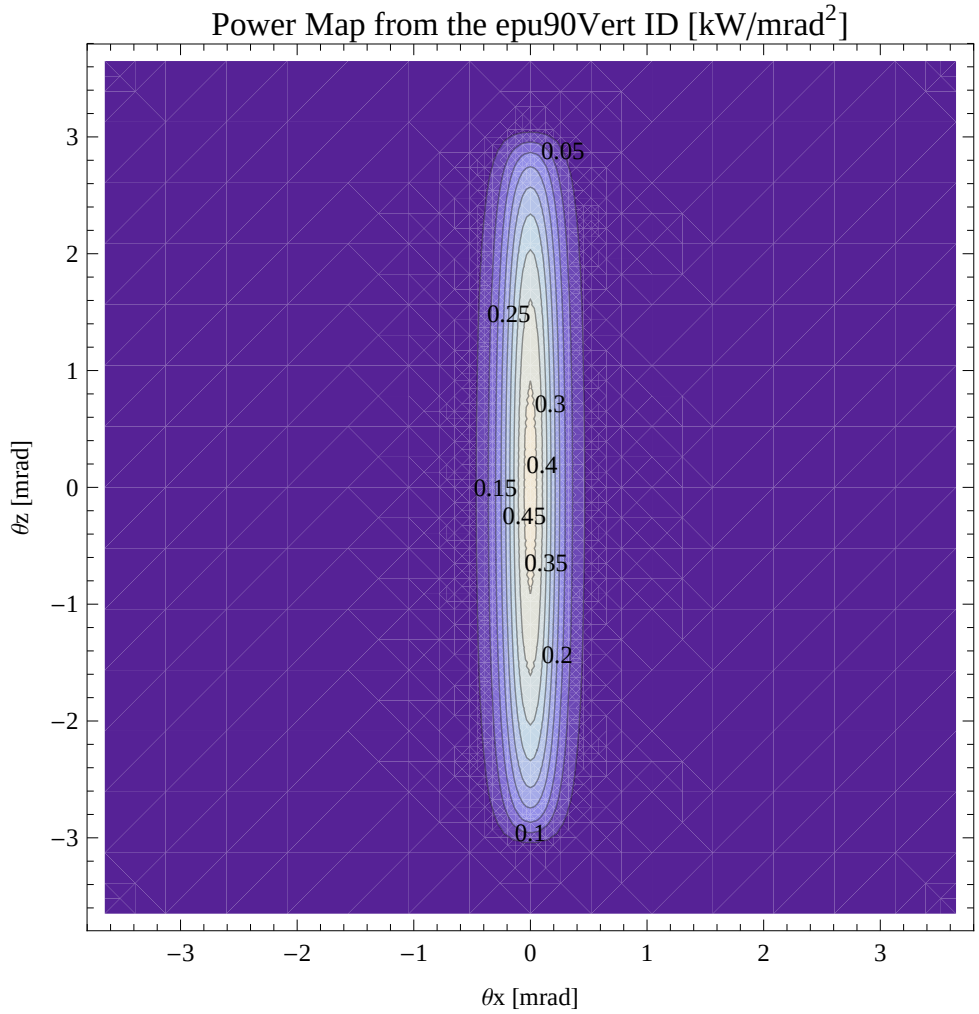

Figure 181: Map of the power distribution of the emitted synchrotron radiation by the epu90Vert

A map of the degree of linear polarisation of the fundamental harmonic of the synchotron radiation emitted by the epu90Vert over the angle of observation is shown in Figure 182.

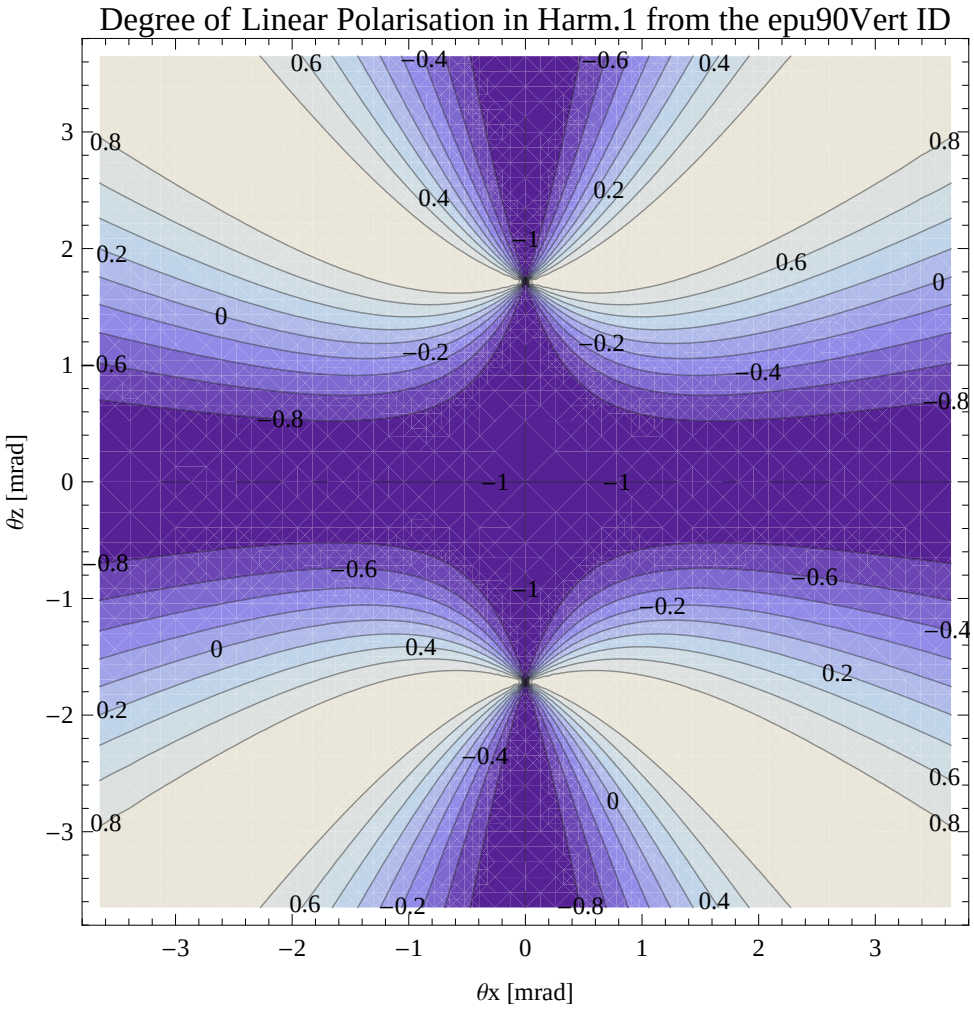

Figure 182: Map of linear polarisation in the fundamental harmonic of the synchotron radiation emitted by the epu90Vert

A map of the degree of 45 degree polarisation of the fundamental harmonic of the synchotron radiation emitted by the epu90Vert over the angle of observation is shown in Figure 183.

A map of the degree of circular polarisation of the fundamental harmonic of the synchotron radiation emitted by the epu90Vert over the angle of observation is shown in Figure 184.

The on axis brilliance at peak energy and the angular spectral flux from the epu90Vert have been calculated with the given beam parameters, which are 0.3 A of stored current, $\beta_H = 5.627$ m, $\varepsilon_H = 5.985$ nmrad, $\beta_V = 2.837$ m, $\varepsilon_V = 59.85$ pmrad, and an energy spread of 0.001.

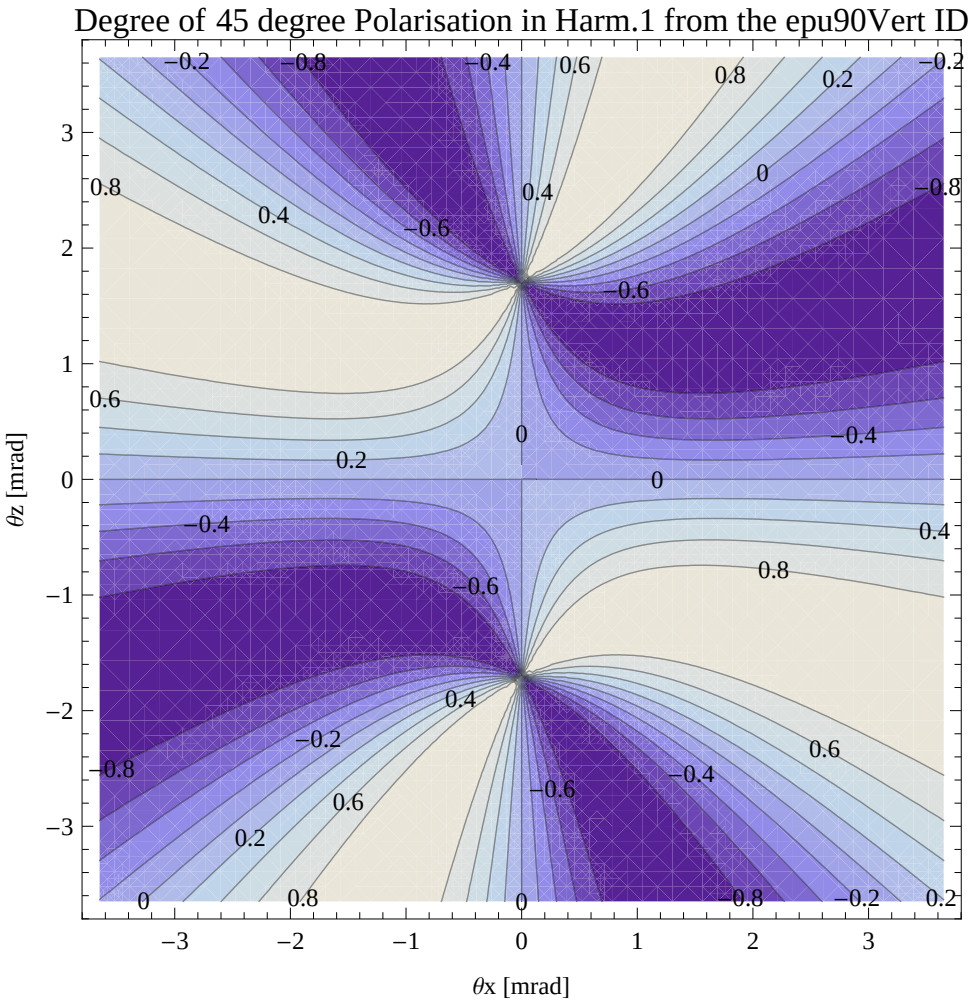

Figure 183: Map of 45 degree polarisation in the fundamental harmonic of the synchotron radiation emitted by the epu90Vert

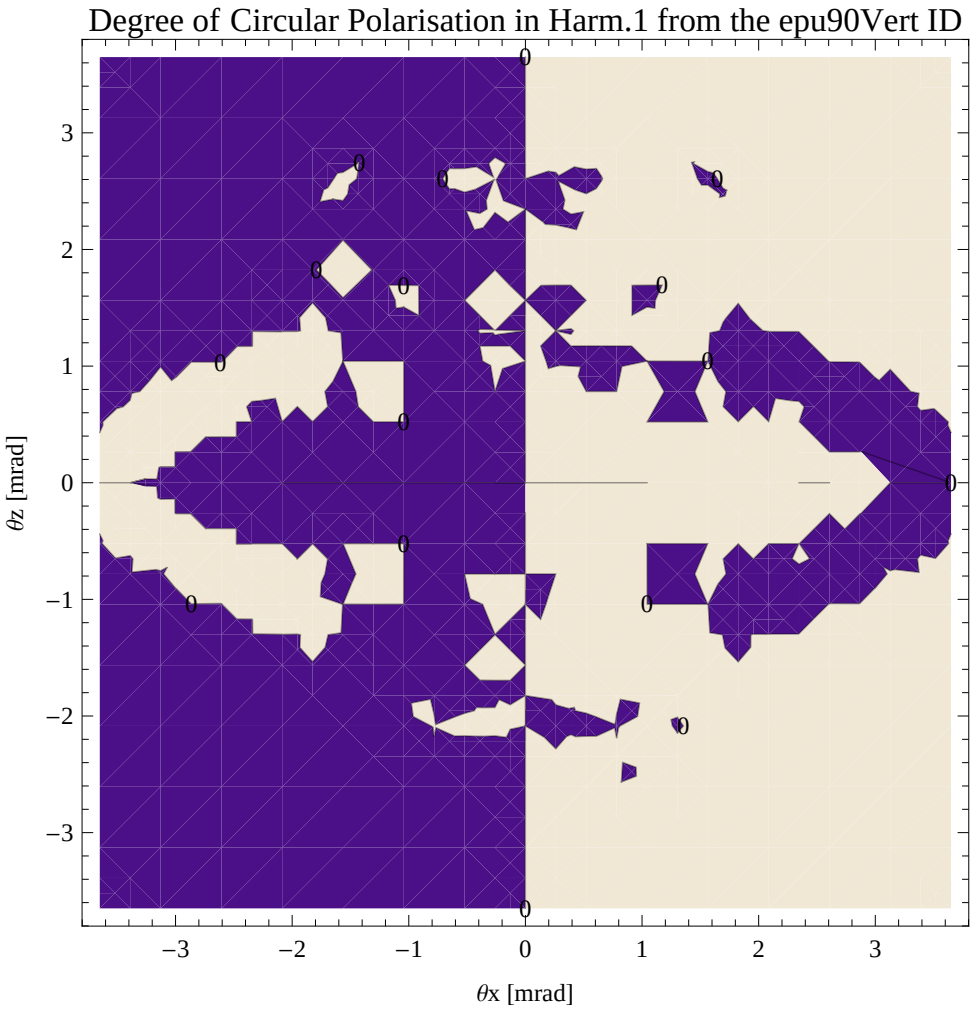

Figure 184: Map of circular polarisation in the fundamental harmonic of the synchotron radiation emitted by the epu90Vert

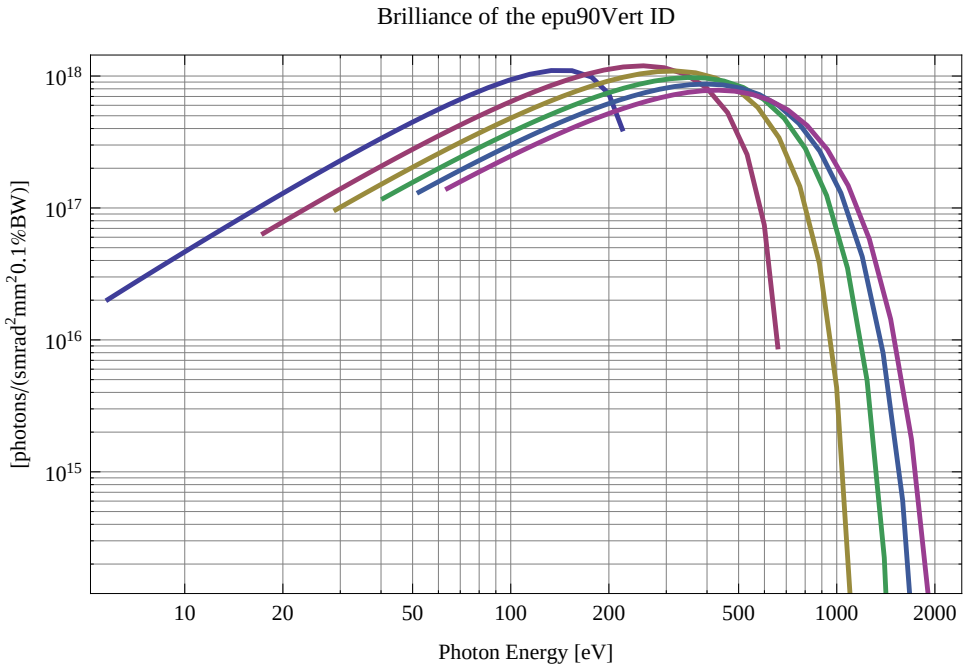

Figure 185: The brilliance at peak energy of the synchotron radiation emitted by the epu90Vert

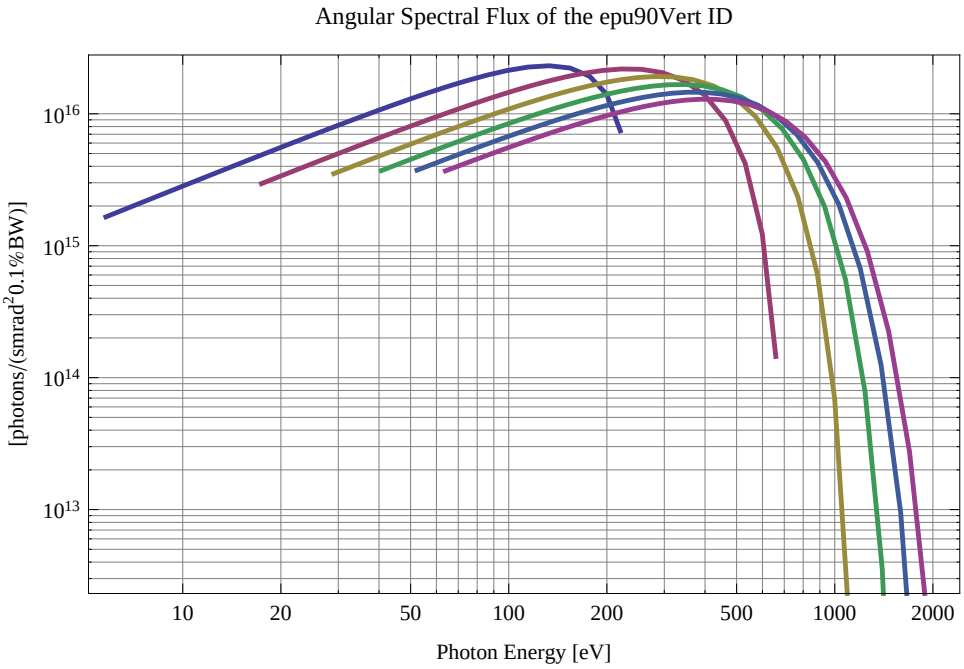

Figure 186: The angular spectral flux of the synchotron radiation emitted by the epu90Vert

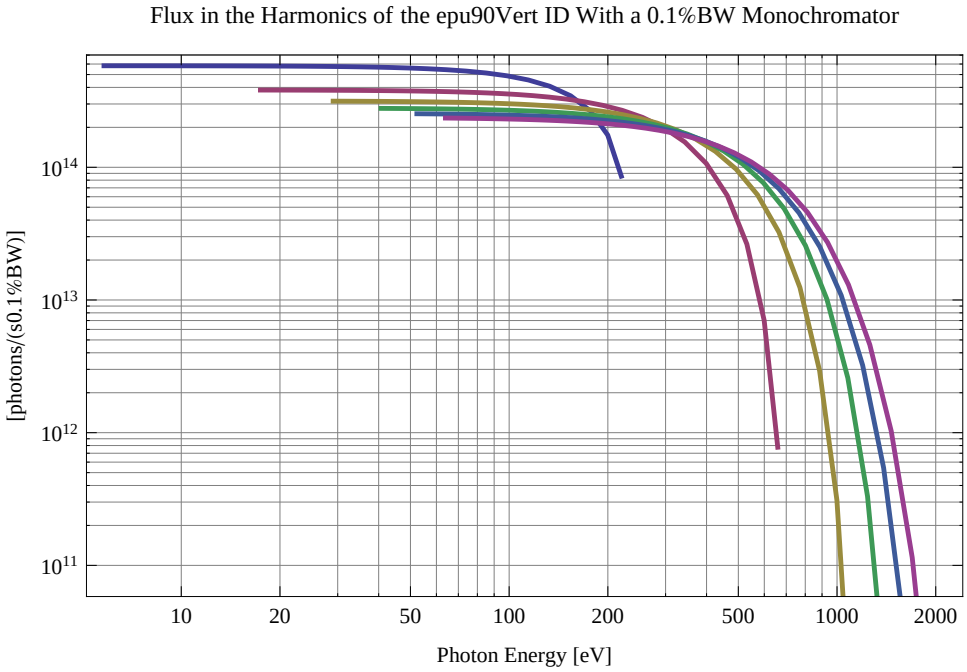

Figure 187: The flux of photons in the harmonics of the emitted synchrotron radiation from the epu90Vert using a 0.1%BW monochromator

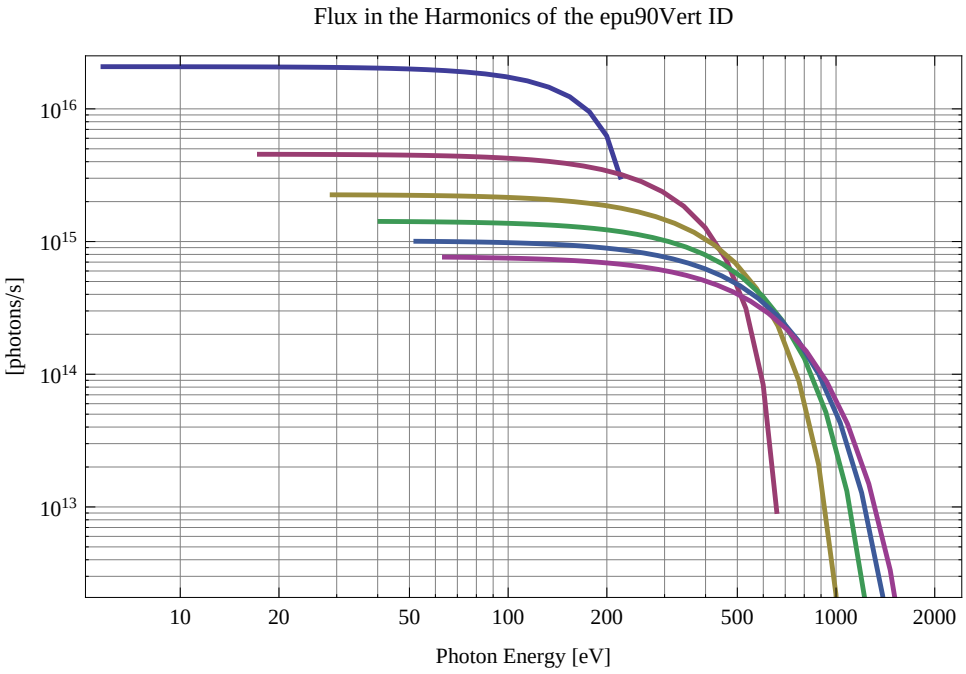

Figure 188: The flux of photons in the harmonics of the emitted synchrotron radiation from the epu90Vert

Figure 189: The power in the harmonics of the emitted synchrotron radiation from the epu90Vert

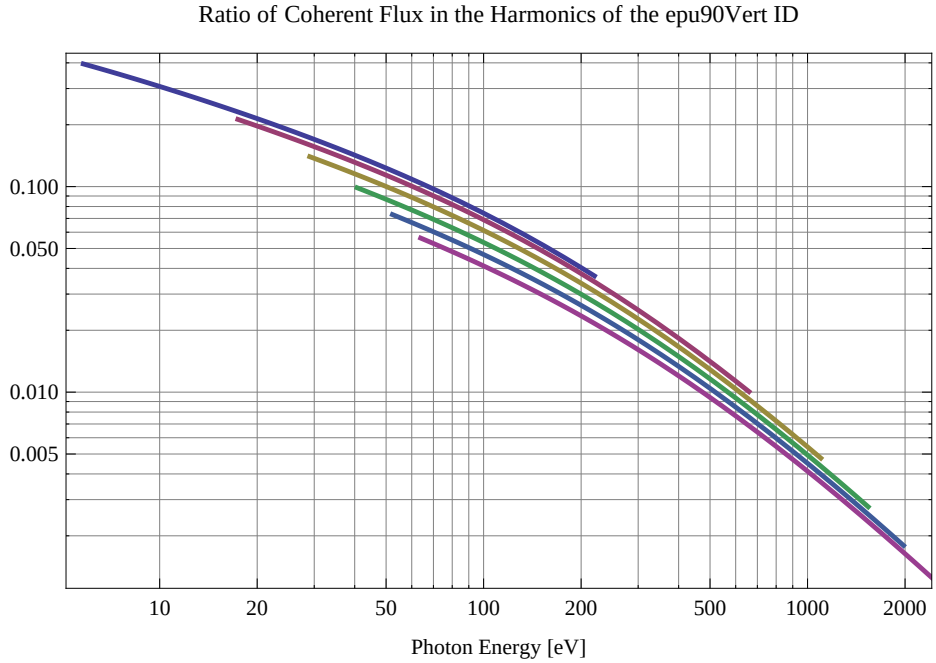

Figure 190: The ratio of coherent flux in the harmonics of the emitted synchrotron radiation from the epu90Vert

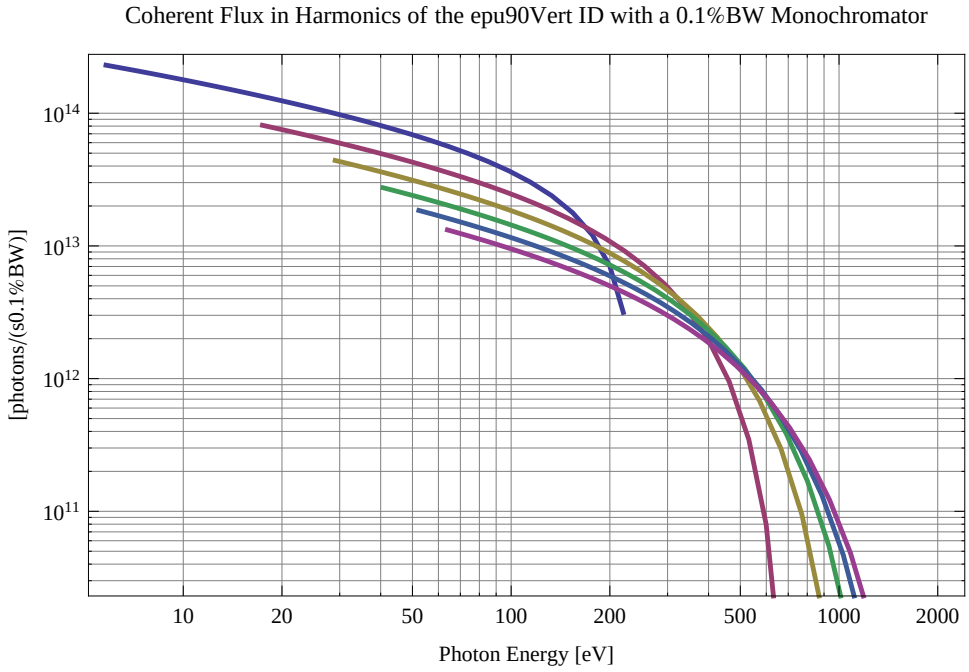

Figure 191: The coherent flux in the harmonics of the epu90Vert using a 0.1%BW Monochromator

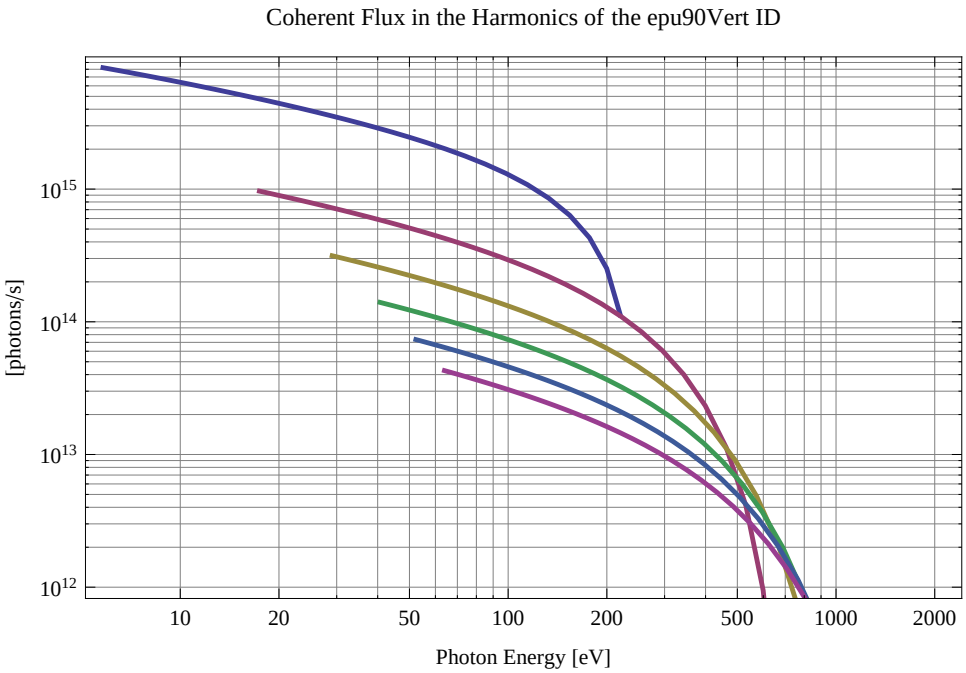

Figure 192: The coherent flux in the harmonics of the epu90Vert

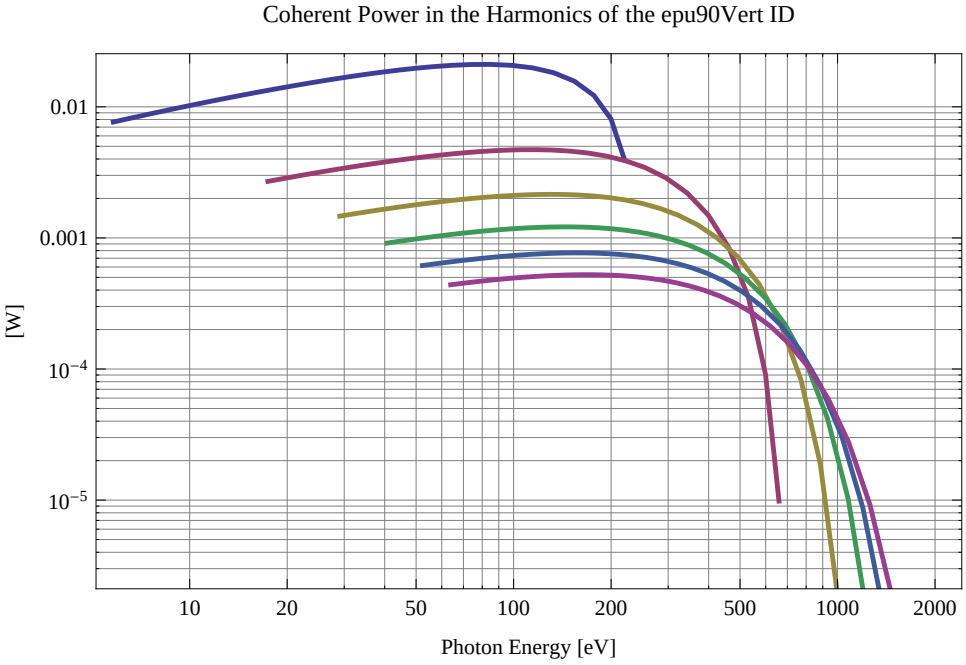

Figure 193: The power of coherent synchrotron radiation in the harmonics of the epu90Vert

The brilliance at peak energy and the angular spectral flux density from the epu90Vert for different harmonics at maximum K-value (8.927) are given in Table 28 and for minimum K-value (0.400) these values are given in Table 29.

Table 28: The brilliance at peak energy and the angular spectral flux density from the epu90Vert for different harmonics at maximum K-value (8.927)

Harmonic	Photon Energy [eV]	Brilliance [Ph./(smrad^{2}mrad^{2}0.1%BW)]	Angular Spectral Flux [Ph./(smrad^{2}0.1%BW)]
1	5.81215	2.02×10^{16}	1.65×10^{15}
3	17.4364	6.42×10^{16}	2.96×10^{15}
5	29.0607	9.68×10^{16}	3.52×10^{15}
7	40.685	1.18×10^{17}	3.71×10^{15}
9	52.3093	1.32×10^{17}	3.74×10^{15}
11	63.9336	1.4×10^{17}	3.69×10^{15}

Table 29: The brilliance at peak energy and the angular spectral flux density from the epu90Vert for different harmonics at minimum K-value (0.4)

Harmonic	Photon Energy [eV]	Brilliance [Ph./(smrad^{2}mrad^{2}0.1%BW)]	Angular Spectral Flux [Ph./(smrad^{2}0.1%BW)]
1	219.824	3.96×10^{17}	7.43×10^{15}
3	659.472	8.84×10^{15}	1.45×10^{14}
5	1099.12	1.15×10^{14}	1.83×10^{12}
7	1538.77	1.3×10^{12}	2.05×10^{10}
9	1978.42	1.4×10^{10}	2.2×10^{8}
11	2418.06	1.47×10^{8}	2.3×10^{6}

3.17 Influence from the epu90Vert on the optics of the stored beam

Figure 194 shows the focusing potential from the epu90Vert over the beam stay clear aperture of the ring aparture.

Figure 195 shows the kick map in the beam energy independant unit T^2m^2 of the kicks induced by the epu90Vert over the beam stay clear aparture.

Figure 196 shows the induced angular kick on the stored beam from the epu90Vert as a function of the vertical distance to the undulator axis.

Figure 197 shows the induced angular kick on the stored beam from the epu90Vert as a function of the horizontal distance to the undulator axis.

Figure 198 shows tune shift induced by the epu90Vert over the beam stay clear aparture. Note that the tune shift depends on the beam size at the.

Figure 199 shows the induced tune shift from the epu90Vert as a function of the vertical distance to the undulator axis.

Figure 200 shows the induced tune shift from the epu90Vert as a function of the horizontal distance to the undulator axis.

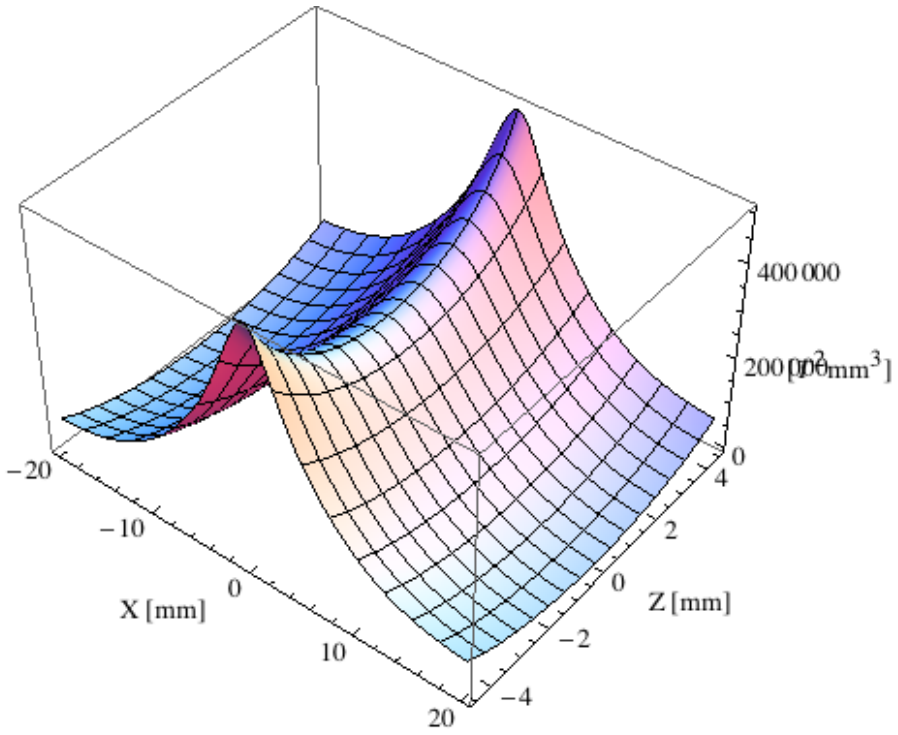

Figure 194: Focusing potential from the epu90Vert over the beam stay clear aparture.

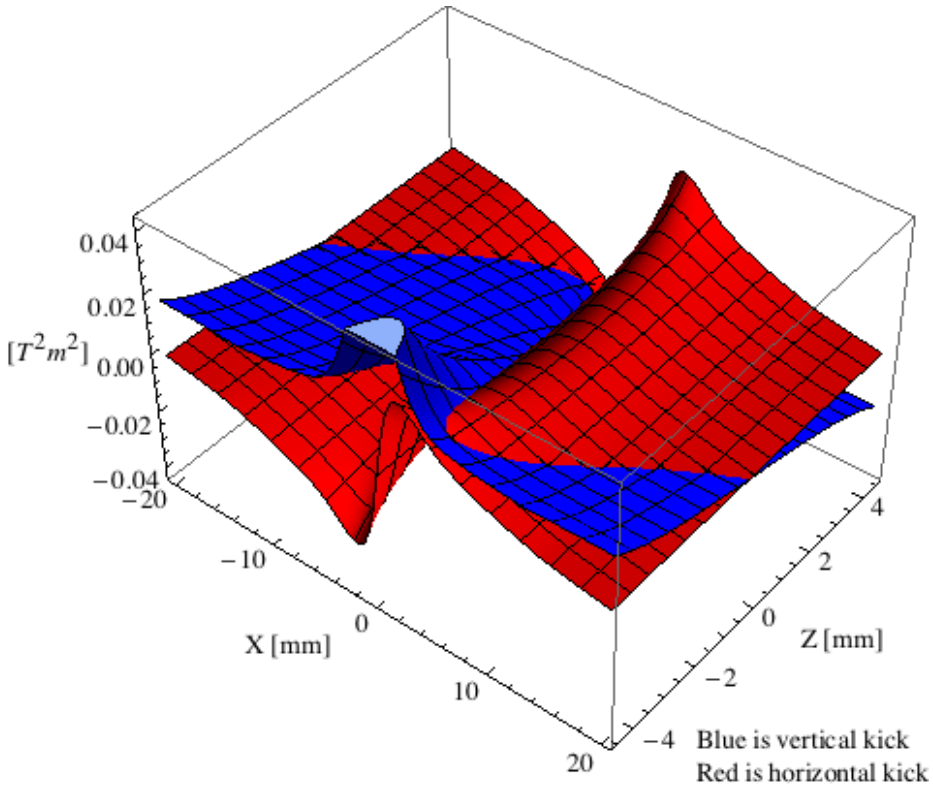

Figure 195: Kick map in the beam energy independant unit T^2m^2 of the kicks induced by the epu90Vert over the beam stay clear aparture.

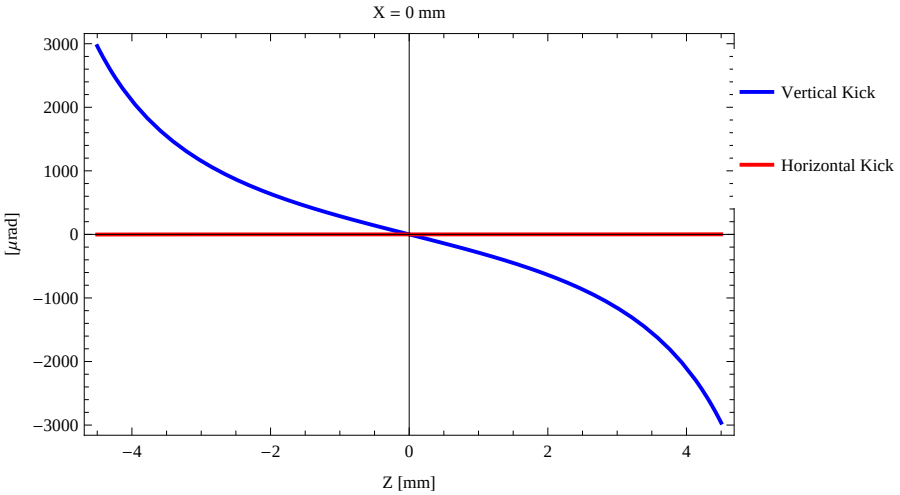

Figure 196: Induced angular kick on the stored beam from the epu90Vert as a function of the vertical distance to the undulator axis.

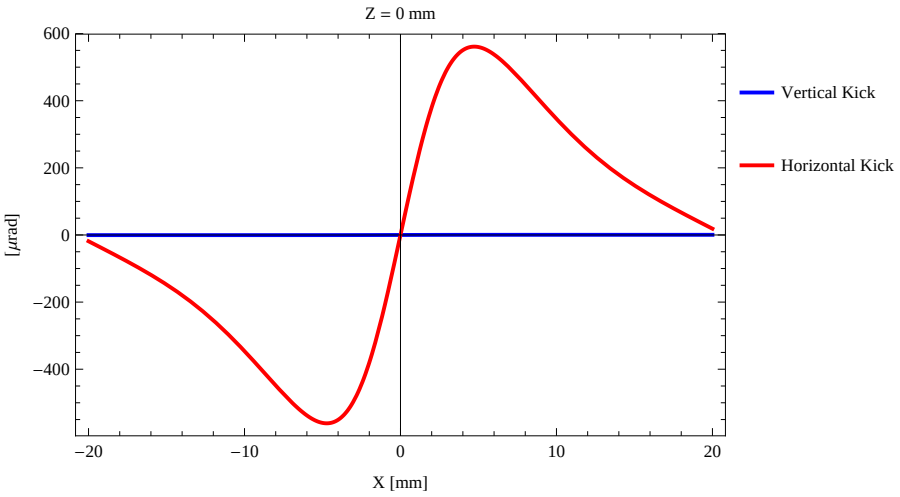

Figure 197: Induced angular kick on the stored beam from the epu90Vert as a function of the horizontal distance to the undulator axis.

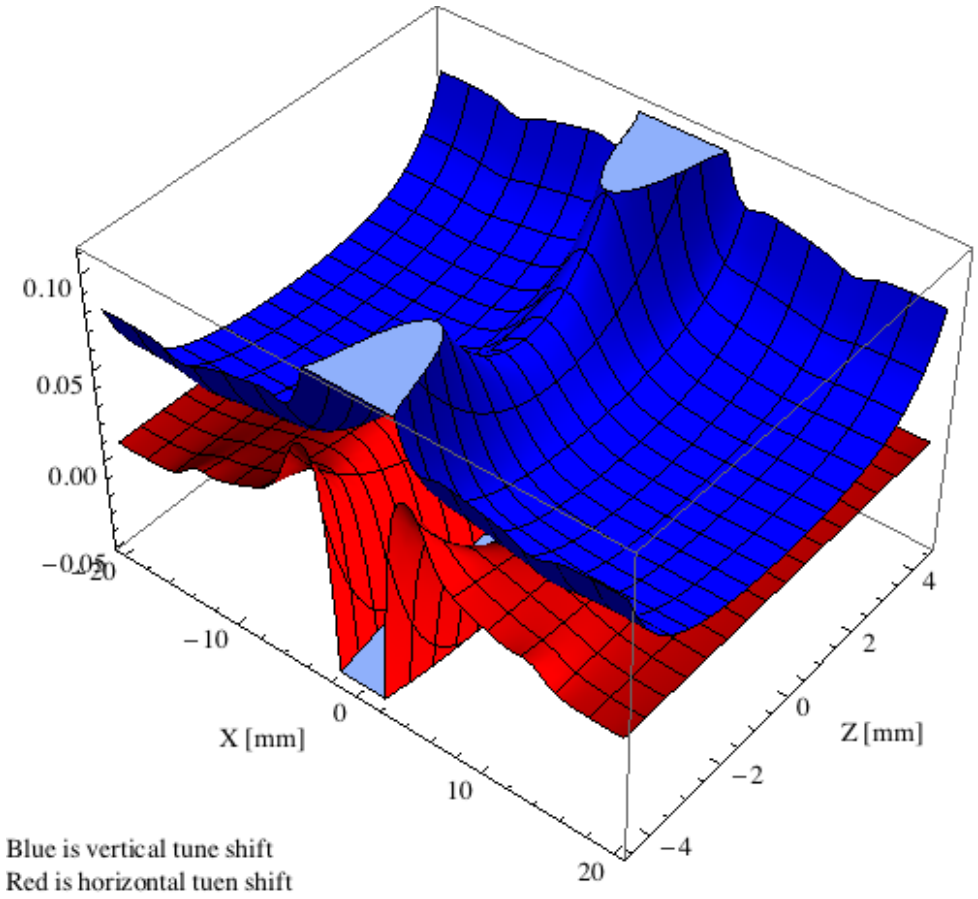

Figure 198: Tune shift induced by the epu90Vert over the beam stay clear aparture.

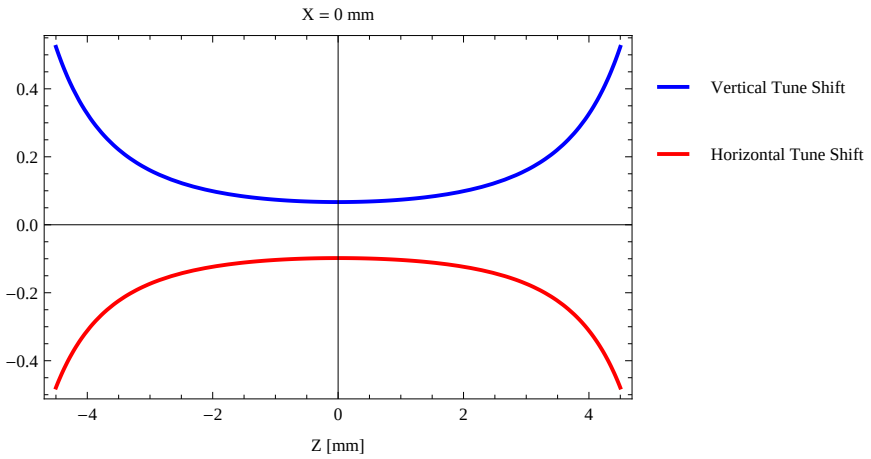

Figure 199: Induced tune shift from the epu90Vert as a function of the vertical distance to the undulator axis.

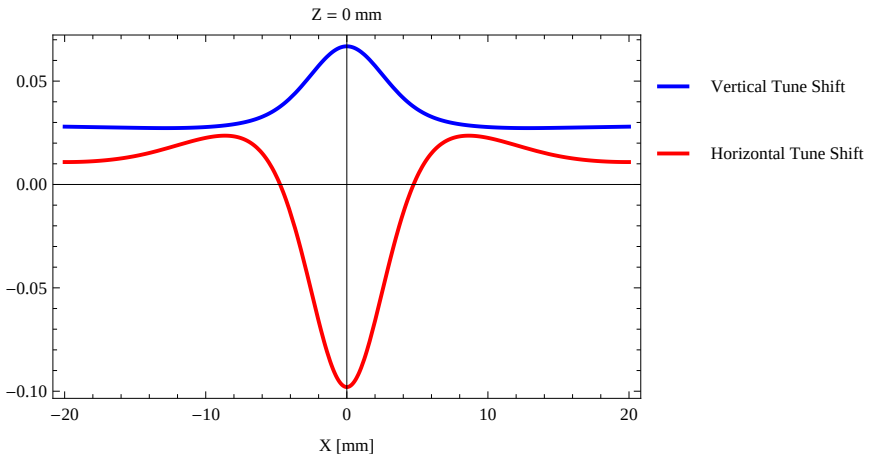

Figure 200: Induced tune shift from the epu90Vert on the stored beam from the as a function of the horizontal distance to the undulator axis.

4 The elliptically polarizing undulator epu72

4.1 Modes of operation in the elliptically polarizing undulator epu72

Horizontal polarisation of the emitted synchrotron radiation from the epu72 (Period=72 mm, Gap=13mm) is found in the planar mode when there is no movement of the sub-girders.

Circular polarisation is found in the elliptical mode of operation for a symmetric sub-grider movement of 20.7303 mm. Figure 201 shows the vertical and horizontal magnetic field for the epu72 when operating in the helical mode.

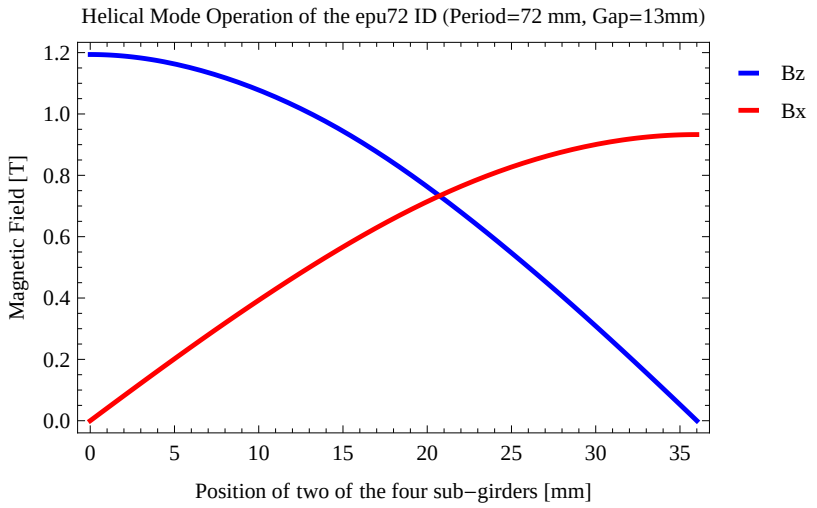

Figure 201: Vertical and horizontal magnetic field for the the epu72 when operating in the helical mode for different positions for two of the four sub-girders

45 degree polarisation is found in the inclined mode of operation for an assymetric sub-grider movement of 19.3793 mm. Figure 202 shows the vertical and horizontal magnetic field for the epu72 when operating in the inclined mode.

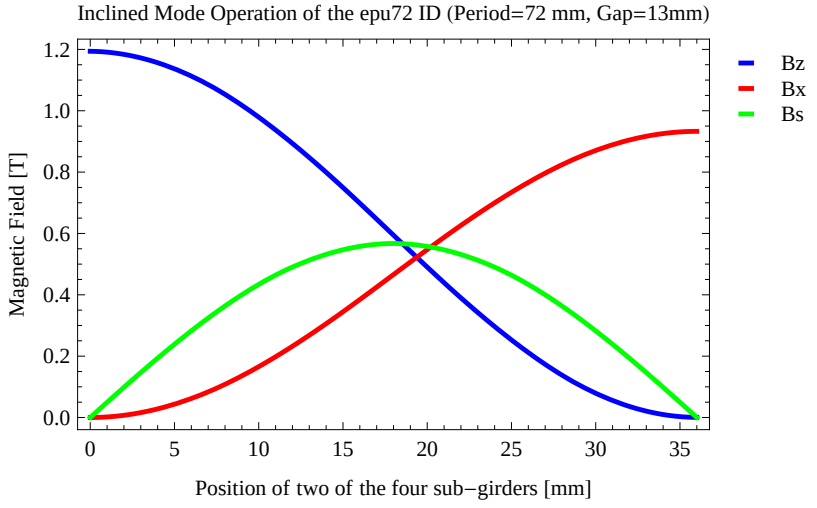

Figure 202: Vertical, horizontal, and longitudinal magnetic field for the the epu72 when operating in the inclined mode for different positions for two of the four sub-girders

The following sub-sections will cover four different situations: The epu72 operating in the planar

mode for horizontal polarisation (epu72Plan); The epu72 operating in the helical mode for circular polarisation (epu72Heli),), the epu72operating in the inclined mode for 45 degree polarisation (epu72Incl); and The epu72 operating in the vertical mode for vertical polarisation (epu72Vert).

4.2 Magnet model of the elliptically polarizing undulator epu72Plan

The Radia [2] magnet model of the epu72Plan is shown in Figure 203. The length of the magnet model is 594.744 mm. The magnetic material in the model is NdFeb with a remanence of 1.33 T. Blocks with vertical magnetisation are blue and blocks with horizontal magnetisation are yellow. The block size is 35.x35.x18. mm^3 and there is a 5. mm cut-out in two of the corners of the blocks. The total length of the epu72Plan is 2610.74 mm.

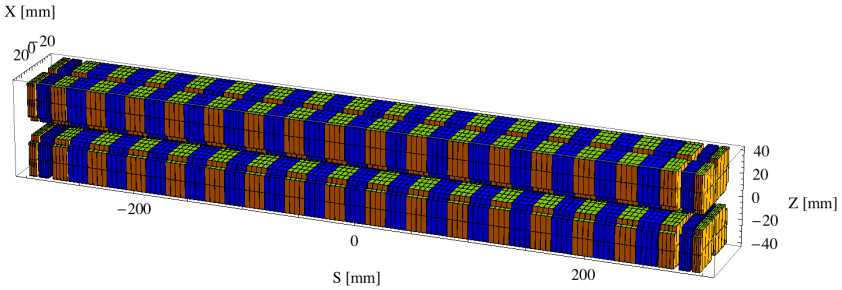

Figure 203: Magnetic model of the epu72Plan. The has been modelled with Radia [2]

4.3 Analysis of the magnetic field of the epu72Plan

The effective magnetic fields on axis and the fundamental photon energy of the epu72Plan are shown in Table 30. The higher harmonic contents in the magnetic field of an elliptically polarizing undulator made of permanent magnets is usually small and the effective field has approximately the same strength as the peak field.

Table 30: Effective Fields on axis and Fundamental Photon Energy of the epu72Plan

Undulator Period	72	mm
Undulator Gap	13	mm
Undulator Mode	Planar	
Undulator Phase	0.000	mm
Vertical Peak Field	1.168	T
effective Vertical Field	1.194	T
Kx (from vert. field)	8.029	
Horizontal Peak Field:	0.000	T
effective Horizontal Field	0.000	T
Kz (from hor. field)	0.000	
Photon Energy, Harm.1	0.009	keV
Emitted Power	1.590	kW
Total Length	2610.7	mm

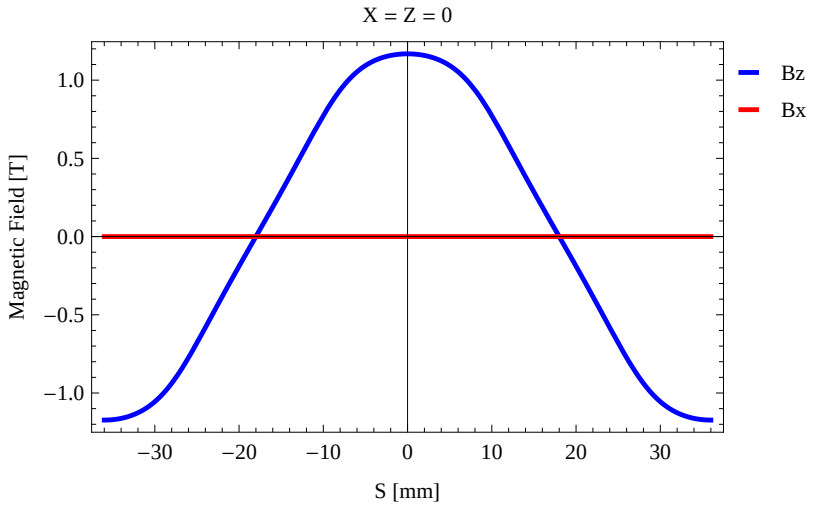

Figure 204: Vertical magnetic field in a central pole of the epu72Plan along the axis, X = Z = 0

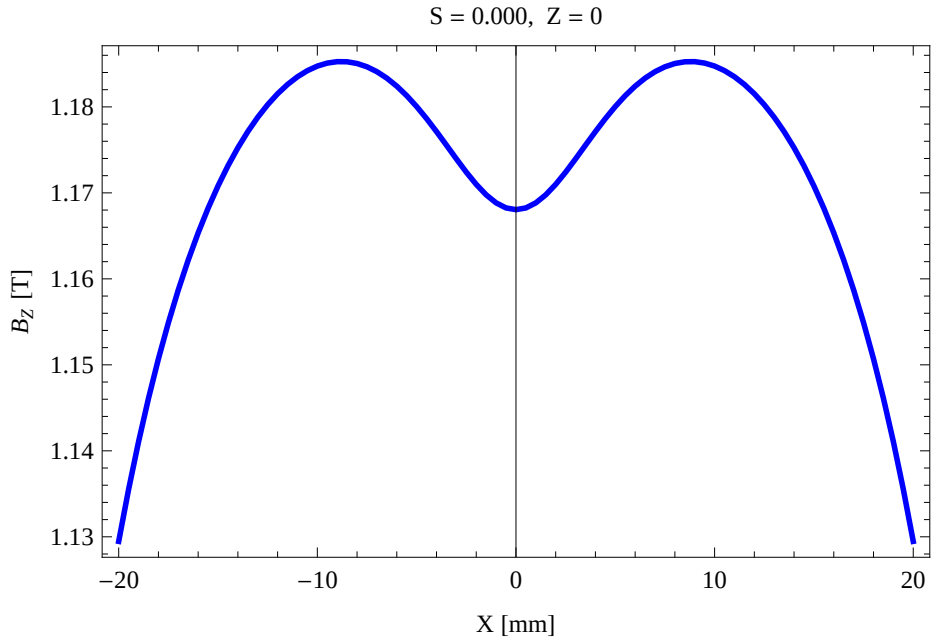

Figure 205: Vertical magnetic field in a central pole of the epu72Plan along the horizontally transverse direction to the axis, S = 0.000, Z = 0

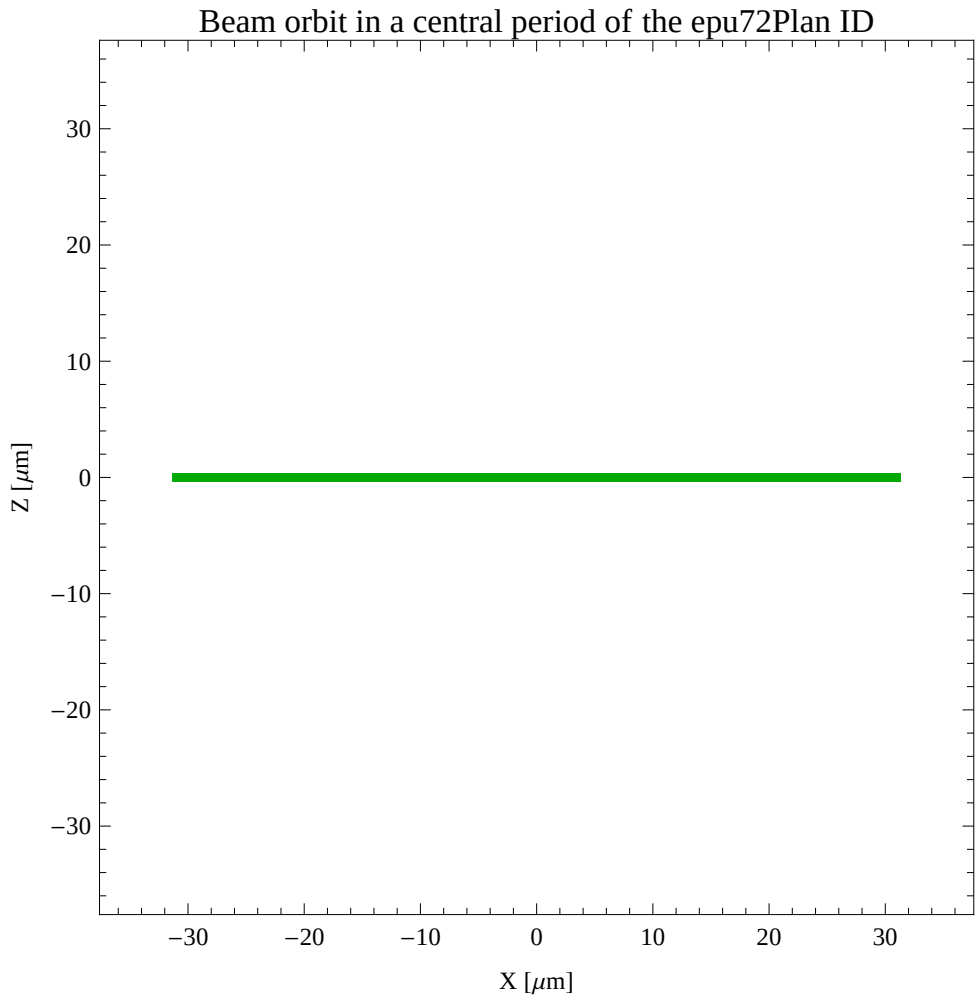

Figure 206: The beam orbit of the electron beam through a central period of the epu72Plan

4.4 Synchrotron radiation from the epu72Plan

The power map of the emitted synchrotron radiation by the epu72Plan, assuming a 0.3 A filament beam with an energy of 1.5 GeV and undulator properties of the synchrotron radiation, is shown in Figure 207. The on-axis power density is 0.687494 kW/mrad^2

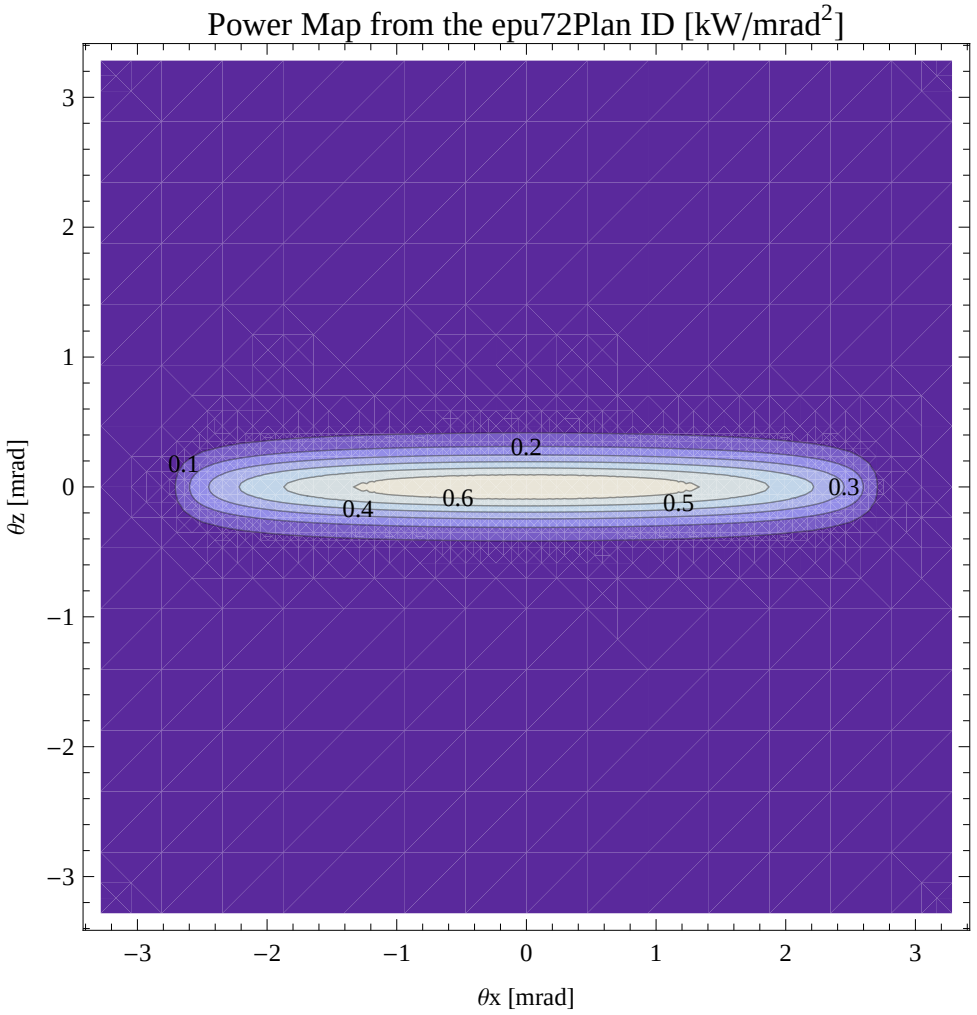

Figure 207: Map of the power distribution of the emitted synchrotron radiation by the epu72Plan

A map of the degree of linear polarisation of the fundamental harmonic of the synchotron radiation emitted by the epu72Plan over the angle of observation is shown in Figure 208.

A map of the degree of 45 degree polarisation of the fundamental harmonic of the synchotron radiation emitted by the epu72Plan over the angle of observation is shown in Figure 209.

A map of the degree of circular polarisation of the fundamental harmonic of the synchotron radiation emitted by the epu72Plan over the angle of observation is shown in Figure 210.

The on axis brilliance at peak energy and the angular spectral flux from the epu72Plan have been calculated with the given beam parameters, which are 0.3 A of stored current, $\beta_H = 5.627$ m, $\varepsilon_H = 5.985$ nmrad, $\beta_V = 2.837$ m, $\varepsilon_V = 59.85$ pmrad, and an energy spread of 0.001.

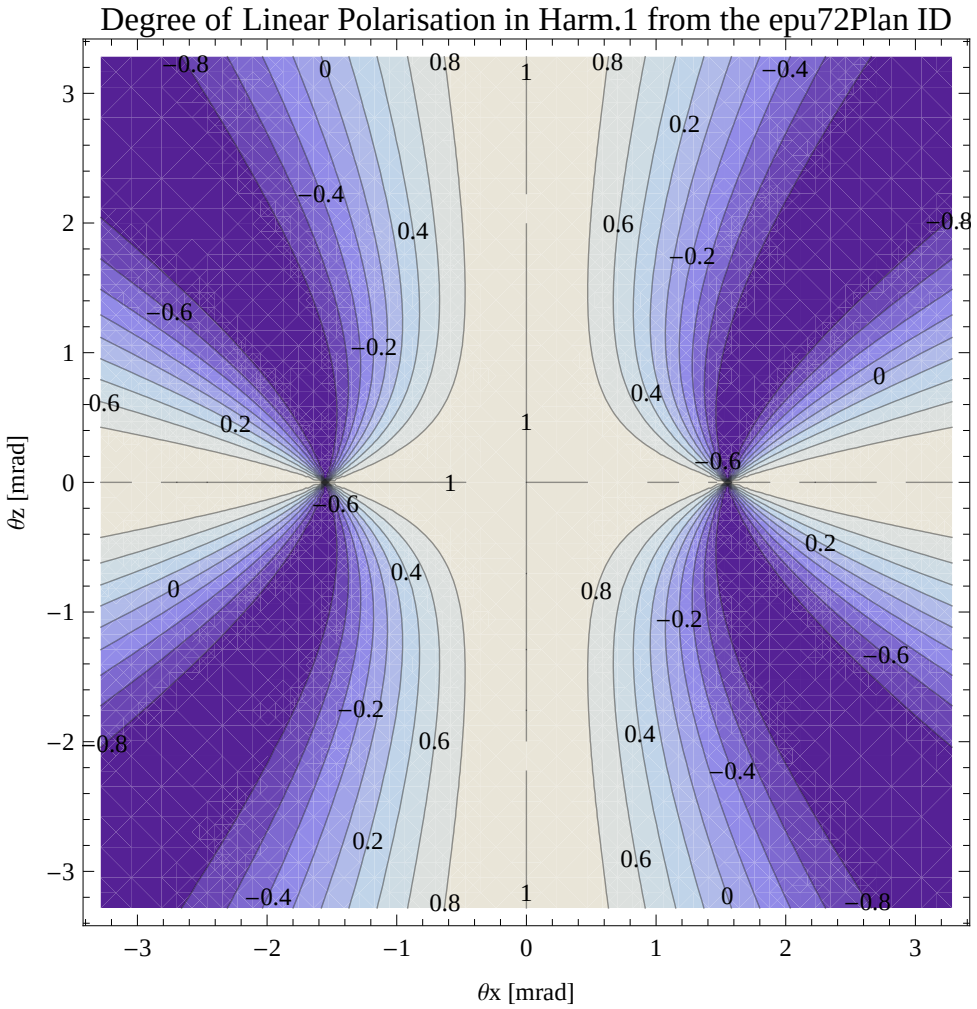

Figure 208: Map of linear polarisation in the fundamental harmonic of the synchotron radiation emitted by the epu72Plan

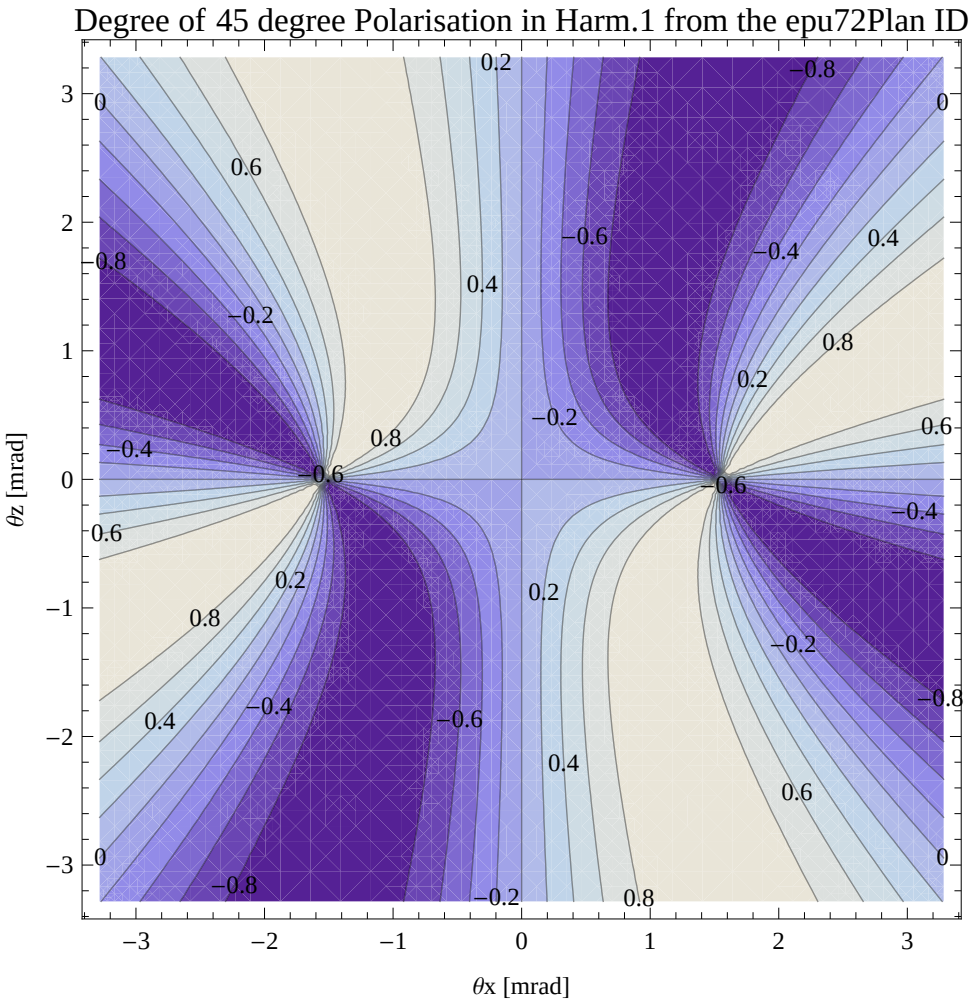

Figure 209: Map of 45 degree polarisation in the fundamental harmonic of the synchotron radiation emitted by the epu72Plan

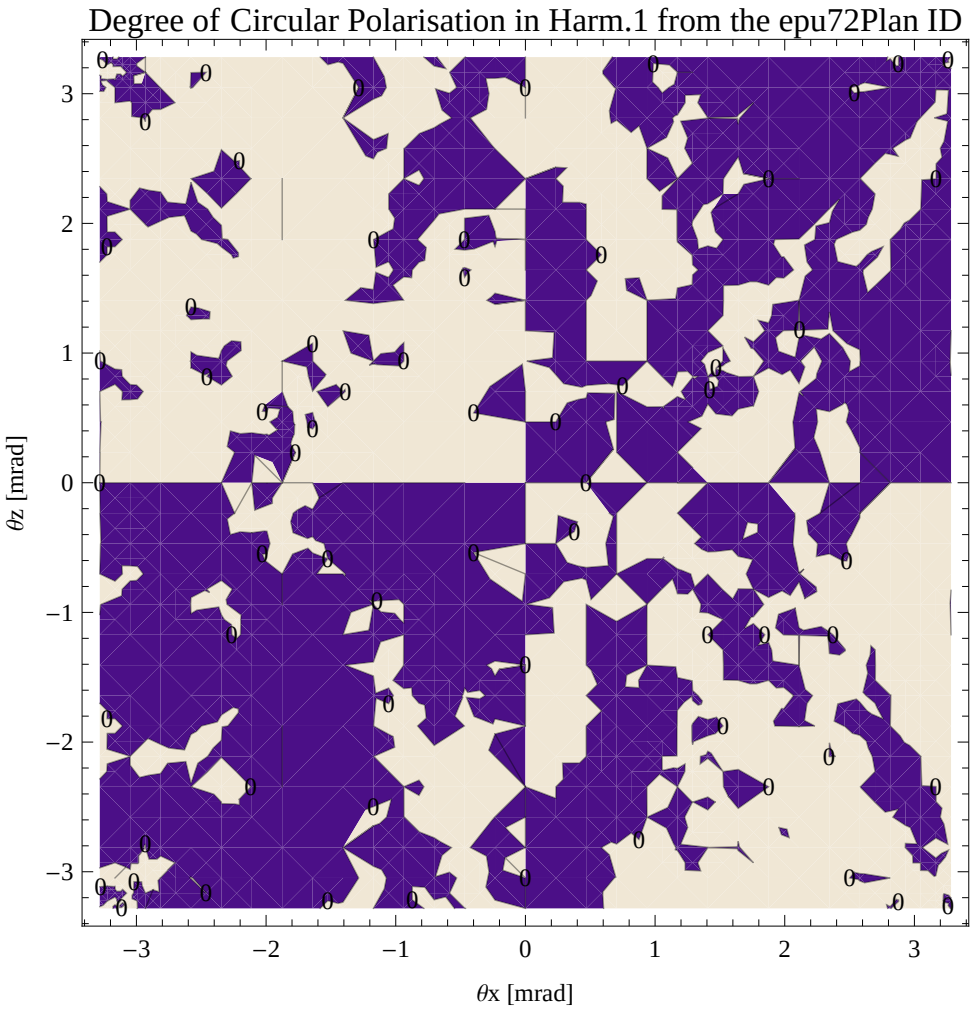

Figure 210: Map of circular polarisation in the fundamental harmonic of the synchotron radiation emitted by the epu72Plan

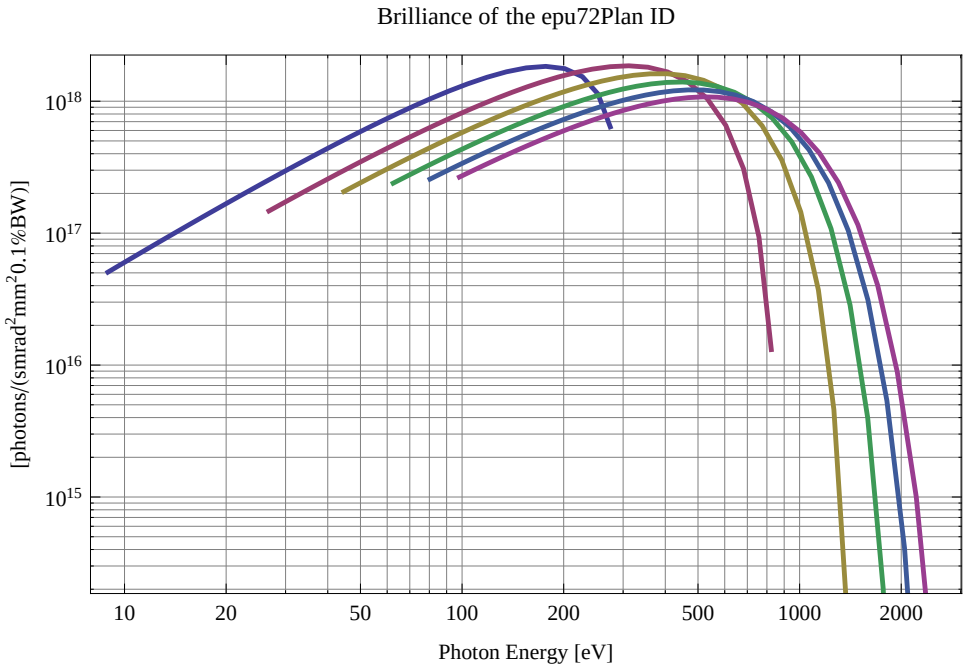

Figure 211: The brilliance at peak energy of the synchotron radiation emitted by the epu72Plan

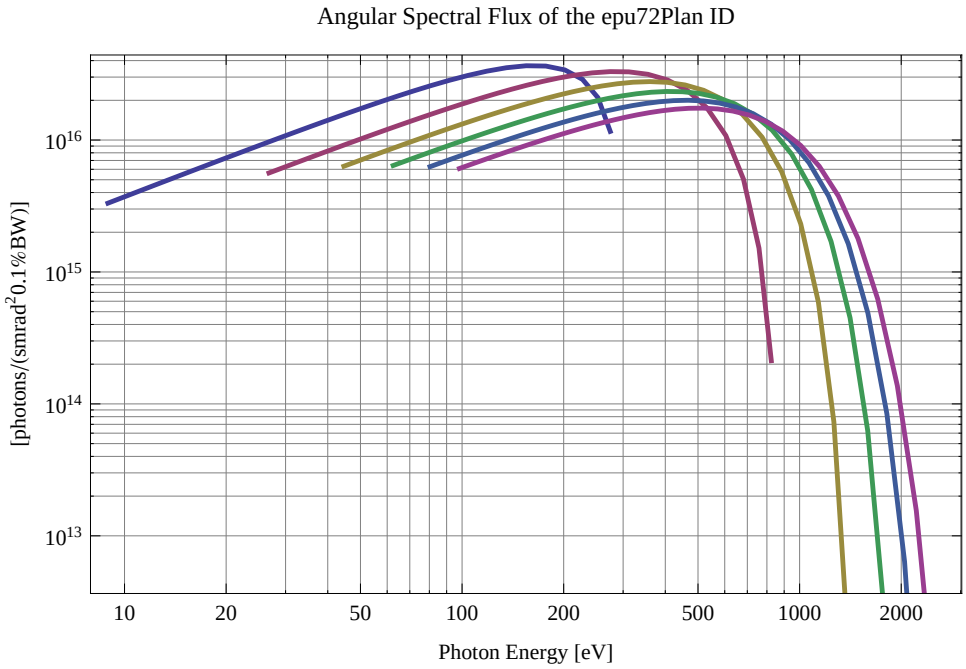

Figure 212: The angular spectral flux of the synchotron radiation emitted by the epu72Plan

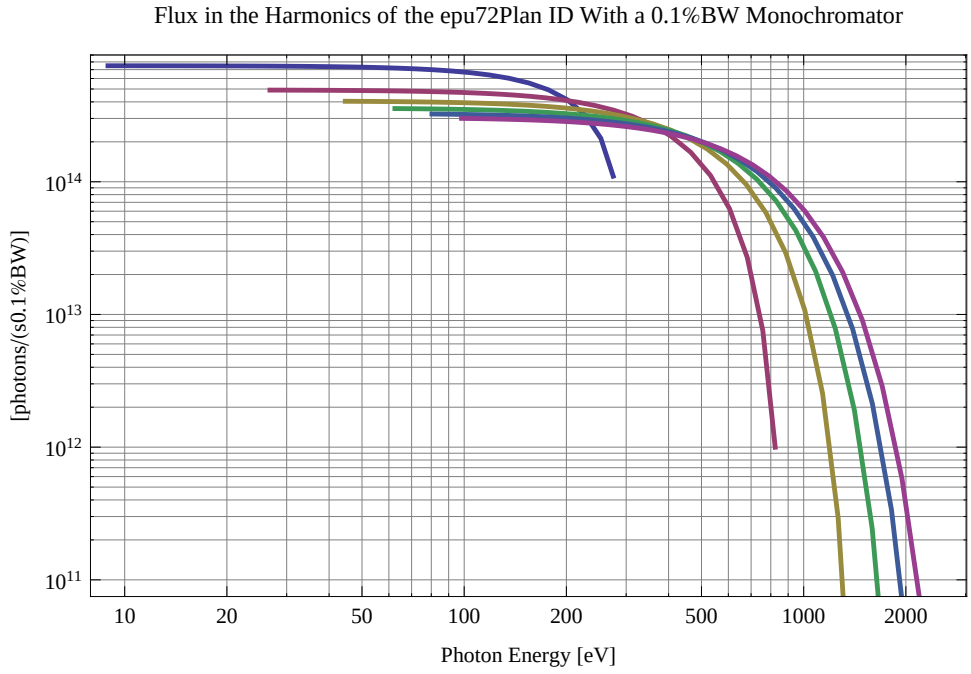

Figure 213: The flux of photons in the harmonics of the emitted synchrotron radiation from the epu72Plan using a 0.1%BW monochromator

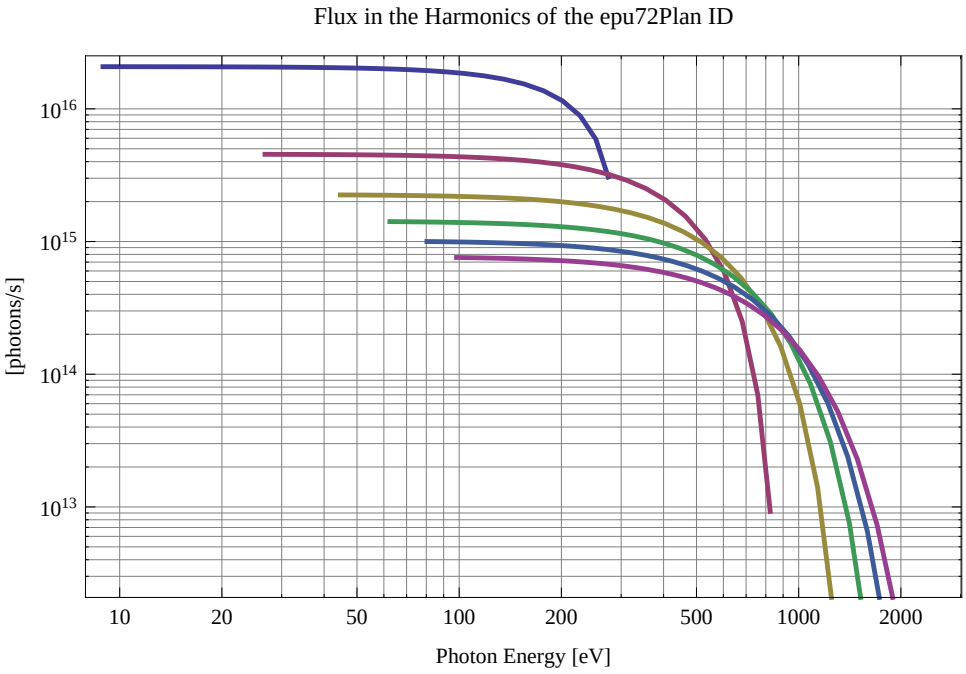

Figure 214: The flux of photons in the harmonics of the emitted synchrotron radiation from the epu72Plan

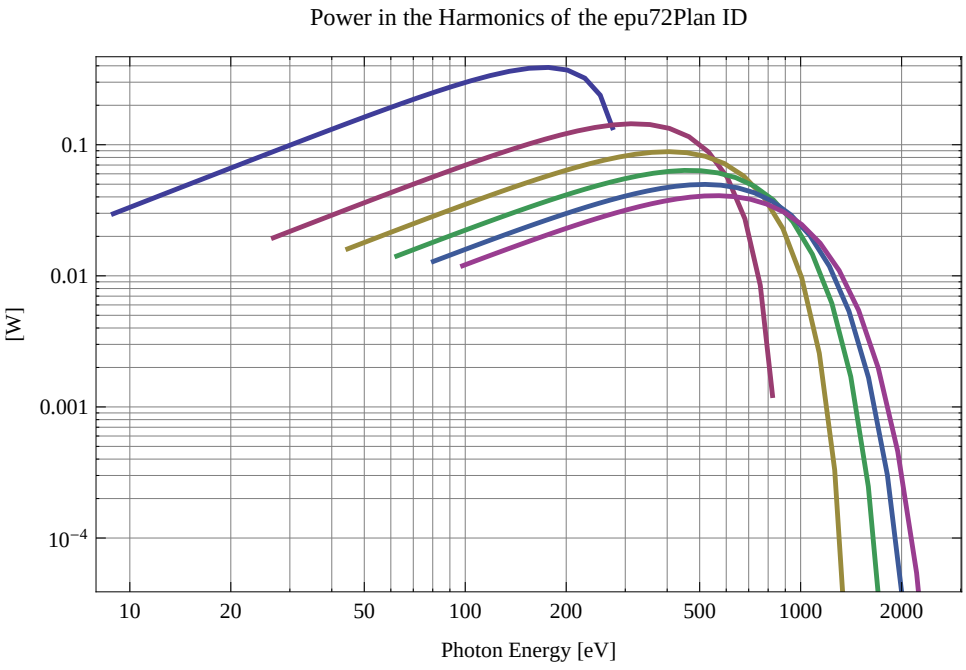

Figure 215: The power in the harmonics of the emitted synchrotron radiation from the epu72Plan

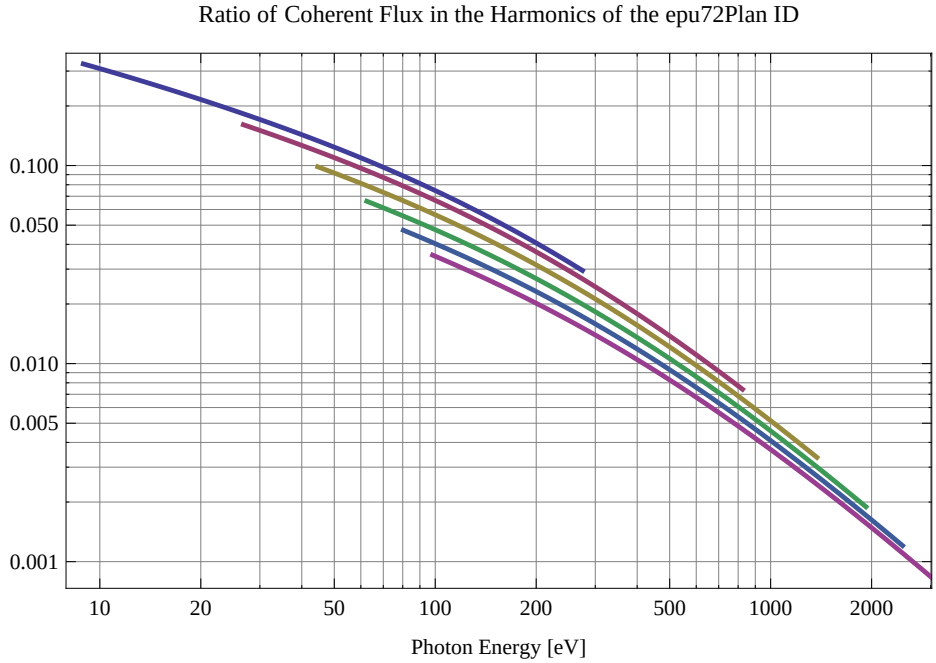

Figure 216: The ratio of coherent flux in the harmonics of the emitted synchrotron radiation from the epu72Plan

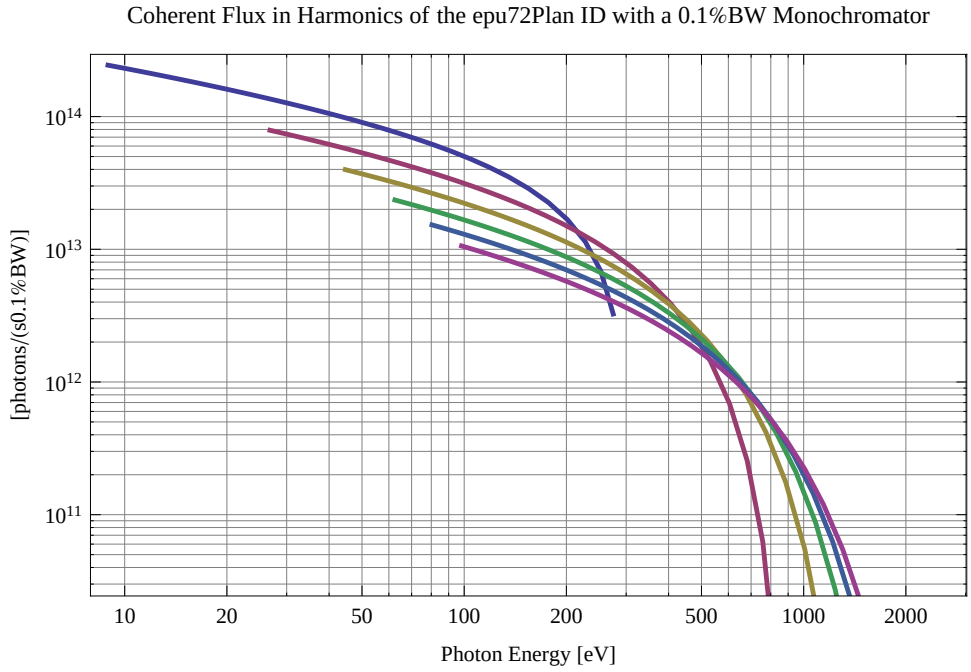

Figure 217: The coherent flux in the harmonics of the epu72Plan using a 0.1%BW Monochromator

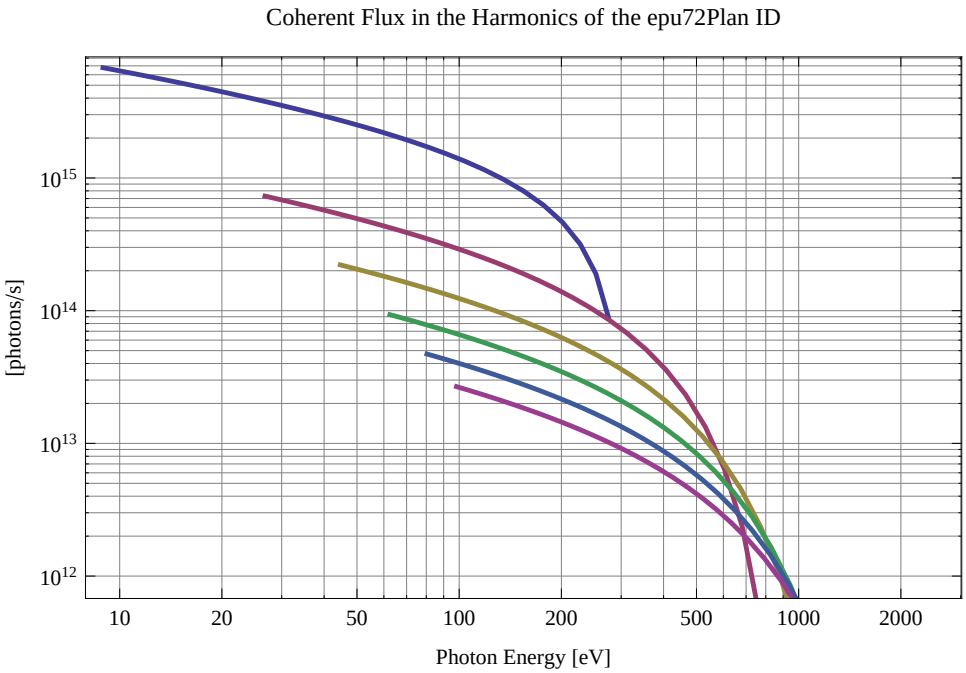

Figure 218: The coherent flux in the harmonics of the epu72Plan

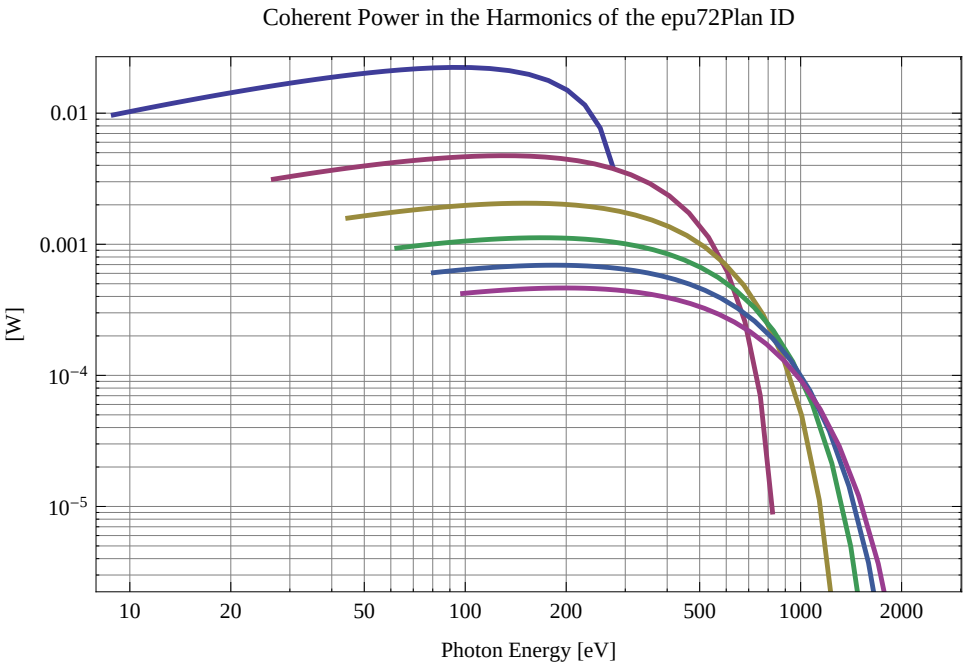

Figure 219: The power of coherent synchrotron radiation in the harmonics of the epu72Plan

The brilliance at peak energy and the angular spectral flux density from the epu72Plan for different harmonics at maximum K-value (8.029) are given in Table 31 and for minimum K-value (0.400) these values are given in Table 32.

Table 31: The brilliance at peak energy and the angular spectral flux density from the epu72Plan for different harmonics at maximum K-value (8.029)

Harmonic	Photon Energy [eV]	Brilliance [Ph./(smrad^{2}mrad^{2}0.1%BW)]	Angular Spectral Flux [Ph./(smrad^{2}0.1%BW)]
1	8.92902	5.06×10^{16}	3.32×10^{15}
3	26.7871	1.47×10^{17}	5.63×10^{15}
5	44.6451	2.07×10^{17}	6.33×10^{15}
7	62.5032	2.39×10^{17}	6.41×10^{15}
9	80.3612	2.57×10^{17}	6.28×10^{15}
11	98.2192	2.66×10^{17}	6.08×10^{15}

Table 32: The brilliance at peak energy and the angular spectral flux density from the epu72Plan for different harmonics at minimum K-value (0.4)

Harmonic	Photon Energy [eV]	Brilliance [Ph./(smrad^{2}mrad^{2}0.1%BW)]	Angular Spectral Flux [Ph./(smrad^{2}0.1%BW)]
1	274.78	6.39×10^{17}	1.16×10^{16}
3	824.34	1.31×10^{16}	2.13×10^{14}
5	1373.9	1.62×10^{14}	2.57×10^{12}
7	1923.46	1.79×10^{12}	2.81×10^{10}
9	2473.02	1.89×10^{10}	2.96×10^{8}
11	3022.58	1.96×10^{8}	3.07×10^{6}

4.5 Influence from the epu72Plan on the optics of the stored beam

Figure 220 shows the focusing potential from the epu72Plan over the beam stay clear aperture of the ring aparture.

Figure 221 shows the kick map in the beam energy independant unit T^2m^2 of the kicks induced by the epu72Plan over the beam stay clear aparture.

Figure 222 shows the induced angular kick on the stored beam from the epu72Plan as a function of the vertical distance to the undulator axis.

Figure 223 shows the induced angular kick on the stored beam from the epu72Plan as a function of the horizontal distance to the undulator axis.

Figure 224 shows tune shift induced by the epu72Plan over the beam stay clear aparture. Note that the tune shift depends on the beam size at the.

Figure 225 shows the induced tune shift from the epu72Plan as a function of the vertical distance to the undulator axis.

Figure 226 shows the induced tune shift from the epu72Plan as a function of the horizontal distance to the undulator axis.

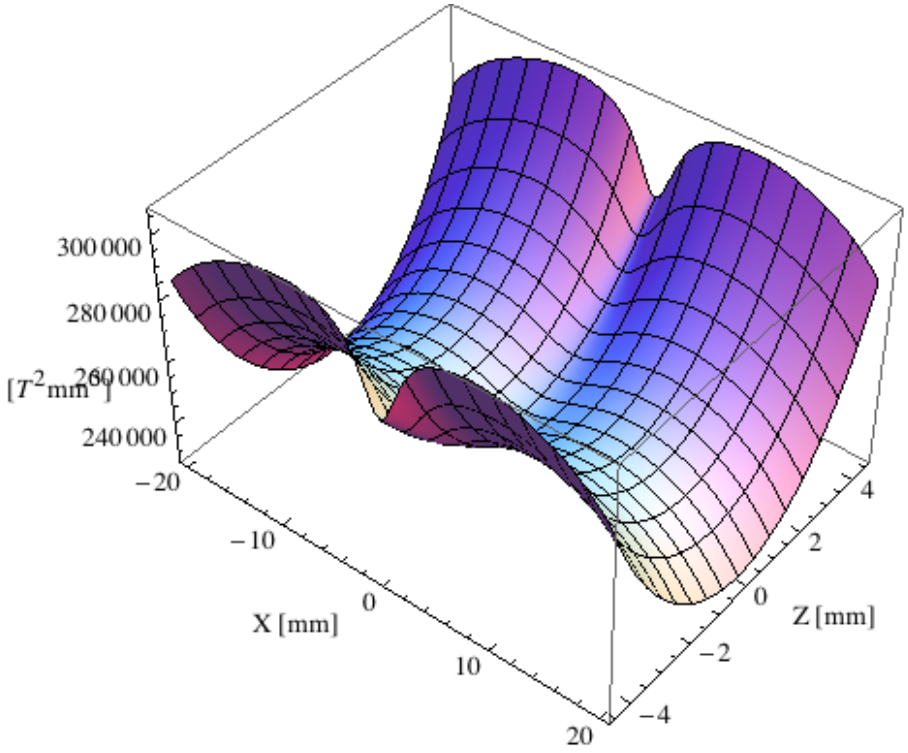

Figure 220: Focusing potential from the epu72Plan over the beam stay clear aparture.

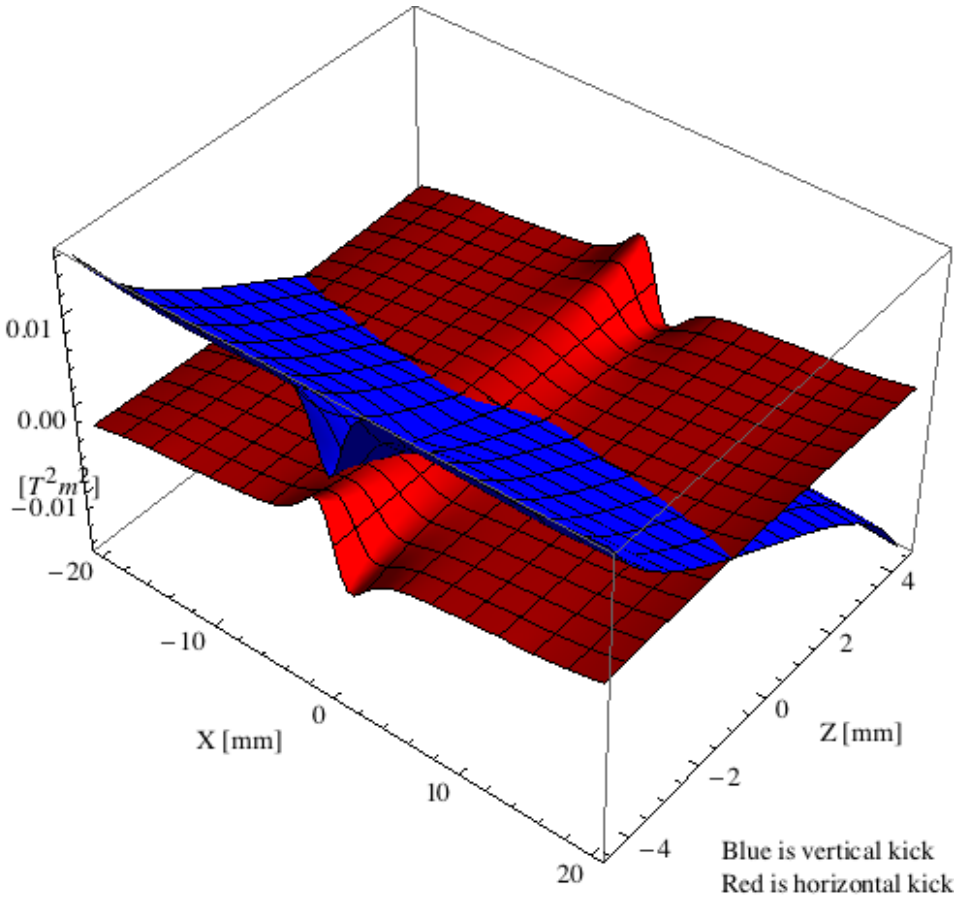

Figure 221: Kick map in the beam energy independant unit T^2m^2 of the kicks induced by the epu72Plan over the beam stay clear aparture.

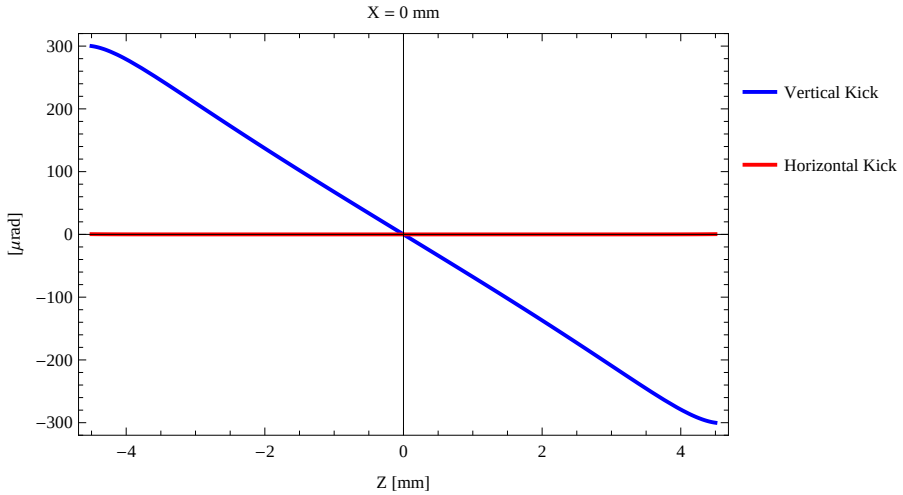

Figure 222: Induced angular kick on the stored beam from the epu72Plan as a function of the vertical distance to the undulator axis.

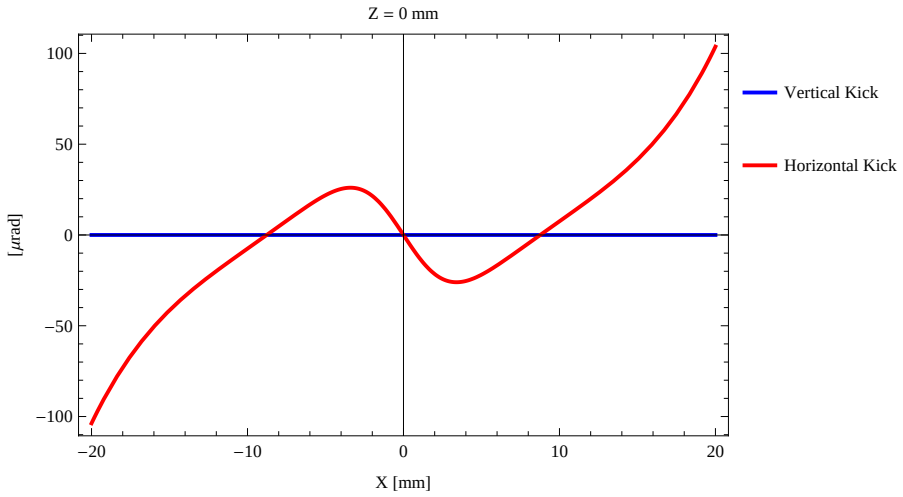

Figure 223: Induced angular kick on the stored beam from the epu72Plan as a function of the horizontal distance to the undulator axis.

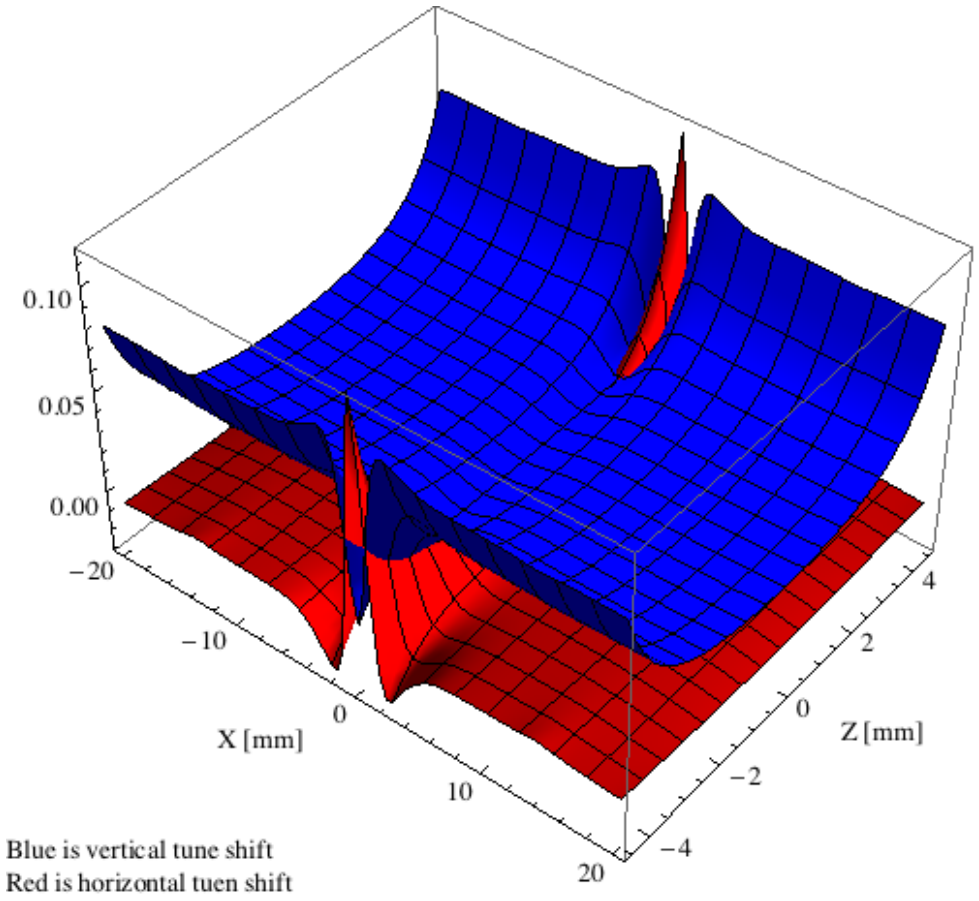

Figure 224: Tune shift induced by the epu72Plan over the beam stay clear aparture.

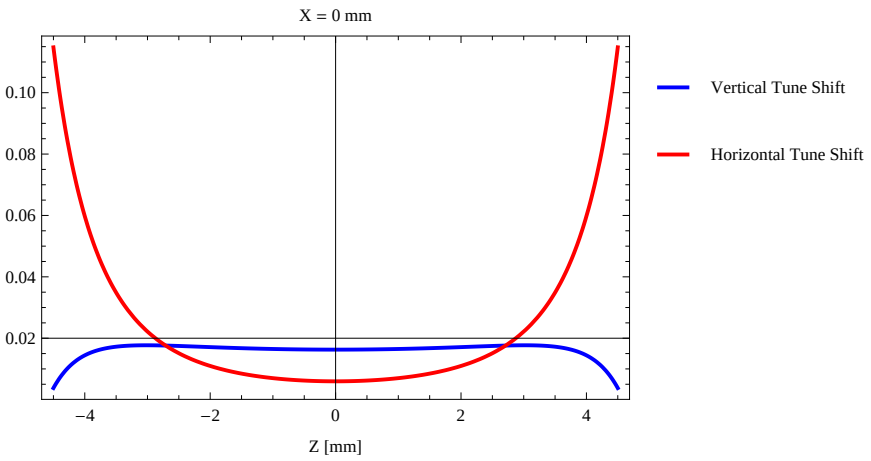

Figure 225: Induced tune shift from the epu72Plan as a function of the vertical distance to the undulator axis.

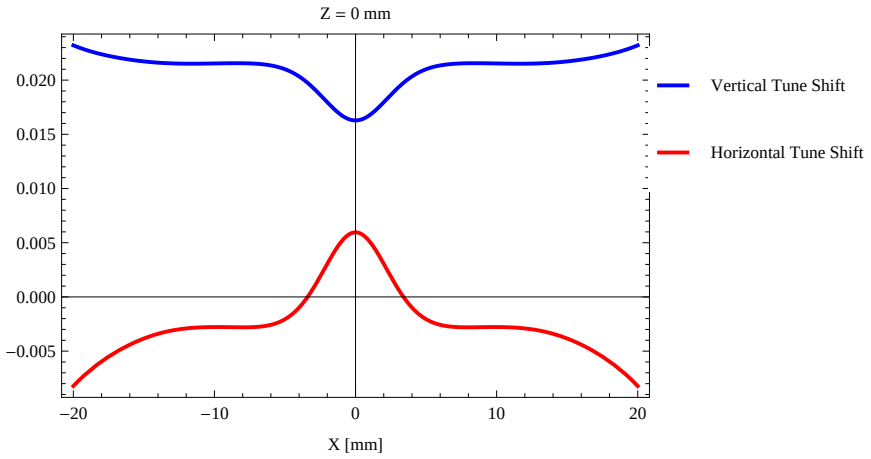

Figure 226: Induced tune shift from the epu72Plan on the stored beam from the as a function of the horizontal distance to the undulator axis.

4.6 Magnet model of the elliptically polarizing undulator epu72Heli

The Radia [2] magnet model of the epu72Heli is shown in Figure 227. The length of the magnet model is 594.744 mm. The magnetic material in the model is NdFeb with a remanence of 1.33 T. Blocks with vertical magnetisation are blue and blocks with horizontal magnetisation are yellow. The block size is 35.x35.x18. mm^3 and there is a 5. mm cut-out in two of the corners of the blocks. The total length of the epu72Heli is 2610.74 mm.

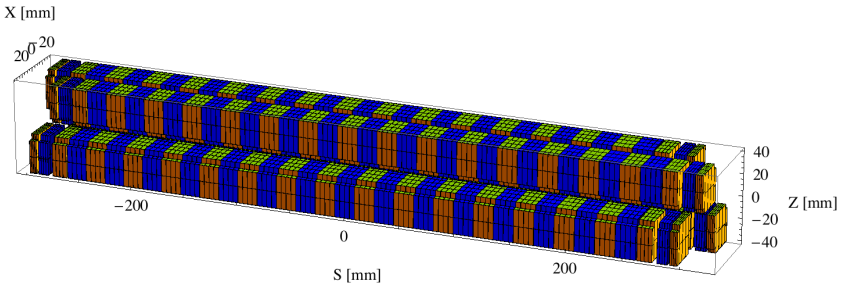

Figure 227: Magnetic model of the epu72Heli. The has been modelled with Radia [2]

4.7 Analysis of the magnetic field of the epu72Heli

The effective magnetic fields on axis and the fundamental photon energy of the epu72Heli are shown in Table 33. The higher harmonic contents in the magnetic field of an elliptically polarizing undulator made of permanent magnets is usually small and the effective field has approximately the same strength as the peak field.

4.8 Synchrotron radiation from the epu72Heli

The power map of the emitted synchrotron radiation by the epu72Heli, assuming a 0.3 A filament beam with an energy of 1.5 GeV and undulator properties of the synchrotron radiation, is shown in Figure 232. The on-axis power density is 0.000588 kW/mrad^2

Table 33: Effective Fields on axis and Fundamental Photon Energy of the epu72Heli

Undulator Period	72	mm
Undulator Gap	13	mm
Undulator Mode	Helical	
Undulator Phase	20.730	mm
Vertical Peak Field	0.734	T
effective Vertical Field	0.733	T
Kx (from vert. field)	4.929	
Horizontal Peak Field:	0.741	T
effective Horizontal Field	0.733	T
Kz (from hor. field)	4.929	
Photon Energy, Harm.1	0.012	keV
Emitted Power	1.198	kW
Total Length	2610.7	mm

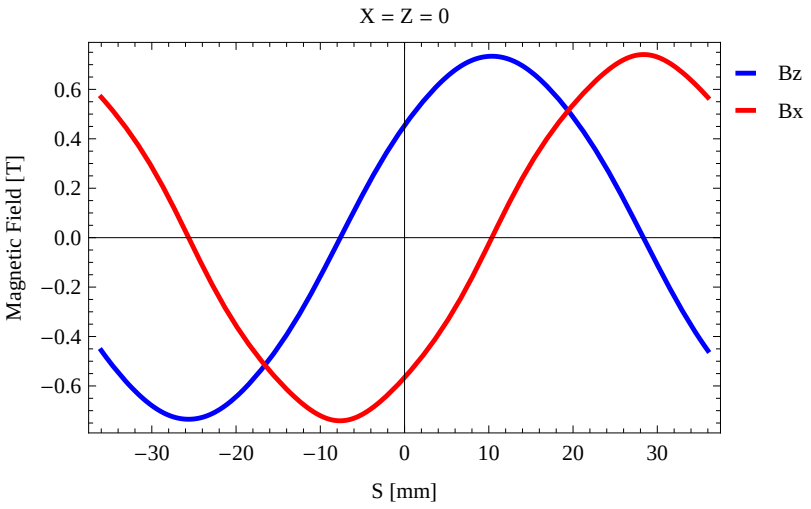

Figure 228: Vertical magnetic field in a central pole of the epu72Heli along the axis, X = Z = 0

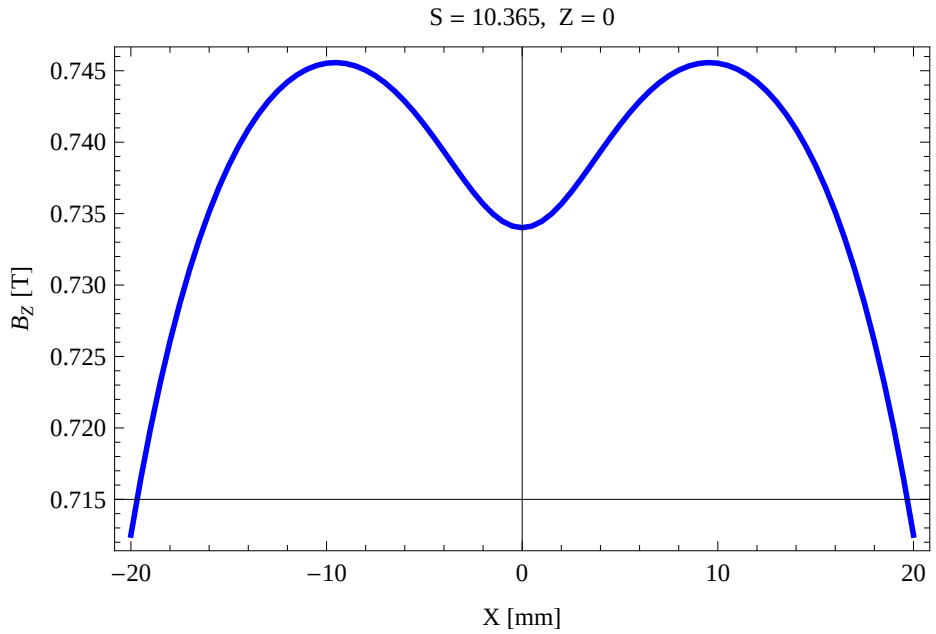

Figure 229: Vertical magnetic field in a central pole of the epu72Heli along the horizontally transverse direction to the axis, S = 10.365, Z = 0

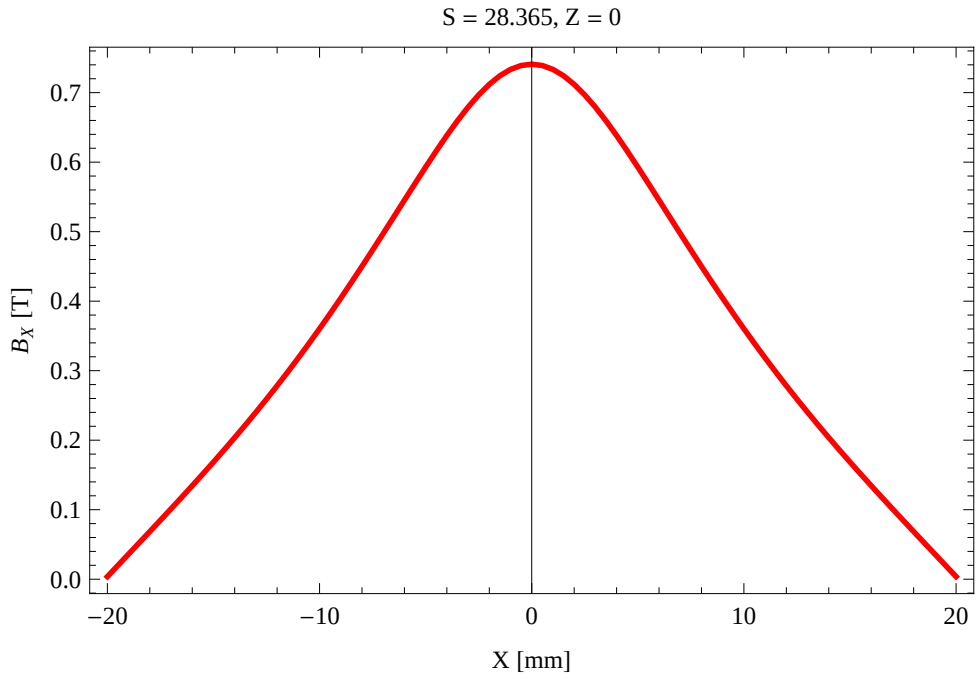

Figure 230: Horizontal magnetic field in a central pole of the epu72Heli along the horizontally transverse direction to the axis, S = 28.365, Z = 0

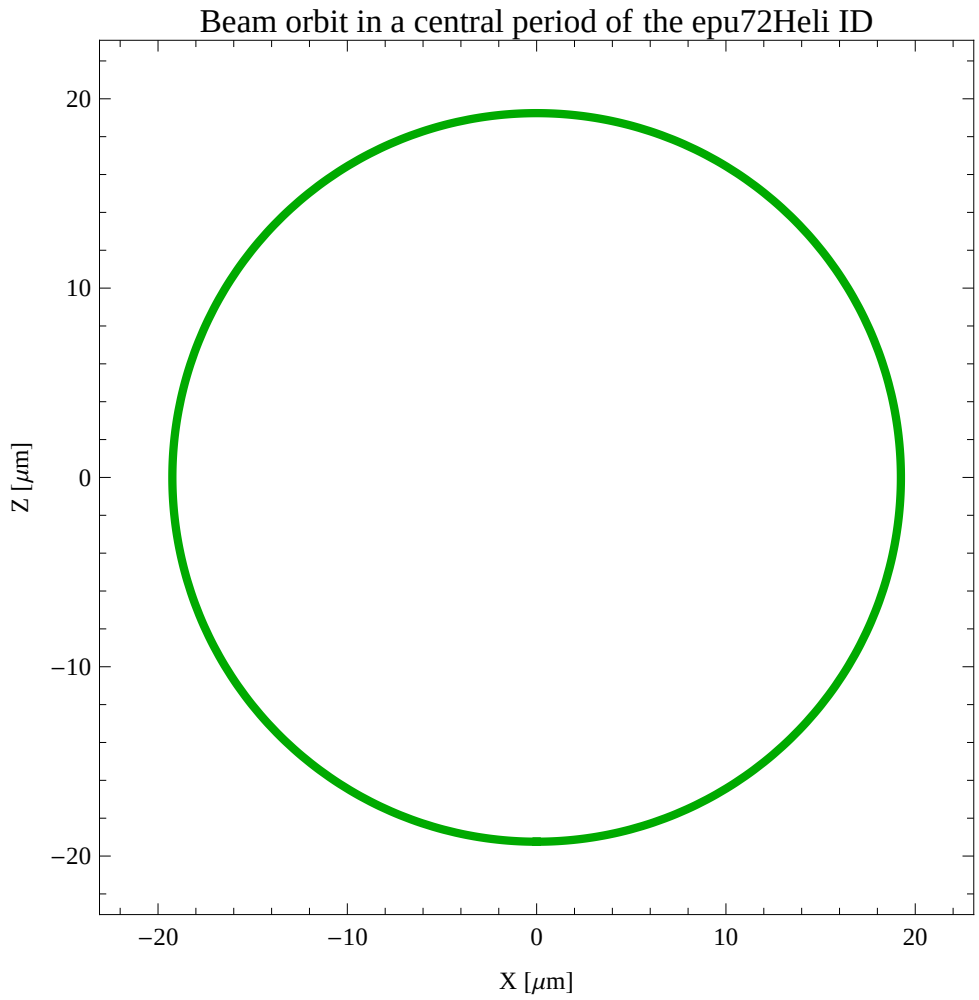

Figure 231: The beam orbit of the electron beam through a central period of the epu72Heli

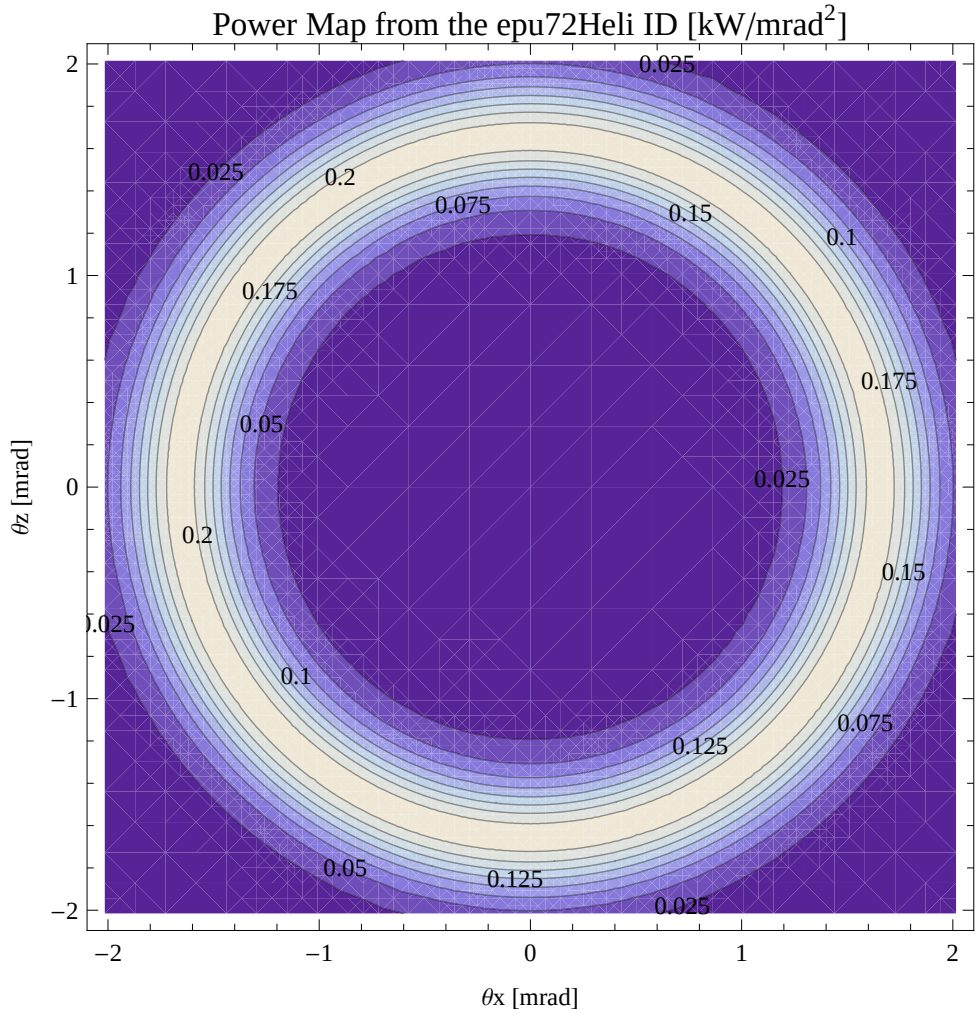

Figure 232: Map of the power distribution of the emitted synchrotron radiation by the epu72Heli

A map of the degree of linear polarisation of the fundamental harmonic of the synchotron radiation emitted by the epu72Heli over the angle of observation is shown in Figure 233.

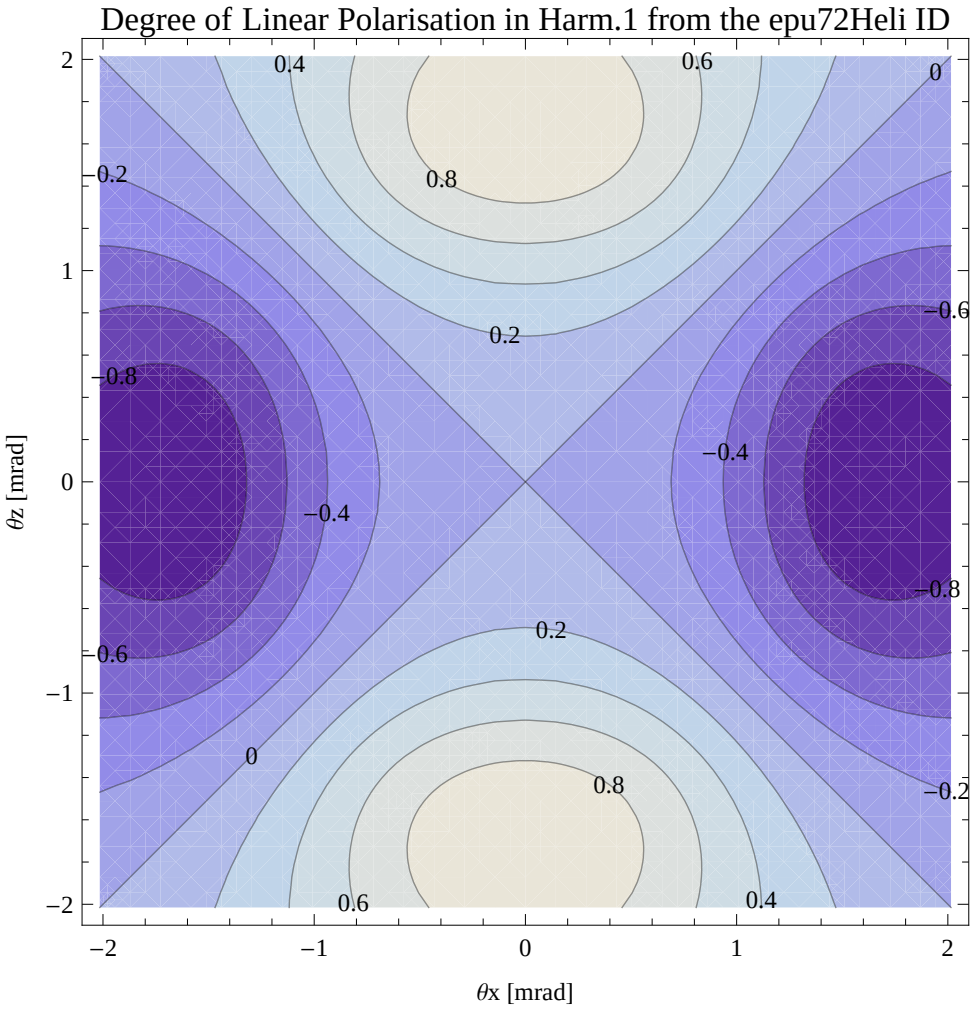

Figure 233: Map of linear polarisation in the fundamental harmonic of the synchotron radiation emitted by the epu72Heli

A map of the degree of 45 degree polarisation of the fundamental harmonic of the synchotron radiation emitted by the epu72Heli over the angle of observation is shown in Figure 234.

A map of the degree of circular polarisation of the fundamental harmonic of the synchotron radiation emitted by the epu72Heli over the angle of observation is shown in Figure 235.

The on axis brilliance at peak energy and the angular spectral flux from the epu72Heli have been calculated with the given beam parameters, which are 0.3 A of stored current, $\beta_H = 5.627$ m, $\varepsilon_H = 5.985$ nmrad, $\beta_V = 2.837$ m, $\varepsilon_V = 59.85$ pmrad, and an energy spread of 0.001.

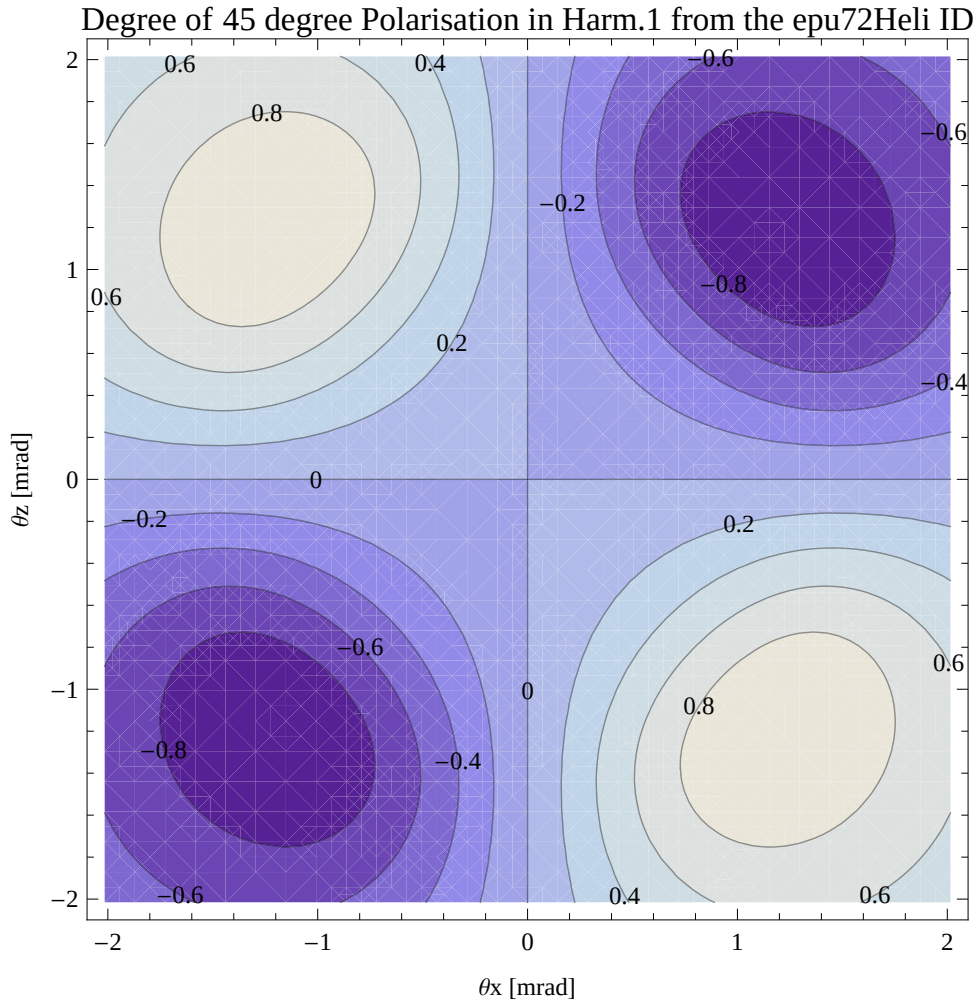

Figure 234: Map of 45 degree polarisation in the fundamental harmonic of the synchotron radiation emitted by the epu72Heli

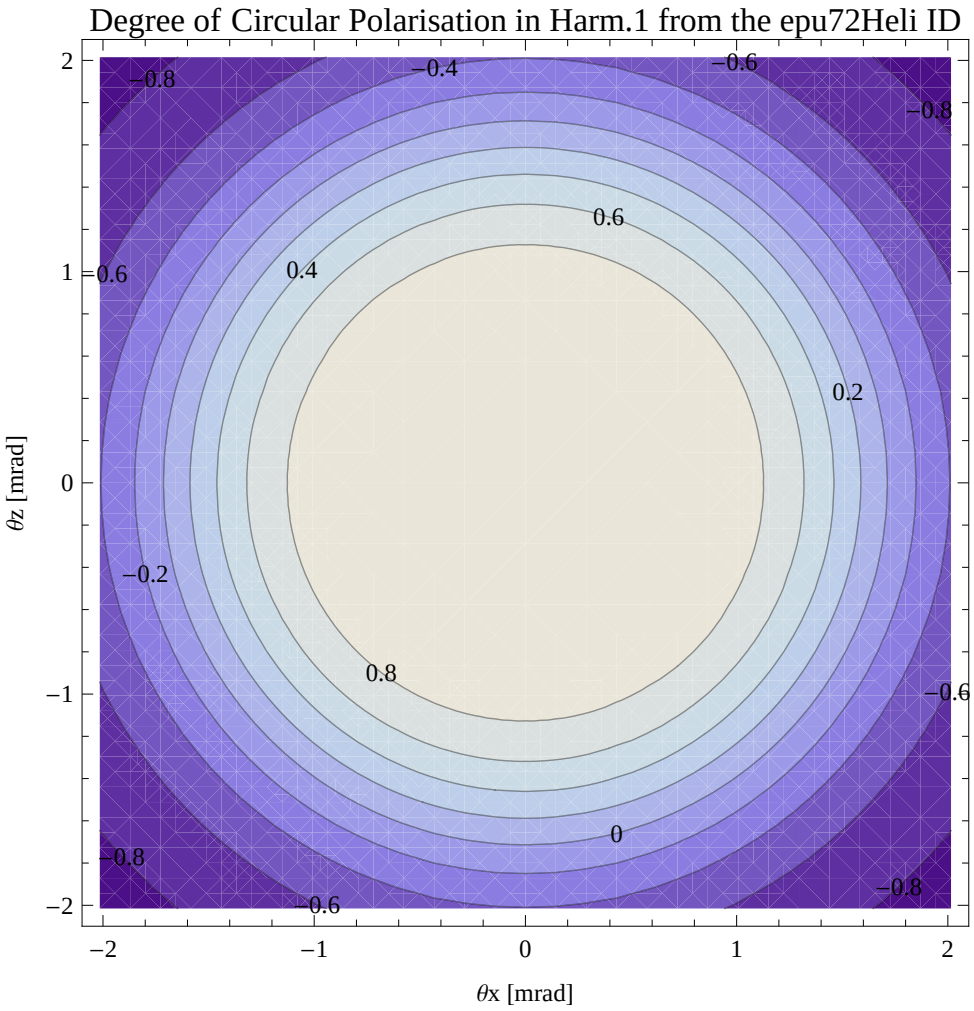

Figure 235: Map of circular polarisation in the fundamental harmonic of the synchotron radiation emitted by the epu72Heli

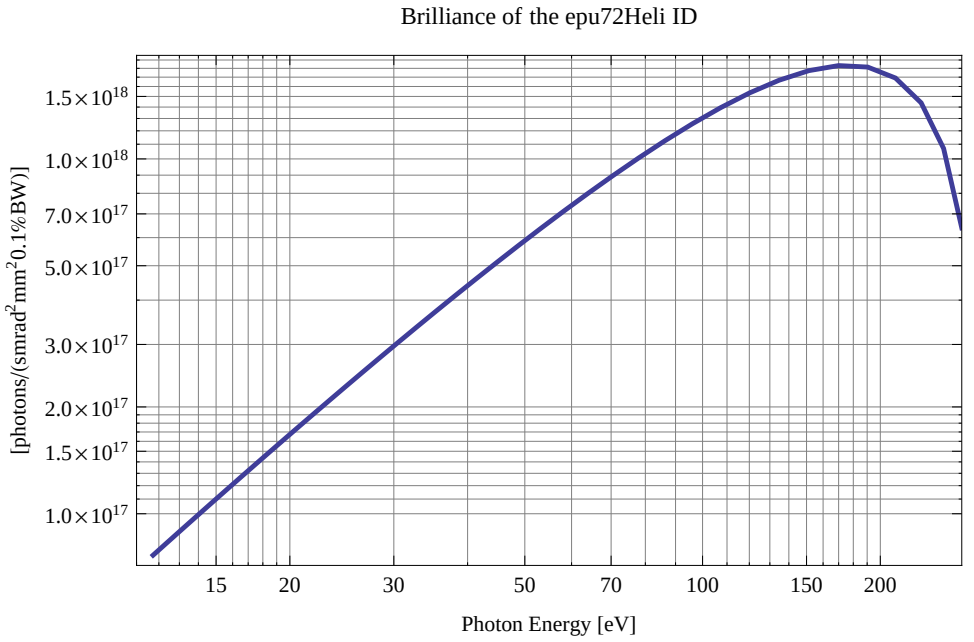

Figure 236: The brilliance at peak energy of the synchotron radiation emitted by the epu72Heli

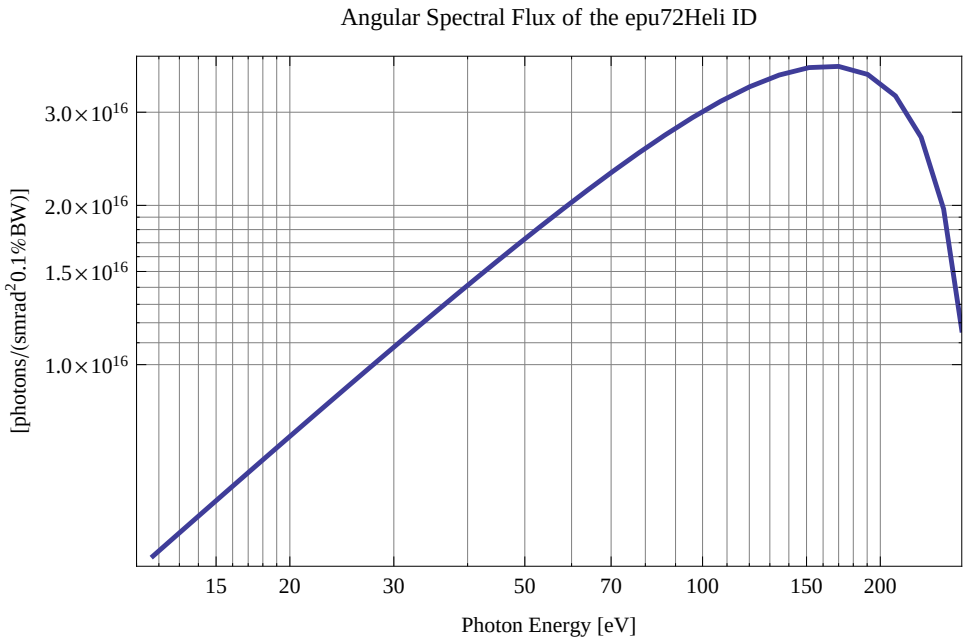

Figure 237: The angular spectral flux of the synchotron radiation emitted by the epu72Heli

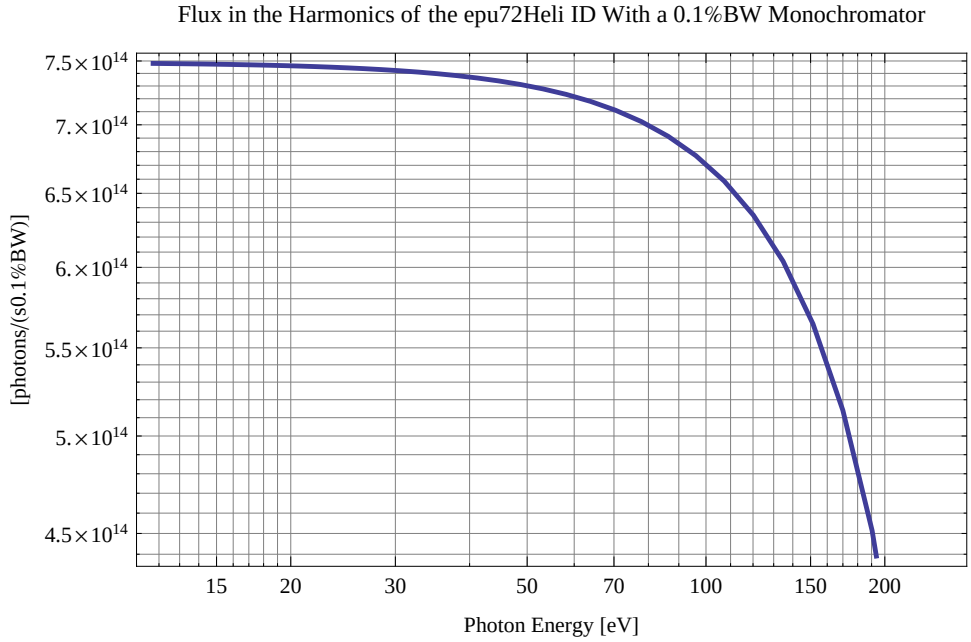

Figure 238: The flux of photons in the harmonics of the emitted synchrotron radiation from the epu72Heli using a 0.1%BW monochromator

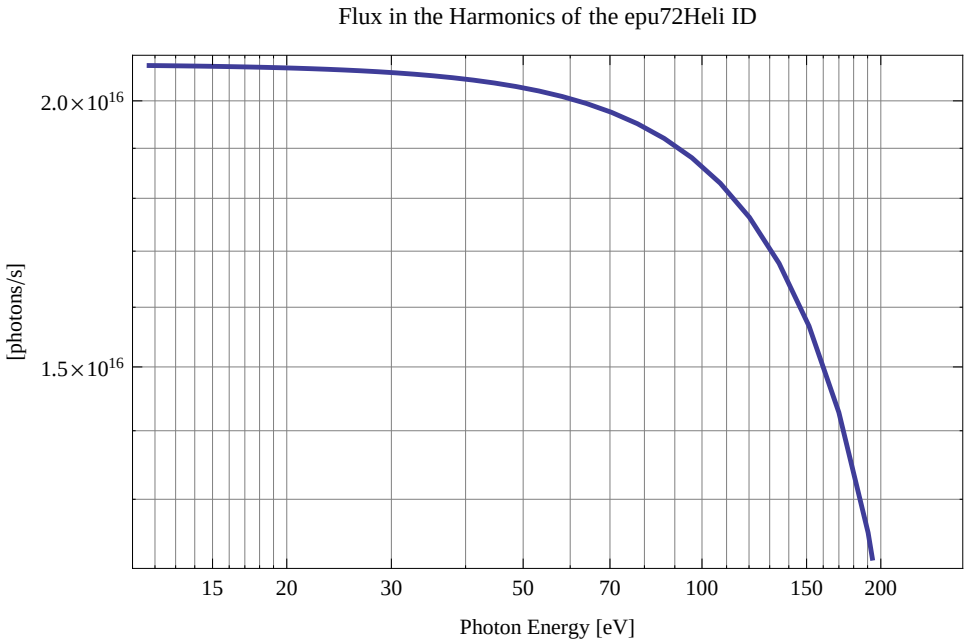

Figure 239: The flux of photons in the harmonics of the emitted synchrotron radiation from the epu72Heli

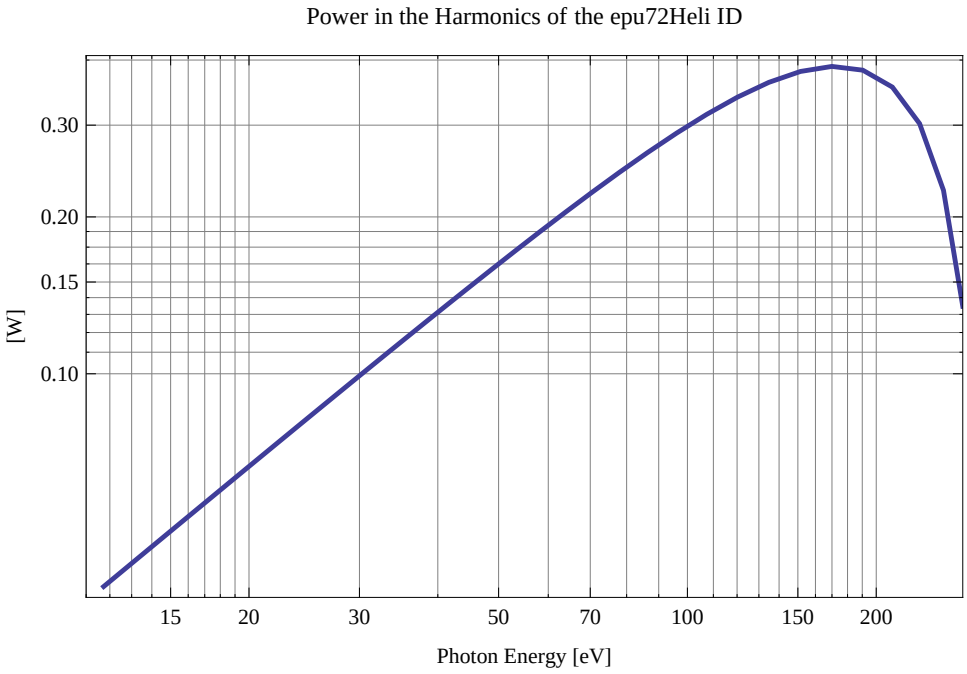

Figure 240: The power in the harmonics of the emitted synchrotron radiation from the epu72Heli

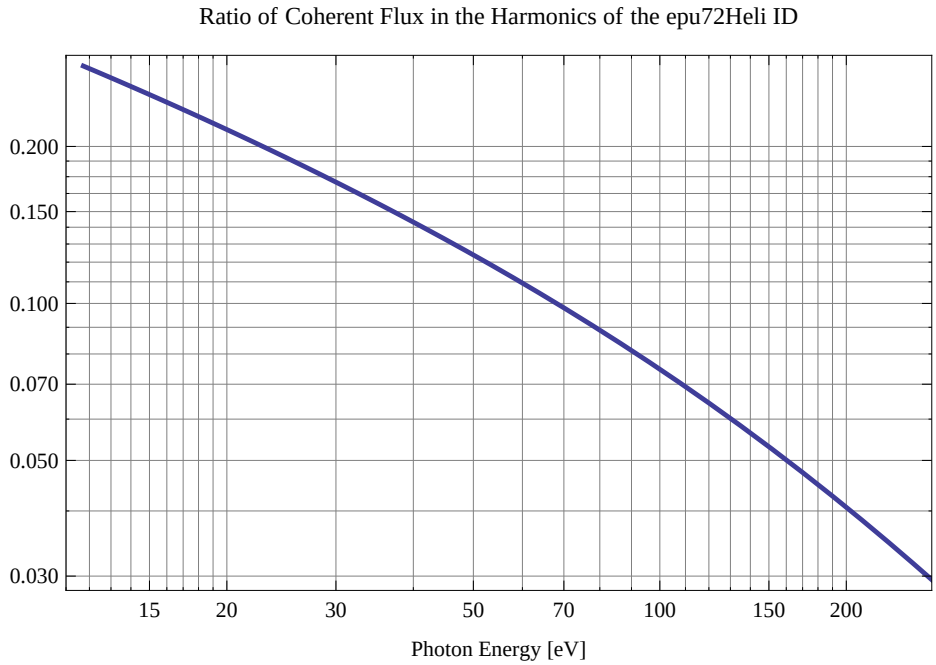

Figure 241: The ratio of coherent flux in the harmonics of the emitted synchrotron radiation from the epu72Heli

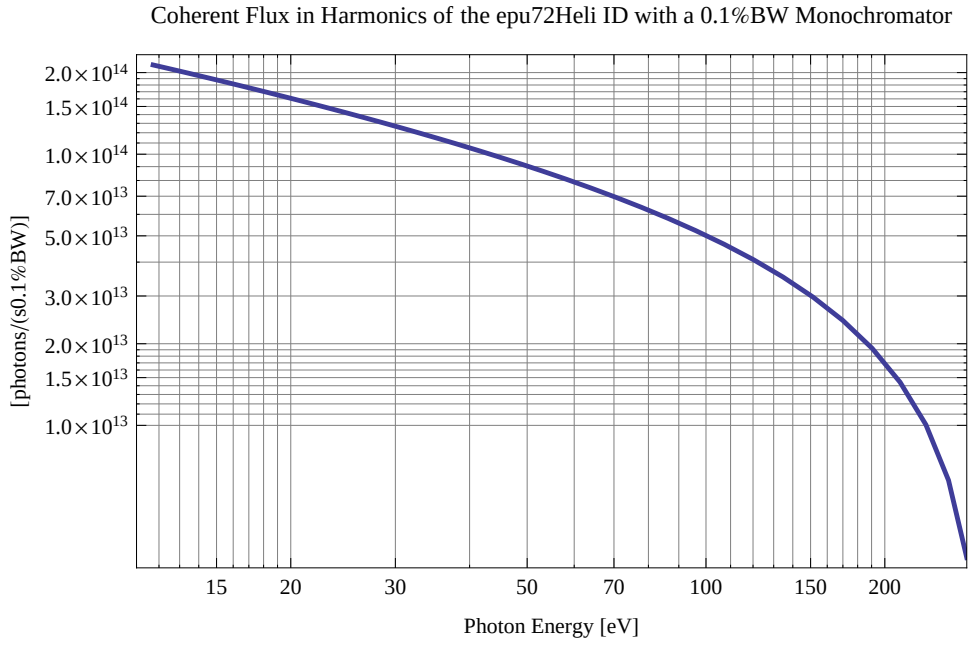

Figure 242: The coherent flux in the harmonics of the epu72Heli using a 0.1%BW Monochromator

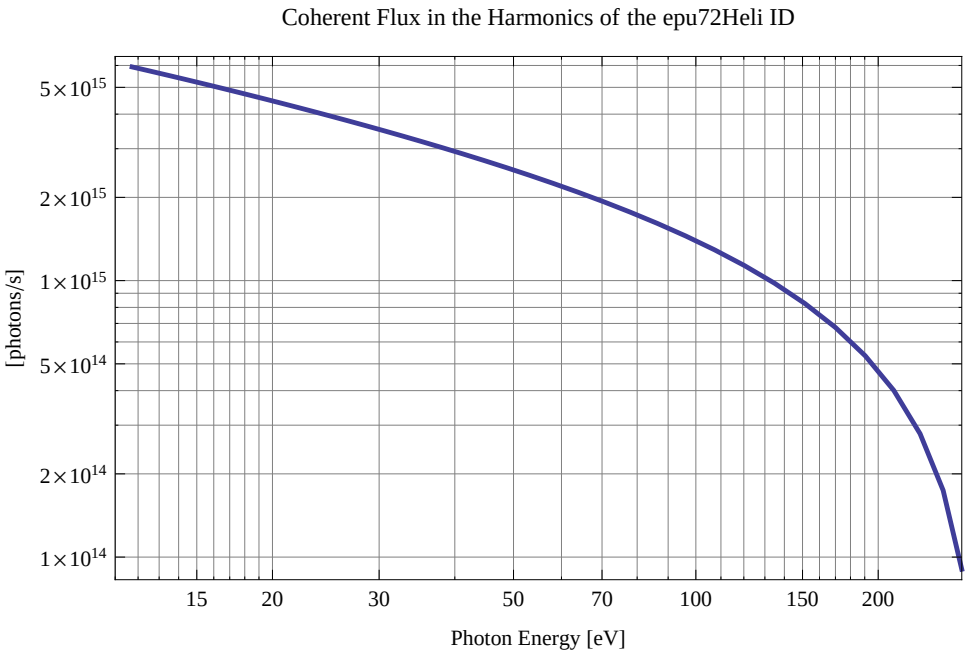

Figure 243: The coherent flux in the harmonics of the epu72Heli

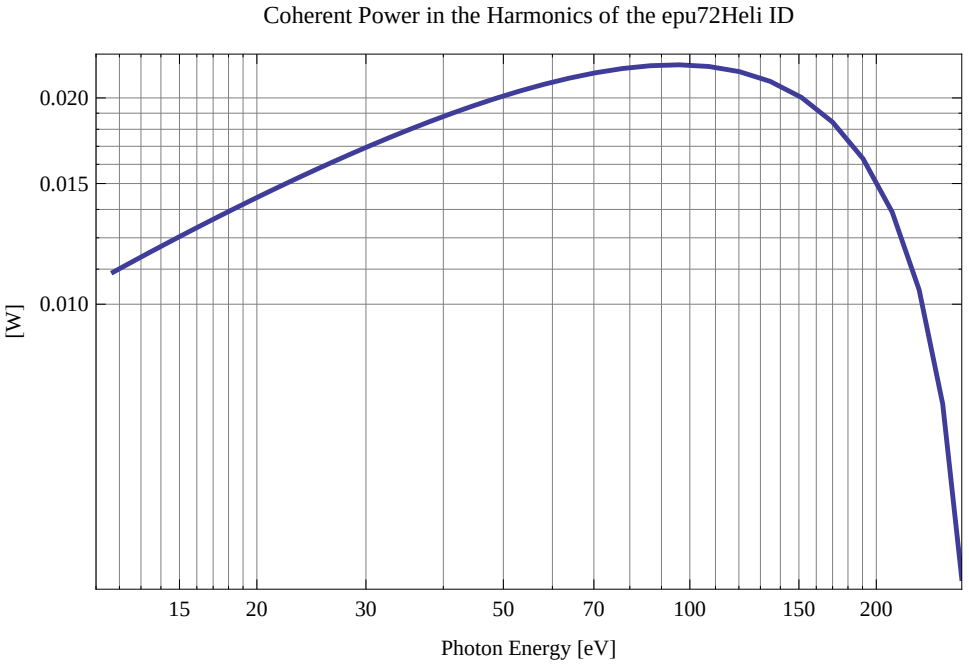

Figure 244: The power of coherent synchrotron radiation in the harmonics of the epu72Heli

The brilliance at peak energy and the angular spectral flux density from the epu72Heli for different harmonics at maximum K-value (6.971) are given in Table 34 and for minimum K-value (0.400) these values are given in Table 35.

Table 34: The brilliance at peak energy and the angular spectral flux density from the epu72Heli for different harmonics at maximum K-value (6.971)

Harmonic	Photon Energy [eV]	Brilliance [Ph./(smrad^{2}mrad^{2}0.1%BW)]	Angular Spectral Flux [Ph./(smrad^{2}0.1%BW)]
1	11.7308	7.64×10^{16}	4.35×10^{15}

Table 35: The brilliance at peak energy and the angular spectral flux density from the epu72Heli for different harmonics at minimum K-value (0.4)

Harmonic	Photon Energy [eV]	Brilliance [Ph./(smrad^{2}mrad^{2}0.1%BW)]	Angular Spectral Flux [Ph./(smrad^{2}0.1%BW)]
1	274.78	6.39×10^{17}	1.16×10^{16}

4.9 Influence from the epu72Heli on the optics of the stored beam

Figure 245 shows the focusing potential from the epu72Heli over the beam stay clear aperture of the ring aparture.

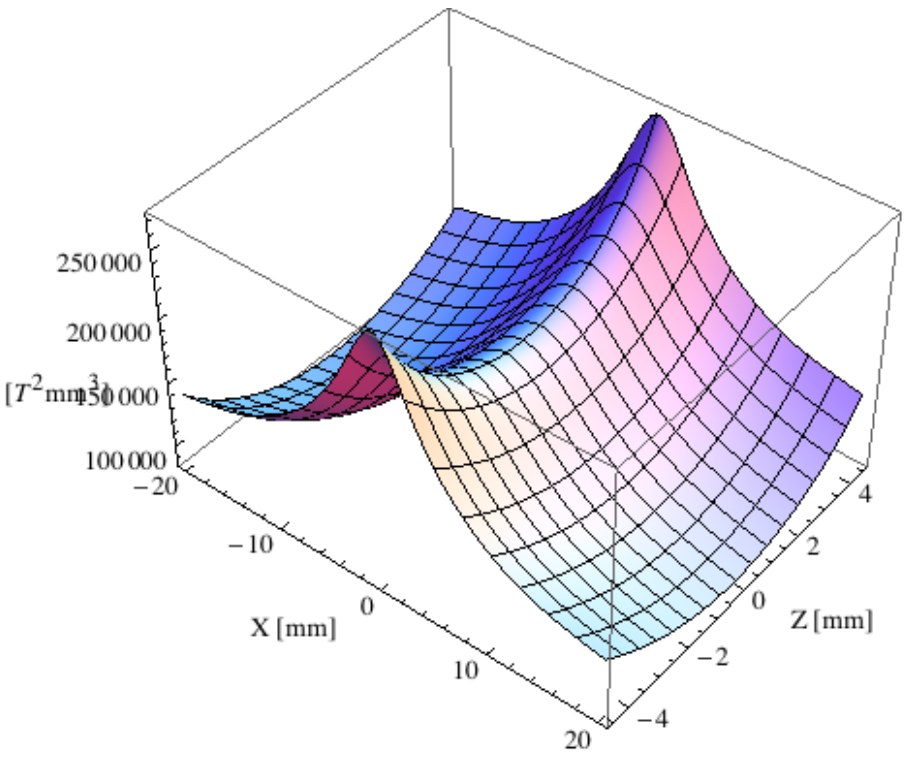

Figure 245: Focusing potential from the epu72Heli over the beam stay clear aparture.

Figure 246 shows the kick map in the beam energy independant unit T^2m^2 of the kicks induced by the epu72Heli over the beam stay clear aparture.

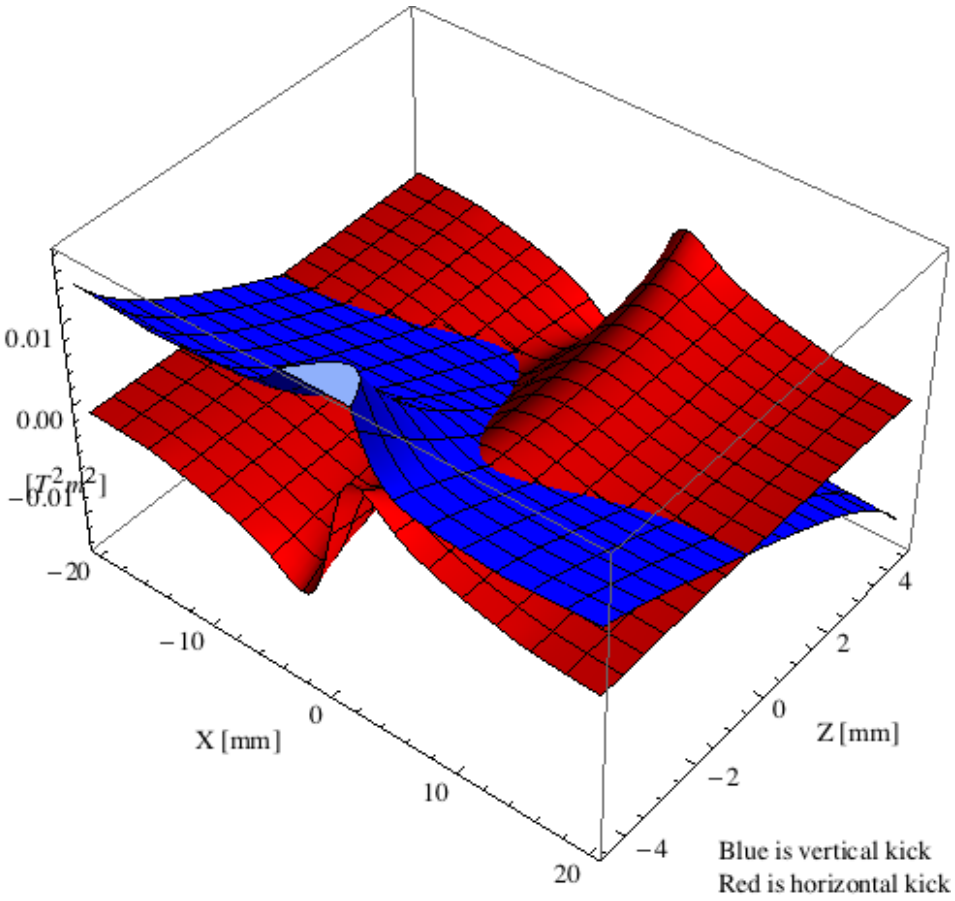

Figure 246: Kick map in the beam energy independant unit T^2m^2 of the kicks induced by the epu72Heli over the beam stay clear aparture.

Figure 247 shows the induced angular kick on the stored beam from the epu72Heli as a function of the vertical distance to the undulator axis.

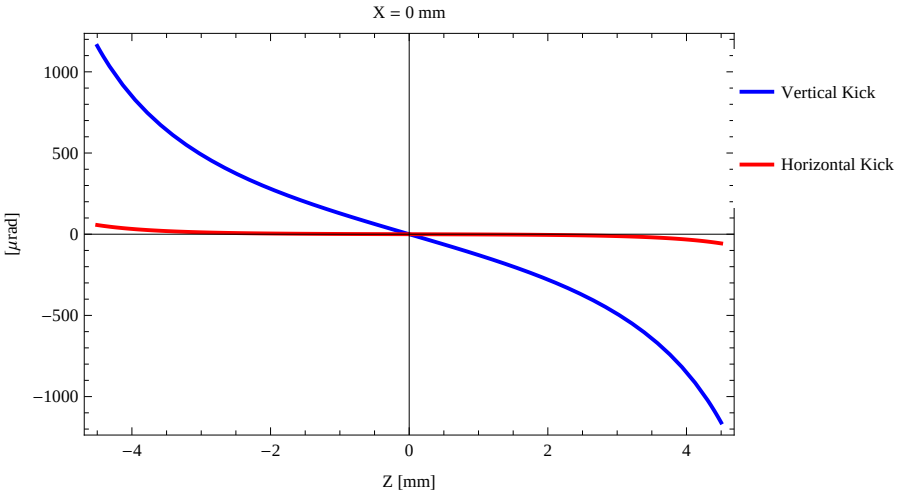

Figure 247: Induced angular kick on the stored beam from the epu72Heli as a function of the vertical distance to the undulator axis.

Figure 248 shows the induced angular kick on the stored beam from the epu72Heli as a function of the horizontal distance to the undulator axis.

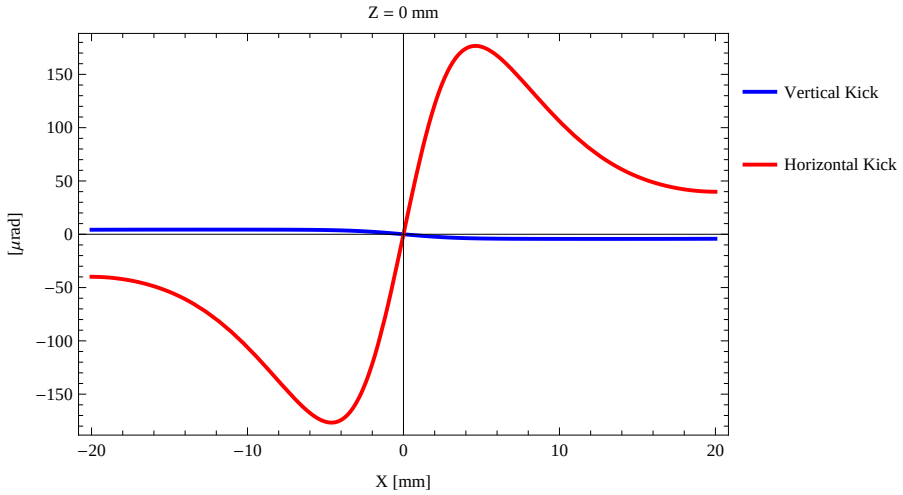

Figure 248: Induced angular kick on the stored beam from the epu72Heli as a function of the horizontal distance to the undulator axis.

Figure 249 shows tune shift induced by the epu72Heli over the beam stay clear aparture. Note that the tune shift depends on the beam size at the.

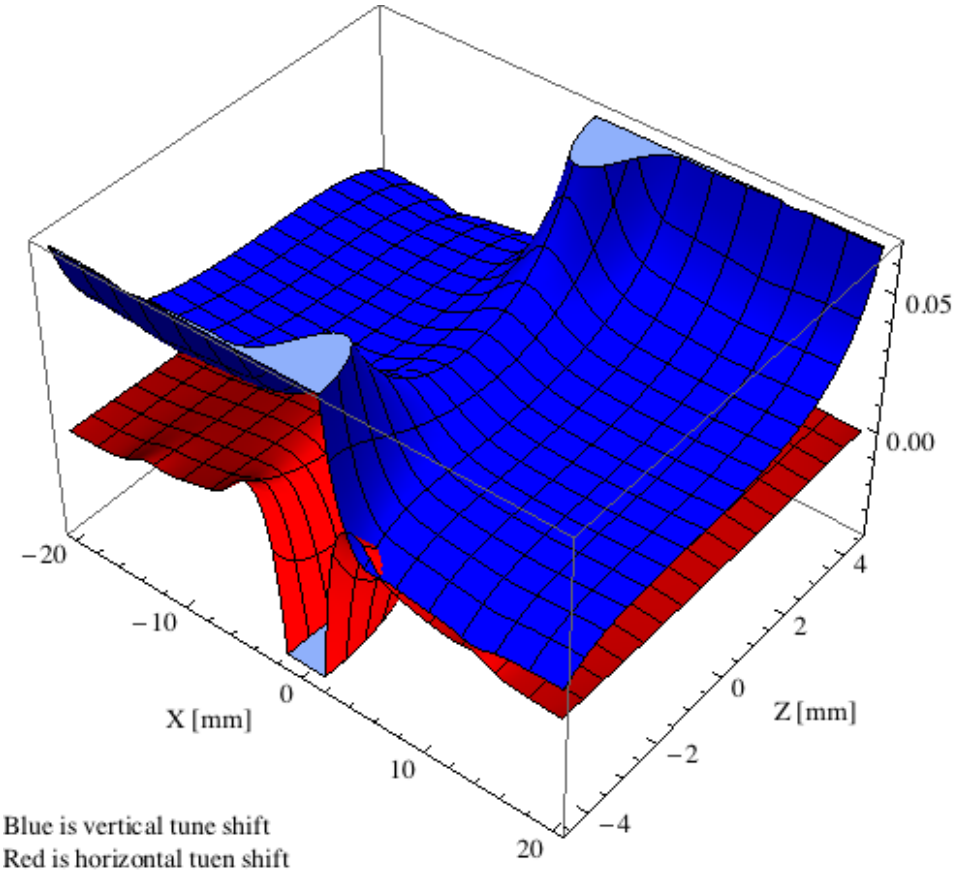

Figure 249: Tune shift induced by the epu72Heli over the beam stay clear aparture.

Figure 250 shows the induced tune shift from the epu72Heli as a function of the vertical distance to the undulator axis.

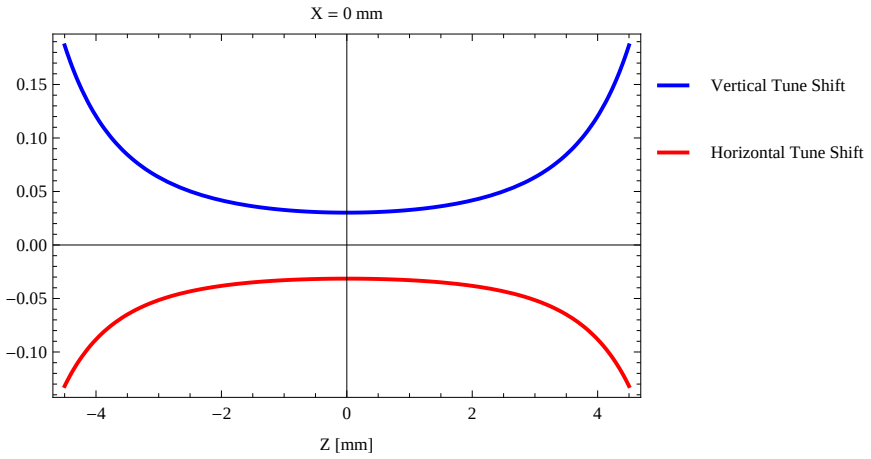

Figure 250: Induced tune shift from the epu72Heli as a function of the vertical distance to the undulator axis.

Figure 251 shows the induced tune shift from the epu72Heli as a function of the horizontal distance to the undulator axis.

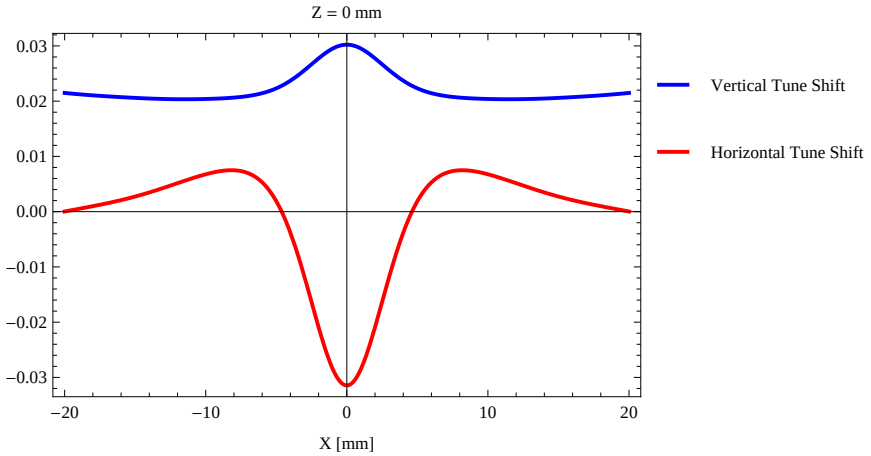

Figure 251: Induced tune shift from the epu72Heli on the stored beam from the as a function of the horizontal distance to the undulator axis.

4.10 Magnet model of the elliptically polarizing undulator epu72Incl

The Radia [2] magnet model of the epu72Incl is shown in Figure 252. The length of the magnet model is 594.744 mm. The magnetic material in the model is NdFeb with a remanence of 1.33 T. Blocks with vertical magnetisation are blue and blocks with horizontal magnetisation are yellow. The block size is 35.x35.x18. mm^3 and there is a 5. mm cut-out in two of the corners of the blocks. The total length of the epu72Incl is 2610.74 mm.

4.11 Analysis of the magnetic field of the epu72Incl

The effective magnetic fields on axis and the fundamental photon energy of the epu72Incl are shown in Table 36. The higher harmonic contents in the magnetic field of an elliptically polarizing

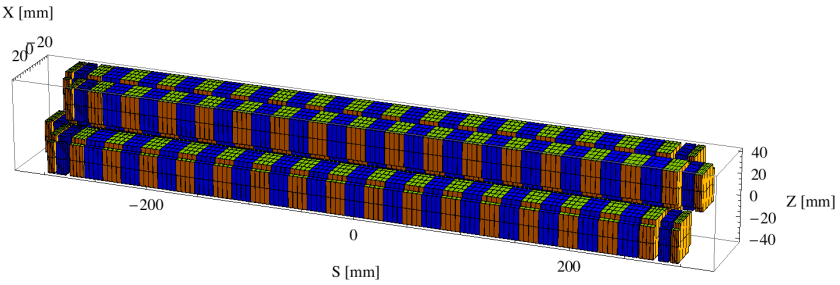

Figure 252: Magnetic model of the epu72Incl. The has been modelled with Radia [2]

undulator made of permanent magnets is usually small and the effective field has approximately the same strength as the peak field.

Table 36: Effective Fields on axis and Fundamental Photon Energy of the epu72Incl

Undulator Period	72	mm
Undulator Gap	13	mm
Undulator Mode	Inclined	
Undulator Phase	19.379	mm
Vertical Peak Field	0.518	T
effective Vertical Field	0.522	T
Kx (from vert. field)	3.510	
Horizontal Peak Field:	−0.515	T
effective Horizontal Field	0.523	T
Kz (from hor. field)	3.517	
Photon Energy, Harm.1	0.022	keV
Emitted Power	0.609	kW
Total Length	2610.7	mm

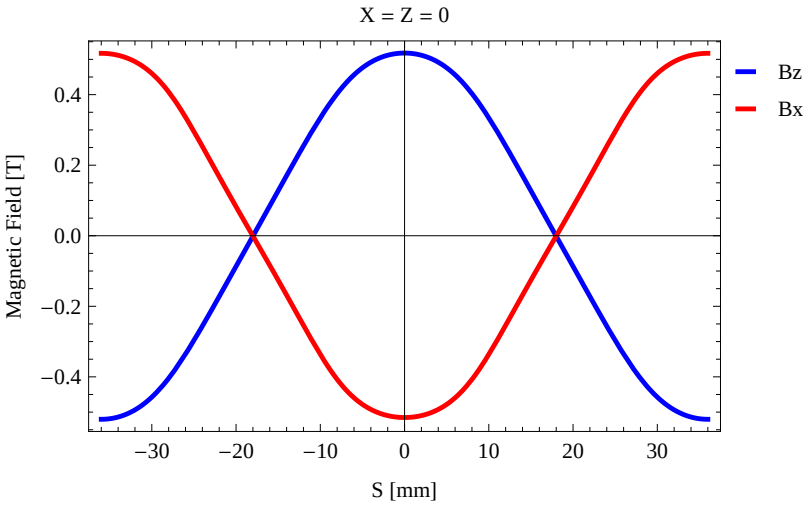

Figure 253: Vertical magnetic field in a central pole of the epu72Incl along the axis, X = Z = 0

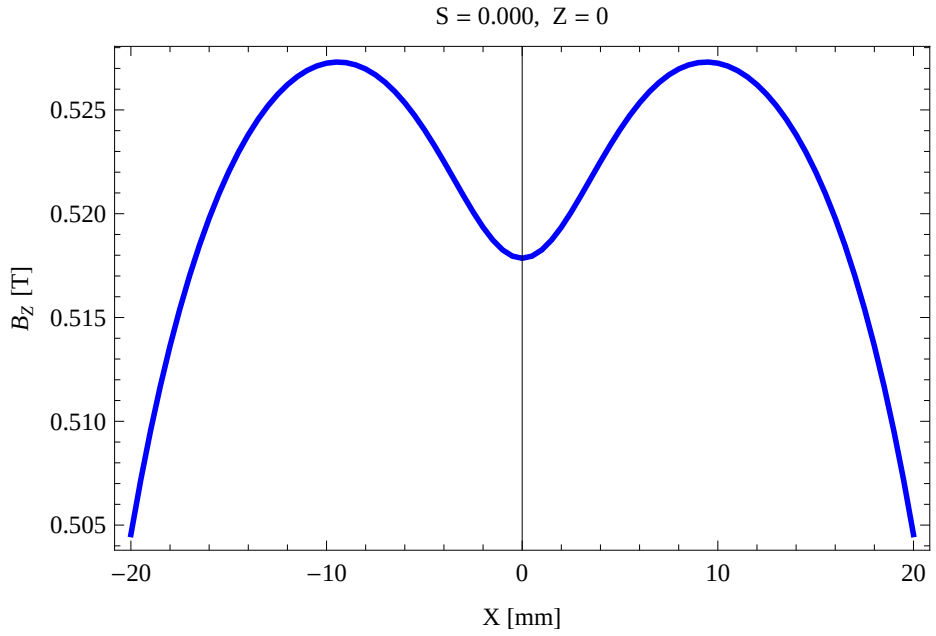

Figure 254: Vertical magnetic field in a central pole of the epu72Incl along the horizontally transverse direction to the axis, S = 0.000, Z = 0

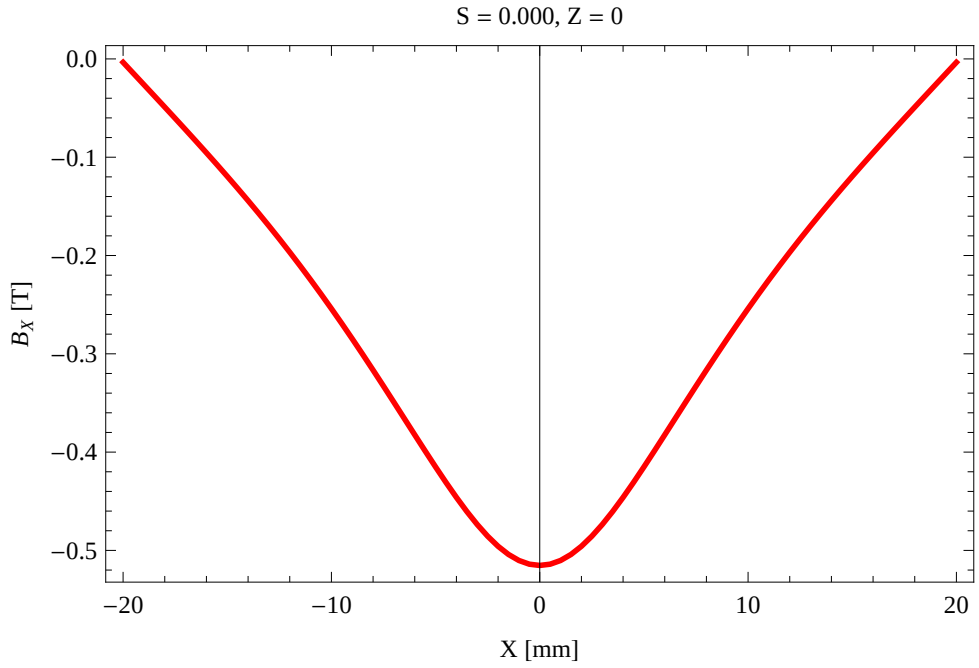

Figure 255: Horizontal magnetic field in a central pole of the epu72Incl along the horizontally transverse direction to the axis, S = 0.000, Z = 0

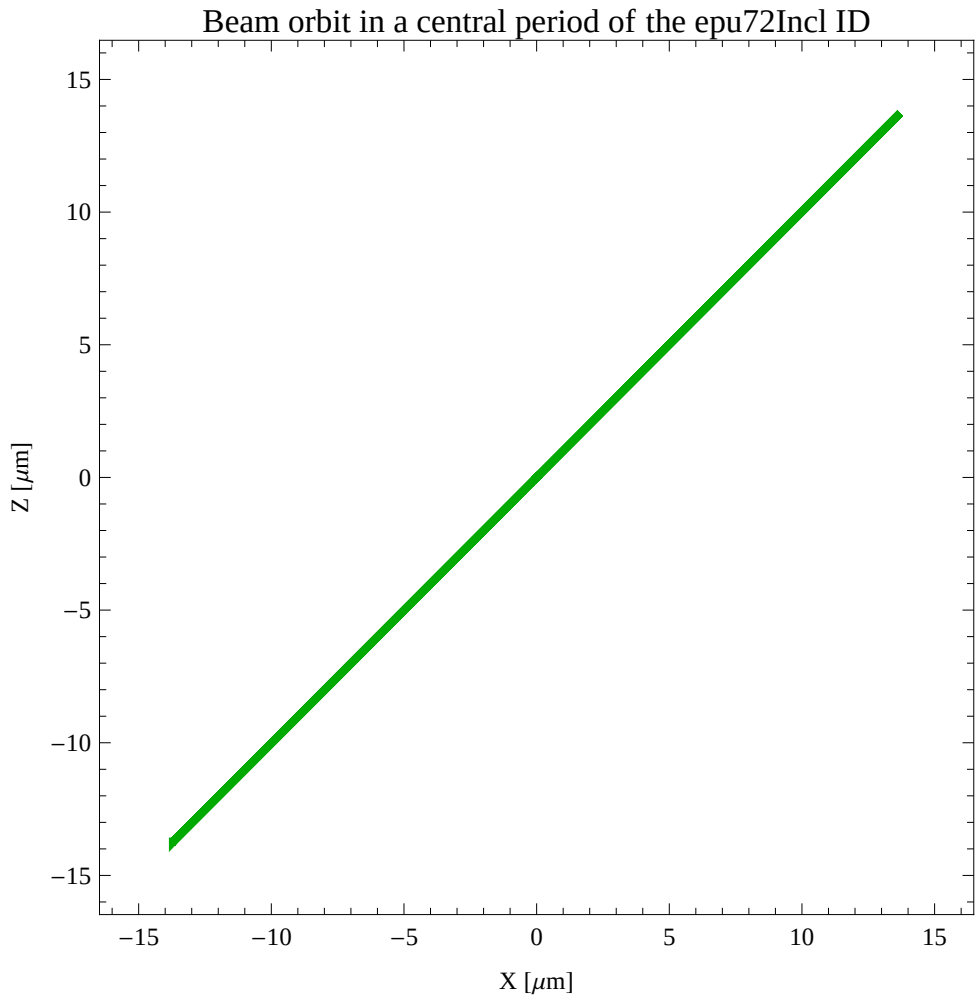

Figure 256: The beam orbit of the electron beam through a central period of the epu72Incl

4.12 Synchrotron radiation from the epu72Incl

The power map of the emitted synchrotron radiation by the epu72Incl, assuming a 0.3 A filament beam with an energy of 1.5 GeV and undulator properties of the synchrotron radiation, is shown in Figure 257. The on-axis power density is 0.424652 kW/mrad^2

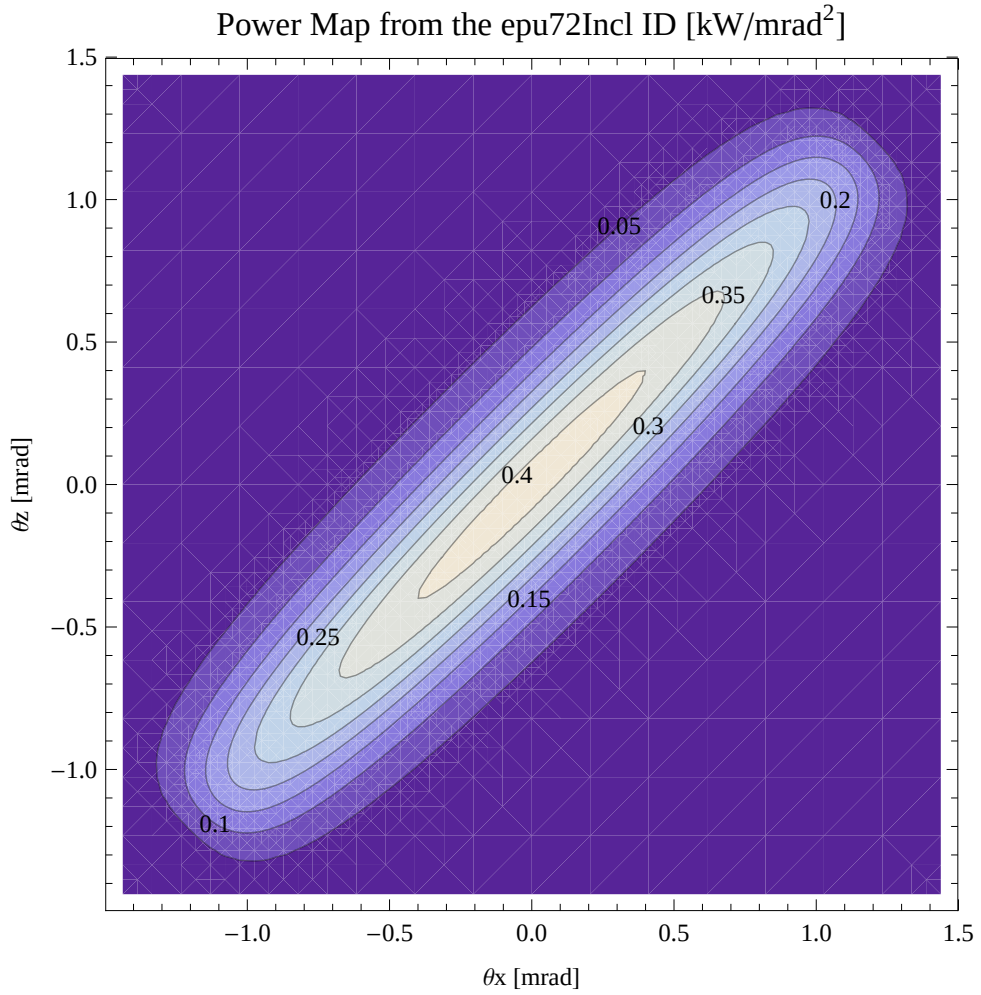

Figure 257: Map of the power distribution of the emitted synchrotron radiation by the epu72Incl

A map of the degree of linear polarisation of the fundamental harmonic of the synchotron radiation emitted by the epu72Incl over the angle of observation is shown in Figure 258.

A map of the degree of 45 degree polarisation of the fundamental harmonic of the synchotron radiation emitted by the epu72Incl over the angle of observation is shown in Figure 259.

A map of the degree of circular polarisation of the fundamental harmonic of the synchotron radiation emitted by the epu72Incl over the angle of observation is shown in Figure 260.

The on axis brilliance at peak energy and the angular spectral flux from the epu72Incl have been calculated with the given beam parameters, which are 0.3 A of stored current, $\beta_H = 5.627$ m, $\varepsilon_H = 5.985$ nmrad, $\beta_V = 2.837$ m, $\varepsilon_V = 59.85$ pmrad, and an energy spread of 0.001.

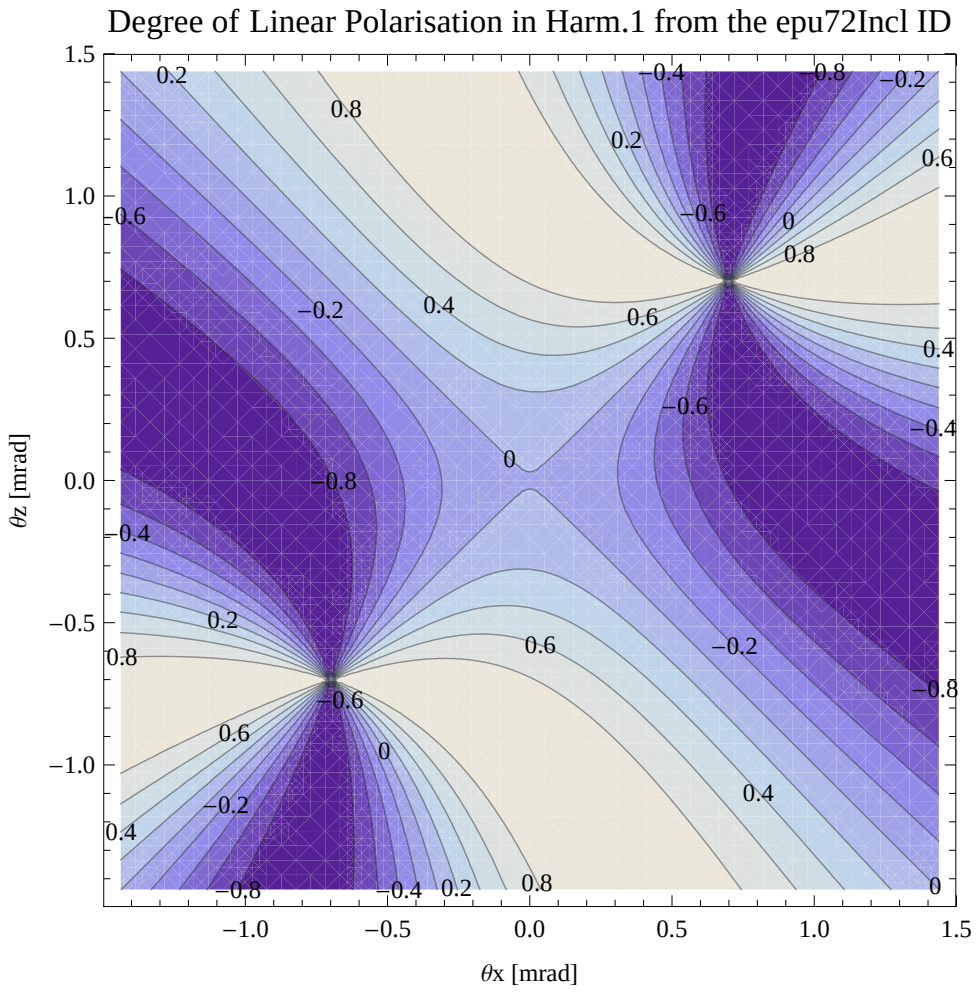

Figure 258: Map of linear polarisation in the fundamental harmonic of the synchotron radiation emitted by the epu72Incl

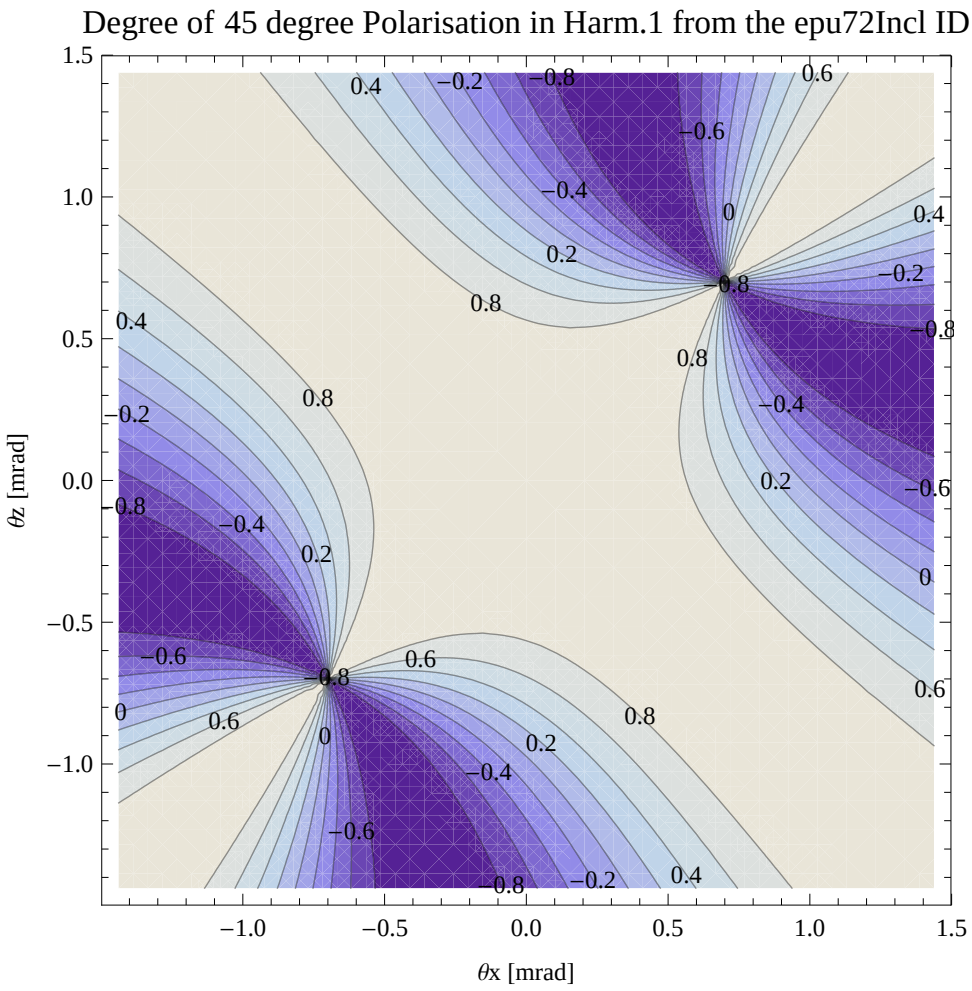

Figure 259: Map of 45 degree polarisation in the fundamental harmonic of the synchotron radiation emitted by the epu72Incl

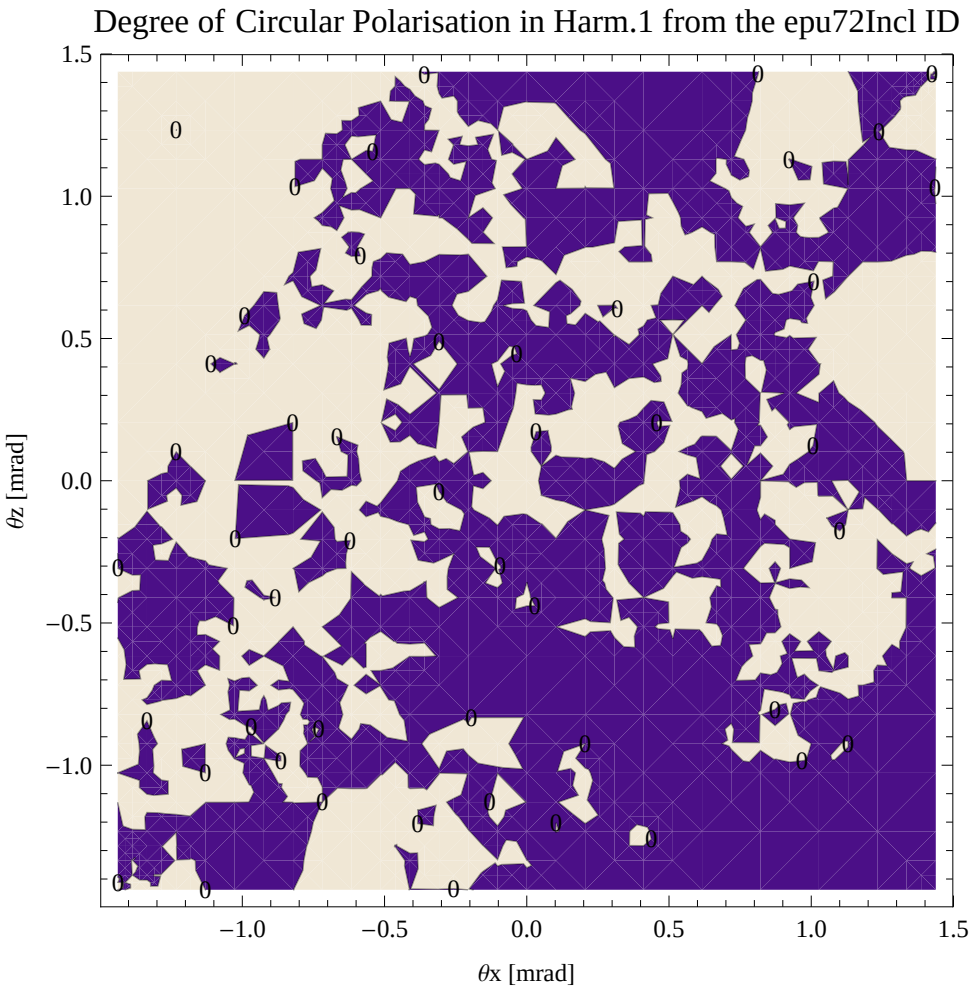

Figure 260: Map of circular polarisation in the fundamental harmonic of the synchotron radiation emitted by the epu72Incl

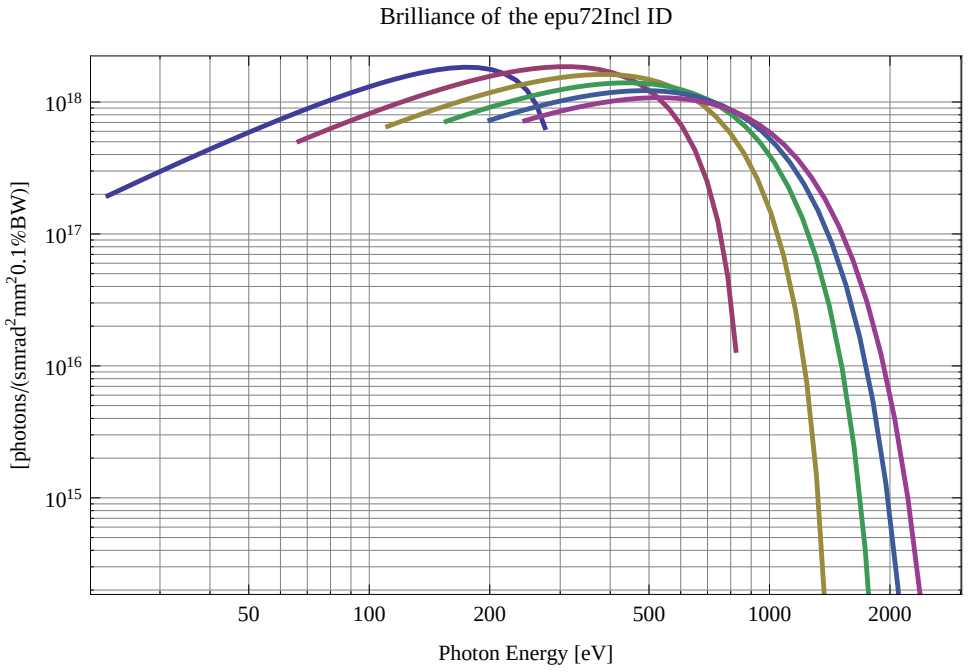

Figure 261: The brilliance at peak energy of the synchotron radiation emitted by the epu72Incl

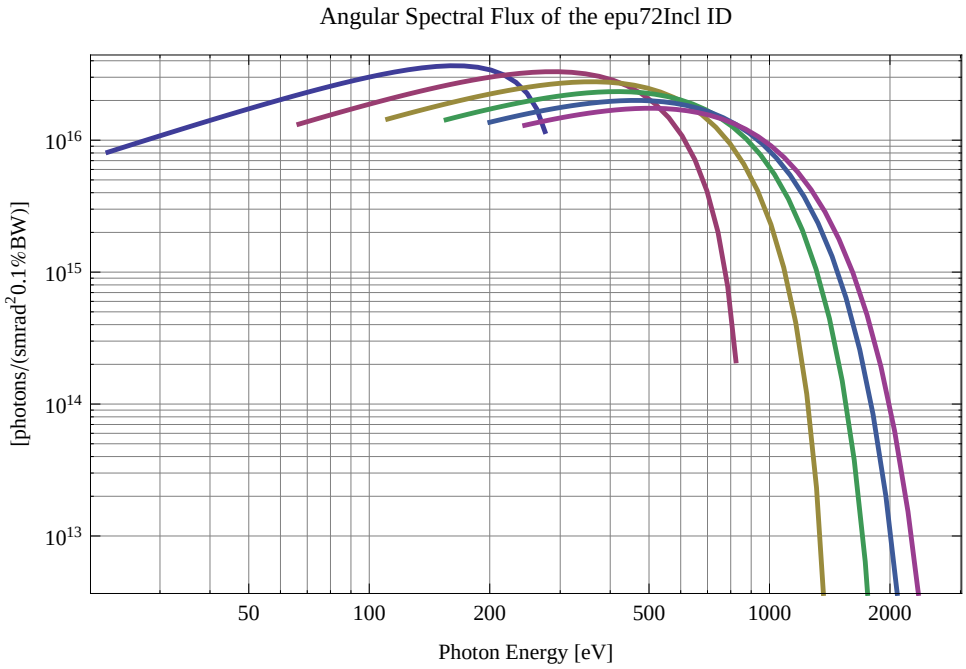

Figure 262: The angular spectral flux of the synchotron radiation emitted by the epu72Incl

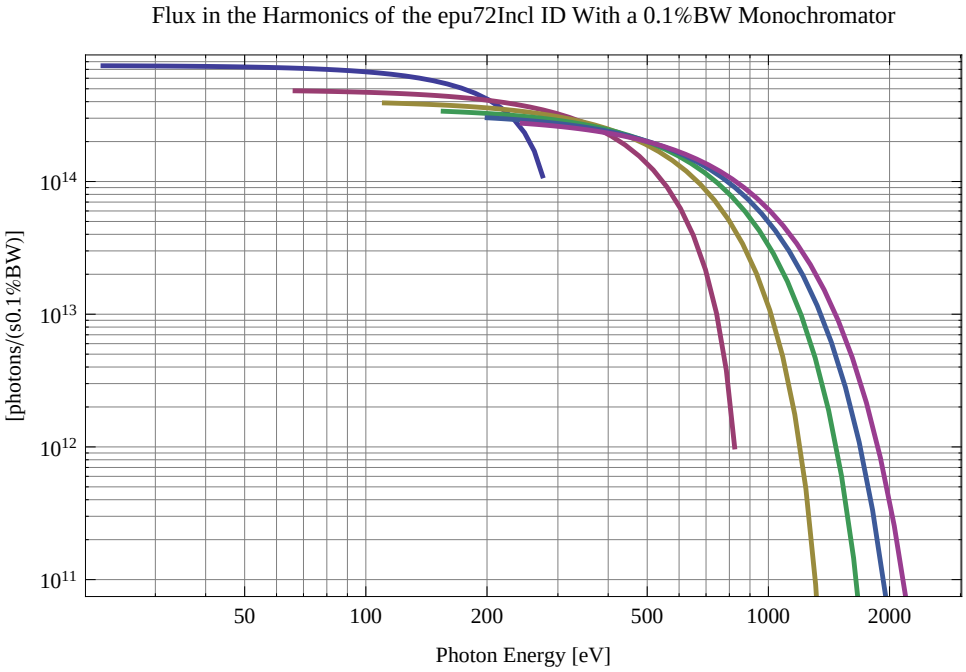

Figure 263: The flux of photons in the harmonics of the emitted synchrotron radiation from the epu72Incl using a 0.1%BW monochromator

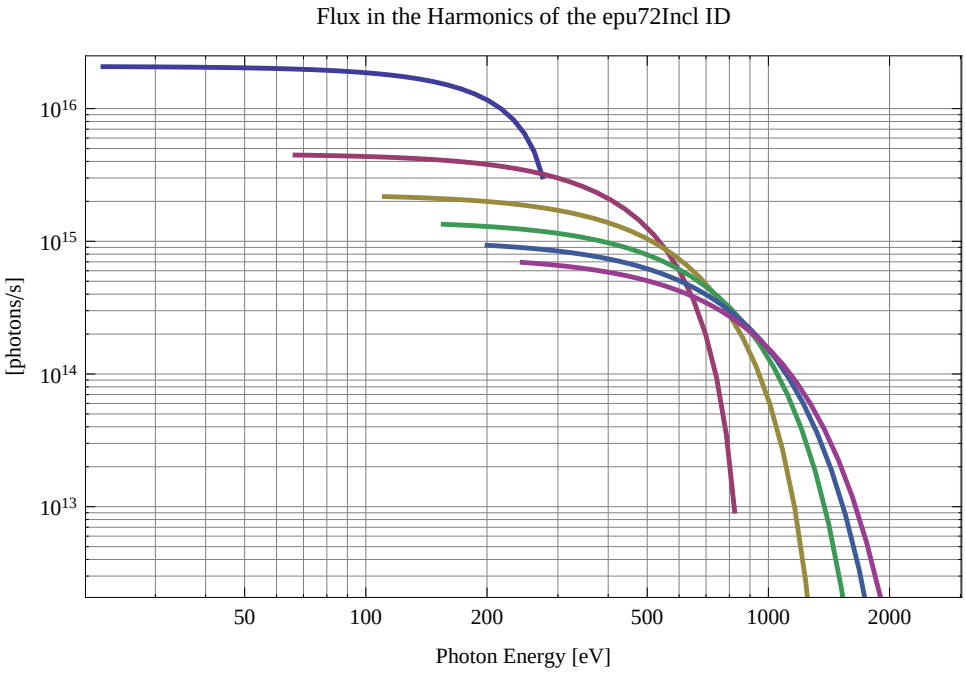

Figure 264: The flux of photons in the harmonics of the emitted synchrotron radiation from the epu72Incl

Figure 265: The power in the harmonics of the emitted synchrotron radiation from the epu72Incl

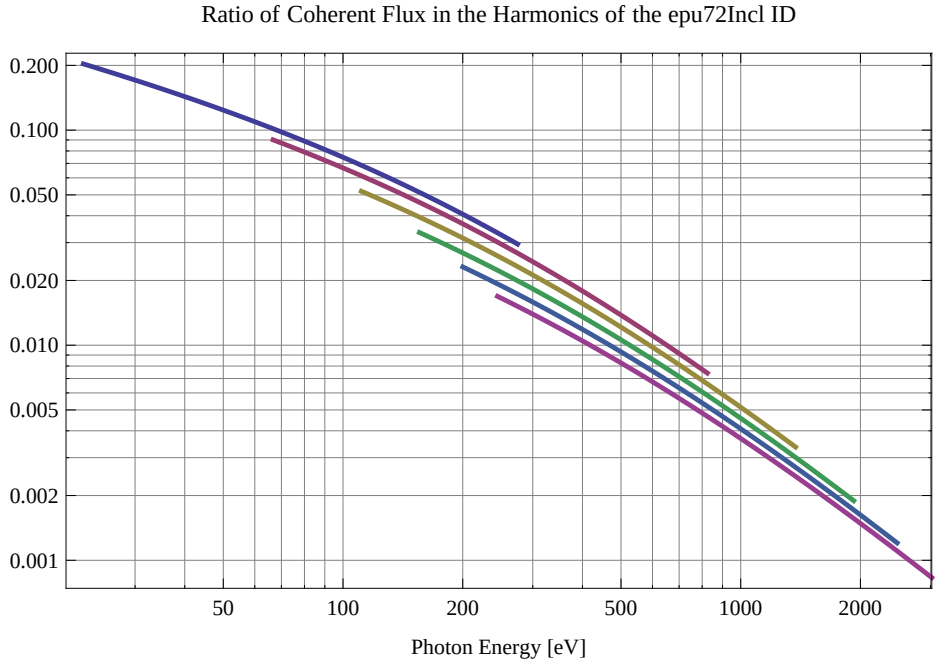

Figure 266: The ratio of coherent flux in the harmonics of the emitted synchrotron radiation from the epu72Incl

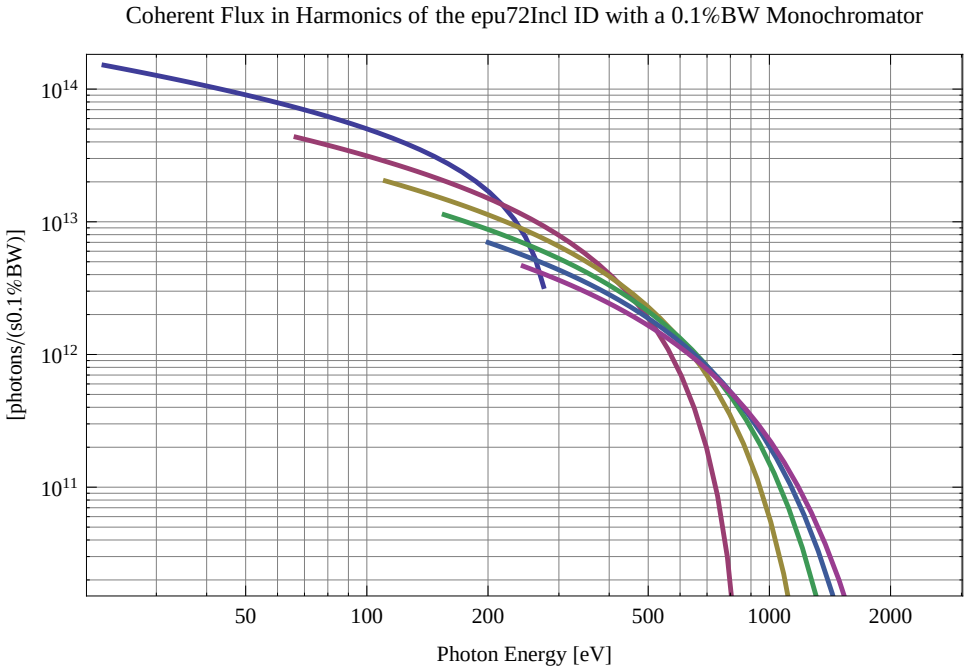

Figure 267: The coherent flux in the harmonics of the epu72Incl using a 0.1%BW Monochromator

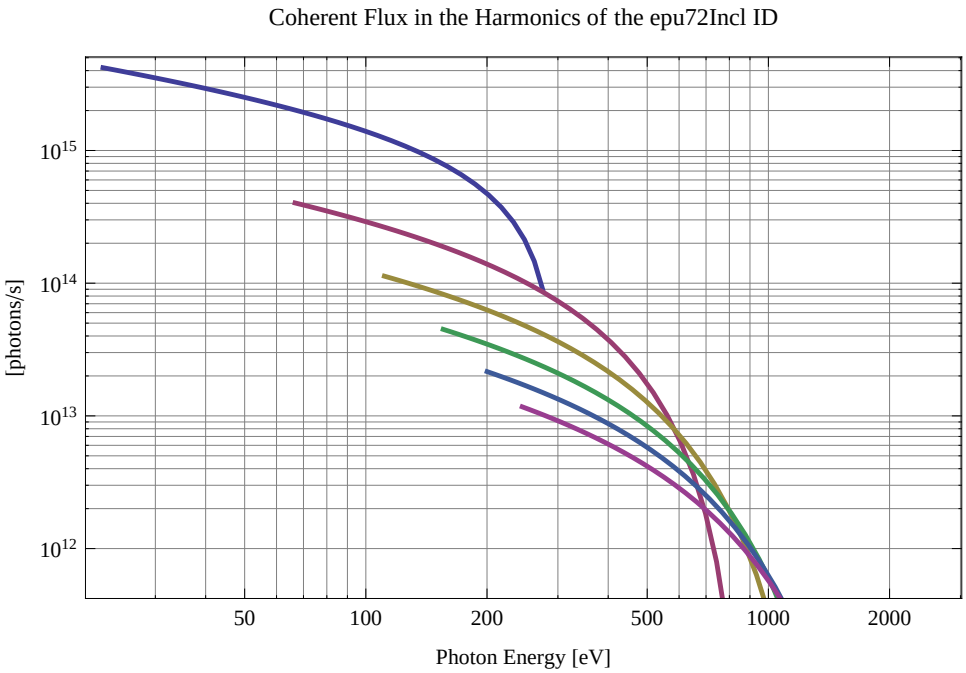

Figure 268: The coherent flux in the harmonics of the epu72Incl

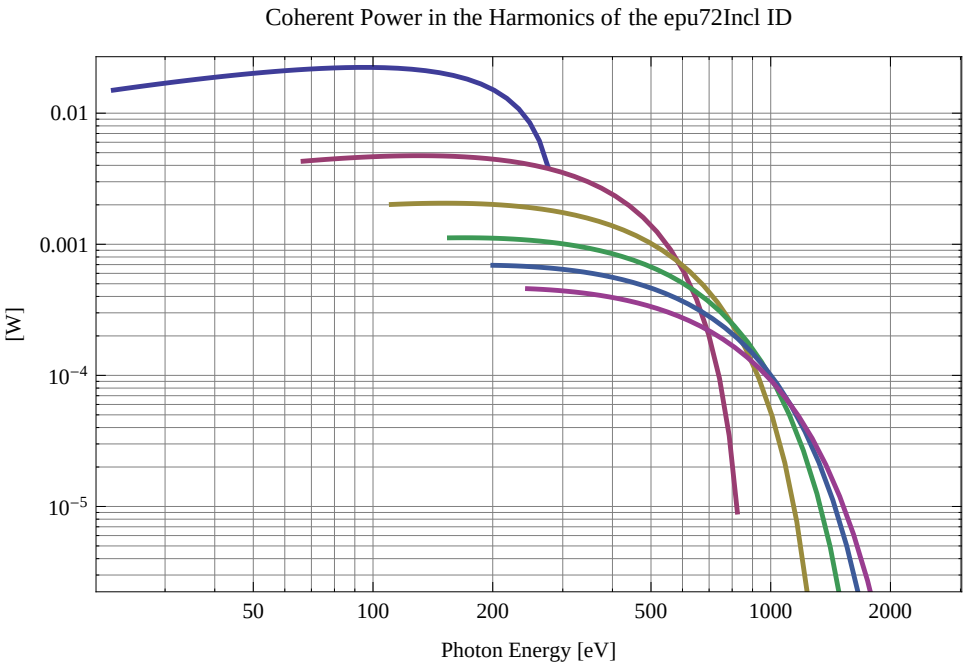

Figure 269: The power of coherent synchrotron radiation in the harmonics of the epu72Incl

The brilliance at peak energy and the angular spectral flux density from the epu72Incl for different harmonics at maximum K-value (4.969) are given in Table 37 and for minimum K-value (0.400) these values are given in Table 38.

Table 37: The brilliance at peak energy and the angular spectral flux density from the epu72Incl for different harmonics at maximum K-value (4.969)

Harmonic	Photon Energy [eV]	Brilliance [Ph./(smrad^{2}mrad^{2}0.1%BW)]	Angular Spectral Flux [Ph./(smrad^{2}0.1%BW)]
1	22.2358	1.95×10^{17}	8.11×10^{15}
3	66.7074	5.03×10^{17}	1.32×10^{16}
5	111.179	6.54×10^{17}	1.45×10^{16}
7	155.651	7.13×10^{17}	1.43×10^{16}
9	200.122	7.28×10^{17}	1.37×10^{16}
11	244.594	7.21×10^{17}	1.3×10^{16}

Table 38: The brilliance at peak energy and the angular spectral flux density from the epu72Incl for different harmonics at minimum K-value (0.4)

Harmonic	Photon Energy [eV]	Brilliance [Ph./(smrad^{2}mrad^{2}0.1%BW)]	Angular Spectral Flux [Ph./(smrad^{2}0.1%BW)]
1	274.78	6.39×10^{17}	1.16×10^{16}
3	824.34	1.31×10^{16}	2.13×10^{14}
5	1373.9	1.62×10^{14}	2.57×10^{12}
7	1923.46	1.79×10^{12}	2.81×10^{10}
9	2473.02	1.89×10^{10}	2.96×10^{8}
11	3022.58	1.96×10^{8}	3.07×10^{6}

4.13 Influence from the epu72Incl on the optics of the stored beam

Figure 270 shows the focusing potential from the epu72Incl over the beam stay clear aperture of the ring aparture.

Figure 271 shows the kick map in the beam energy independant unit T^2m^2 of the kicks induced by the epu72Incl over the beam stay clear aparture.

Figure 272 shows the induced angular kick on the stored beam from the epu72Incl as a function of the vertical distance to the undulator axis.

Figure 273 shows the induced angular kick on the stored beam from the epu72Incl as a function of the horizontal distance to the undulator axis.

Figure 274 shows tune shift induced by the epu72Incl over the beam stay clear aparture. Note that the tune shift depends on the beam size at the.

Figure 275 shows the induced tune shift from the epu72Incl as a function of the vertical distance to the undulator axis.

Figure 276 shows the induced tune shift from the epu72Incl as a function of the horizontal distance to the undulator axis.

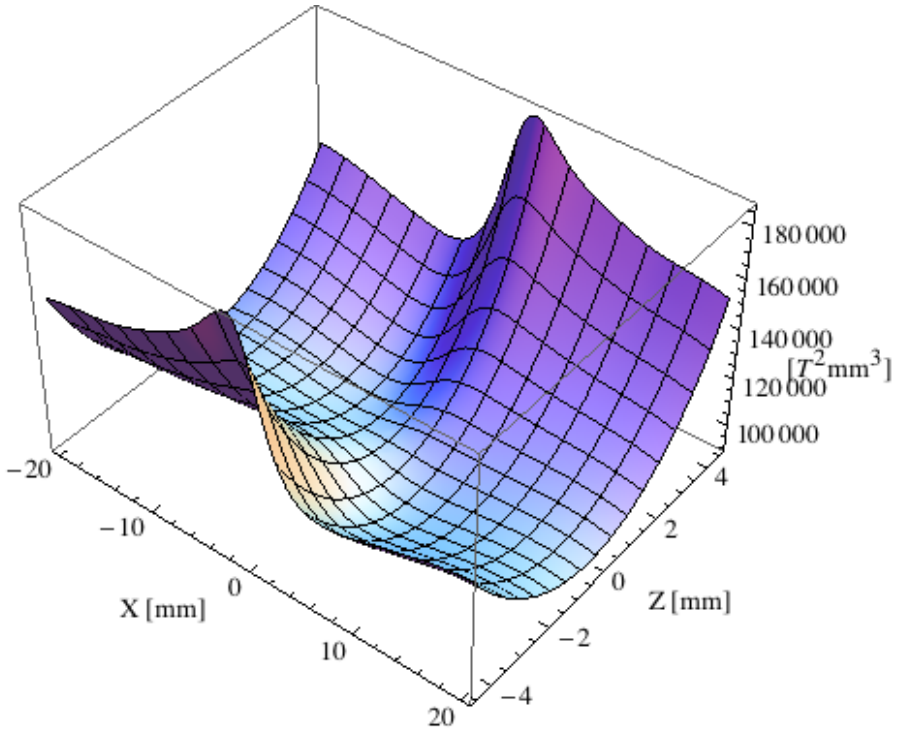

Figure 270: Focusing potential from the epu72Incl over the beam stay clear aparture.

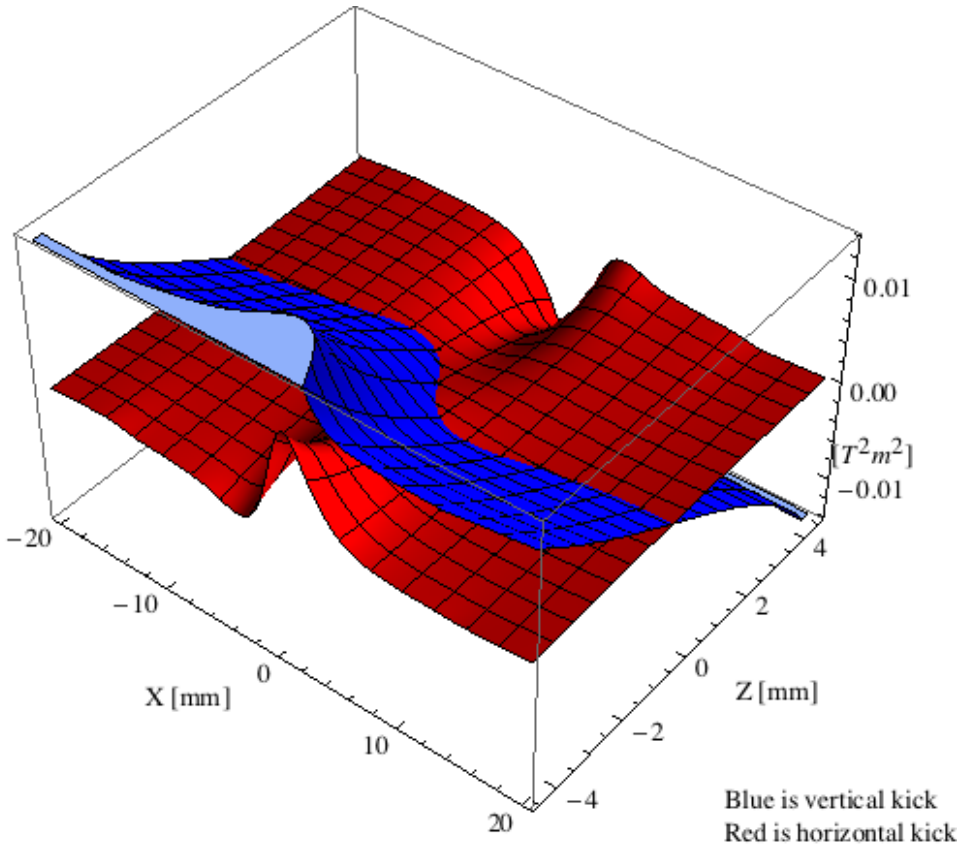

Figure 271: Kick map in the beam energy independant unit T^2m^2 of the kicks induced by the epu72Incl over the beam stay clear aparture.

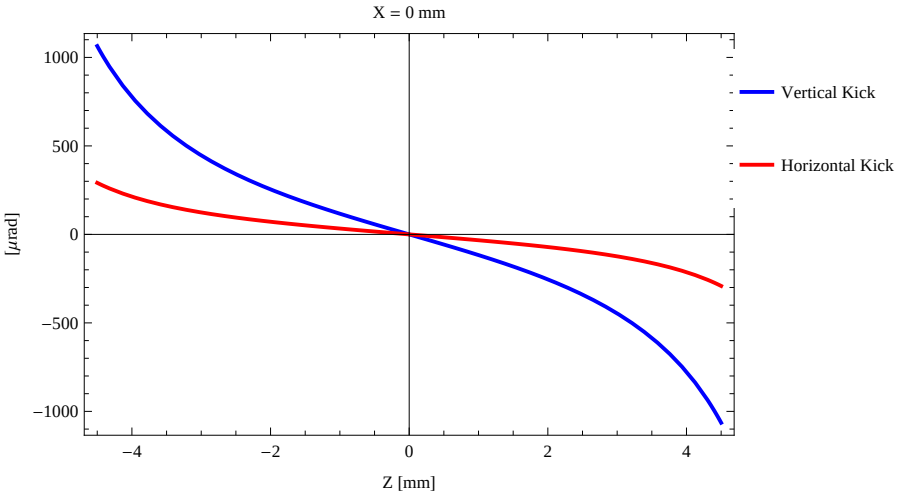

Figure 272: Induced angular kick on the stored beam from the epu72Incl as a function of the vertical distance to the undulator axis.

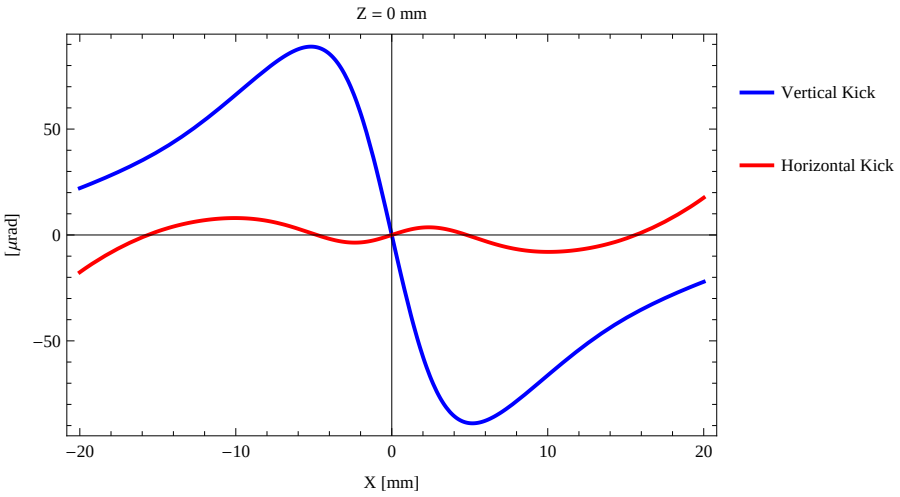

Figure 273: Induced angular kick on the stored beam from the epu72Incl as a function of the horizontal distance to the undulator axis.

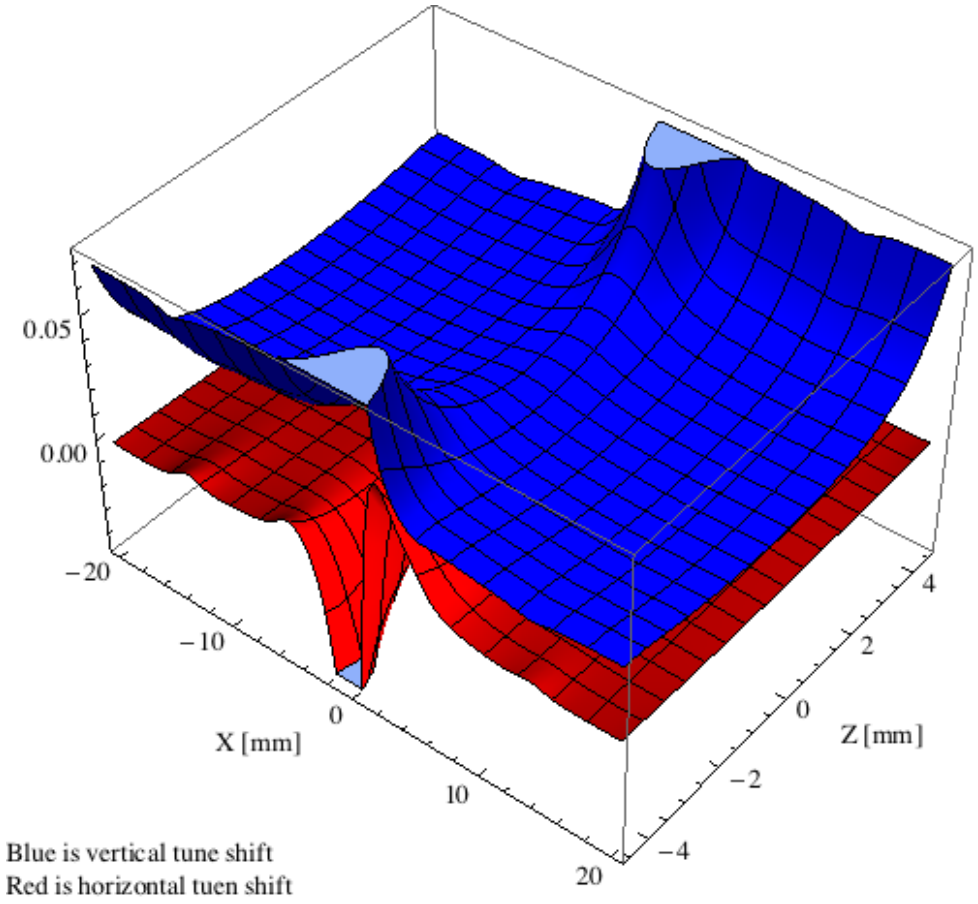

Figure 274: Tune shift induced by the epu72Incl over the beam stay clear aparture.

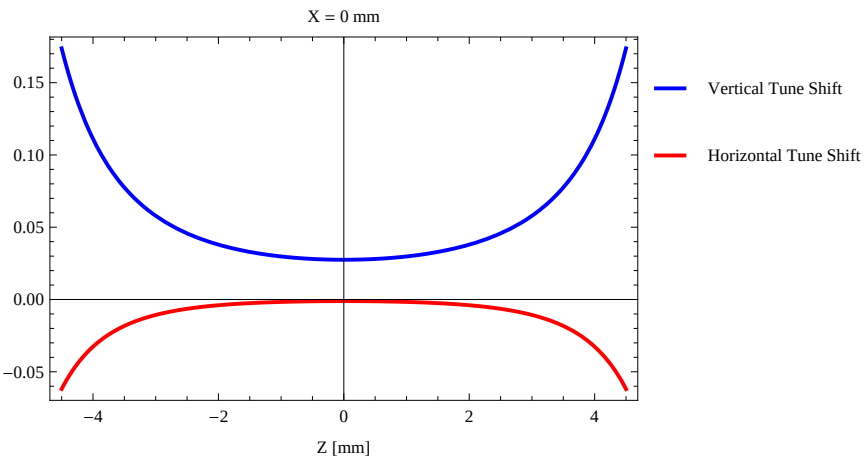

Figure 275: Induced tune shift from the epu72Incl as a function of the vertical distance to the undulator axis.

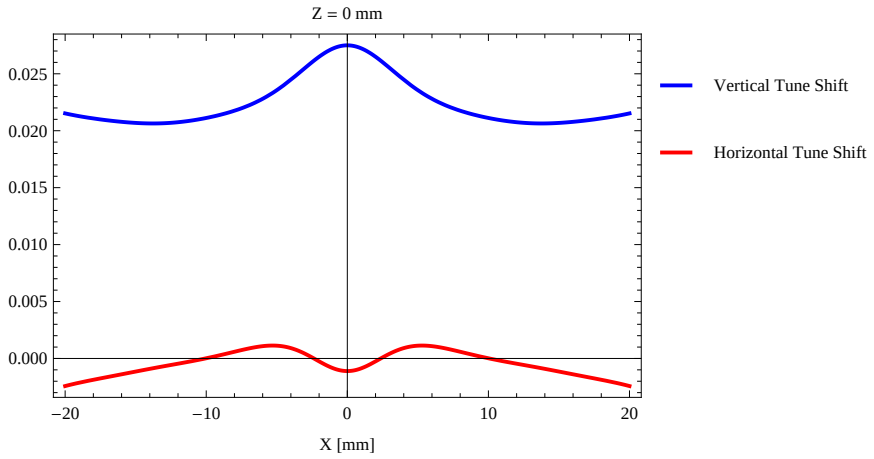

Figure 276: Induced tune shift from the epu72Incl on the stored beam from the as a function of the horizontal distance to the undulator axis.

4.14 Magnet model of the elliptically polarizing undulator epu72Vert

The Radia [2] magnet model of the epu72Vert is shown in Figure 277. The length of the magnet model is 594.744 mm. The magnetic material in the model is NdFeb with a remanence of 1.33 T. Blocks with vertical magnetisation are blue and blocks with horizontal magnetisation are yellow. The block size is 35.x35.x18. mm^3 and there is a 5. mm cut-out in two of the corners of the blocks. The total length of the epu72Vert is 2610.74 mm.

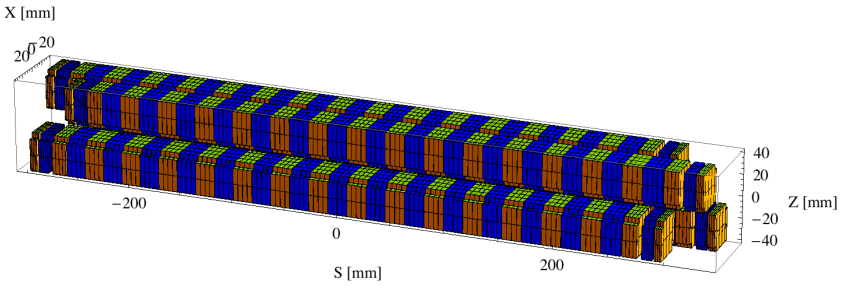

Figure 277: Magnetic model of the epu72Vert. The has been modelled with Radia [2]

4.15 Analysis of the magnetic field of the epu72Vert

The effective magnetic fields on axis and the fundamental photon energy of the epu72Vert are shown in Table 39. The higher harmonic contents in the magnetic field of an elliptically polarizing undulator made of permanent magnets is usually small and the effective field has approximately the same strength as the peak field.

4.16 Synchrotron radiation from the epu72Vert

The power map of the emitted synchrotron radiation by the epu72Vert, assuming a 0.3 A filament beam with an energy of 1.5 GeV and undulator properties of the synchrotron radiation, is shown in Figure 281. The on-axis power density is 0.536810 kW/mrad^2

Table 39: Effective Fields on axis and Fundamental Photon Energy of the epu72Vert

Undulator Period	72	mm
Undulator Gap	13	mm
Undulator Mode	Vertical	
Undulator Phase	36.000	mm
Vertical Peak Field	0.000	T
effective Vertical Field	0.000	T
Kx (from vert. field)	0.000	
Horizontal Peak Field:	0.930	T
effective Horizontal Field	0.933	T
Kz (from hor. field)	6.274	
Photon Energy, Harm.1	0.014	keV
Emitted Power	0.971	kW
Total Length	2610.7	mm

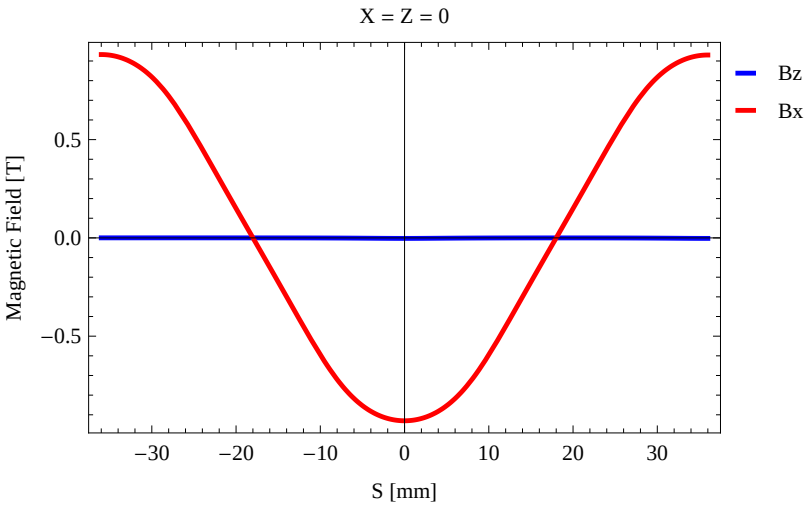

Figure 278: Vertical magnetic field in a central pole of the epu72Vert along the axis, X = Z = 0

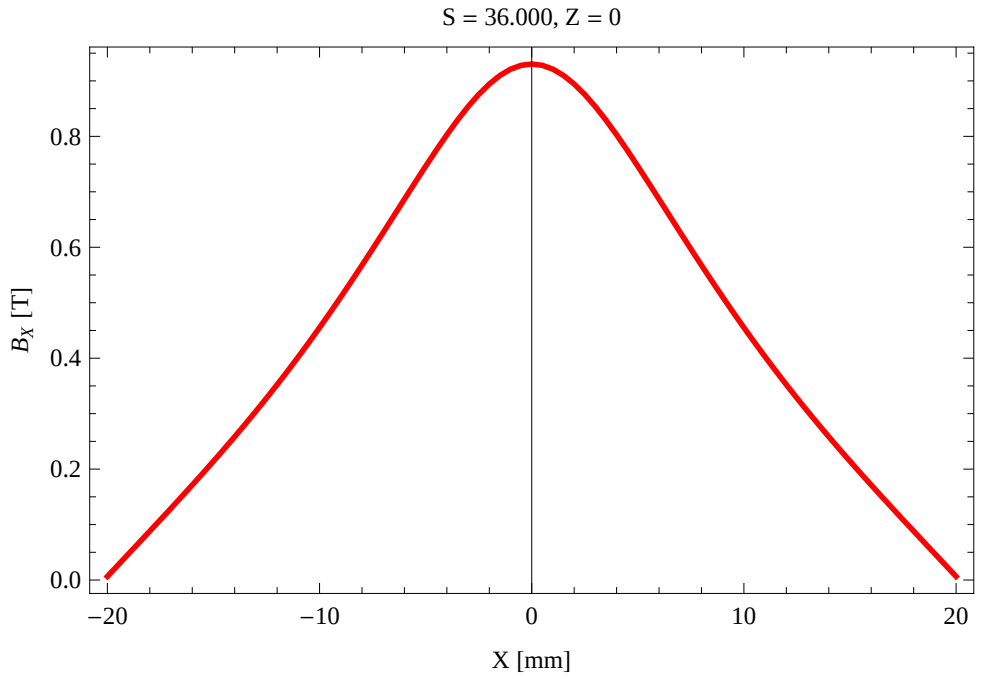

Figure 279: Horizontal magnetic field in a central pole of the epu72Vert along the horizontally transverse direction to the axis, S = 36.000, Z = 0

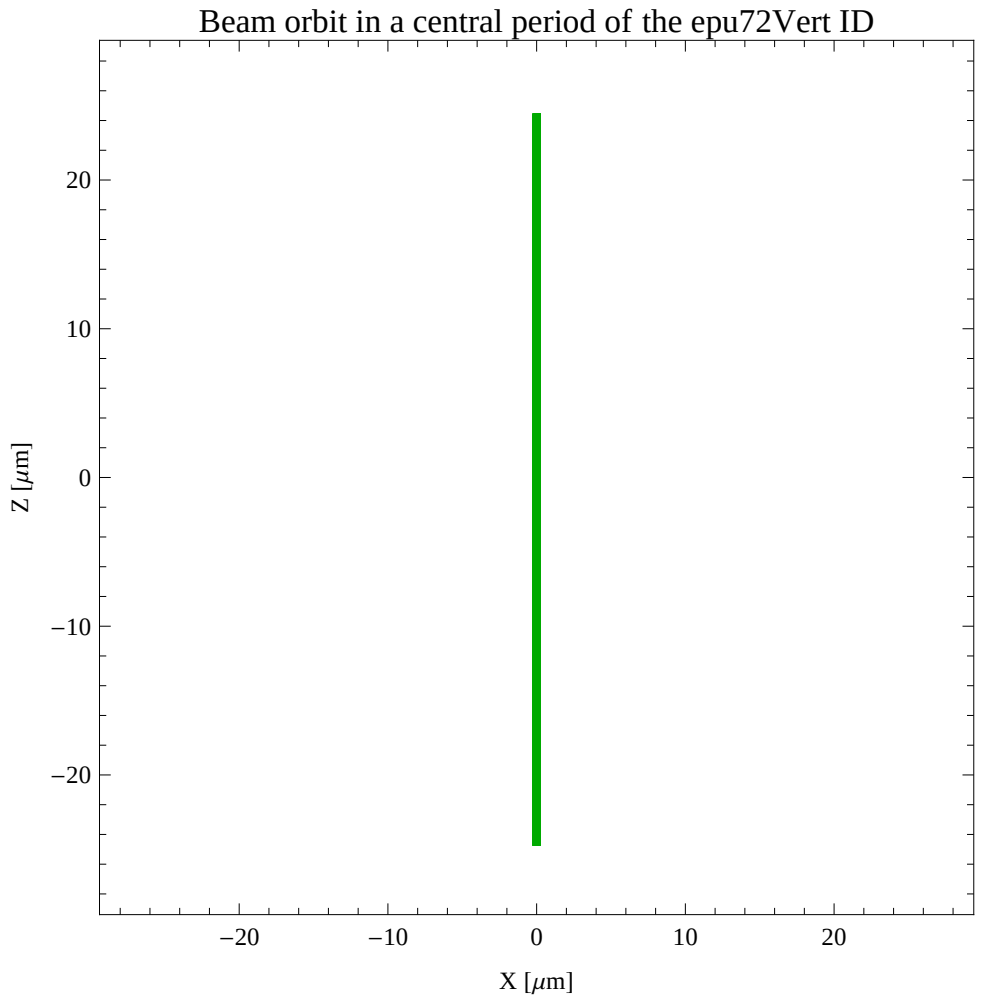

Figure 280: The beam orbit of the electron beam through a central period of the epu72Vert

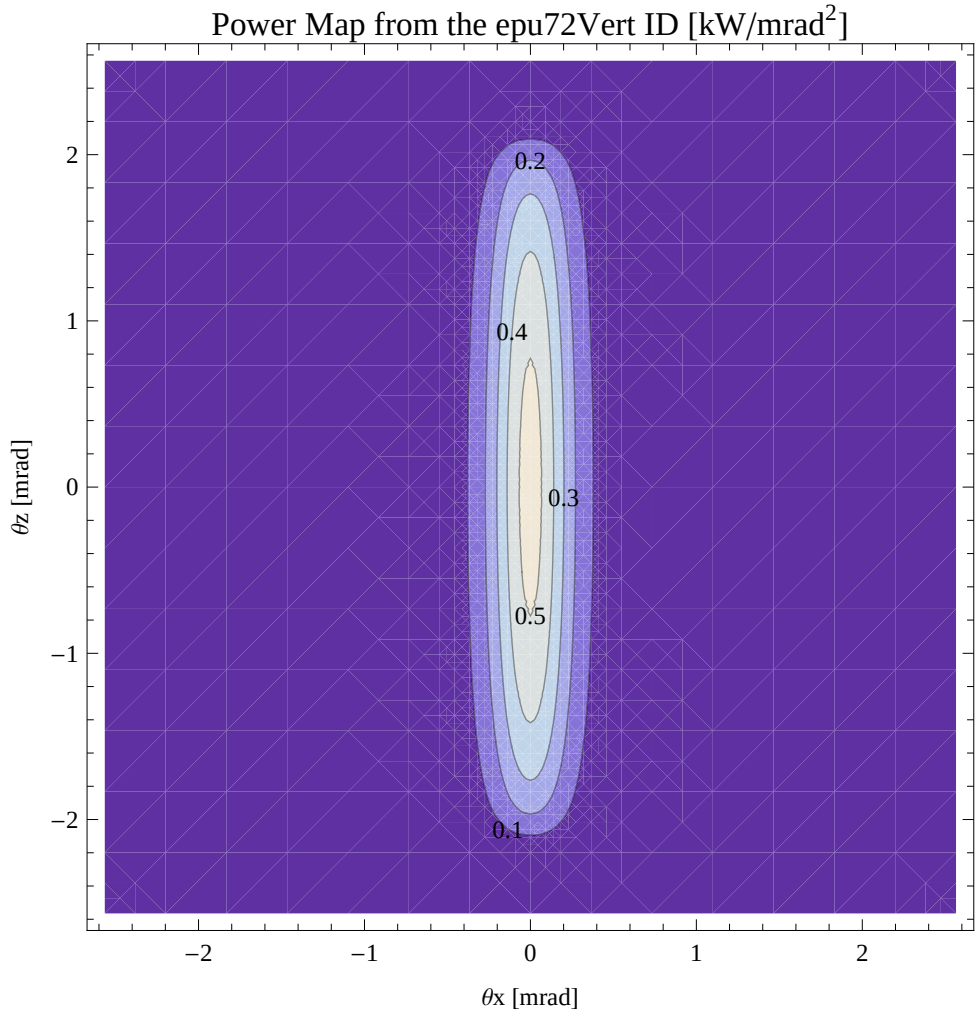

Figure 281: Map of the power distribution of the emitted synchrotron radiation by the epu72Vert

A map of the degree of linear polarisation of the fundamental harmonic of the synchotron radiation emitted by the epu72Vert over the angle of observation is shown in Figure 282.

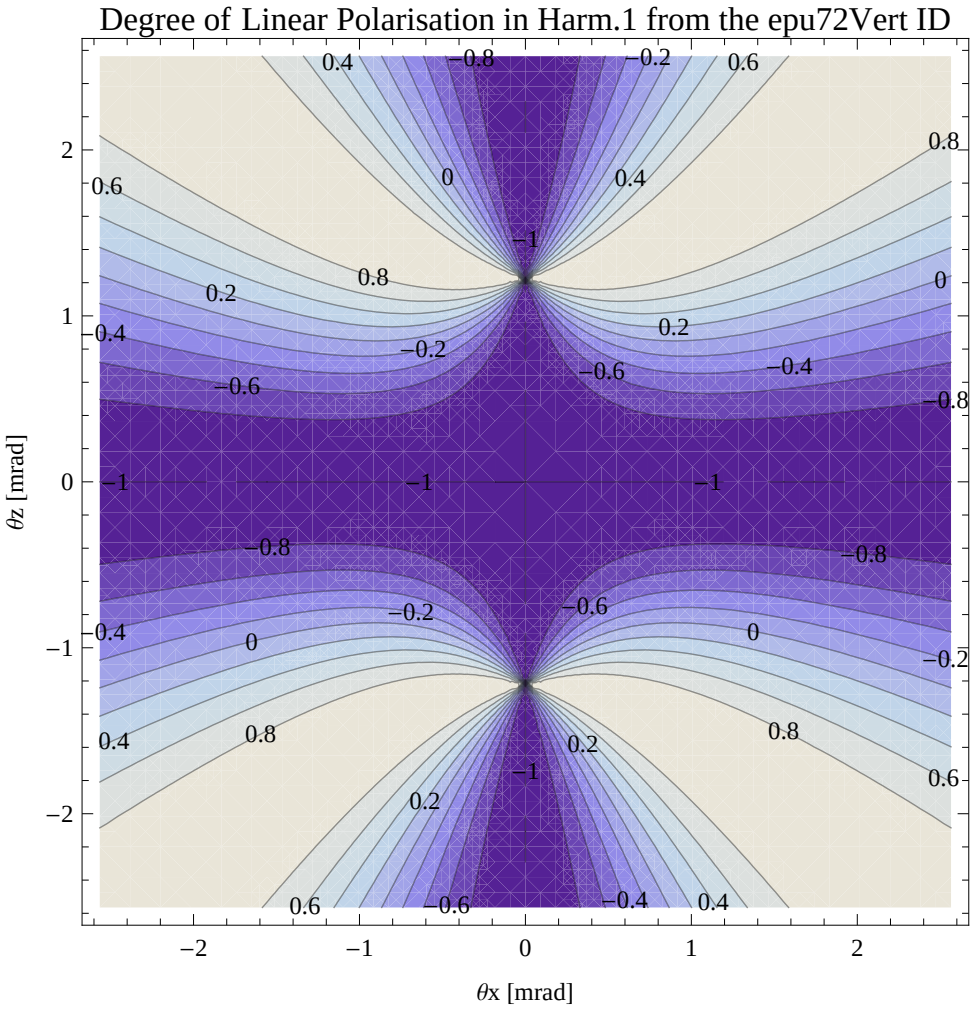

Figure 282: Map of linear polarisation in the fundamental harmonic of the synchotron radiation emitted by the epu72Vert

A map of the degree of 45 degree polarisation of the fundamental harmonic of the synchotron radiation emitted by the epu72Vert over the angle of observation is shown in Figure 283.

A map of the degree of circular polarisation of the fundamental harmonic of the synchotron radiation emitted by the epu72Vert over the angle of observation is shown in Figure 284.

The on axis brilliance at peak energy and the angular spectral flux from the epu72Vert have been calculated with the given beam parameters, which are 0.3 A of stored current, $\beta_H = 5.627$ m, $\varepsilon_H = 5.985$ nmrad, $\beta_V = 2.837$ m, $\varepsilon_V = 59.85$ pmrad, and an energy spread of 0.001.

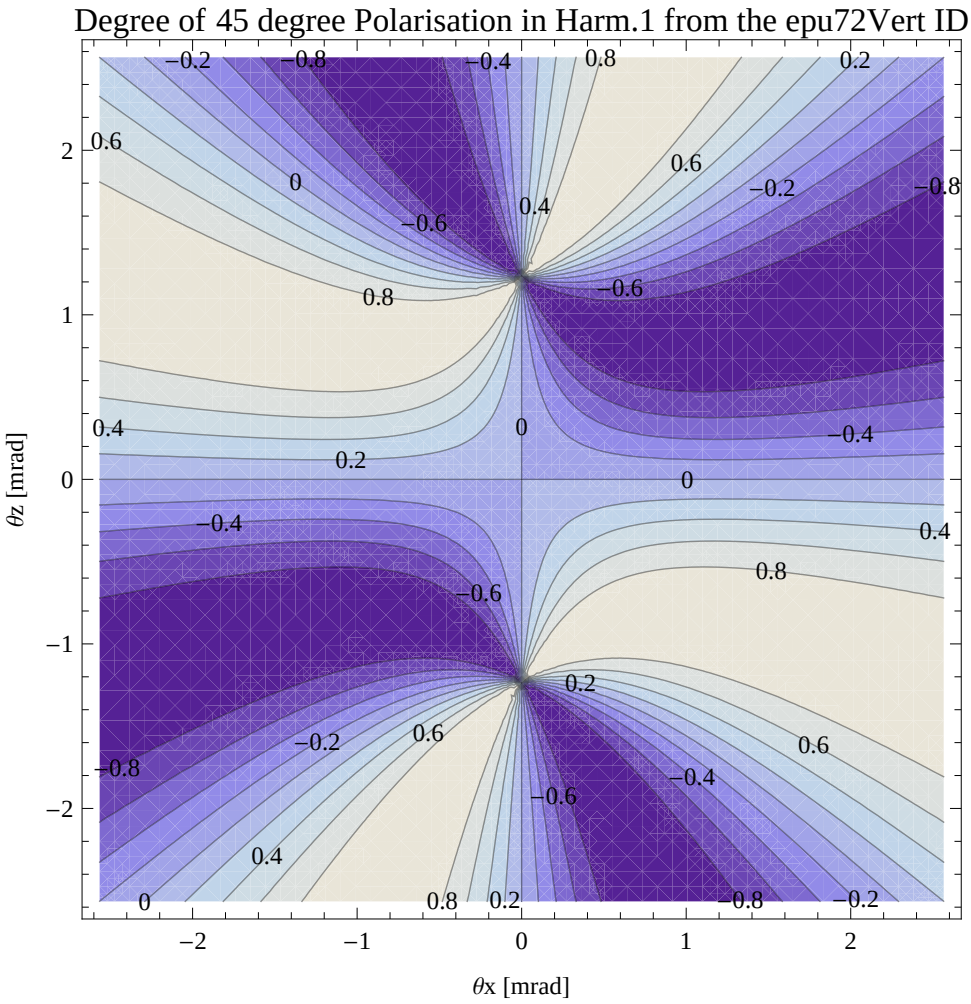

Figure 283: Map of 45 degree polarisation in the fundamental harmonic of the synchotron radiation emitted by the epu72Vert

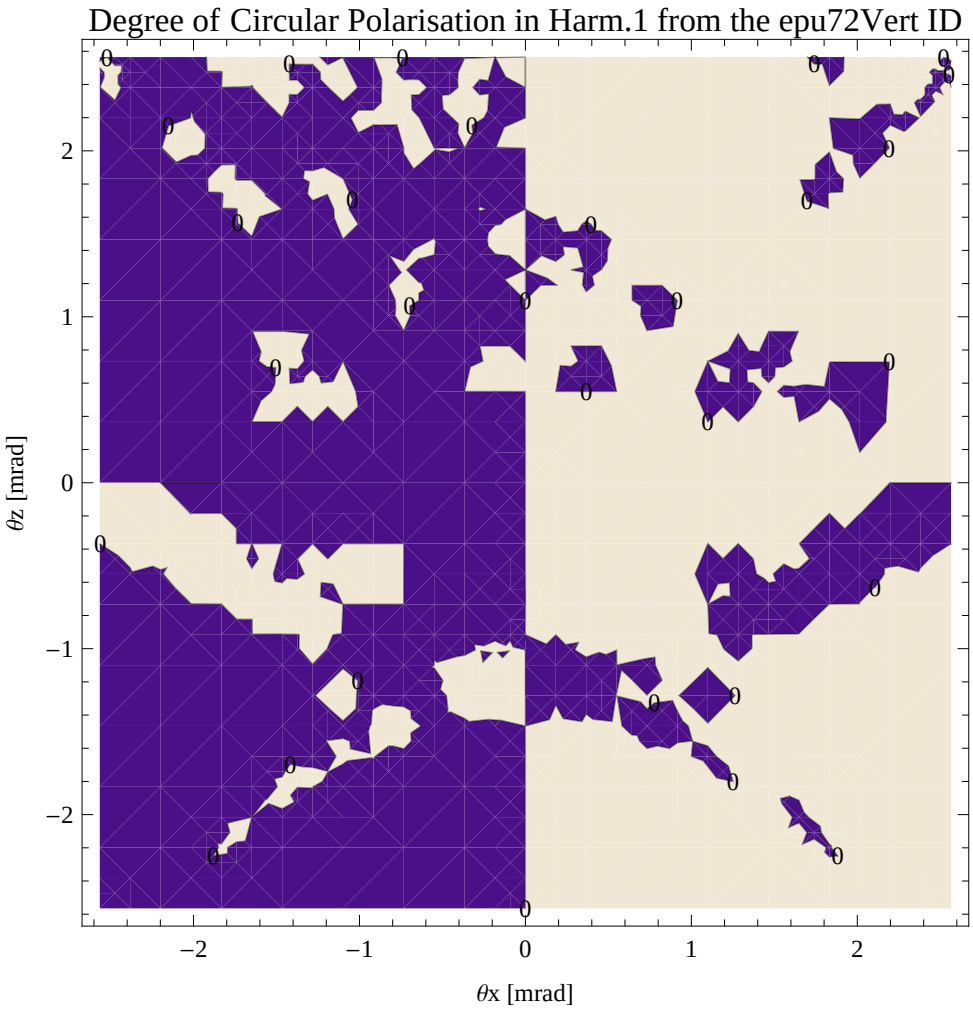

Figure 284: Map of circular polarisation in the fundamental harmonic of the synchotron radiation emitted by the epu72Vert

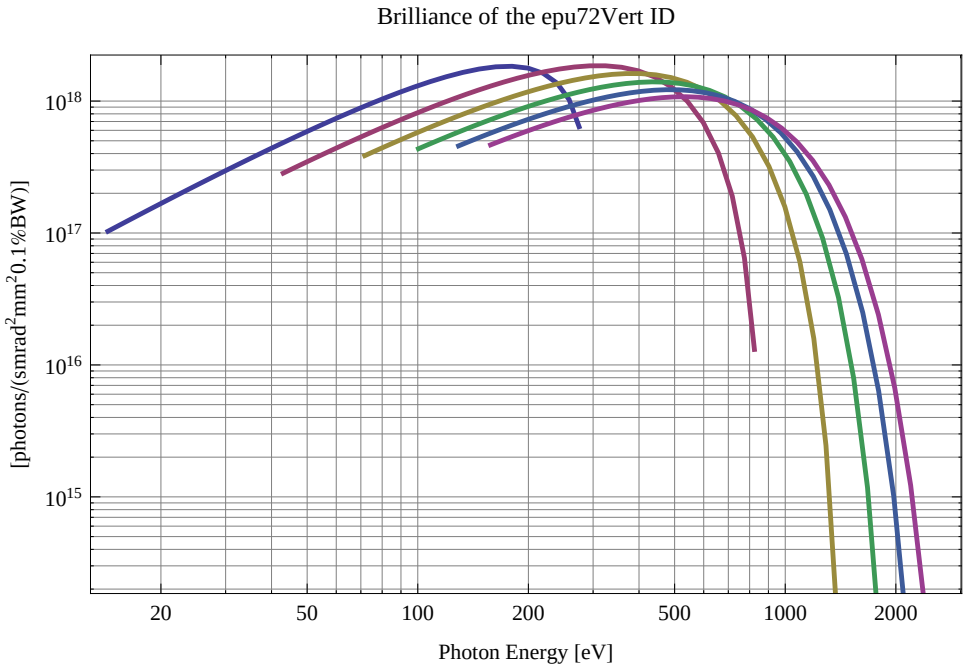

Figure 285: The brilliance at peak energy of the synchotron radiation emitted by the epu72Vert

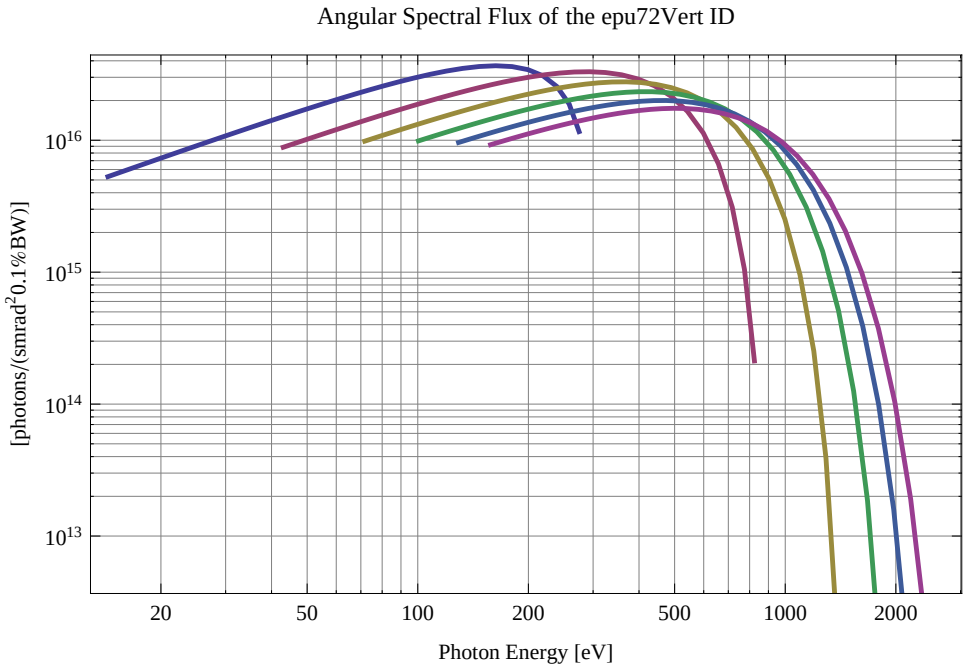

Figure 286: The angular spectral flux of the synchotron radiation emitted by the epu72Vert

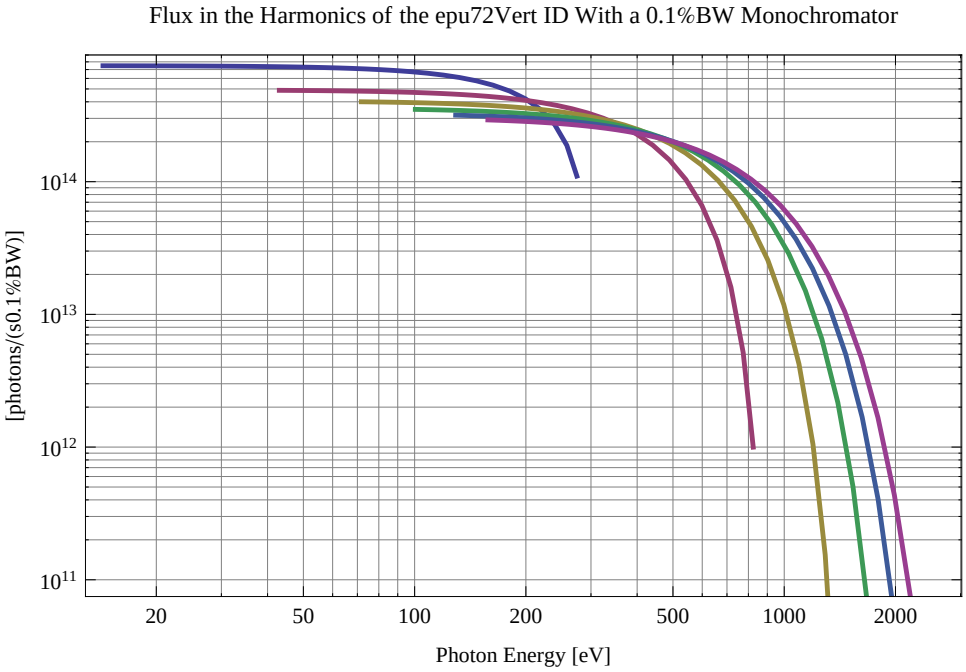

Figure 287: The flux of photons in the harmonics of the emitted synchrotron radiation from the epu72Vert using a 0.1%BW monochromator

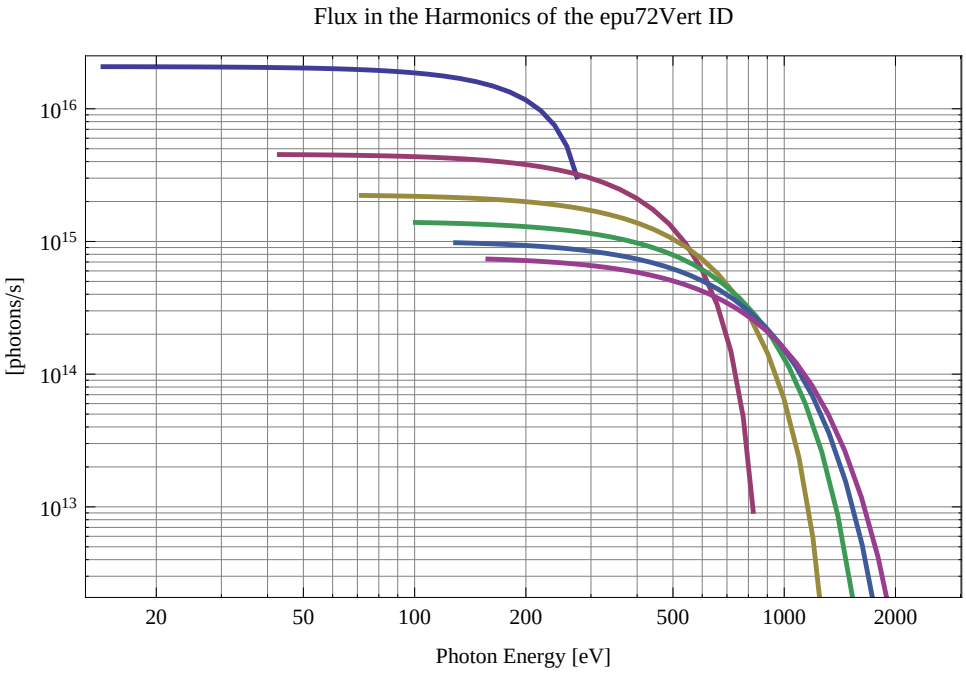

Figure 288: The flux of photons in the harmonics of the emitted synchrotron radiation from the epu72Vert

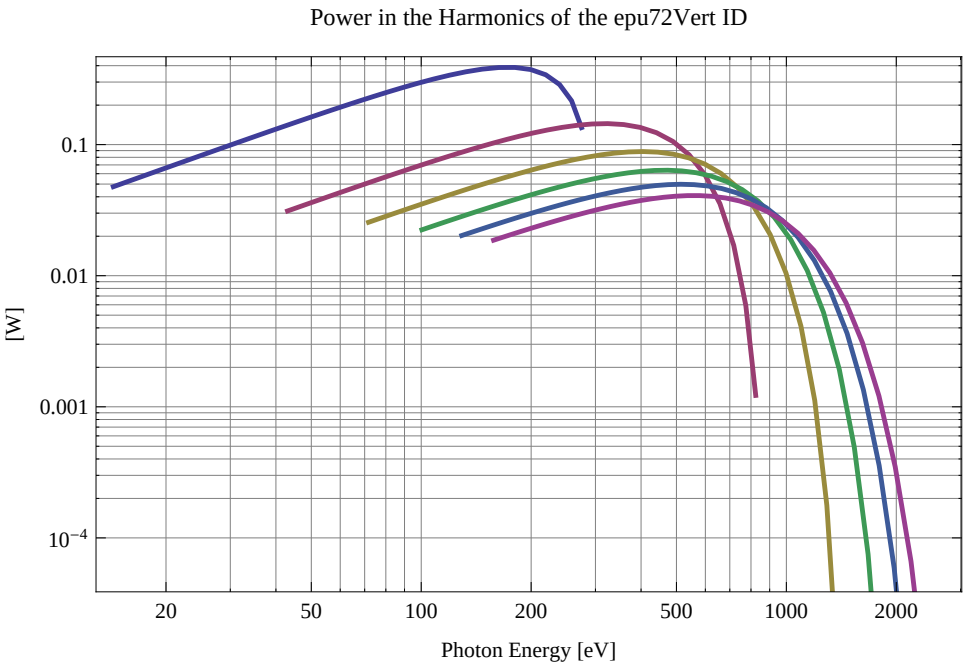

Figure 289: The power in the harmonics of the emitted synchrotron radiation from the epu72Vert

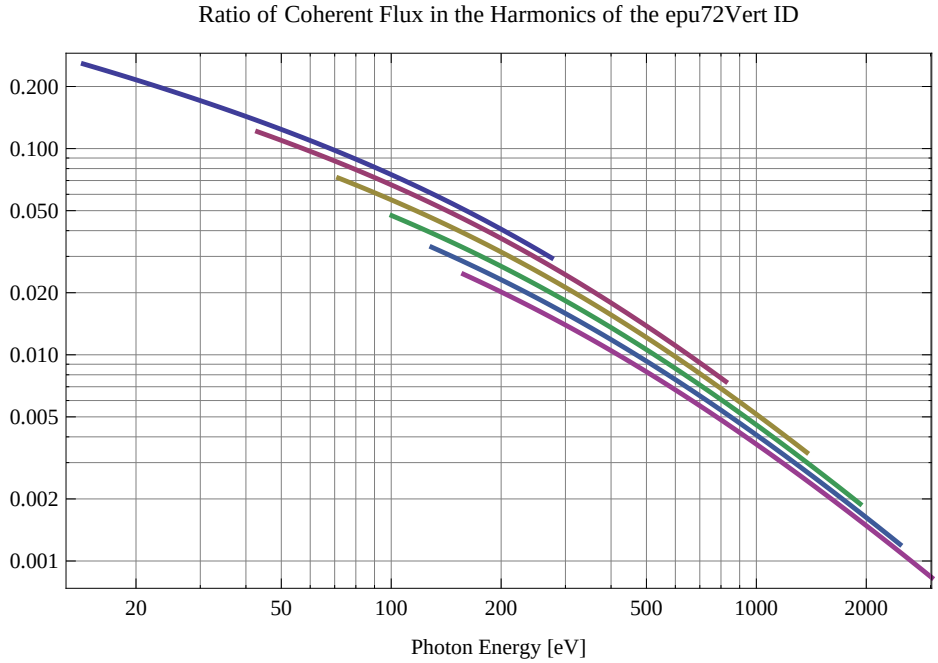

Figure 290: The ratio of coherent flux in the harmonics of the emitted synchrotron radiation from the epu72Vert

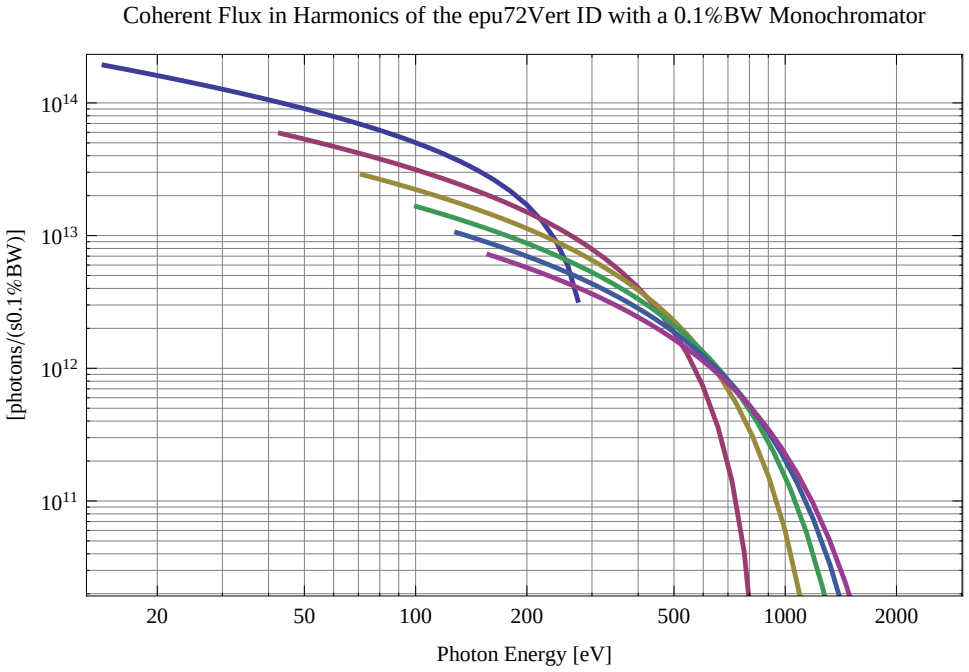

Figure 291: The coherent flux in the harmonics of the epu72Vert using a 0.1%BW Monochromator

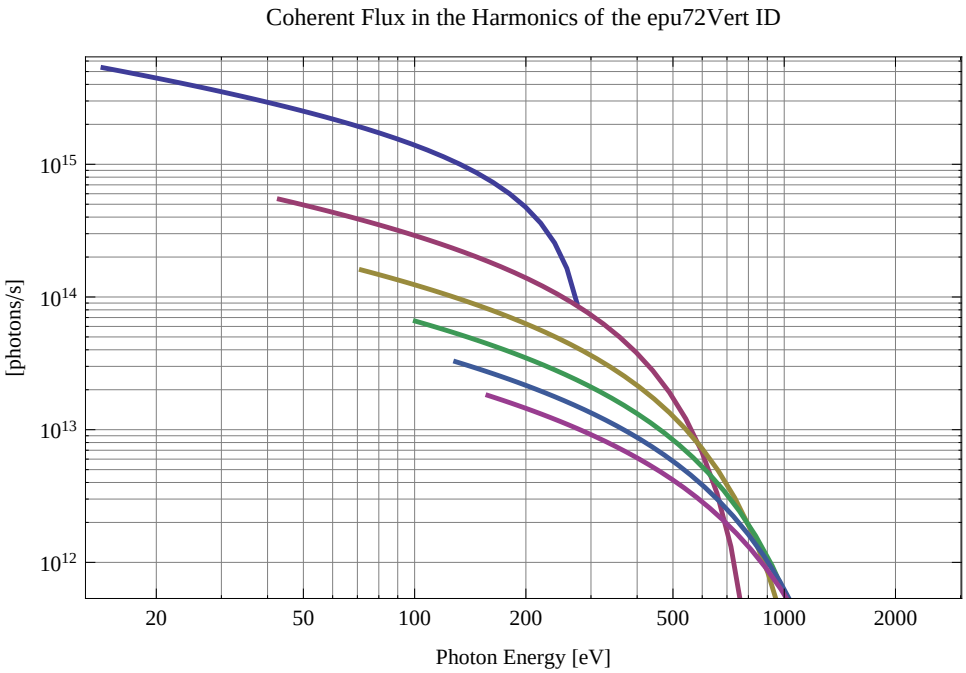

Figure 292: The coherent flux in the harmonics of the epu72Vert

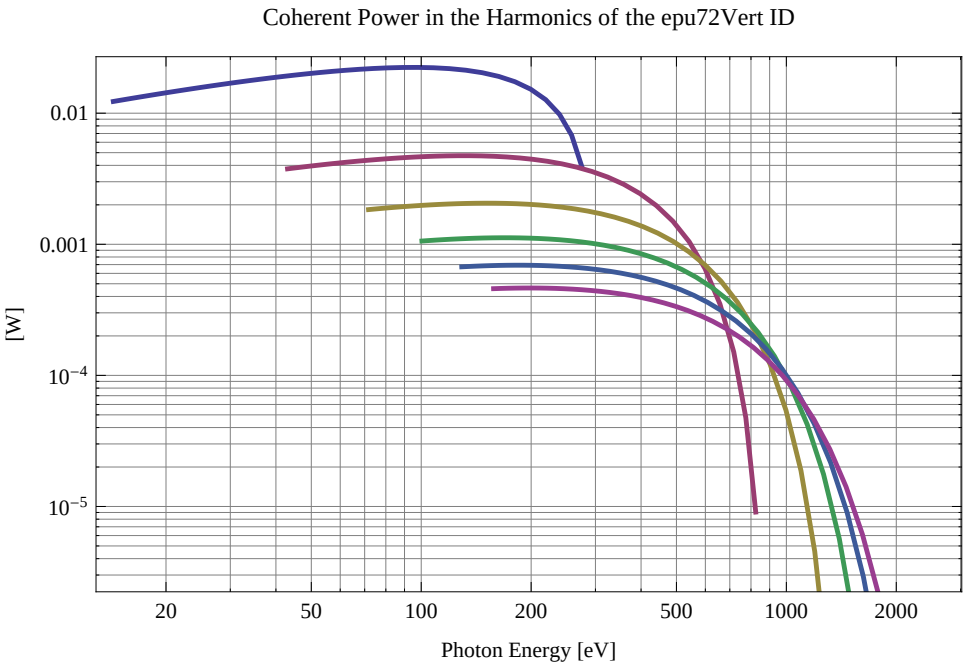

Figure 293: The power of coherent synchrotron radiation in the harmonics of the epu72Vert

The brilliance at peak energy and the angular spectral flux density from the epu72Vert for different harmonics at maximum K-value (6.274) are given in Table 40 and for minimum K-value (0.400) these values are given in Table 41.

Table 40: The brilliance at peak energy and the angular spectral flux density from the epu72Vert for different harmonics at maximum K-value (6.274)

Harmonic	Photon Energy [eV]	Brilliance [Ph./(smrad^{2}mrad^{2}0.1%BW)]	Angular Spectral Flux [Ph./(smrad^{2}0.1%BW)]
1	14.3481	1.03×10^{17}	5.3×10^{15}
3	43.0443	2.84×10^{17}	8.85×10^{15}
5	71.7406	3.86×10^{17}	9.84×10^{15}
7	100.437	4.35×10^{17}	9.89×10^{15}
9	129.133	4.57×10^{17}	9.61×10^{15}
11	157.829	4.66×10^{17}	9.25×10^{15}

Table 41: The brilliance at peak energy and the angular spectral flux density from the epu72Vert for different harmonics at minimum K-value (0.4)

Harmonic	Photon Energy [eV]	Brilliance [Ph./(smrad^{2}mrad^{2}0.1%BW)]	Angular Spectral Flux [Ph./(smrad^{2}0.1%BW)]
1	274.78	6.39×10^{17}	1.16×10^{16}
3	824.34	1.31×10^{16}	2.13×10^{14}
5	1373.9	1.62×10^{14}	2.57×10^{12}
7	1923.46	1.79×10^{12}	2.81×10^{10}
9	2473.02	1.89×10^{10}	2.96×10^{8}
11	3022.58	1.96×10^{8}	3.07×10^{6}

4.17 Influence from the epu72Vert on the optics of the stored beam

Figure 294 shows the focusing potential from the epu72Vert over the beam stay clear aperture of the ring aparture.

Figure 295 shows the kick map in the beam energy independant unit T^2m^2 of the kicks induced by the epu72Vert over the beam stay clear aparture.

Figure 296 shows the induced angular kick on the stored beam from the epu72Vert as a function of the vertical distance to the undulator axis.

Figure 297 shows the induced angular kick on the stored beam from the epu72Vert as a function of the horizontal distance to the undulator axis.

Figure 298 shows tune shift induced by the epu72Vert over the beam stay clear aparture. Note that the tune shift depends on the beam size at the.

Figure 299 shows the induced tune shift from the epu72Vert as a function of the vertical distance to the undulator axis.

Figure 300 shows the induced tune shift from the epu72Vert as a function of the horizontal distance to the undulator axis.

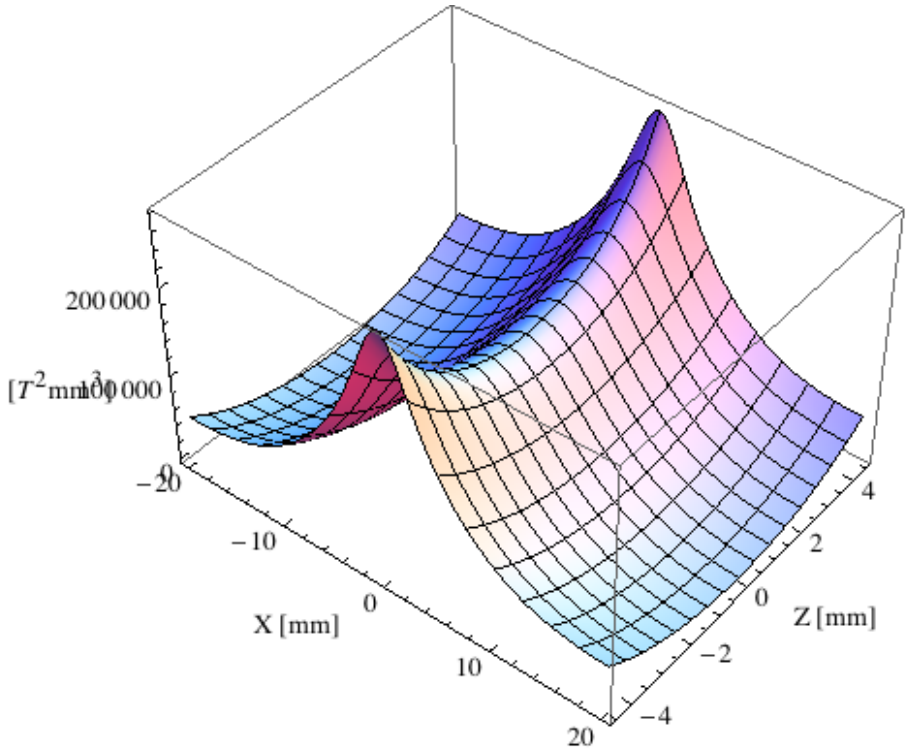

Figure 294: Focusing potential from the epu72Vert over the beam stay clear aparture.

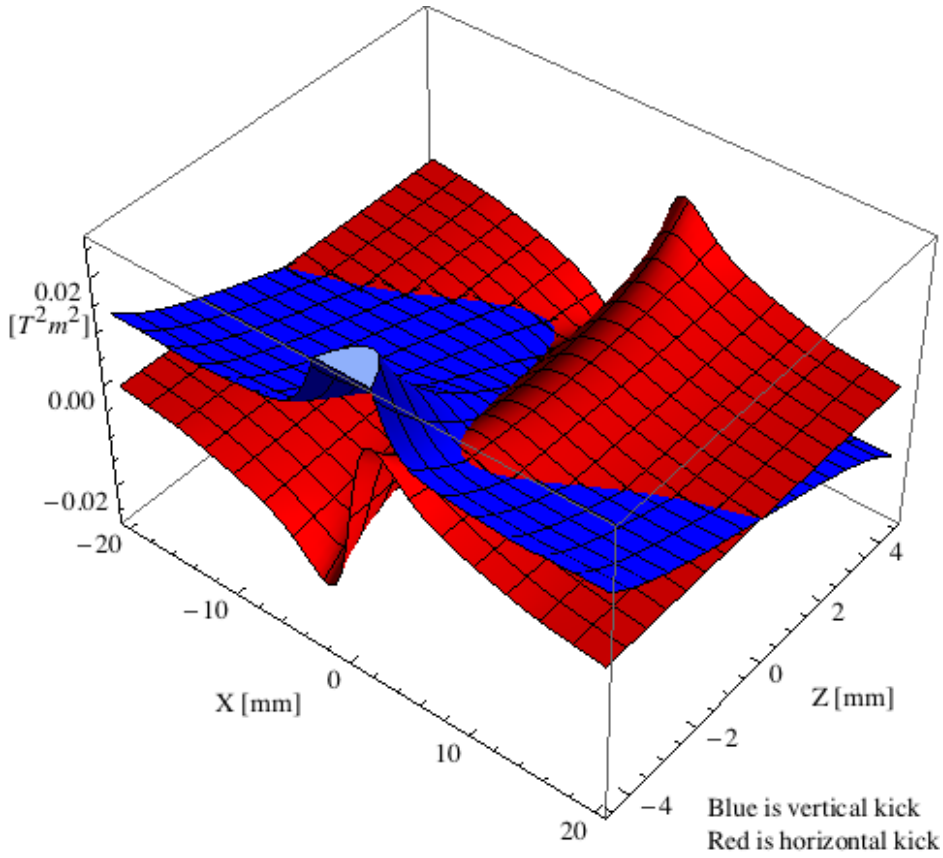

Figure 295: Kick map in the beam energy independant unit T^2m^2 of the kicks induced by the epu72Vert over the beam stay clear aparture.

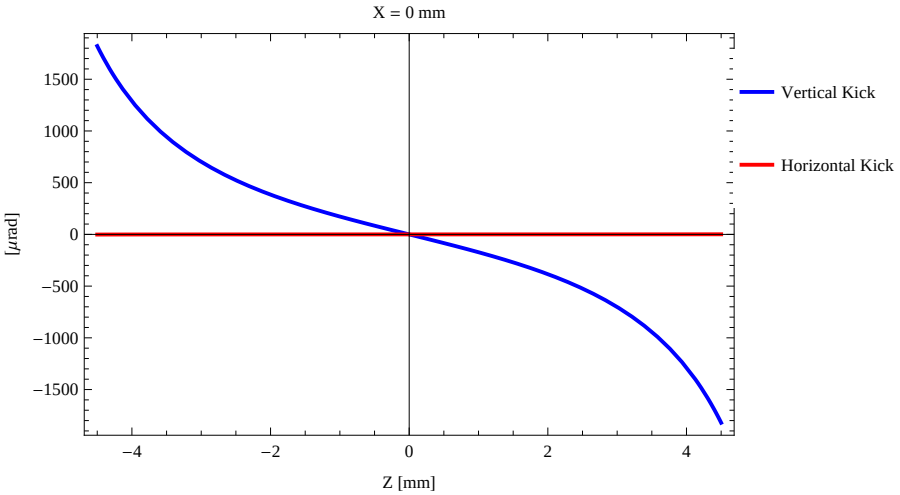

Figure 296: Induced angular kick on the stored beam from the epu72Vert as a function of the vertical distance to the undulator axis.

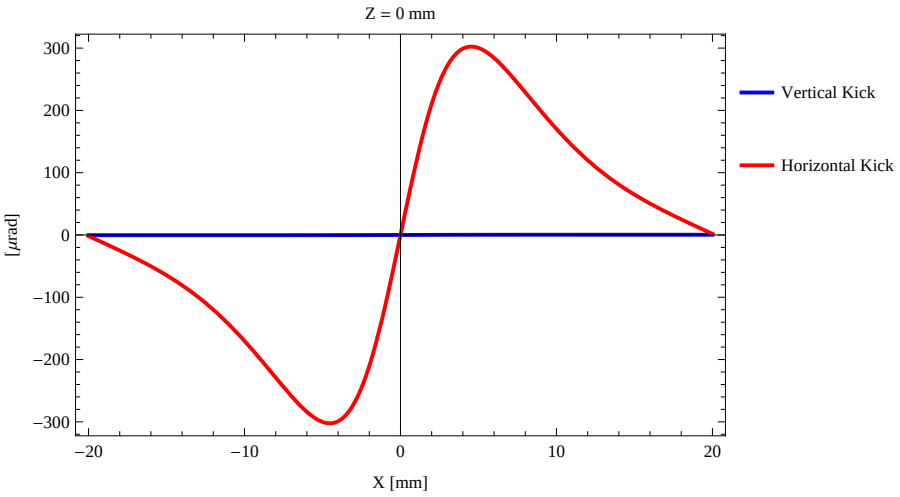

Figure 297: Induced angular kick on the stored beam from the epu72Vert as a function of the horizontal distance to the undulator axis.

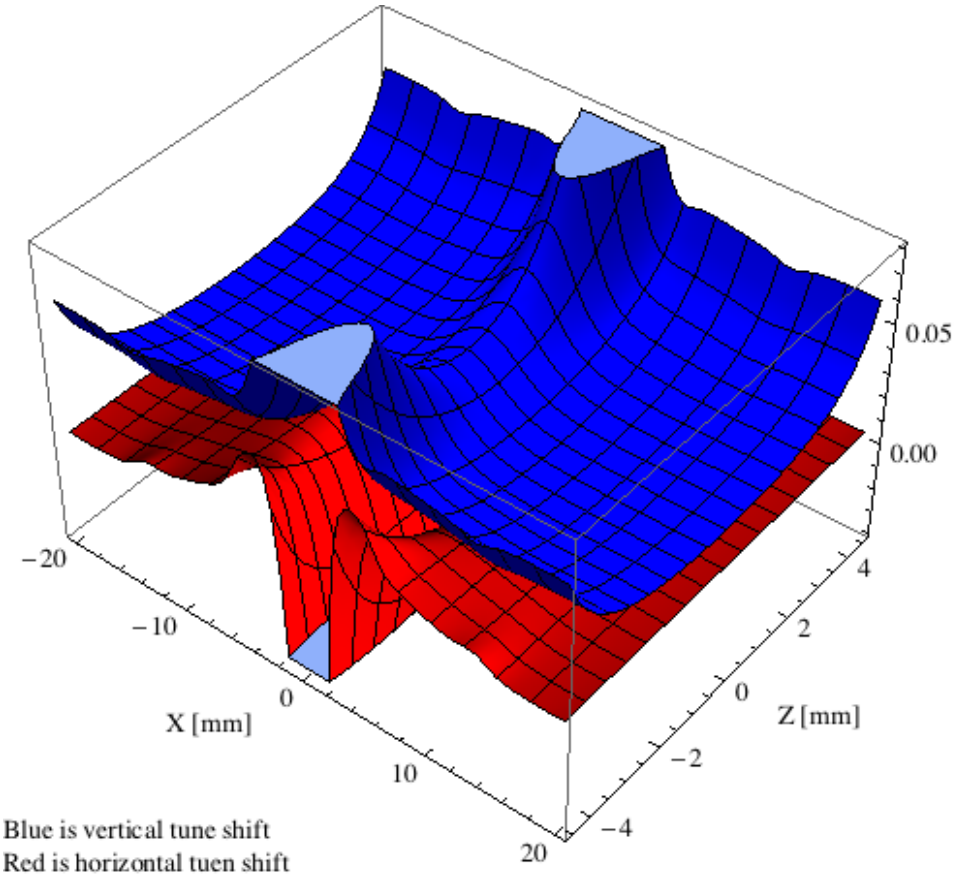

Figure 298: Tune shift induced by the epu72Vert over the beam stay clear aparture.

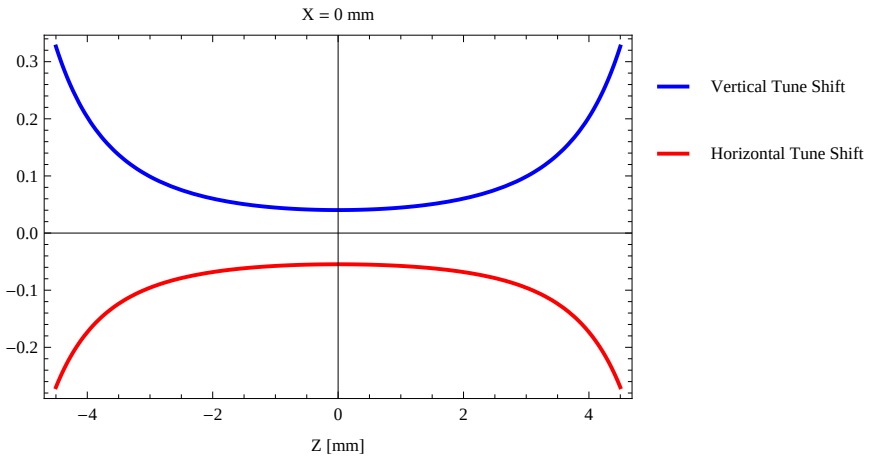

Figure 299: Induced tune shift from the epu72Vert as a function of the vertical distance to the undulator axis.

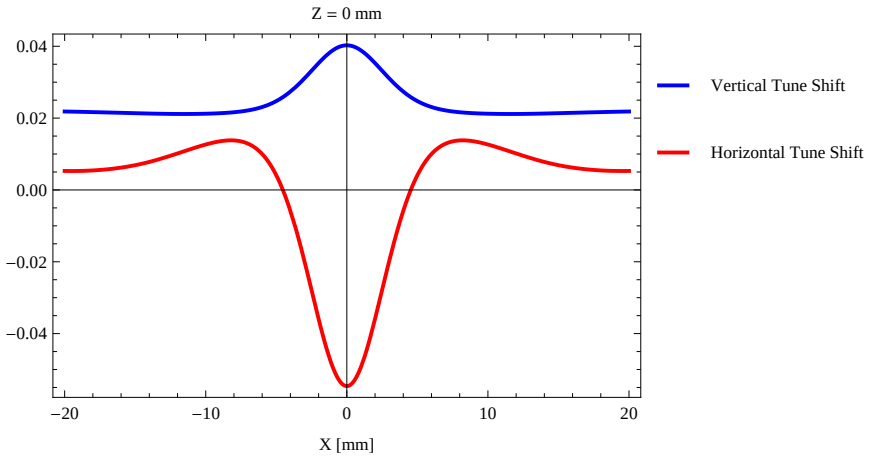

Figure 300: Induced tune shift from the epu72Vert on the stored beam from the as a function of the horizontal distance to the undulator axis.

References

[1] http://www.synchrotron.uj.edu.pl/.

[2] O. Chubar, P. Elleaume and J. Chavanne. *Journal of Synchrotron Radiation*, 5:481, 1998.

[3] http://www.maxlab.lu.se/maxlab/max4/max_iv_reports_public/accelerators_machine/1_5GeV/Lattice/Internal_Note_20111102_Updated_Lattice_111124.pdf.

[4] Johannes Bahrdt and Godehard Wüstefeld. Symplectic tracking and compensation of dynamic field integrals in complex undulator structures. *Phys. Rev. ST Accel. Beams*, 14:040703, Apr 2011.

List of Tables

List of Figures